Investigation into the mechanical performance of pipe grade HDPE with included silicon chips as a basis for future sensors

Anna Magdalena Kolonko

A thesis submitted to The University of Birmingham
for the degree of Doctor of Philosophy

School of Civil Engineering
University of Birmingham
April 2011

UNIVERSITY OF BIRMINGHAM

University of Birmingham Research Archive

e-theses repository

Abstract

Several hundreds of thousands of kilometres of pipes are buried beneath the roads in the UK. These pipes are 'dumb', i.e. they do not routinely have sensors attached to or integrated within them. One possibility of overcoming this is to utilize the Micro-Electro-Mechanical Systems technology (MEMS), which can produce micro sensors in large numbers and cheaply. If these sensors are to be integrated within the pipe, it is important to assess their impact on the structural integrity of the pipes. As most modern pipes are made of polyethylene, this has been the focus of this project. In order to test a large number of samples, small polyethylene samples were produced using compression moulding and tested in different stress modes such as tension, bending, Charpy impact and flexural creep. In addition, pipe joints were investigated. The samples were tested with respect to different chip sizes (4 and 16mm²), shapes (circle and square), numbers (one and two), orientations and position as well as sample dimensions and chip-polyethylene interface.

It was discovered that the square chip contributes to the highest increase in the stiffness of the polymer, but significantly reduces its ductility. The 4mm² circle causes the smallest disruption in the integrity of polymer, especially when including multiple chips, and it also acts as reinforcement when its volume is sufficiently large relative to the volume of the polymer matrix, e.g. multiple chips or smaller volume of matrix.

The optimal chip orientation for improving the impact strength and reducing the embrittlement effect in tension is parallel to the applied stress. A slight deviation from this orientation leads to a significant reduction in the ductility and yield stress of the sample. This is especially true when the chip is perpendicular to the tension direction as this produces the

greatest reduction in the cross-section of the polymer matrix, and when the proportion of the chip size to the sample size is large.

In the short and long term bending stress modes, the effect of the 4mm² circular chip was insignificant, while the 16mm² circular chip perpendicular to the load direction failed at large strains.

It was discovered that the bond between the silicon chips and the polymer matrix is important and a number of different chip coatings and hot melt adhesives were tested indirectly (in the tensile and bending tests). In addition, the hot melt adhesives were also tested directly (in the pull-off test). It was discovered that the chip causes the smallest embrittlement when there is no adhesion.

To my family

Acknowledgements

Table of Contents

List of Figures

List of Tables

Glossary of Symbols and Abbreviations

A	area of the sample cross-section (initial)
a	size of flaw, defect
A_0	initial sample area
A_{max}	maximum area of the samples cross-section
A_{min}	minimum area of the samples cross-section
a_N	impact strength of the notched sample
A_p	area of the platens
ASTM	American Society for Testing of Materials
a_U	impact strength of the unnotched sample
B	material constant associated with properties of the flaw
b	specimen width
b_N	remaining specimen width (under the notch)
BP	best practice
BS	British Standard
BSI	British Standards Institution
D	sample diameter
D_0	initial sample diameter
DN	nominal (outside) diameter
DSC	differential scanning colorimetry
E	Young's (tensile, elastic) modulus
E_a	energy absorbed
E_C	modulus of the composite
$E_c(t)$	time dependent creep modulus
E_{C1}	longitudinal modulus of the composite
E_f	flexural modulus
E_F	modulus of the filler
E_{fc}	flexural creep modulus
E_{fc50}	flexural creep modulus at 50 years
E_M	modulus of the matrix
EN	European Norm

$E_r(t)$	time dependent relaxation modulus
F	force
F_{13}	load at a stress of 13MPa
$F_{3.25}$	load at a stress of 3.25MPa
$F_{6.5}$	load at a stress of 6.5MPa
F_p	force applied to the platens
FSRM	Swiss Foundation for Research in Microtechnology
F_y	load applied at yield
G	shear modulus
g	standard gravity
GPC	gel permeation chromatography
h	specimen thickness (depth)
HDPE	high density polyethylene
h_m	thickness of the mould
HMA	hot melt adhesive
HMA1	Yparex 9702ES
HMA2	Yparex 9404
h_s	thickness of the sheet
I	moment of inertia
ICI	Imperial Chemical Industries
ISO	International Organization for Standardization
$J_c(t)$	time dependent creep compliance
K	compressive modulus and stress concentration factor
L	support span
l	extension, final length
L_0	load maintained constant
l_0	gauge length of the specimen, initial length
LC	large circle (16mm²)
LDPE	low density polyethylene
LLDPE	linear low density polyethylene
L_p	load applied to the platens
LSQ	large square (16mm²)

m	mass of the specimen
$M_{90°}$	bending moment at 90°
MDPE	medium density polyethylene
MEMS	Micro-Electro-Mechanical Systems
MFR	melt flow rate
m_H	mass of the specimen in Heptane
M_n	molecular weight (number average)
m_p	mass of the polymer
MW, M_w	molecular weight (weight average)
MWD	molecular weight distribution
n	number of measurements
NDE	non-destructive examination
PDI	polydispersivity index
PE	polyethylene
PENT	Pennsylvania edge notch tensile test
PP	polypropylene
P_p	pressure applied to the platens
PS	polystyrene
PSA	pressure sensitive adhesive
PTFE	Teflon
PVC	polyvinyl chloride
r	rate of cross-head motion
R^2	coefficient of determination
S	shrinkage
s	deflection
SC	small circle (4mm²)
SD	standard deviation
SDR	pipe diameter to wall thickness ratio
SSQ	small square (4mm²)
T	Temperature and torque
t	time
t(PENT)	failure lifetime in a PENT test

t(pipe)	failure lifetime of a pipe
$T_{f,c}$	temperature at the start of crystallization
$T_{f,m}$	temperature at the end of melting
$T_{i,c}$	temperature at the end of crystallization
$T_{i,m}$	temperature at the start of melting
$T_{p,c}$	temperature at the crystallization peak
$T_{p,m}$	temperature at the melting peak
t_{SR}	stress rupture time
TWI	The Welding Institute
UKWIR	UK Water Industry Research
UTS	ultimate tensile strength
V	final sample volume
V_0	initial sample volume
V_F	volume fraction of the filler
V_M	volume fraction of the matrix
V_m	volume of the mould
WaterRF	Water Research Foundation
X	arbitrary value used in equations
x	measured value
$\overline{x}$	average value
X_c	crystallinity
Y	arbitrary value used in equations and geometric factor
y_{max}	maximum deflection
Z	arbitrary value used in equations
z	strain rate

Greek Symbols

γ	shear strain
Δ	error of the quantity, e.g. ΔA – error of the area of the sample cross-section
ΔH	enthalpy of fusion
ε	axial strain
$\varepsilon(t)$	time dependent strain

ε_0	strain, maintained constant
ε_C	strain at break of the composite
ε_f	flexural strain in 3-point bending
ε_{f4}	flexural strain in 4-point bending
ε_l	lateral strain
ε_M	strain at break of the matrix
η	viscosity
θ	shear angle
ν	Poisson's ratio
ρ	density
ρ_H	density of Heptane
ρ_p	density of the polymer
σ	tensile stress
$\sigma(t)$	time dependent stress
σ_0	stress maintained constant
$\sigma_{0.0025}$	stress value at strain 0.0025
$\sigma_{0.005}$	stress value at strain 0.005
σ_{com}	compressive stress
σ_f	flexural stress in 3-point bending
σ_{f4}	flexural stress in 4-point bending
σ_{fp}	flexural peak
σ_h	hoop stress
σ_{yC}	yield stress of the composite
σ_{yM}	yield stress of the matrix
τ	shear stress
φ	angle of twist
ψ	debonding angle

Chapter 1   INTRODUCTION

Several hundreds of thousands of kilometres of pipes are buried beneath the roads in the UK. The old pipes laying in the ground are made from the full spectrum of materials, such as cast and ductile iron, asbestos cement, steel, PVC and PE, while these days the majority of water pipes installed in the UK are made from HDPE (Parker, 2007). In 2000-2003 it was 86% HDPE, while 7% was laid in ductile iron and the remaining 7% in PVC (MacKellar, 2007).

These pipes are exposed to many environmental factors, which accelerate their failure and contribute to contamination of their content, for example water, which should be prevented (American Water Works Service Co., Inc., 2002). This requires continuous real time monitoring of the condition of the pipes and their contents. The accurate location of buried utilities is also a challenge (Metje et al., 2007). Current techniques are expensive and time consuming and they allow only for local and occasional monitoring (Kamdem et al., 2004; Kwietniewski et al., 2005). Thus, there is a need for improvement and the development of new technologies. Therefore, the project "Smart Sensors for Buried Utility Location and Performance Monitoring" (Chapman et al., 2009) was proposed by the UKWIR (UK Water Industry Research) and WaterRF (Water Research Foundation). It aims to develop a sensor system, which would fulfil the challenges faced by the water industry. The current research originates from this project.

It is thought that micro/nano sensors could help to fulfil some of the challenges faced by the water sector. The idea of using micro scale sensors has arisen due to advances in Micro-Electro-Mechanical Systems engineering technology (MEMS) and the potential to enhance current monitoring techniques (Ko, 2007). There are many challenges associated with implementing lots of microsensors within the water distribution system, such as power

supply, signal transmission, and data analysis and management. The microsensors will have to be specially designed and located depending on the parameters they are targeted to measure. The majority of microfabricated sensors are made on silicon as the base material (Gad-el-Hak, 2002).

In this project the placement of silicon chips in the pipe walls is considered. Pipe grade high density polyethylene (HDPE) is used, as it is the most common pipe material. This requires a fundamental investigation of the mechanical compatibility between the polyethylene matrix and silicon chips, as no information was found in the literature on silicon within polyethylene samples nor pipes. In order to do this investigation the chips need to be introduced into polyethylene samples and pipes. The incorporation of the chips through mixing with the molten polyethylene during the pipe manufacturing process and the complex pipe tests would have consumed a lot of resources, especially time, energy, materials, and as a result money that was not available to the researcher. In addition, the required laboratory facilities were not available to carry out these complex procedures. Therefore, the tests were limited to compression moulded samples and also fusion joints connecting the sections of the pipes. The advantage of using small-scale polymer samples is that it allowed the testing of a large number of samples with a large number of different conditions.

This project does not aim to find a solution to the microsensors perse. It is researching the problems associated with embedding silicon chips within the polyethylene. The methods of introducing chips into compression moulded polyethylene and pipe joints will be developed and the integrity of the polyethylene matrix with silicon chips will be investigated. This will show if the incorporation of advanced MEMS in polyethylene for different applications, e.g. water pipes, is feasible and what the challenges and limitations are.

1.1 Aim

This project aims to investigate the effect of inclusions of silicon chips on the performance of pipe-grade polyethylene.

1.2 Objectives

1) To conduct a critical literature review of polyethylene and the effects of inclusions.

2) To develop a method of producing repeatable compression moulded polyethylene samples containing silicon chips for use in tensile, bending and Charpy impact tests.

3) To test the integrity of polyethylene samples containing silicon chips in tension, bending and impact with respect to chip size, shape, orientation, number and sample thickness.

4) To investigate the effect of bonding between the silicon chips and the polyethylene.

5) To carry out flexural creep tests for polyethylene samples containing chips in order to investigate the effect of inclusions on the long term performance of polyethylene.

6) To develop a method of introducing the chips into pipe butt fusion joints and to assess their impact by conducting tensile tests.

1.3 Thesis layout

The thesis is arranged in the following Chapters.

Chapter 2: Critical literature review focusing on the properties of materials and the effects of inclusions in polymers.

Chapter 3: Characterization of materials: The materials used in the project are introduced and the structural and physical properties of polymers, such as molecular weight (MW), molecular

weight distribution (MWD), melt flow rate (MFR), density, and crystallinity, obtained in the complementary tests are analysed.

Chapter 4: Methodology: Summary of sample production and test procedures is provided. Preliminary test results are presented to show the quality of the data and highlight issues related to sample production.

Chapter 5: Results & discussion of the impact of various parameters of the silicon chips and samples on the polyethylene in different stress modes such as tension, bending and Charpy impact.

Chapter 6: Results & discussion of adhesion tests: The strength of the bond formed by the hot melt adhesives between silicon and polyethylene is investigated in the pull-off test and the impact of different coatings on the performance of the samples with chips is analysed in the tensile and flexural bending tests.

Chapter 7: Results & discussion of the flexural creep test: The influence of the chips on the long term properties of polyethylene is investigated.

Chapter 8: Conclusions and recommendations for further work: The key findings are summarised, the conclusions are derived, the shortcomings of the current research are determined and the directions of further possible research are proposed.

Chapter 2   LITERATURE REVIEW

2.1 Introduction

In this chapter the composition and mechanical properties of silicon and polyethylene as well as the basic tests in which they are determined are discussed. Further, the role of inclusions and holes within a matrix is analysed and the factors identified by the researchers to influence the integrity and mechanical properties of such structures are discussed. At the end of the chapter the research gaps are specified.

2.2 Materials

In the introduction it was demonstrated that there is a need to monitor pipes routinely and one approach is to use MEMS technology. The most common pipe material for new pipes in the UK is currently HDPE, although, other materials are used. Therefore, polyethylene and silicon as the basis pipe and chip material are reviewed. Clearly, not only pipes are made of polyethylene.

2.2.1   Silicon

The basic most common material of MEMS sensors is a single crystal silicon. It is classified as a metalloid, which has intermediate properties between metals and non-metals (Sherman & Weston, 1966). Silicon was first prepared in a crystalline form by Deville in 1854. The Czochralski process is commonly used to produce single crystals of silicon, which have a diamond (cubic) structure, so the crystal lattice has three main directions (Haynes, 2010).

Silicon has semiconductive properties and has been used as a structural material and/or substrate of Micro-Electro-Mechanical Systems (MEMS) since Smith (1954) published a paper describing the piezoresistive effect in silicon. In the 1980s it became the primary

material for MEMS, which have a function to sense and locally control mostly physical parameters at the microscale (Gad-el-Hak, 2002).

The structures of microdevices are batch fabricated on wafers of diameter over 50mm using two primary processes: etching and deposition. They are composed of one structural material (usually silicon) and additional layers of a few micrometers in thickness in which the sensor is micromachined. Surfaces of microdevices are often lubricated or covered with special coatings to prevent their wear, friction and stiction (Gad-el-Hak, 2002).

Silicon is very rigid and brittle with a Young's modulus of about 190GPa comparable to steel (210GPa), but techniques of micromachining flexible substrates were developed. The silicon strength is controlled by flaws and grain boundaries. The physical effects dominating at microscale differ from those at macroscale so the strength of silicon structures reduces as the size decreases, while the electrostatic attraction and Van der Walls forces become important at the microscale (Gad-el-Hak, 2002). Silicon has a very smooth mirror-like surface of nanometre scale roughness (Tay et al., 2004).

2.2.2 Polyethylene

Polyethylene (PE) belongs to thermoplastic polymers together with polyvinyl chloride (PVC), polypropylene (PP), polystyrene (PS), and other (Plastics Pipe Institute, 2007). Polyethylene and polypropylene are classified as polyolefins as they are produced from a simple olefin monomer with the general formula C_nH_{2n}.

As material molecular structure has an influence on its mechanical properties. The details of polyethylene molecular structure are introduced in next sections. Further, its influence on polyethylene mechanical properties is studied.

2.2.2.1 Molecular structure of polyethylene

Polyethylene was invented by the Imperial Chemical Industries (ICI) company in England in 1933 and its production process has evolved since this time to allow the variation of the density and improve the properties (Hoechst Plastics, 1982).

It is made of ethylene monomers in the polymerization process of gaseous ethylene, as illustrated in Figure 2.1 (Mills, 2005).
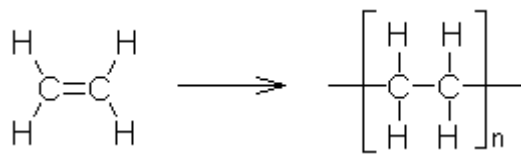
Figure 2.1 Forming of polyethylene in the polymerization process (Mills, 2005).

Polyethylene chains are three dimensional and have different lengths, consisting from a few to several hundred thousands ethylene units. They can have additional chain branches (an example is illustrated in Figure 2.2) formed from the same structure or from introduced comonomers. In Figure 2.3 different molecular structures of polyethylene are illustrated.
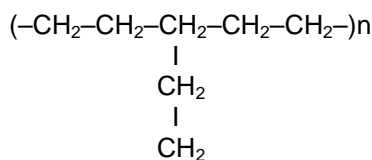
Figure 2.2 Polyethylene chain with a side branch (Plastics Pipe Institute, 2007).
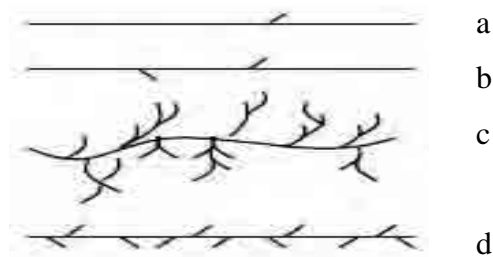
Figure 2.3 Molecular structures of (a) High Density Polyethylene (HDPE) Homopolymer with almost no branching, (b) HDPE Copolymer with no long branches, (c) High Pressure Low Density Polyethylene (LDPE) with many long branches, (d) Linear LDPE with many short branches (Brydson, 1999).

Both, the length of the main chains and the number, length and type of side branches are controlled in the polymerization process and are reflected in the Molecular Weight (MW) and Molecular Weight Distribution (MWD) of polyethylene (Plastics Pipe Institute, 2007).

The distribution of the molecules size (weight) in polyethylene usually follows the bell shaped normal distribution curve known from the Gaussian probability theory, which can have a different spread influencing the material properties. Narrow MWD means that the polymer contains molecules of similar weight, while broad MWD reflects a wide range of molecule sizes. The MWD curve can also have a bimodal shape, which means that the polymer is composed of very long and very short polymer molecules (Plastics Pipe Institute, 2007). All three MWDs are presented in Figure 2.4.
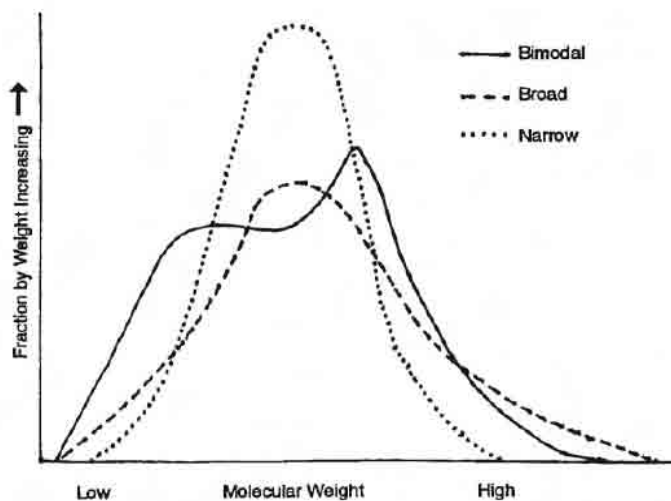
Figure 2.4 MWD curves (Plastics Pipe Institute, 2007).

MWD is expressed via the Polydispersity Index (PDI), which has a value greater or approaching one when the polymer chains approach a uniform chain weight (Rane & Choi, 2005).

Processing of polymers is likely to give some changes in MW and MWD due to degradation of some molecules; however, this depends on the particular material and the processing conditions (Holding, 2010; Peacock, 2000).

MW and MWD of polymer molecules determine their arrangement, which has an influence on the physical and mechanical properties, and is studied in the next section.

2.2.2.2 Arrangement of molecular chains

The polyethylene chains are highly random in the molten state. The long chains can entangle as illustrated in Figure 2.5.
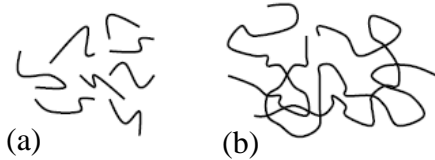
Figure 2.5 Entanglement of polymer chains: (a) short chains at low molecular weight (b) long chains at high molecular weight (Özbek, 2008).

During crystallization (setting) of polyethylene the chains arrange themselves in an ordered way. Polyethylene is a semi-crystalline polymer, i.e. it consists of both amorphous regions – made of randomly arranged tangled molecular chains, and crystalline regions – highly ordered and layered. The proportion of these regions within a sample determines its degree of crystallinity (Peacock, 2000).

Keller's (1957) observations of polymer crystals' growth from dilute solutions revealed that they form around 10nm thick platelets (lamellae) made of folded chains (Figure 2.6). The lamellae radiate outward from a single nucleation site in the centre and form spherulites of a spherical shape (Figure 2.7). In between the lamellae are the amorphous regions with the tie-chain molecules connecting adjustment lamellae (Callister, 2007; Peacock, 2000). At the end of the crystallization process the spherulites change their shape as they impinge on one another (Figure 2.8).

Figure 2.6 The chain folded lamella (Callister, 2007).
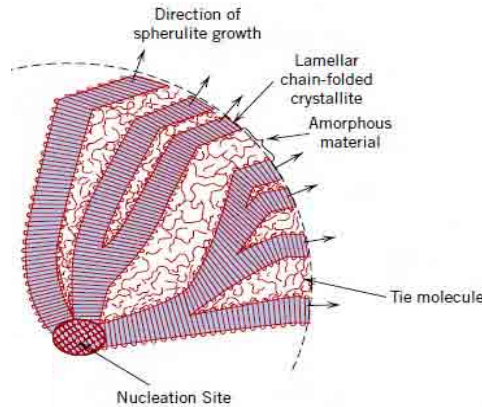
Figure 2.7 The structure of a spherulite (Callister, 2007).
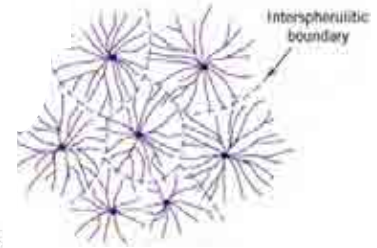
Figure 2.8 Adjacent spherulites (Callister, 2007).

In contrast to the spherulite formation from a dilute solution, in a melt the chain entanglement plays an important role and the spherulites adopt a more irregular form.

The size of the lamellae (and thus spherulites) depends on the time the chains have for the arrangement (processing conditions), and on the polyethylene molecular structure (Peacock, 2000). Amornsakchai et al. (2000) observed that the size of spherulites is indirectly proportional to MW of polymer. In the studies of HDPE only early stage small spherulites were observed. Some polyethylene resins do not develop spherulite structures at all, which is attributed to a larger number of branches, entanglements and tie molecules preventing their formation (Paizis, 2004).

The side branches usually prevent polymer chains from packing closely and additionally contribute to formation of defects in the crystalline material. The chain defects such as vacancies and atoms dissimilar to normal chain units, and impurities and imperfections within spherulites distract the polymer structure and reduce its crystallinity (Peacock, 2000).

When the polymer molecules have similar weights (narrow MWD), it crystallizes faster and more uniformly.

The density is directly proportional to the crystallinity as the packing of crystalline regions is better than amorphous regions (Callister, 2007; Peacock, 2000). On the basis of density, the polyethylene grades are classified as shown in Table 2.1.

Table 2.1 The density ranges of polyethylene (ASTM, 2005).

Type of polyethylene	Density, g/cm³	Standard designation
Very Low Density Polyethylene	< 0.910	Type 0
Low Density Polyethylene (LDPE)	0.910 – 0.925	Type I
Medium Density Polyethylene (MDPE)	0.926 – 0.940	Type II
High Density Polyethylene (HDPE)	0.941 – 0.960	Type III
Very High Density Polyethylene	> 0.961	Type IV

In the next section the dependency between polymer molecular properties and mechanical properties of the final product is studied.

2.2.2.3 The influence of polymer molecular structure on its mechanical properties

In the previous section the typical arrangement of polymer molecules was introduced and the influence of polymer molecular composition on the variations in this arrangement was analysed. In this section, the influence of these variations and the role of the tie chains on the mechanical properties of the final product are studied.

The basic physical and mechanical properties of polyethylene are explained in Table 2.2. Some of them will be discussed later in detail and also other properties will be introduced.

Table 2.2 The physical and mechanical properties of polymers (Callister, 2007; Jaarsma, 2000).

Property	Definition/description
Tensile strength	The maximum tensile load per unit area a material can withstand.
Tensile elongation	Expresses how much the material length increases in response to a tensile load. Elongation at break is the maximum elongation the polymer can undergo.
Flexural stiffness	The maximum bending load a material can withstand before it ruptures.
Impact strength	Evaluates how well the material absorbs energy from an impact loading. In the case of testing a notched sample, it is related to the ease of crack propagation.
Stress Crack Resistance	The resistance to propagation of a crack under constant load conditions.
Creep	Material deformation and/or failure under a constant load (tension, compression or flexure) over time.
Fatigue	Material deformation and/or failure under a cyclically applied load (tension, compression or flexure) over time.
Abrasion resistance	The resistance to wear and tear.
Hardness	The resistance to deformation due to surface indentation or abrasion.
Ductility	Expresses how well a material can deform without fracture and can be evaluated via tensile elongation.
Brittleness	The opposite to ductility; the tendency of the material to fracture under the application of load without or with small previous deformation.
Toughness	The ability to absorb mechanical energy without fracturing. It is proportional to the impact strength.
Viscosity	The resistance of polymer to flow in a molten state by the shear forces. It is indirectly proportional to the Melt Flow Rate (MFR).

The interlamellar connections (tie chains) formed especially by the molecules having high MW hold the crystallites together and transmit forces between them. Without the tie chains polyethylene would be a brittle material with little physical strength (Peacock, 2000). Under the application of stress they reduce polymer 'mobility', hindering elongation during stretching and increasing the tensile strength (Fu et al., 2003; Seguela, 2005). However, in some cases the samples with low MW might reach a higher tensile strength due to higher elongation (Callister, 2007). Further, high MW improves the polymer durability, long term strength, and fatigue. However, it also increases the viscosity and reduces the Melt Flow Rate (MFR) (ability to flow in a molten state), which is important in polymer processing.

A wide range of molecular weights indicates a polymer with a good stress crack resistance, and good impact resistance. The bimodal MWD ensures both good material physical properties and processing behaviour required e.g. for pipe-grade polymers (Plastics Pipe Institute, 2007).

Table 2.3 shows the correlation between the polyethylene molecular structure, crystallinity and density, and the mechanical properties of the end product.

Table 2.3 Correlation between polyethylene molecular structure, crystallinity and density, and mechanical properties of the end product (Crawford & Kearns, 2003; Peacock, 2000; Plastics Pipe Institute, 2007).

	MW	MWD	Crystallinity and Density	MFR
Physical property	As the molecular property increases/broadens, the physical property:			
Tensile Strength	Increases	-	Increases	Decreases
Tensile Elongation/ Ductility	Decreases	Increases	Decreases	Decreases
Flexural Stiffness	Increases	Decreases Slightly	Increases	Decreases Slightly
Impact Strength	Increases	Increases	Decreases	Decreases
Stress Crack Resistance	Increases	Increases	Decreases	Decreases
Resistance to Creep	Increases	-	Increases	Decreases Slightly
Fatigue Endurance	Increases	Increases	Increases	Decreases Slightly
Abrasion Resistance	-	-	Increases	Decreases
Hardness	-	-	Increases	Decreases Slightly
Shrinkage	-	Increases	Increases	Decreases

As indicated in section 2.2.2.2 the size of the spherulites depends on the processing conditions besides polyethylene molecular structure. Therefore, the influence of the processing conditions on polyethylene crystallinity as well as different methods of polyethylene processing are studied in the next section.

2.2.3 Processing of polyethylene

It was already briefly explained that polyethylene can be in a molten and solid state. In a molten state it is a viscous liquid (which can be shaped) with randomly arranged molecules, while in a solid state (final product) the polyethylene chains are ordered (Peacock, 2000). The state of polyethylene depends mostly on its temperature.

Thus, the manufacturing process of polyethylene comprises three main stages (Figure 2.9). Firstly, the material is heated into the melt state. Secondly, it changes its shape as it flows or is compressed under a relatively high pressure required due to its high viscosity. Thirdly, it is cooled to solidify (Mills, 2005).

| Heat to melt | → | Change shape | → | Cool to solidify |

Figure 2.9 Schematic of the stages in processing thermoplastics (Mills, 2005).

The level of order of the chains (crystallinity) depends on both, their molecular structure and the processing conditions such as pressure applied during cooling and the cooling rate. The cooling rate is only important at the temperatures at which the polyethylene crystallizes, thus this is studied in the next section. Further, different polyethylene manufacturing techniques are introduced.

2.2.3.1 Crystallization and melting temperature

Crystallization usually takes place over a range of temperatures as the sample cools because every polymer is composed of molecules having a variety of MWs, thus different sizes of lamellae and spherulites form. The polymer structural properties favouring quick and intensive crystallization were mentioned in section 2.2.2.2. At lower temperatures, the chain movement is inhibited; however, the formation of stable nuclei (from which the crystallites originate) is favoured. Thus, the highest rate of crystallization occurs at an absolute temperature of approximately the equilibrium melting temperature multiplied by 0.8 (Peacock, 2000).

The melting temperature increases with increasing thickness of lamellae determined by the factors specified in section 2.2.2.2, and with increasing heating rate (Callister, 2007; Peacock,

2000). Similar to crystallization, the melting of polymers takes place over a range of temperatures due to a varied crystalline structure associated with varied MWs.

In the next section the polyethylene manufacturing methods are introduced.

2.2.3.2 Polyethylene manufacturing techniques

The main methods of polyethylene production are compression moulding, injection moulding, and extrusion.

In the compression moulding process the polymer granules are introduced into the metal mould and melted in the preheated press. Then the pressure is applied to the mould in the vertical direction and further the material is cooled down to solidify usually by passing cold water through the mould. Different types of moulds can be used and one of them is illustrated in Figure 2.10.
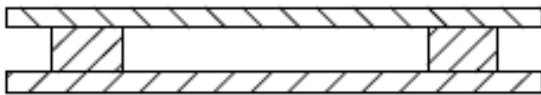
Figure 2.10. Flash "picture frame" mould (BSI, 2005a).

Shrinkage is a common phenomenon associated with crystallization, orientation and thermal contraction of polymer. The higher the crystallinity of the material associated with its molecular structure, the higher the shrinkage (Peacock, 2000). This causes thickness variation and a wavy surface of the product (BSI, 1998).

Injection moulding allows the production of different shapes of plastics. An example of an injection moulding machine is shown in Figure 2.11. The polymer granules drop from the feed hopper into the heated barrel. An extruder type screw in a barrel rotates to transport, melt and pressurise material, which is further forced through the nozzle into the mould cavity. After the mould is filled the cooling starts.
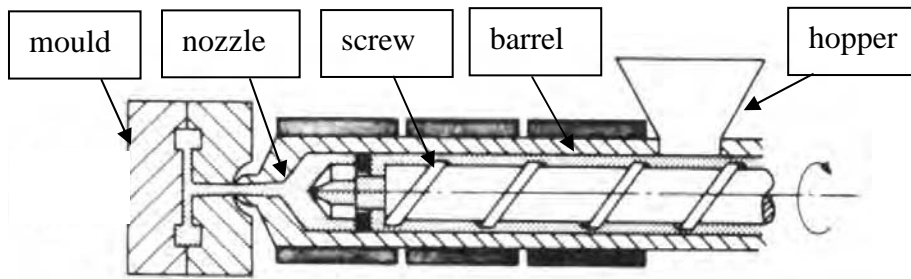
Figure 2.11. Schematic of an injection moulding machine (Crawford, 1987).

In the extrusion process the material, instead of being injected into the mould, is pushed through the die, which distributes the polymer melt around a solid mandrel forming it into an annular shape of controlled size. The pipe is pulled through the immersion or spray cooling system. The speed of the extruder screw and the speed of pulling determine the wall thickness (Plastics Pipe Institute, 2007). The modern equipment is fully automatized.

In the compression and injection moulding the product is usually cooled from outside so the highest crystallinity is inside, where the cooling rate is the lowest. The pipe can be cooled from one side (usually outside), so the crystallinity is the highest on the inner side of the pipe wall, or from both sides so the middle of the wall has the highest crystallinity (Peacock, 2000; Plastics Pipe Institute, 2007). The residual stresses formed due to cooling cause compression on the outer side and tension on the inner side of the pipe wall (Sandilands and Bowman, 1986).

Schouwenaars et al. (2007) measured the tensile properties of specimens cut out from external, central, and internal parts of HDPE tubes of various sizes (see Figure 2.12). In the case of the 40mm tube, cooling was applied from both sides of the pipe wall, therefore the UTS and E distribution through the pipe wall is symmetrical.
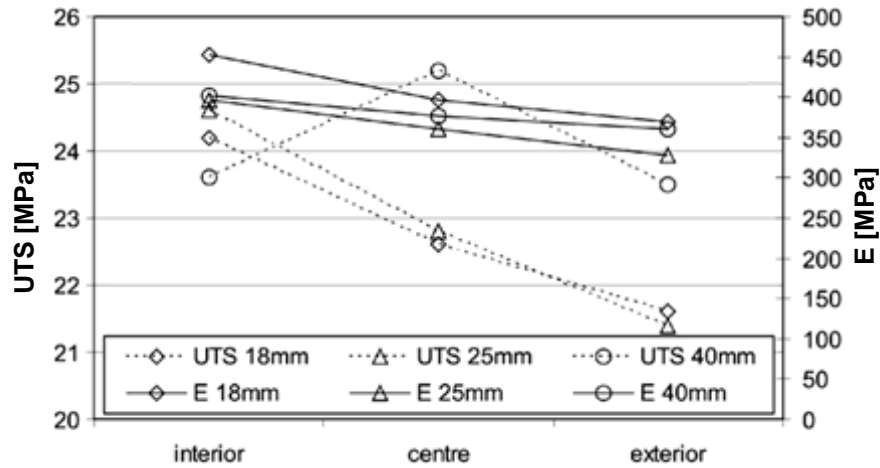
Figure 2.12 UTS and Young's modulus of HDPE samples taken at different positions in tubes of different wall thickness (Schouwenaars et al., 2007).

The variations associated with the molecular structure of polyethylene can change the failure time of a pipe due to crack growth by a factor of 10^4, while the processing conditions (residual stresses due to cooling, etc.) can change it only by a factor of 2, which is insignificant (Lu et al., 1994).

Polymer properties can be improved by different types of additives added to the material in the polymerization process or during manufacturing. Their names are connected with the functions they fulfil. Among the common additives are heat stabilizers preventing depolymerisation, antioxidants, UV protection agents, flame retardants, colorants, plasticizers reducing the viscosity and stiffness, and modifiers improving a specific property (e.g. impact resistance) (Farshad, 2006).

The molecular structure and physical properties of materials determine how they react and deform when a force is applied. Therefore, the response typical for most materials is further introduced and then the behaviour characteristic for polyethylene is studied.

2.2.4   Deformation due to the applied load

2.2.4.1 Typical stress-strain response of materials

The stress-strain behaviour (material deformation) is best characterized in tension and the degree of deformation depends on the magnitude of an imposed stress. At low stress levels the strain is directly proportional to the stress for most materials what was first observed by Hooke in 1678 and termed Hooke's law (Kurrer, 2008). It was, for example, described by Callister (2007) amongst others and is shown in Equation 2.1.

$$= E \cdot \qquad\qquad \textbf{2.1}$$

where: σ – tensile stress (axial force F per unit area), N/m² (Pa)

E – Young's (tensile, elastic) modulus, N/m² (Pa)

ε – axial strain as dimensionless ratio of the sample elongation to its original length

The greater the Young's modulus the stiffer the material. In the case of anisotropic materials, e.g. single crystals like silicon, the Young's modulus varies depending on the crystallographic direction in which measurements are taken (Callister, 2007).

Elastic deformation is non-permanent, i.e. when the applied load is released, the material returns to its original shape. For larger strains most materials exhibit plastic behaviour (permanent deformation).

The moment at which the plastic deformation begins, marked in Figure 2.13, is called the yield point. Most structures are designed to ensure that no plastic deformation will occur i.e. the yield stress will not be exceeded.

The stress-strain curve is usually plotted for the engineering stress (or just stress) obtained as the measured force to the initial sample cross-section (Peacock, 2000). In practice, the cross-section usually reduces as the sample elongates (Figure 2.14a). The stress, which considers the change in the sample cross-section, is called nominal stress and the degree of contraction is a characteristic of material called Poisson's ratio. It was discovered by Poisson in the first half of the 19th century (Kurrer, 2008) and is expressed by Equation 2.2 (Mitchell, 2004).
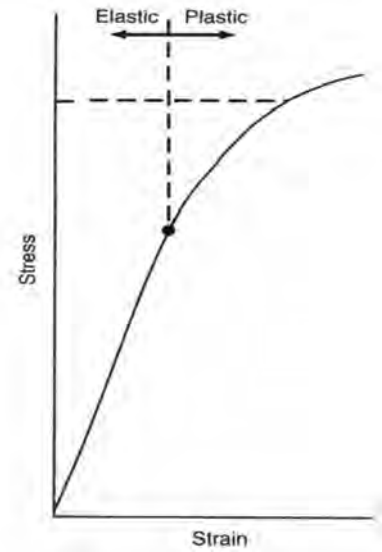
Figure 2.13 Stress-strain curve for silicon (Gad-el-Hak, 2002).

$$= -\frac{\varepsilon_l}{\varepsilon}$$

2.2

where: ν – Poisson's ratio

ε_l – lateral strain as dimensionless ratio of the diameter reduction (contraction) to the initial sample diameter, $(D_0 - D)/D_0$

ε – axial strain as a dimensionless ratio of sample elongation to its original length, $(l_0 - l)/l_0$

Apart from tension, the stress can also be applied in other modes such as compression (Figure 2.14b), shear (Figure 2.14c), torque (Figure 2.14d), or combinations thereof (e.g. in bending), which can also evoke elastic and plastic behaviour. The compressive modulus (also called the bulk modulus) is expressed as (Mitchell, 2004):

$$\sigma_{com} = K \cdot (V / V_0)$$

2.3

where: σ_{com} – compressive stress, N/m² (Pa)

K – compressive modulus, N/m² (Pa)

V/V_0 – relative change in volume, where V_0 is the initial value and V is the final value

20

The compressive modulus and elastic modulus are related through Poisson's ratio (Mitchell, 2004):

$$K = \frac{E}{3(1-2\nu)}$$

2.4

As for most materials Poisson's ratio is constant within the elastic range, usually between 0.25 and 0.35, always smaller than 0.5 (which indicates no change in volume), the stress-strain characteristics at low stress levels are the same for both tensile and compressive situations, i.e. $K \approx E$ (Callister, 2007).

In the bending mode the external fibres of the sample are subject to tension while the internal to compression. Flexural modulus is also determined within the elastic region of the stress-strain curve.

The shear stress-strain relationship is also linear for low stresses as expressed in Equation 2.5 (Callister, 2007).

$$\tau = G \cdot \gamma$$

2.5

where: τ – shear stress, N/m² (Pa)

G – elastic shear modulus (modulus of rigidity), N/m² (Pa)

γ – shear strain equal to tanθ (where θ is the shear angle as illustrated in Figure 2.14c)

For isotropic materials shear (G) and elastic moduli (E) are related to each other and to Poisson's ratio (ν) through Equation 2.6 (Callister, 2007).

$$G = \frac{E}{2(1+\nu)}$$

2.6

21

Torsion is a variation of pure shear where a sample is twisted. In this stress mode a shear stress is a function of the applied torque and shear strain is related to the angle of twist (φ) (Callister, 2007).

Figure 2.14 Schematic representation sample deformation in (a) tension, (b) compression, (c) shear, (d) torsion. Dashed lines represent the shape before deformation; solid lines, after deformation; A_0 – initial area, D_0 – initial diameter, l_0 – initial length, l – extension, F – force, T – torque, θ – shear angle and φ – angle of twist (Callister, 2007).

All these parameters and relationships are valid for most materials. The next section focuses on the deformation behaviour characteristic for polyethylene associated with its molecular structure.

2.2.4.2 Deformation of polyethylene

The deformation behaviour of polyethylene depends on the stress mode, speed and magnitude of the applied load. It involves rearrangement of the molecules and change in the morphology, which is elastic (recoverable) at low stress levels. It can proceed in a ductile mode (involving plastic deformation) and brittle mode (rapid fracture without plastic deformation).

The extent and speed of deformation of polymers depend on many factors such as strain rate, temperature, and chemical nature of the environment (the presence of water or organic solvents). Increasing the rate of deformation and decreasing the temperature have the same

influence on the polyethylene performance as an increase in crystallinity (and density). When taken to extremes, a rapid application of strain or very low temperature can convert an otherwise ductile sample into a brittle one so it fractures without previous deformation. The brittle failure is not preferred as it is usually rapid, thus difficult to prevent and often catastrophic (Callister, 2007). Other factors promoting brittle failure are increasing the specimen thickness and/or presence of notches and flaws, etc. The defects (deliberate or non-deliberate) cause stress concentration initiating cracks. The stress is amplified at the crack tips leading to crack propagation and accelerated failure (Callister, 2007).

One of the most common stress modes investigated for polyethylene is tension, which delivers a lot of information on material properties and deformation mechanism (Peacock, 2000). The shape of the stress-strain curve with marked characteristic stages obtained in the tensile test presented in Figure 2.15 reflects the complexity of the deformation process. Figure 2.16 illustrates the rearrangement of polyethylene molecules in tension.

Within the elastic region (Figure 2.15) the deformation is elastic and homogenous. The tie chains in the amorphous regions elongate in the direction of the applied stress (Figure 2.16, Stage 1) (Callister, 2007). The elastic modulus is approximately proportional to the degree of crystallinity as it requires more stress to elongate the sample with less amorphous regions (and thus less tie chains) to the same degree (Peacock, 2000).

The yield point, which is the first maximum in the stress-strain curve (Figure 2.15), initiates heterogeneous and plastic deformation (necking). The yield stress also increases with increasing crystallinity.

During the necking stage the neck narrows down as the adjacent chains in the lamellae slide past one another causing tilting of the lamellae so that the chain folds become more orientated with the tensile axis (Figure 2.16, Stage 2) (Callister, 2007).

Further, in the cold drawing stage (plateau) the neck propagates along the sample (Figure 2.15). Crystalline block segments separate from the lamellae but remain attached to one another by the tie chains (Figure 2.16, Stage 3).

Then the blocks and tie chains become orientated in the direction of the tensile axis forming microfibrils (micronecking) (Figure 2.16, Stage 4), which are very strong and stable due to many tie molecules connecting the lamellae (Callister, 2007). The tie molecules partially unfold and become taut, which increases their length and the distance between the blocks (Meinel & Peterlin, 1971).

The stress is sustained by the taut tie chains. If their concentration is insufficient to sustain the stress required to destroy the crystallites (plastic deformation), they break prior to ductile yielding and the failure is brittle. The stress required to destroy the crystallites is proportional to their volume, thus material crystallinity. Therefore, the tie chains concentration should be sufficient for a specific degree of crystallinity to ensure ductile failure. Thus, both, a high MW increasing the concentration of tie chains, and chain branching decreasing the degree of crystallinity reduce the possibility of brittle failure (Meinel & Peterlin, 1971; Peacock, 2000).

The strain at the end of the plateau is termed the natural draw ratio (Figure 2.15). In the subsequent strain hardening stage the neck and the fibrous material deform uniformly until the sample breaks (Callister, 2007), which is associated with chain slippage and fracture (Peterlin, 1971).

The entanglements and branches associated with a high MW limit the slippage of chains past one another and thus limit elongation. Thus samples with a low MW rather reach higher tensile strength, even though the higher MW sample may require a greater force to break it (Callister, 2007).
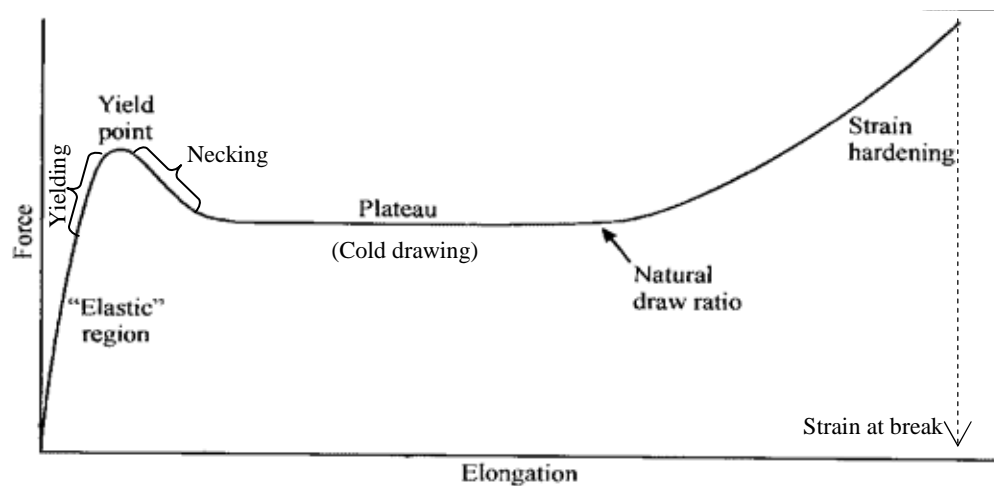
Figure 2.15 Typical force versus elongation curve for polyethylene with the key stages marked after Peacock (2000) and Powell (1983).
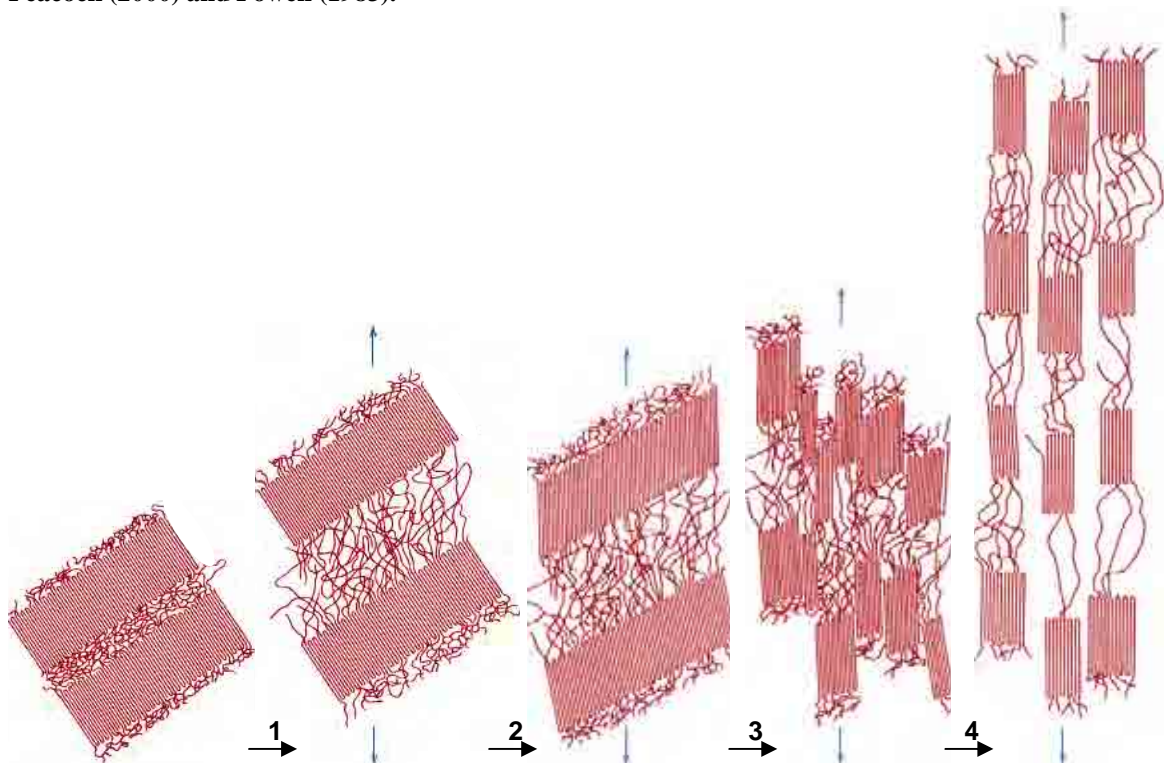
Figure 2.16 Stages in the deformation of a semicrystalline polymer (Callister, 2007). Note: individual pictures and stages explained in the main text.

The compressive, shear, and flexural properties of polyethylene are controlled by the same morphological characteristics that control the tensile properties.

So far it was shown that the deformation mechanisms for polyethylene are very different to typical engineering materials such as steel or concrete. Therefore, the fracture properties of polyethylene associated with a rapid application of tensile or flexural stresses leading to formation of new surfaces are investigated further.

2.2.4.3 Fracture of polyethylene

The fracture strength of polymers is lower than of metals and ceramics. It is a measure of polymer toughness and is normally determined in the impact test where the crack is often induced by a deliberately introduced notch and propagates perpendicularly to the direction of the applied stress. The fracture of polyethylene involves two processes that absorb energy, the inelastic deformation and the formation of a new surface area, and can also be in a ductile and brittle mode (Peacock, 2000).

In the ductile failure the crack formation is followed by crazing and plastic yielding prior to fracture. Crazes lead to the formation of small microvoids connected by fibrillar bridges leading to the orientation of the chains (Figure 2.17a). Stretched fibrillar bridges elongate and break so the microvoids grow and coalesce turning into cracks leading to ultimate material fracture (Figure 2.17b) (Callister, 2007). The type of fracture can be distinguished on the basis of stress-strain curves and on the basis of microscopic observation of the fractured surface (fractographic examination). The brittle failure usually results in a flat fracture surface.

(a)   (b)
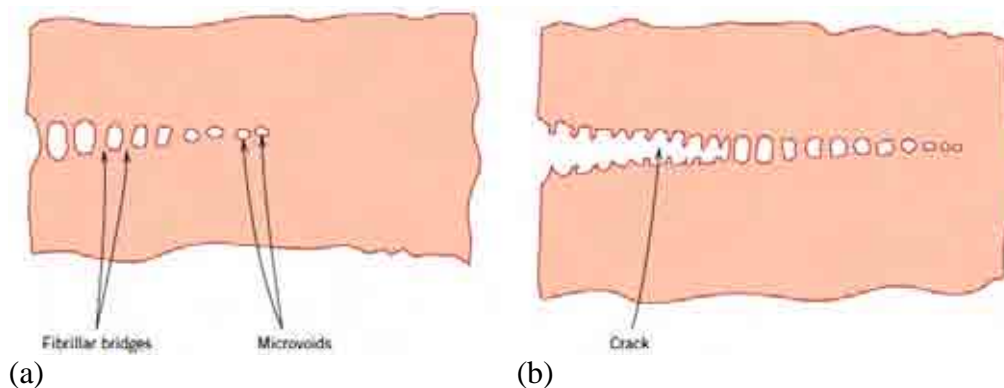
Figure 2.17 Schematic of (a) a craze showing microvoids and fibrillar bridges, and (b) a craze followed by a crack (Hearle, 1982).

The polyethylene high speed fracture is controlled by the same factors as low stress brittle failure explained in the previous section. High concentration of tie chains and low crystallinity ensure high impact resistance (Channel & Clutton, 1992).

As the method of testing and the sample geometry have a great influence on the results and failure mode, especially in impact, the fracture strengths of polymers are quoted in terms of the energy required to break a sample of standard dimensions under specific standardized testing conditions (e.g. Charpy impact). The same applies to the tear strength, which is an energy required to tear a film using a standard test configuration. The materials can be compared if tested under identical conditions (Peacock, 2000).

Due to viscoelasticity of polyethylene it behaves differently if the load is applied for a prolonged time. The viscoelasticity phenomenon and the long term properties of polyethylene and introduced in the next section.

2.2.4.4 Long term mechanical properties of polyethylene associated with its viscoelasticity

The polymers in a molten state at the highest temperatures exhibit viscous liquid-like behaviour, while below the melting temperature they are viscoelastic combining the mechanical characteristics of an elastic solid and a viscous liquid (Mitchell, 2004).

27

The elastic behaviour follows Hook's law, which was explained in section 2.2.4.1. It can be symbolized by the spring stiffness E illustrated in Figure 2.18a. In the viscous behaviour the strain depends on the time for which the stress (load) is applied and it remains constant after the stress (load) is removed illustrated by a dashpot of viscosity η in Figure 2.18b. It was discovered by Newton (1643-1773) and is termed Newton's law of viscosity expressed as (Mitchell, 2004):

$$\tau = \eta \frac{d\gamma}{dt} \qquad\qquad 2.7$$

where: τ – shear stress, Pa

η – viscosity, Pa·s

γ – shear strain, m

t – time, s
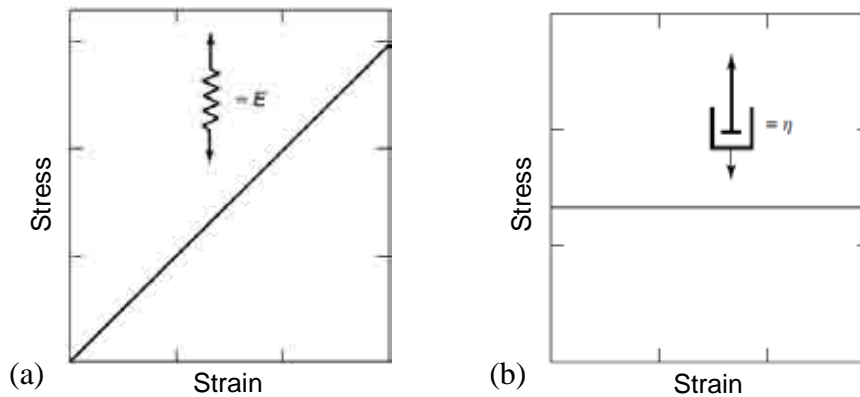
(a)   Strain   (b)   Strain

Figure 2.18 Stress–strain behaviour of (a) spring with stiffness E and (b) dashpot of viscosity η after Cowie (1991).

Molten polyethylene is extremely viscous, up to many orders of magnitude more than water; however, it displays certain elastic properties and therefore is termed a viscoelastic liquid. A viscoelastic liquid can be distinguished from a viscoelastic solid in that, under the application of a constant force, the liquid deforms indefinitely, whereas the deformation of a solid is

limited. The viscosity and extent of elastic recovery are functions of the entanglement of the molecules. (Peacock, 2000).

Due to the viscoelasticity and morphological instability of polyethylene the application of prolonged stress (even much lower than that required to cause instantaneous yielding) results in a gradual rearrangement of the molecules either on a local basis, as in the case of brittle failure and stress cracking, or throughout a large portion of the sample, as in creep and stress relaxation. The low stress brittle failure and cracking are often initiated by deliberate or non-deliberate defects, which act as stress concentrators (Peacock, 2000).

Creep means that the imposition of a constant load results in an instantaneous elastic strain, which is followed by a viscous, time-dependent strain. The time dependent creep modulus is expressed as (Callister, 2007):

$$E_c(t) = \frac{\sigma_0}{\varepsilon(t)} \qquad \textbf{2.8}$$

where: $E_c(t)$ – time dependent creep modulus, Pa

σ_0 – stress maintained constant, Pa

$\varepsilon(t)$ – time dependent strain

Sometimes creep is expressed as creep compliance, $J_c(t)$, which is a reciprocal of the creep modulus.

In Figure 2.19 the creep response is explained on the basis of combined Maxwell and Kelvin models, which is one of the approaches of explaining viscoelastic behaviour (Peacock, 2000).
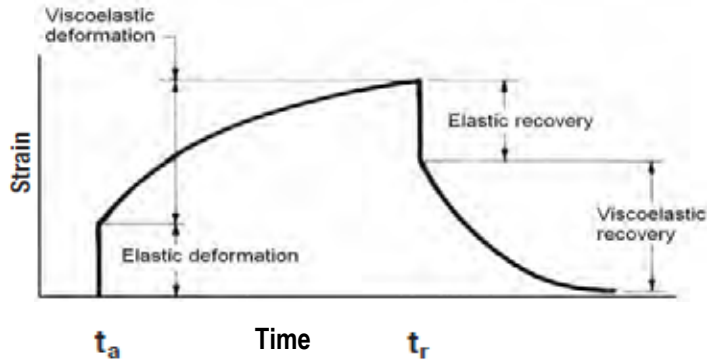
Figure 2.19 Strain versus time response to the constant load applied instantaneously at time t_a and released at time t_r for viscoelastic behaviour after Callister (2007) and Crawford (1987).

In the viscoelastic behaviour the imposition of stress results in an instantaneous elastic deformation followed by a gradual viscoelastic deformation (Figure 2.19c). After the load is released, first the immediate elastic recovery occurs followed by viscoelastic recovery. The sample does not recover completely due to some plastic deformation (Callister, 2007; Crawford, 1987).

Relaxation is a decrease in stress at a constant strain. The stress gradually decreases (relaxes) with time due to molecular relaxation processes that take place within the polymer. Thus, after the load is removed, only part of the strain disappears. The longer the load is applied, the more permanent the strain is. The time-dependent relaxation modulus is expressed as (Callister, 2007):

$$E_r(t) = \frac{\sigma(t)}{\varepsilon_0}$$

2.9

where: $E_r(t)$ – time dependent relaxation modulus, Pa

$\sigma(t)$ – time dependent stress, Pa

ε_0 – strain, maintained constant

Susceptibility to creep and relaxation decreases as the degree of crystallinity increases. The enhanced temperature or presence of some organic solvents lower the creep and relaxation

modulus, thus accelerate polymer ageing and failure, which is often brittle in a hostile environment (Callister, 2007). High density polyethylene is relatively resistant to such environmental stress cracking due to its molecular structure and high crystallinity (Peacock, 2000).

2.2.4.5 Failure due to cyclic loading

Polymers may also experience fatigue failure under conditions of cyclic loading. It follows the same general trend as low stress brittle failure; however, it proceeds at a faster rate as a function of total time under load. Additional factors influencing fatigue failure are the frequency of loading, relaxation time, and the waveform of the applied stress (Peacock, 2000). The fatigue lifetime of some materials, e.g. some polyethylene grades, often exceeds 10^6 cycles, thus the test is very time consuming and requires specialized equipment (Khelif et al., 2008). Cycling polymers at high frequencies and/or relatively large stresses can also cause localized heating and as a result the failure may be due to the softening of the material rather than due to typical fatigue processes (Callister, 2007).

In order to predict the lifetime of a component subject to constant strain, stress or cyclic loading the creep, relaxation or fatigue curves are constructed on the basis of data from many different tests and the desired values are extrapolated.

The tests can be carried out in different environments, e.g. at elevated temperatures, under UV light and/or in chemicals, simulating the operating conditions or deliberately accelerating the failure to obtain the data quicker from which further values are extrapolated (Kukureka, 1989; Peacock, 2000). However, the conversion of the data obtained in the environment accelerating aging is complicated and sometimes gives wrong results (Hoàng & Lowe, 2008; Whelton & Dietrich, 2009).

2.2.4.6 Failure and tests of the structures

So far the focus has been on testing using small samples in the laboratory in order to investigate the behaviour of structures. However, in some cases tests on the whole structure are required not only in specific environments but also in the stress modes similar to those in which they operate. This is the case for plastic water pipes. For operational purposes a specific pipe has to sustain a specific pressure for a specific period of time, so the hydrostatic strength is tested via the application of internal water pressure to a piece of pipe. The time to failure under pressure is another important parameter. As these tests could take a long time, the material ageing can be accelerated in the tests at an enhanced temperature of 80ºC. The 50 year hydrostatic strength at 20ºC is a key parameter to estimate the strength of the pipe and can be extrapolated from the obtained results (BSI, 2003a; UK Water Industry, 2001).

The short term surge pressure expresses the resistance of the pipe to dynamic loading (experienced e.g. during water hammer) and is measured via increasing the pressure in the pipe at a specific rate until failure. As cracks within pipes are a common source of their failure (Schouwenaars et al., 2007), the long term stress crack resistance is often measured for a notched pressurised pipe at 80ºC. Resistance to rapid crack propagation is another important property investigated as this can cause a catastrophic failure (BSI, 2003a; UK Water Industry, 2001). However, the modern PE100 pipes are very resistant to slow or rapid crack propagation, thus the failure times measured at 20ºC reach between 70 and 1000+ years (Bowman, 2008).

In the tests, the pipes filled with water are placed in air, water or another liquid, while in practice they are surrounded by soil, so the stresses are unevenly spread and partly balance the hoop stress due to water pressure giving the total maximum value at the inner wall, on the top and bottom of the pipe (Schouwenaars et al., 2007). In practice, not only the operation

conditions but also the loading modes are usually more complex including fatigue and/or bending (due to loading from traffic and/or point loads) (Farshad, 2006). Therefore, in some cases non-standard pipe field tests are additionally carried out. Analyses of the pipes which failed in service are also useful for material justification (Greig et al., 1992).

The tests of connections (joints) between structures are another important field of study as they are often the weakest part of the system (Zhao et al., 2002). The pipe joints are usually tested in similar pressure tests as the whole pipe sections and in the tensile test, where the joint strength is determined (UK Water Industry, 2008).

As indicated, the holes and other defects within structures are the sources of stress concentration and accelerate development of cracks and failure. Therefore, their influence on materials, especially polyethylene, is studied in more detail.

2.3 Inclusions and holes in the matrix

The integrity of a polyethylene matrix depends on the matrix material itself as well as any deliberate or non-deliberate inclusions or holes. If the inclusions are deliberate such as solid fillers the materials are called composites. The role of fillers is to improve mostly the mechanical, magnetic, and/or processing properties of materials, which are utilized especially in the construction, transportation and automotive industries (Xanthos, 2010). Further types of inclusions are sensors, which measure the properties of the matrix. An example are sensors placed in narrow holes in aircraft composite structures to detect potential damage (Kousourakis et al., 2008). The inclusion can also be the main part of the structure, i.e. in the situation when the matrix serves as an encapsulant protecting the main rigid component from applied loads and the surrounding environments, which is utilized in the automotive,

aerospace, and electronic industries, e.g. for microelectronic chip packages (Reedy & Guess, 2001).

Inclusions can also be non-deliberate and are considered as defects accidentally introduced into the object. This usually happens during production or field assembly of the product, e.g. pipes. Schouwenaars et al. (2007), who studied fractured surfaces of HDPE pipes, found retained HDPE pellets (Figure 2.20a) and calcium and iron containing crystals (deposited from water) (Figure 2.20b). Bowman et al. (1984) tested off-the-shelf polyethylene pipes and also recognized iron based flaws (Figure 2.20c) (probably from wear and damage to the manufacturing equipment) and calcium based flaws (from additives) (Figure 2.20d). Wu et al. (2001) additionally found gel particles in the tested HDPE pipes.
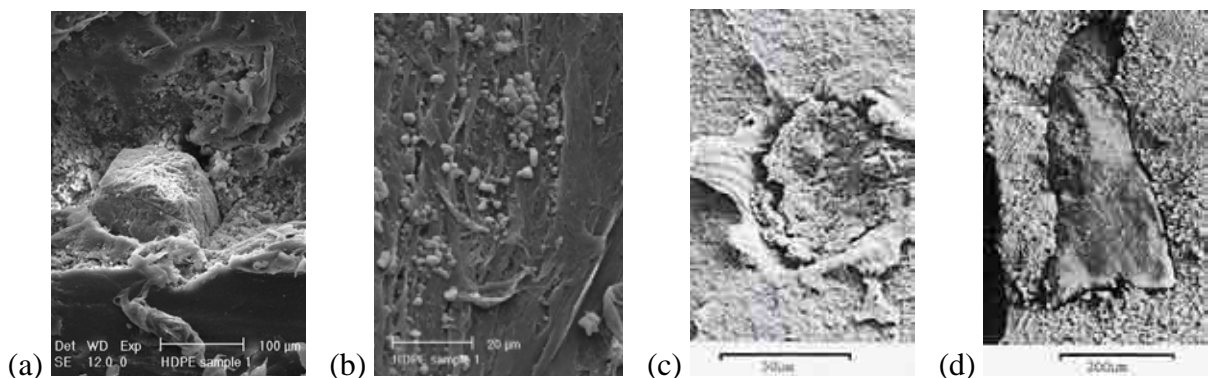
Figure 2.20 Different types of defects as sources of cracks found in polyethylene pipes by (a, b) Schouwenaars et al. (2007) and (c, d) Bowman et al. (1984).

The introduction of the defects during assembly is a significant problem especially during the fusion jointing process of pipes done on side. The defects such as dust, oil and water can attach themselves to the hot plate or to the weld directly and be frozen within the structure (Marshall, 1991; Troughton, 2001).

A hole within the matrix can have a similar effect as a rigid inclusion, which does not adhere to the matrix. Holes and cracks are usually non-deliberate, often formed during processing (voids, local thermal degradation of material) (Lang et al., 1997) and/or handling and

34

installation of the structure (American Society of Metals, 2003). As plastics are relatively soft (Xiang et al., 2001), when laying pipes in a trench these can be subject to scratches on the surface due to friction between the pipe wall and improper filling material in a trench or some random stones and other sharp object (Farshad, 2006; Madryas et al., 2002).

There was a lot of research done on materials with inclusions and defects, and various parameters were determined to influence the integrity of the structure. They are discussed in the next sections, although, first the fillers and the methods of composite manufacturing are introduced.

2.3.1 Fillers

Xanthos (2010) defines fillers as rigid particulate materials (inorganic and organic) of irregular, fibrous, plate-like or sphere-like shapes used usually in volumes greater than 5%. However, some fillers are soft, e.g. organic microspheres which are added to polymers and expand forming a foam and improve the thermal insulation, sound dampening and impact resistance (Jönsson, 2005). Beside various shapes they have various chemical composition, sizes, and inherent properties. They are usually immiscible with the matrix in both molten and solid states.

Examples of particulate fillers are talc and clay, wood flour or calcium carbonate ($CaCO_3$), fibres – glass, carbon and cellulose fibres, flakes – mica or glass flakes, and spheres – glass beads. The critical properties improved by mineral fillers are material stiffness and heat resistance.

Further, the ways of introducing fillers into the matrix are studied.

2.3.2 Manufacturing of composites

Fillers are incorporated into the matrix often in a standard polymer production process using batch or continuous (extrusion) equipment with some modifications depending on the product requirements.

For most composite applications extruders are used. The filler (often pre-treated for enhanced adhesion) is mixed within the matrix by the screws and extra pressure and shearing forces. Due to large forces applied during the melting of polymer, fillers can agglomerate causing wear of screws and barrels and also a non-uniform composition of the end product. Therefore, the dispersion and distribution of a filler illustrated schematically in Figure 2.21 controlled by the method of manufacture is important (McCrum et al., 1997). The uniform distribution and dispersion of the filler ensures uniform properties of the product. The agglomeration of the particles in one place can cause wakening of the structure. Agglomeration can be avoided by feeding the filler downstream after the polymer is fully melted (Xanthos, 2010).
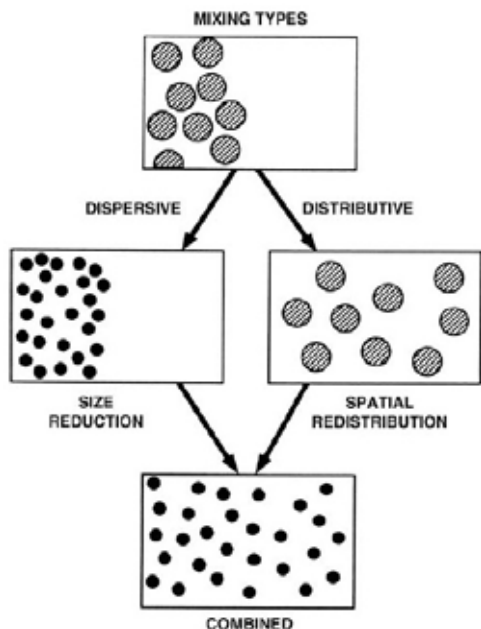
Figure 2.21 Dispersive and distributive mixing aspects (Paul et al., 2004).

When mixing the filler with the matrix air can be entrapped due to the high viscosity of polymer melts hindering dispersion of a filler and also causing a weakening of the structure, therefore venting of the composite is another significant stage (Xanthos, 2010).

The orientation of fibres or flakes in a composite influences its final properties, thus needs to be controlled. It is normally parallel to the flow direction in the case of composites produced in the extrusion process. It can also be controlled and modified in the injection and compression moulding. Kuelpmann et al. (2005) produced the HDPE composite sheets with mica flakes oriented parallel to the sample surface as illustrated in Figure 2.22 by repeated remelting of multiple thin layers of composite.
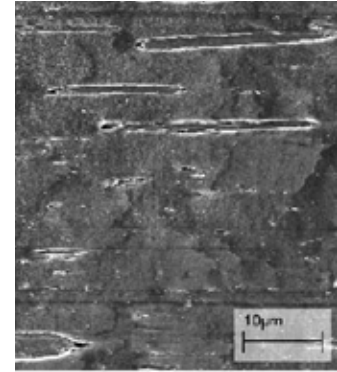
Figure 2.22 SEM micrograph of mica flakes composite (Kuelpmanna et al., 2005).

All industrial composite manufacturing processes are explained in detail and illustrated in the North American Mixing Forum's Handbook (Paul et al., 2004) and Plastics Compounding: Equipment and Processing book (Todd, 1998).

After discussing the manufacturing processes of composites, the parameters of the deliberate and non-deliberate inclusions or holes affecting the integrity of the structures are determined.

2.3.3   Parameters of the inclusions or holes influencing the mechanical performance of the structures

The researchers distinguished different parameters of the inclusions or holes controlling the morphology and properties of the polymer structures such as concentration, size, shape, orientation, rigidity, density, modulus, strength, and surface chemistry influencing the nature of interface between the filler and the matrix, which can be varied via special surface treatment. The matrix properties are also crucial. In the case of non-deliberate defects their

parameters are more random thus the investigation of some parameters and associated research is limited unless artificial flaws are introduced.

2.3.3.1 Concentration of inclusions or holes

The concentration of particles and associated distance between them determine how the stress is transferred from one to another (Piggott, 1980). The volumetric concentration of a typical filler ranges from 5 to 70% in highly orientated composites with long fibres. Other fillers constitute up to 30-40% of the composite (Raghupathi, 1990; Xanthos, 2010).

The effect of small particles uniformly distributed within the composite matrix, particularly with respect to their concentration, has been widely examined by researchers. Liang & Li (1998) and Liang (2007) who tested PP reinforced with glass beads (up to 20%) noticed that the stiffness and toughness improve with the addition of filler, however the material becomes more brittle. Yang et al. (2008) also observed improved stiffness with increasing filler content in the same type of composite for tested concentrations of 10-40% especially for the largest particles, while the toughness improved only for particles of diameter up to 10μm and dropped for greater particles. Similar observations were made by Majeed (2001) who tested glass flake reinforced MDPE. The Young's modulus (strength) increased and the strain at break (ductility) decreased with increasing filler content (up to 40%), while the toughness improved with the addition of 10% flakes and then dropped. Liang & Yang (2007) also noticed an increase in a reinforcing effect in HDPE with increasing mica flakes content (in the range of 0-15% by weight), which was linear for flexural modulus and strength. The strain at break increased for up to 5% filler content and then dropped, while the impact strength reduced with the addition of filler. In each introduced case the yield stress reduced, which is also in accordance with research of Lu et al. (1992) who tested glass bead filled HDPE. They also analysed the influence of particles on the long term properties and recorded an increase in

creep resistance with the addition of filler. Similar observations were made by Chevali et al. (2009) who studied the flexural creep characteristics of glass fibre composites based on PP and HDPE, and Hawley (1987) who investigated mica flakes as a polymer filler.

Different researchers tried to work out the equations, which allow the estimation of the mechanical parameters (mostly tensile) of a composite on the basis of the properties of the filler and the matrix, filler volumetric content, and other factors. Bigg (1987) collected and listed various equations in his paper, which assume uniform dispersion of a filler and some adhesion between the filler and the matrix. The very first developed by Einstein in 1906 applies to small filler concentrations (Bigg, 1987):

$$E_C = E_M(1 + 2.5V_F)$$
 2.10

where: E_C – modulus of the composite, MPa

E_M – modulus of the matrix, MPa

V_F – volume fraction of the filler

Nicolais and Narkis (1971) who studied the mechanism of stretching of a composite observed that fillers often induce yield points in the stress-strain curve and the yielding is due to crazing and dewetting (debonding) of the filler from the matrix. They deducted that the yielding or dewetting behaviour depends on the surface area of the filler and thus is a function of $V_F^{2/3}$, so the yield stress of a composite can be expressed as:

$$\sigma_{yC} = \sigma_{yM}(1 - V_F^{2/3})$$
 2.11

where: σ_{yC} – yield stress of the composite, MPa

σ_{yM} – yield stress of the matrix, MPa

V_F – volume fraction of the filler

Similarly the reduced strain at break is a consequence of debonding of the filler from the matrix and reduced volume of the matrix to sustain the load. It can be calculated as (Nielsen, 1974):

$$\varepsilon_C = \varepsilon_M (1 - V_F^{1/3})$$ **2.12**

where: ε_C – strain at break of the composite, MPa

ε_M – strain at break of the matrix, MPa

V_F – volume fraction of the filler

Majeed (2001) investigated the MDPE pipes reinforced with glass flakes and observed an improvement in the hoop strength for 10% concentration and a reduction for greater filler content, where in addition the failure was brittle. No other related work was found on the concentration effect of the defects within structures themselves; however, Schouwenaars et al. (2007) studied broken HDPE pipes and concluded that the more defects there are the more crack initiation sides there are.

Many equations also consider the orientation of the fillers in the case of fibres and flakes, which is another factor influencing the mechanical performance of a material and are discussed in the next section.

2.3.3.2 Orientation and location

Attempts have been made to model and predict orientation distributions in fibre and flake composites (Clegg & Collyer, 1986; Wang et al., 2008). For flakes and fibres the orientation during extrusion, injection moulding, or blow moulding is predominantly parallel to the flow direction, with a region of misalignment in the core (Xanthos, 2010). This can be modified by the variation of equipment and process parameters. Majeed (2001) observed that the

orientation of glass flakes in MDPE pipe becomes more random around the hoop direction with increasing concentration.

The research proved that the positive effect of reinforcement is especially noticed when there is a minimum misalignment of fibres or flakes from the direction of applied stress (longitudinal orientation) (Liang & Yang, 2007; Xanthos, 2010). Piggott (1980) claimed that the polymer uniformly and symmetrically reinforced with platelets at the longitudinal orientation (in the direction of the applied stress) obeys the 'rule of mixtures' for modulus, which is equal to:

$$E_1 = V_F E_F + V_M E_M \qquad\qquad \textbf{2.13}$$

where: E_{C1} – longitudinal modulus of the composite, MPa

$\qquad$ E_F – modulus of the filler, MPa

$\qquad$ V_M – volume fraction of the matrix

$\qquad$ V_F – volume fraction of the filler

$\qquad$ E_M – modulus of the matrix, MPa

While the filler arranged perpendicularly to the stress direction (transverse orientation) has little effect and the modulus is down to the matrix, thus the first part of Equation 2.13 referring to the filler is excluded (Piggott, 1980).

More equations were developed to calculate tensile and other mechanical parameters of the composite. They consider also other factors such as the aspect ratio (proportion of the greatest to the smallest dimension) of the filler and the interaction between the filler and the matrix, i.e. interfacial shear stress and adhesion and can be found among other in Bigg's (1987) paper and Piggott's (1980) and Xanthos' (2010) books.

In the impact stress mode the alignment of the fibres or platelets also matters. After Piggott (1980) when the crack front is normal to the reinforcement (Figure 2.23a), the propagation of the crack is inhibited by the soft matrix layers. When the crack front is parallel to the reinforcement (Figure 2.23b), the stress concentration is reduced due to separation of the layers and the crack is diverged.

In the case of the platelets (schematic in Figure 2.24) the extra pull-out and debonding work increases the amount of energy required to break the sample also improving the impact resistance (Nielsen, 1974; Piggott, 1980).

(a)

(b)
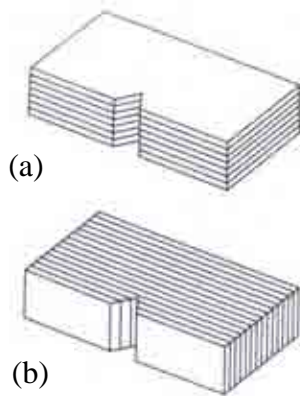
Figure 2.23 Alignment of the fibres in the impact test mode: (a) crack divider and (b) crack arrester (Piggott, 1980).

(a)   (b)
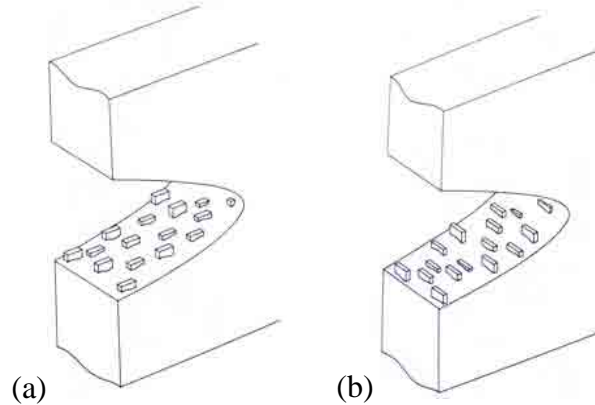
Figure 2.24 Alignment of the platelets (a) parallel and (b) across to the crack propagation direction (Piggott, 1980).

Kousourakis et al. (2008) who studied the influence of thin and long holes (galleries) designed for the health monitoring sensors for tensile and compressive properties of aerospace carbon/epoxy laminates also noticed that the longitudinal orientation is the best.

Not much relevant information on the orientation effect of the defects within polymer structures was found in the literature. Majeed (2001) recorded improvement in the hoop stress of glass flakes reinforced MDPE pipes for the flakes aligned around the hoop direction. Marshall et al. (1984) who studied mica reinforced polyethylene pipes observed that the

flakes, which initiated fracture, lay totally in the fracture plane always defined by the pipe axis and radial direction.

Concerning the most disadvantageous location of defects within structures Wu et al. (2001) and Schouwenaars et al. (2007) observed that most fractures were generated at the inner surface of the pipes probably due to higher residual stress and pressure in this region. In addition, the fracture always started in the central parts of the tubes away from welds, which seem to stop or mitigate the cracks. Sandilands & Bowman (1986) who produced polyethylene pipes with artificial flaws also noticed that the fracture initiated usually at the internal side of the pipe and occasionally in the centre of the wall in the case of larger defects. An example of a fractured pipe wall surface with initiating defects is shown in Figure 2.25.
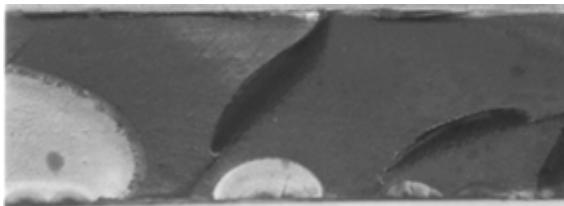
Figure 2.25 Fracture initiation sites on the inner wall of failed HDPE pipes (Schouwenaars et al., 2007).

As some studies on concentration effect indicated (e.g. Yang et al., 2008) the size is another factor influencing the mechanical properties of a composite and is discussed in the next section.

2.3.3.3 Size

The size of a standard filler does not exceed a few hundred micrometers. Exceptions are fibres, which can be longer. Liang & Li (1998), who looked at the size aspect in the PP reinforced with glass beads, observed that the tensile modulus reduces with increasing filler size. The same observations were made by Pukánszky (1990) who investigated combinations of various fillers and LDPE and PP matrix materials.

A big particle gives the same effect as particle agglomeration, which accelerates sample failure even though it may sometimes increase the modulus (Xanthos, 2010). This is due to the fact that after dewetting occurs, the larger the particle the larger the void/crack which forms around it (Nielsen, 1974). Jilkén et al. (1991) who tested PP reinforced with various mechanical fillers noticed that the high impact strength is obtained only for sufficiently fine fractions and reduces with increasing particle size.

However, the research of Lauke & Schüller (2002) on stress concentration around particles suggest that without considering the boundary conditions, the stress fields around the particle do not depend on its size, although, the volume of the matrix, which experiences the stress concentration, increases with particle size and it is more likely to find a large flaw within this vast region (Griffith, 1920; Nielsen, 1974).

When considering the boundary conditions, Durelli and Murray (1943), Durelli et al. (1966) and Williams (1984), who carried out the theoretical studies on holes within an elastic matrix, noticed that the smaller the distance between the hole and the specimen boundary the lower the stress the sample can sustain. Similar observations were made by Lauke & Schüller (2002) who stated that the load the bond can sustain depends highly on the ratio between the particle diameter and the cross-section of the sample, which again proves that the size of a sample is important.

In the bending mode different behaviour was observed by the researchers. Chen et al. (2006) who tested wood flour-HDPE composite noticed that the flexural strength and modulus increased with the size of particle and the highest was for sizes over 1.18mm. Yang et al. (2008) who tested glass bead filled PP at sizes up to 15μm and different contents also noticed a significant increase in flexural properties with increasing filler size, while the yield strength and impact strength were the highest for the smallest particles.

Kousourakis et al. (2008) determined the critical diameter of the galleries used in aerospace structures to be approximately 1-3mm for longitudinal and 0.3-0.7mm for transverse galleries. They also noticed that the galleries (even though filled with sensors) reduced the load bearing area of the matrix.

Extensive research on the size aspect of inclusions and holes within structures was carried out for polyethylene pipes, which normally fail due to cracks induced by flaws. Bowman et al. (1984) found various sizes of defects within the off-the-shelf HDPE pipes and observed that the pipe lifetime reduces with increasing filler size, thus, recommended to filter the melt to exclude large defects, which is current practice during pipe manufacturing (section 2.2.3.2).

Lu et al. (1994) also analysed defects within HDPE pipes and found the largest defect of 100μm, of irregular shape. Wu et al. (2001) studied two types of HDPE pipes produced in different ways and the size distribution of detected defects is shown in Figure 2.26.
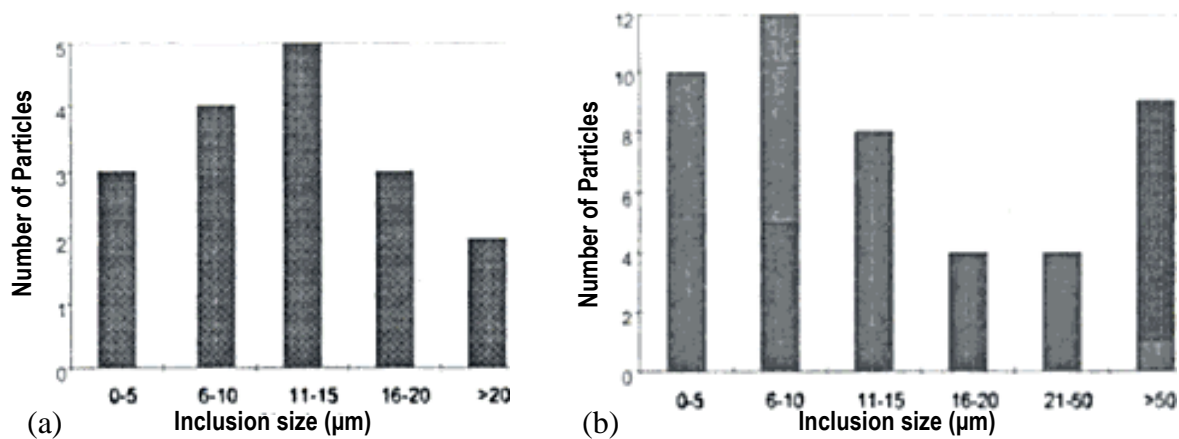
Figure 2.26 Size distribution of particles observed at fracture surfaces for pipes made of two different materials (Wu et al., 2001).

Surprisingly, the pipes with larger particles (Figure 2.26b) had a longer lifetime suggesting that other factors beside the defect size influence the mechanical performance of the structure (Wu et al., 2001). The size of the cracks generated by defects was also only slightly dependent on their size as indicated in Figure 2.27.
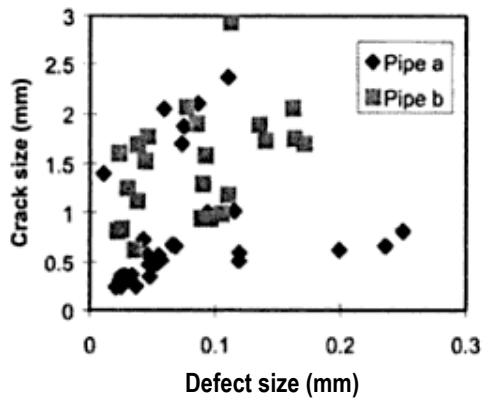
Figure 2.27 Defect size versus crack size (Wu et al., 2001).

Sandinals & Bowman (1986) produced different combinations of MDPE and HDPE pipes with artificial defects of different sizes. Aluminium particles (180-600μm) and glass spheres (100-200μm) were added at a maximum concentration of 0.5% by weight. Some pipes were produced via filtering the melt to 150 and 45μm. Figure 2.28 presents the data for some pipes.
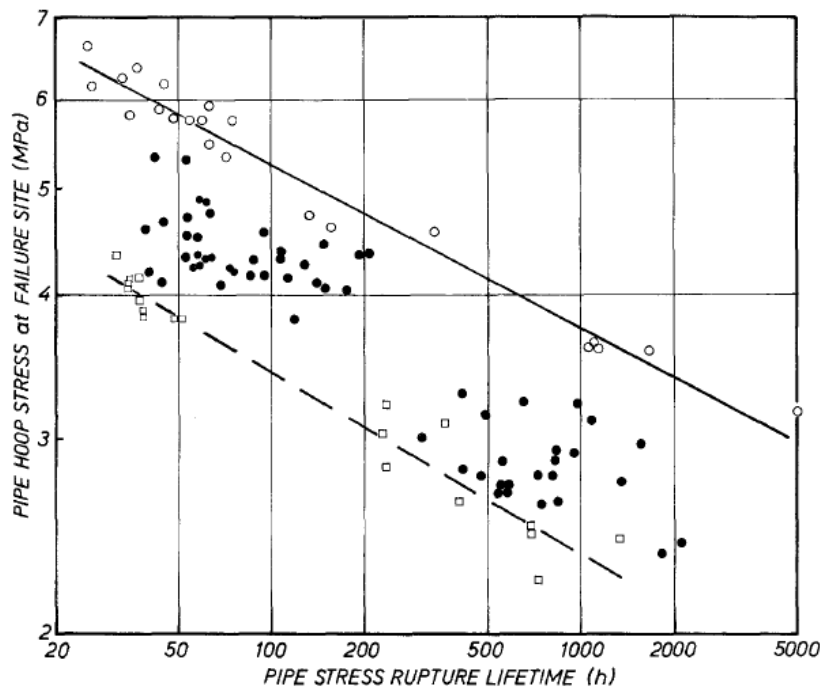
Figure 2.28 Stress rupture data for HDPE pipes: □ - with 180-212μm aluminium flaws, ● - filtered to 150μm, ○ - filtered to 45μm, tested at 79ºC (Sandilands & Bowman, 1986).

It was indicated that the 180-212μm aluminium particles reduced the pipe lifetime by a factor of twenty in comparison with the pipe extruded from the melt filtered to 45μm and the finest

filtered pipe was six times more durable than the weakest pipe filtered to 150μm. This research confirms that a pipe lifetime reduces with defect size and the bigger the size variation, the bigger the data scatter as in the case of HDPE pipes filtered to 150μm. They also found out that the stress rupture curve for one flaw size can allow the prediction of the behaviour for another size of flaw on the basis of Equation 2.14 (Bowman et al., 1984).

$$t_{SR} \cdot a^{[(B/2)-1]} = \text{constant}$$

2.14

where: t_{SR} – stress rupture time, hrs

a – sizes of flaw, μm

B – material constant associated with properties of the flaw

Some research was done on the defects within joints, which are a common problem, thus their impact on the structure needs to be known. Marshall (1991) introduced the defects of known sizes into MDPE SDR11 DN125, DN250 and DN355 pipes. Circular discs of diameters 0.5-8mm were produced from 20μm thick aluminium foil and placed in the weld after the removal of the heater plate. Tensile test samples were cut out and examined and the critical defect size causing embrittlement, which disqualifies the joint in accordance with UK Water Industry (2008), was determined. Figure 2.29 presents examples of ductile and brittle failure of the welds in a tensile test.

(a)   (b)
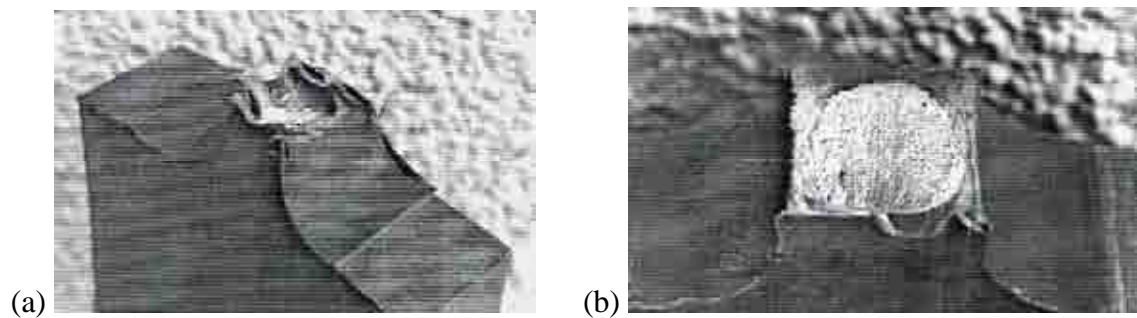
Figure 2.29 (a) Ductile and (b) brittle failure modes in polyethylene pipes (Marshall, 1991).

For DN125 pipes ductile failures occurred for inclusion size up to 6mm; for DN250 pipes the maximum size of defect was 3mm and for DN355 pipes it was 2mm. This means that the critical defect size (causing embrittlement) reduces with increasing wall thickness. This conclusion is in accordance with practical experience as the evaluation of service welds shows that thin-walled welded pipe sections seldom fail in a brittle manner.

In The Welding Institute (TWI) laboratories artificial defects were also introduced into PE100 pipe joints (Troughton, 2001). They included contamination such as talc particles ($< 45\mu$m) and graded natural silica sand (150-300μm), or planar discs of different sizes (1, 2, 3, 4 and 8mm) one or eight per joint as illustrated in Figure 2.30. The flaws were adhesively bonded to one end of the pipe at the mid-wall position after the trimming stage.

Figure 2.30 Location of planar flaws of different sizes (Troughton, 2001).

The optical analysis of the weld indicated that larger flaws broke during the welding process.

The acceptable size levels of contaminants were determined using a tensile creep rupture test of jointed 125mm pipes; however, due to the high cost of the test performance on pipes the specimens cut out from the pipes were examined for most 125 and 315mm welds according to BSI (2000). Examples of failed welds containing contaminants are shown in Figure 2.31.
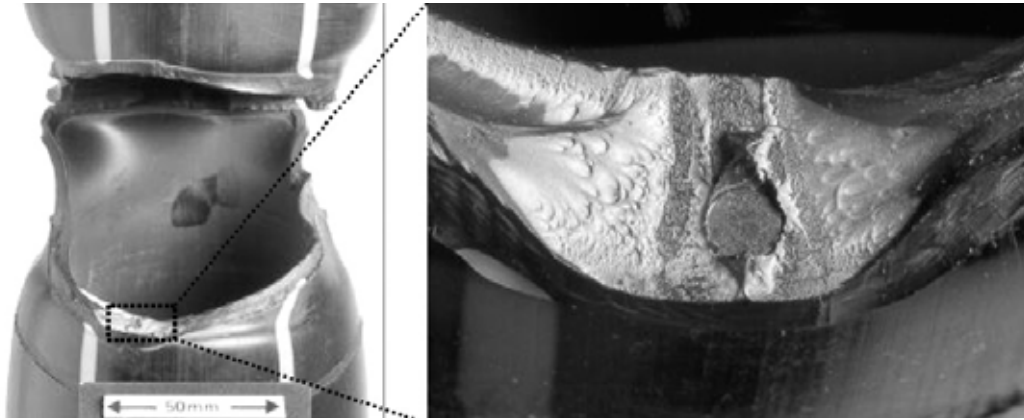
Figure 2.31 Photographs of a failed weld in 125mm pipe containing 4mm diameter planar flaw (Troughton, 2001).

Figure 2.32 presents the results of the tests on a logarithmic scale as time to failure vs. flaw size. The actual results are confidential.
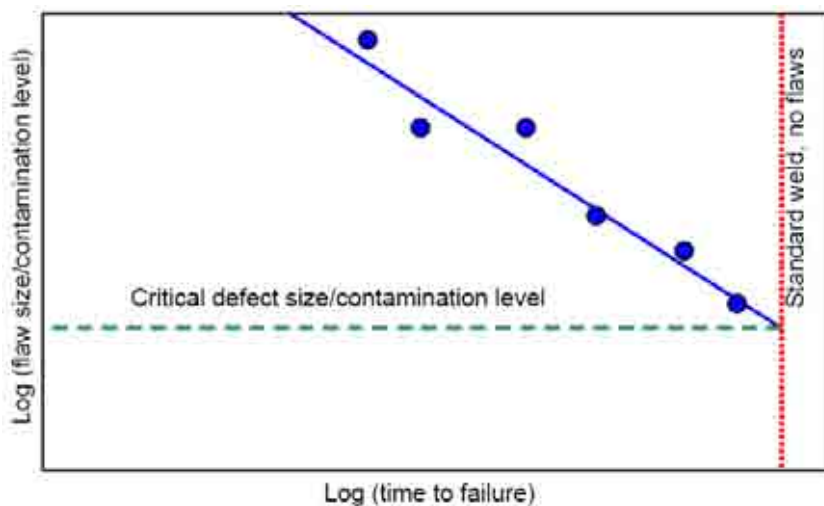
Figure 2.32 Time to failure vs. flaw size curve determined on the basis of test results (Troughton, 2001).

These analyses also confirmed that the time to failure reduced with increasing flaw size.

Another important parameter determined to influence the mechanical performance of the structures with inclusions or holes is their shape.

2.3.3.4 Shape

The shape of defects is rather random while in the case of fillers it is better controlled and chosen for particular composite applications. Maine & Shepherd (1974) who reviewed the

49

literature on reinforced plastics noticed that flakes and fibres are a more efficient reinforcement than spheres and the high aspect ratio is favoured (Xanthos, 2010). Pukánszky (1990) who investigated the effect of filler type/shape on tensile properties of reinforced LDPE and PP, made the same observations.

A high aspect ratio is also favoured in terms of the flexural strength and modulus as the research conducted by Lusis et al. (1973) on polymer/mica flakes composites indicated. Jilkén et al. (1991) who analysed various mineral-filled PP composites, also obtained higher modulus and strength values for high aspect ratio fillers like mica, while a very high impact strength, at high filler content, was obtained for low aspect ratio particulate fillers. Piggott (1980) assigns reduced impact strength due to inclusion of high aspect ratio fillers such as flakes or platelets to the sharp corners and irregularities, which cause stress concentration. Nielsen (1974) recognizes that additional stress concentrations might form due to air bubbles squeezed between the filler and the matrix.

Bowman et al. (1984) examined the influence of the filler shape on the lifetime of polyethylene pipes by adding near spherical, platelet and fibre particles. The 180-212μm globular aluminium particles and 180-220μm wide and 40μm thick mica platelets presented in Figure 2.33 were introduced in the pipe extrusion process. Figure 2.34 shows the results.

(a)   (b)
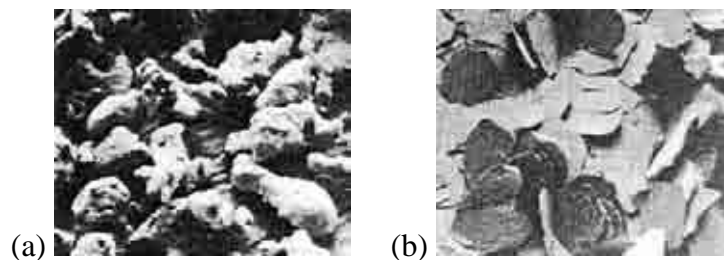
Figure 2.33 (a) Aluminium particles and (b) mica pellets of similar size (Bowman et al., 1984).
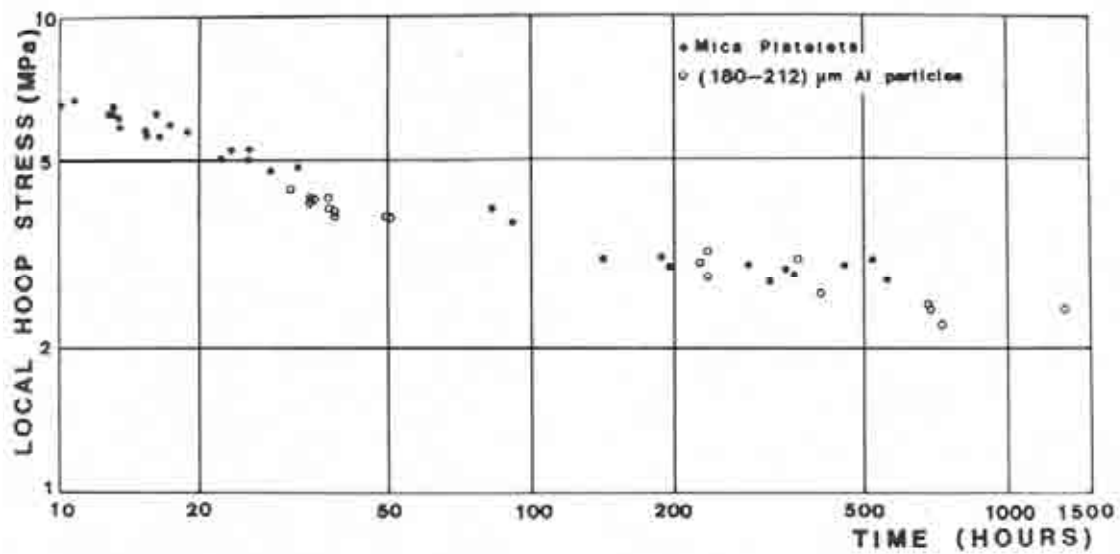
Figure 2.34 Comparison of stress rupture data between pipes containing mica and aluminium particles of the same size (Bowman et al., 1984).

There was no significant difference in the lifetime of pipes containing particles of similar size but different shape; however, no fracture was initiated by the glass beads, which suggests lower stress concentration imposed by these inclusions.

The lifetime of the reinforced pipe was similar to the lifetime of a pipe made of polymer filtered to 150μm. The reason for that might be the orientation of the inclusions usually in the pipe extrusion direction (as explained in 2.3.2) causing insignificant stress intensification (Bowman et al., 1984).

Even though here the shape of inclusions had no impact on pipe lifetime (Bowman et al., 1984), it influenced the performance of other polymer composites. It has an effect on the stress concentration around inclusions or holes, which is the highest at the corners (Feingold et al., 1972) and was widely studied by many researchers from a theoretical and practical point of view and is further analysed.

51

2.3.3.5 Stress concentration

A higher stress concentration accelerates the formation and propagation of cracks and thus, the final failure. It is expressed by the stress concentration factor (K), which is the relation between the local stress and the overall stress applied to the sample.

Most theoretical studies on the stress distribution around the inclusions or holes apply to the elastic behaviour of the matrix, the most common stress mode analysed is tension, and the most common shape investigated is a circle. Timoshenko & Goodier (1951) who did a 2D model of the stress distribution around a circular particle obtained the maximum $K \approx 3$ at the equator, which gives a different result than in the 3D model done by Lu et al. (1992) where the highest stress concentration was at the poles.

Savin (1961) calculated the modulus around the edges (M_θ) of a circular hole within a bent thin sheet. The results (relative moduli) are presented in Figure 2.35. The largest value of a moment is obtained at 90° (poles), $M_{90°} = 1.788M$, thus at this point the crack might initiate in the case of short or long term bending (creep test).

Figure 2.35 Bending moments (M_θ/M) along the contour of a circular hole in a plate when ν (Poisson's ratio explained in section 2.2.4.1) = 0.3 (Savin, 1961).

Some experimental studies were done on the composites with spherical particles in the tensile stress mode. Lu et al. (1992) determined the stress distribution in the glass bead filled HDPE and also noticed the highest stress concentration ($K \approx 2$) at the poles, where the crack tip forms, which was in accordance with their theoretical predictions. The value obtained by

Thibodeau & Wood (1938) experimentally and via the calculations for a hard circular inclusion within a soft-rubber sheet was $K \approx 1.5$.

Zhuk et al. (1992) who observed the crack propagation along the inclusion-matrix interface in PP, PE, and epoxy resin filled with glass beads under transmitted polarized light noticed that the debonding of the inclusion from the polymer matrix leads to an alteration of the local stress-strain distribution. The debonding stress depends on the size and shape of the inclusion, and on the adhesion between the filler and the matrix. Therefore, the adhesion is another important parameter influencing the mechanical performance of the samples with inclusions.

The shapes including corners were also studied by some researchers. Savin (1961) who calculated the stress concentration factors around different shapes of holes within an infinite elastic plate noticed that in the case of a rectangle at 30º towards the tension direction the value is four times larger than in the case of a circle. He also analysed, although less extensively, other shapes and stress modes.

Mirza & Ansari (1974) who analysed the stress distribution around square inclusions within a rigid plastic matrix utilizing the photoelasticity method found out that the highest stress concentration at the corners reaches a maximum (4.1) when the sides are oriented at 45º towards the tension direction in comparison with the orientation at 0º and 90º for which the lowest stress concentration (2.7) was obtained.

Some approaches to model the slow crack growth within polyethylene pipes were carried out, which is their most common failure mode and depends on the stress concentration imposed by the initial crack/notch as proven by Chan & Williams (1983). Chudnovsky & Shulkin (1999) tried to model the slow crack growth within polyethylene as dependent on the load, temperature and specimen dimensions, in tension. However, it has to be noted that the stress

analysis of a crack within polymer is very complex due to the non-linearity, time-dependency, material anisotropy and non-uniform stress distribution. To estimate the stress intensity for an elliptical crack emanating from surface defects it often has to be assumed that the material is linearly elastic, isotropic and homogeneous (Schouwenaars et al., 2007).

Anderson (2005) developed some complicated formulae to calculate the stress concentration imposed by a semi-elliptical crack within an infinite flat plate and thin walled tube under combined tension and bending. Schouwenaars et al. (2007) applied these formulas in his analysis of the failed pipes of a wall thickness of 40mm taking into account the additional hoop stress in the operating buried pipe. In Figure 2.36 the stress concentration factor (K) as a function of crack length is shown.
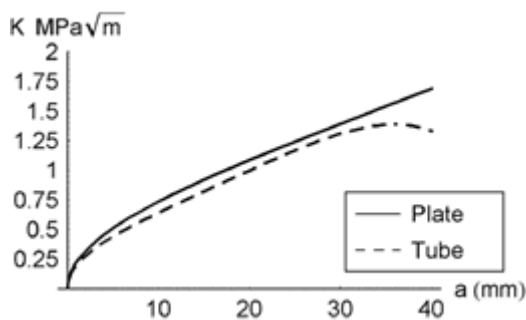
Figure 2.36 Stress intensity for a linearly elastic material with an elliptical crack of length 2c and penetration depth a (a/c = constant = 2/3), subject to bending and tensile stress (Schouwenaars et al., 2007).

Schouwenaars et al. (2007) indicated that the crack tip opening displacement and stress concentration increases till a critical point when it starts to blunt (Figure 2.36). After this critical stage the stress concentration drops and is too small to induce localized crazing. The crack stops to propagate locally and the general yielding starts.

Brown (2007) developed the Pennsylvania Edge-Notch Tensile Test (PENT) (ASTM, 2007a) on which basis the lifetime of a pipe associated with the slow crack growth can be determined from Equation 2.15 (Brown, 2007).

$$t(\text{pipe}) = 29 \pm 11 \cdot t(\text{PENT})$$

2.15

where: t(pipe) – failure lifetime of a pipe, hrs

t(PENT) – failure lifetime in a PENT test, hrs

The standard PENT test is carried out at 80ºC for a specific geometry of the samples made of the same resin as the pipe. However, as polyethylene is a complex non-linear viscoelastic material, stress intensities measured in one environmental and geometrical conditions cannot be directly transferred to other (Schouwenaars et al., 2007). Therefore, to obtain the accurate value of t(pipe) on the basis of t(PENT) the size of the largest defect (stress concentration) within the pipe and the operating temperature have to be known and the Williams' conversion theories applied (1984). The stress concentration due to an external notch is obtained from Equation 2.16 given by Rooke & Cartwright (1976).

$$K = \sigma_h Y (\pi\, a)^{1/2}$$

2.16

where: a – size of defect (flaw), mm

Y – geometric factor

σ_h – hoop stress, MPa

The more complex version of this equation considers the dimensions of the pipe. On the basis of Williams' (1984) equations the thinner the pipe wall and the larger the crack in relation to the pipe wall thickness, the larger the stress concentration.

Another important parameter influencing the mechanical performance of the structure with deliberate or non-deliberate inclusions is adhesion to the matrix.

2.3.3.6 Adhesion

Polyethylene is a non-polar material with low surface energy, thus it does not adhere to most materials. A non-polar molecule has symmetrically distributed electrons and therefore does not have an abundance of charges at the opposite sides (they all cancel each other out). In order to improve the adhesion its surface needs to be modified by breaking the molecular bonds leading to an increase of the surface tension (energy) (Huntsman Corporation, 2009).

In the case of deliberate fillers the interface can be improved by some additives. Silane coupling agents are frequently used for polyethylene or polypropylene reinforced with mica, glass or other fillers as they increase the polarity of the normally non-polar matrix (Borup & Weissenbach, 2010). They "form 'molecular bridges' to create strong, stable, water and chemical resistant bonds between two otherwise weakly bonded surfaces" (Borup & Weissenbach, 2010).

Marshal et al. (1985) who tested mica filled HDPE and Shucai et al. (1996) who tested mica filled PP observed that the reinforcing effect of a filler is better when there is good adhesion between the filler and the matrix. Adur & Flynn (1987) who tested wood flour reinforced plastics, observed that when adhesion is poor, the reinforcement can even reduce the tensile and flexural strengths of the composite.

Similar observations had Zhang & Tanner (2008) and Joseph at al. (2002) who investigated polyethylene reinforced with ceramic fillers (hydroxyapatite) of different surface roughness, shown in Figure 2.37. Stronger interfacial bonding resulted in higher (falling weight) impact strength of the composite. However, in their researches it was controlled by the surface morphology and the stronger bond was observed for the smooth filler surface. The reason for that is that during processing, the polymer matrix does not completely fill all the cavities on the rough surface (Figure 2.37a) due to the poor wettability of particles to polyethylene. Thus,

more voids or weak points are present in this composite leading to poorer adhesion and a weaker interface. During impact testing, the voids or weak points initiate the formation of cracks and the particles debond easily from the matrix and less plastic deformation occurs before fracture resulting in lower impact strength. While the smooth surface of other particles (Figure 2.37b) leads to increased contact between the two phases and some smooth particles are even still wrapped inside the polyethylene matrix after testing. As a result, more and larger matrix fibrils are pulled out during testing and resulting in more impact energy being absorbed.

Joseph et al. (2002) also stated that the larger plastic deformation of the composite with smooth particles is due to a larger amount of polymer matrix required to wet the surface and form an immobile layer on the rough particles during processing, hence less matrix is available for flow during deformation, resulting in less energy dissipation.

(a) (b)
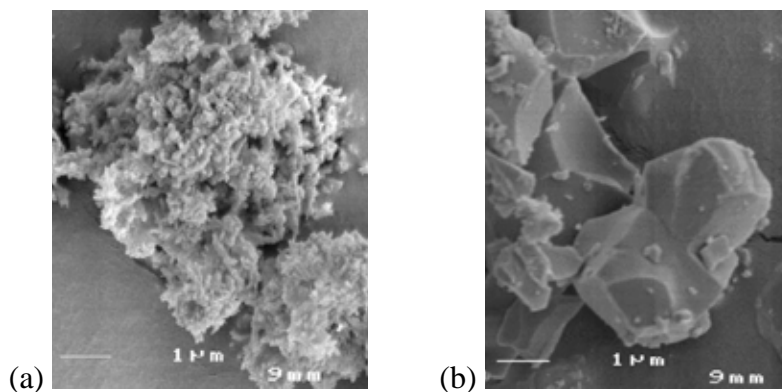
Figure 2.37 Scanning electron micrograph of (a) rough and (b) smooth hydroxyapatite particles (marker bar=1μm) (Joseph et al., 2002).

Different observations were made by Beaumont & Philips (1972) who discovered that the debonding, as a result of poor adhesion, makes the composite less sensitive to cracks and notches thus improves its toughness. The same was observed by Wypych (2000) in PP filled with calcium carbonate. After Bramuzzo et al. (1985) the debonding of mica in PP composite

usually leads to microductility ahead of the crack tip: the matrix pulls away from the filler and stretches, which improves the fracture toughness.

Similarly, Vu-Khanh & Fisa (1986) obtained a higher impact strength for the poor adhesion between mica flakes and polypropylene matrix. This might be due to the reasons explained by Friedrich & Karsch (1981) who claim that the stretching of the matrix requires much more energy than the formation of voids and cracking of the matrix-filler interface, thus fracture toughness of the matrix itself is higher than that of the composite.

Concerning the long term properties after Nielsen (1974) and Joseph et al. (2002) observed that good adhesion between the filler and the matrix reduces the creep rate with increasing filler content. Wu et al. (2001) who investigated the influence of defects on the pipe lifetime claim that this is because good adhesion lowers the stress concentration delaying the initiation of cracks. However, at high strains and loading times when debonding occurs and/or cracks develop, the creep rate may dramatically increase and the time to rupture decrease (Nielsen, 1974).

Better adhesion is ensured when the rigidity of the particle and the matrix are similar (Wu et al., 2001).

The last important parameter determining the behaviour of composites or structures with inclusions, holes or defects is the toughness of the matrix.

2.3.3.7 Toughness of the matrix

The toughness of the material is reflected in the susceptibility to crack growth (initiation and propagation), which can be induced by the inclusions or holes causing stress concentration (Lu et al., 1994).

Friedrich & Karsh (1981) who tested PP reinforced with particulate silicon discovered that the optimal concentration of the filler depends on the toughness of the matrix. In the case of highly crystalline polymer even a small amount of the filler (2.2%) weakened the material, while the toughness of more ductile polymer dropped for a concentration over 10%. The results obtained here are also in accordance with Nielsen (1974) who states that the composites with ductile matrix have a high impact strength due to the crazing mechanism.

Sandilands & Bowman (1986) introduced defects of known sizes into the polyethylene pipes with different fracture toughness and the longer lifetime (tougher) pipe grade resin showed a better resistance to failure caused by the included flaws. In addition, high toughness MDPE with particles in the size range of 250-600μm performed better than lower toughness HDPE pipe filtered to 150μm (Bowman et al., 1984).

Marshall (1991) observed that material toughness also influences the mechanical performance of pipe welds. Welds made of MDPE were classified as extremely tough while HDPE welds were more sensitive to contamination and induced embrittlement.

Further parameters influencing mechanical performance of composites and materials with inclusions are the same as for the plain polymer. This includes parameters associated with the testing environment, i.e. temperature and presence of chemicals, method and mode of testing, geometry of the samples and others as explained in section 2.2.4.2.

2.4 Summary and gaps

The focus in the literature review was on the composition and properties of materials, their deformation in different stress modes and methods of testing with the emphasis on polyethylene. Different methods of polyethylene production were introduced. The role and types of inclusions and holes within materials and structures were discussed and the up-to-date research on composites including manufacturing methods was summarised. Further, the parameters of inclusions and holes found to influence the integrity of the structures were discussed on the basis of available literature related to modelling, testing, and analysis of failed defected polyethylene structures, pipes and pipe joints. The key findings from the literature can be summarised as:

- It was demonstrated that polyethylene deforms very differently to typical engineering materials such as steel or concrete. In the tensile mode, after the yield point, there is a necking stage, followed by cold drawing and strain hardening all associated with large elongations. The ductility of polyethylene depends mostly on its molecular structure and to some extent on the processing conditions. Sometimes additives are used to improve a particular property of the product. These factors need to be taken into account when studying the mechanical properties of polyethylene.

- Several researchers have looked into the effects of inclusions on the structural integrity of polyethylene. The most common deliberate inclusions consist of glass fibres or beads, mica flakes, clays, talk, and calcium carbonate, and are inserted into the matrix during typical polymer manufacturing processes such as extrusion and injection or compression moulding, uniformly distributed at volumetric concentrations from 5 to 70%. Many researchers investigated the influence of different parameters on the final mechanical properties of the matrix. Their findings are summarized in a general form in Table 2.4.

Table 2.4 The dependency between parameters of the filler and mechanical properties of the polymer composite.

	Mechanical property of the composite				
	Strength (Young's modulus)	Stiffness (flexural modulus)	Ductility (elongation)	Toughness (impact resistance)	Creep resistance
Property of the filler	As the filler property increases, composite mechanical property:				
Concentration	Increases		Decreases	Increases or Decreases	Increases
Size	Decreases	Increases	Decreases	Decreases	Decreases
Aspect ratio	Increases	Increases	Decreases	Decreases	Decreases
Adhesion (between the filler and the matrix)	Increases	Increases	Increases or Decreases	Increases or Decreases	Increases

- It was shown that the orientation of the fillers such as fibres or flakes influences the properties of the structures. The best orientation with regards to the composite strength and impact toughness is in the direction of the applied stress, while the least reinforcing effect of the filler was observed for the orientation perpendicular to the stress direction (Piggott, 1980; Xanthos, 2010). The literature indicated that the toughness of the matrix is another parameter influencing the mechanical performance of the composite; the tougher the matrix, the less sensitive it is to the cracks and notches. In addition, the distance between the filler and the edge of the sample is important; the smaller the distance, the greater the stress concentration induced by the inclusion and the more brittle the sample.

- It was shown that the adhesion between the filler and the matrix is an important parameter characterising the composites and influencing their mechanical performance. Coupling agents have been proven to work for polyethylene containing mineral fillers.

- In the literature it was highlighted that sometimes tests on real scale structures in an environment simulating the operating conditions are required to get a better understanding of the large-scale behaviour. Some researchers investigated pipes with non-deliberate defects (e.g. Schouwenaars et al., 2007), others introduced inclusions into pipes (e.g. Majeed, 2001) and pipe joints (e.g. Troughton, 2001). Their findings supported the results shown in Table 2.4 on composites, although, fewer filler parameters and composite mechanical properties were investigated for these structures. In addition, Marshall (1991) found out that the size of the particle causing brittle failure, which disqualifies pipes and pipe joints, decreases with increasing pipe wall thickness.

The literature has shown that many aspects of polyethylene and other materials with and without deliberate and non-deliberate inclusions have already been explored; however, there are some research gaps, which still need to be filled:

- Although, different types of polyethylene were explored in detail by many researchers, most of the studies were conducted on the old generation of materials, whereas, modern grades have been less thoroughly investigated. The new materials are much tougher, and are thus less sensitive to defects and very resistant to crack propagation. The lifetime of modern PE100 theoretically reaches up to 1000+ years (Bowman, 2008). Therefore, there is a need to analyse different properties of modern polyethylene grades, both with and without inclusions.

- Although lots of research was found on fillers within the polymer matrix, this applied to small uniformly distributed particles at high concentrations. The chips based on MEMS technology are expected to be up to a few millimetres in size and half a millimetre thick. Thus, research is required on the effects of different discrete chip shapes, sizes and their placement and orientations. In addition, the method of inserting chips into the

polyethylene matrix in a controlled way also needs to be developed. These will be the subject of this research.

- It was indicated that the filler-matrix interface has an impact on the mechanical properties of the composite and the silane coupling agents were proven to improve the adhesion. Therefore, the bond between the silicon chip and the polymer matrix needs to be investigated and varied in this research and different types of adhesives are worthwhile exploring.

- The literature review showed that standard engineering material tests such as tensile, bending, impact, creep and fatigue tests can be used in this project to test the structural integrity of polyethylene. Thus, these tests will be used to determine the structural integrity of polyethylene samples with silicon chips embedded in them.

- Although other researchers have investigated non-deliberate defects and deliberate inclusions in pipes, the silicon chips used here are different in size, shape and material. This suggests that the tests on large-scale pipes would aid the interpretation of the data and provide confidence in the results. Alternatively, the chips can be introduced into pipe joints. For this purpose, the techniques of inserting chips into pipes and joints need to be developed.

Not all of the problems listed above could be solved in this project due to various limitations. Pipes containing silicon chips could not be investigated due to a lack of access to the equipment needed to produce the pipes with chips and subsequently test them. However, most of the research gaps identified previously were investigated, and the methodology developed to research these gaps is introduced in Chapter 4.

Before the sample production and testing procedures are described, the materials used in the project are introduced and characterized. The literature has indicated that the polyethylene mechanical properties depend strongly on its molecular structure, therefore it is specified for the tested materials. Both, the molecular structure and processing conditions affect polymer crystallinity and thus density, therefore these physical properties are also determined. As the processing conditions of the samples are introduced and discussed in detail in the methodology Chapter, their impact on the density and crystallinity is analysed also there. The information about the properties of tested polymers and their variations associated e.g. with changing manufacturing conditions (during compression moulding of the samples) should help in interpretation of the results of the main mechanical tests of the samples with and without silicon chips.

Chapter 3   CHARACTERIZATION OF MATERIALS

In this chapter the materials used in the project are introduced. Further, the material characterization tests such as melt flow rate (MFR), molecular weight (MW), molecular weight distribution (MWD), crystallinity, and density analyses are described and their results presented and discussed. These complementary tests will help to understand the connection between the materials' performance in the main tests conducted and their structure.

3.1 Description of materials

This section describes all the materials used in this research project. The characteristics of the main materials used, i.e. silicon and polyethylene, were already generally introduced in section 2.2.

3.1.1   High density polyethylene (HDPE)

Different polyethylene grades were used to study the effects of embedding silicon chips on the structural integrity. Two main types of high density polyethylene (HDPE) were used: natural colour pipe-grade HDPE (BorStar HE 3493-LS-H produced by Borealis) and off-the-shelf HDPE (produced by DOW). In the preliminary tests a blue pipe-grade HDPE (Eltex TUB124 produced by INEOS Polyolefins Europe) was also used. All materials were supplied in granular form and the pipe grades were both supplied by Radius Systems.

3.1.2   Single crystal silicon

Single crystal silicon was investigated in the form of chips as an inclusion in the polyethylene matrix. This is a common base material for Micro-Electro-Mechanical Systems (MEMS) used to manufacture small sensors. The sensing layer in these microsensors has a thickness of just a few microns. Therefore, its influence on the shape and structural performance of the chips is

not likely to be significant and hence the plain single crystal silicon chips can represent a working microsensor.

As the sensor is manufactured on one side of silicon wafer, only one side of the surface is polished and is very smooth with the irregularities at the nanometre scale (Figure 3.1). The morphology of the unpolished structure differs and the irregularities are a few micrometers deep as the scanning electron micrograph of the rough surface indicated (Figure 3.2). However, as there are no standards specifying the roughness of the rough side of a silicon wafer, its morphology differs from wafer to wafer and sometimes the unpolished side looks very smooth and shiny and no difference can be noticed with the naked eye.
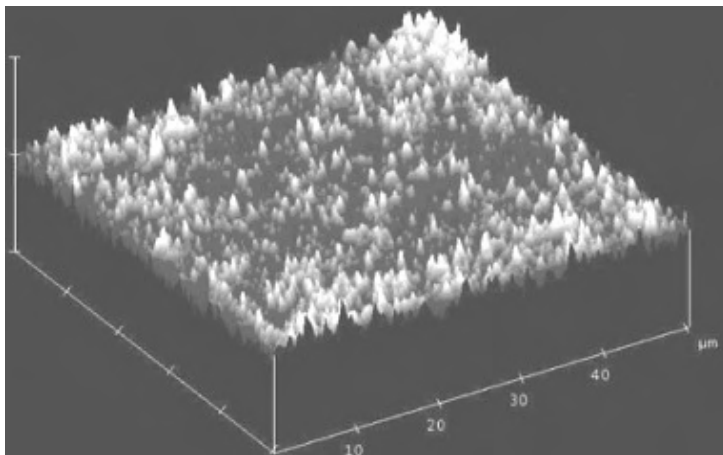
Figure 3.1 Surface morphology of a smooth (polished) side of a silicon wafer (Tay et al., 2004).
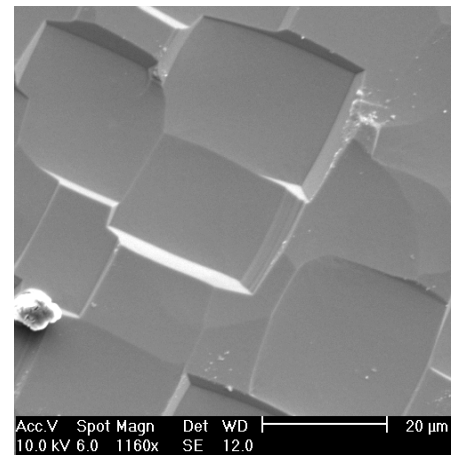
Figure 3.2 Scanning electron micrograph of a rough side of a silicon wafer (marker bar = 20µm).

3.1.3   Hot melt adhesive

Hot melt adhesive (HMA) was used to alter the bond strength between the silicon chip and the HDPE. It is vastly used for the multilayer pipes to bind e.g. polyethylene and aluminium layers (DSM Engineering Plastics, 2004). It was supplied by DSM in the form of granules. Two grades were used: Yparex 8702ES (HMA1) and Yparex 9403 (HMA2). They are composed of chemically modified linear low density polyethylene (LLDPE).

3.1.4 Photoresist

The photoresist is a material used in the MEMS manufacturing process. It is a photosensitive polymer, which is spread over the wafer surface. After the sensor is produced, the remaining photoresist is removed (FSRM, 2003). However, in this case, it was applied to alter the silicon-polyethylene bond and thus the chips were fully coated with the photoresist. The material used was MEGAPOSIT SPR 220-7 manufactured by Rohm and Haas Electronic Materials.

3.1.5 Teflon

The Teflon (PTFE) lubricant was used as another silicon chip coating. In industry, Teflon is considered as the material, which ensures low friction and a non-stick surface (Roberts, 1989). This coating was used in order to investigate the chip-polymer interaction when there is no adhesion between both materials. The Dry PTFE spray manufactured by Rocol was applied.

In the next section the tests used to characterize different polyethylene grades are described.

3.2 Material characterization tests

The main mechanical tests on the samples are complimented by tests to characterise the polymers themselves and include melt flow rate (MFR), molecular weight (MW), molecular weight distribution (MWD), crystallinity, and density analyses. The samples for theses tests were cut using a cutter or a knife depending on their dimensions.

3.2.1   Melt flow rate (MFR)

This is a standard test in which the mass of the material flowing under specified conditions of temperature, load, and time is determined (BSI, 2005b). The apparatus used is shown in Figure 3.3. First, the cylinder with an internal diameter of 9.55mm was cleaned to remove any polymer residues from previous tests. Then, it was heated up to 190ºC and a few grams of polymer granules were inserted into the cylinder, pushed in by a feeder. A piston was then inserted into the cylinder and the weight was applied; 5 and 2.16kg in the case of pipe-grade and off-the-

(a)

(b)
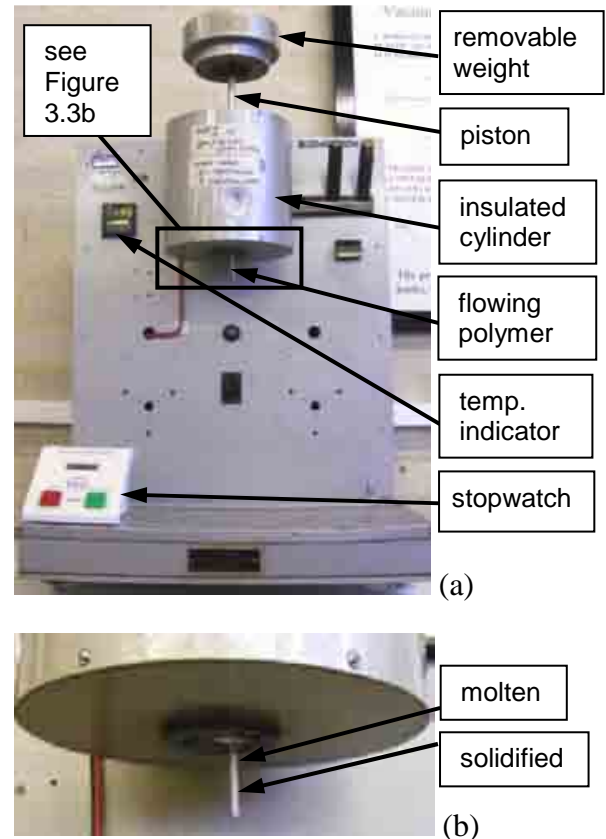
Figure 3.3 (a) Melt flow rate apparatus, (b) enlarged view of a flowing polymer sample.

shelf polyethylene grades, respectively. Once the polymer flow was continuous (no air bubbles) and steady (see Figure 3.3b), the extruded polymer was cut off and the stop watch started. The 10- and 1-min portions of the extruded pipe-grade and off-the-shelf polyethylene, respectively, were sampled. The lower weight and shorter sampling time were used in the case of the off-the-shelf polymer due to its very high flow rate.

A minimum of three samples of each polymer should be taken in accordance with BSI (2005b). In this case five cut-offs were taken as this was the maximum number of samples which could be taken from one filling of the cylinder with pipe-grade polyethylene. The extra samples prolonged the testing time by just a few minutes and increased the accuracy of the result.

3.2.2 Molecular Weight (MW) and Molecular Weight Distribution (MWD)

The MW and MWD were determined using High Temperature Gel Permeation Chromatography (GPC) by the commercial company Smithers Rapra (Holding, 2010). The method is based on the rule that molecules in a solution adopt random coil configurations, the volume of which is proportional to their molecular weight. Separating the molecules according to their random coil dimensions allows the MWD to be determined. The separation is achieved by pumping the polymer solution through a column packed with microscopic beads with porous surfaces. The smaller the molecules, the larger the fraction of pores is accessible for them to diffuse through and thus it takes them longer to pass through the column. Chromatography is used to detect the weight concentration of the polyethylene in a solution on the basis of the differences in the refractive index (Peacock, 2000).

The molecular weight is expressed as a weight average (Peacock, 2000):

$$M_w = \frac{\text{Total weight of each size} \times \text{Respective weights}}{\text{Total weight of all molecules}}$$

3.1

and number average:

$$M_n = \frac{\text{Total weight of all molecules}}{\text{Total number of molecules}}$$

3.2

where M_w is always larger.

The polydispersity index (PDI) is also determined as a measure of the distribution of molecular mass within the polymer sample and is calculated as (Rane & Choi, 2005):

$$PDI = \frac{M_w}{M_n}$$

3.3

3.2.3 Crystallinity

The crystallinity was determined using the thermal differential scanning colorimetry (DSC). In addition, the melting and glass transition temperatures for the material were determined. In this method the sample and the empty reference crucible are heated and cooled at a controlled rate and under controlled conditions as specified in the standards (ASTM, 2006; BSI, 2009). The general arrangement of the equipment is shown in Figure 3.4.
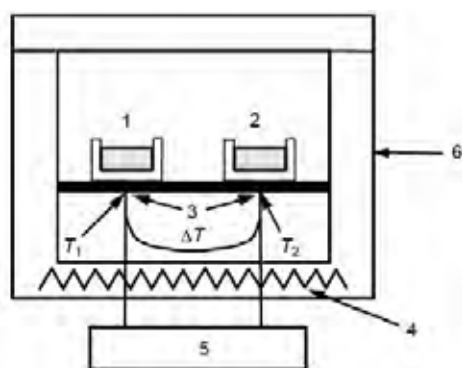
Figure 3.4 General arrangement for the DSC heat-flux test illustrating the basic components; T – temperature, 1 – sample position, 2 – reference position, 3 – thermocouples, 4 – heater, 5 – measurement circuit of T, 6 – surrounding oven (BSI, 2009).

The amount of heat/energy required to increase the temperature of a sample differs depending on the material due to differences in material heat capacity. This causes a difference in heat flow rate into the sample and reference positions (Figure 3.4, positions 1 and 2, respectively), which is continuously monitored and recorded against the temperature.

A transition of material state between liquid and solid is marked by absorption (or release) of energy by the specimen resulting in a corresponding endothermic (or exothermic) peak in the heating (or cooling) curve (ASTM, 2006; Hubert et al., 2001).

In the test, around 5-10mg polymer samples were first held at 25ºC for 1min. Then they were heated at a rate of 10ºC/min till the temperature of 160ºC exceeding the melting point was reached. In order to standardize the physical state of the materials prior to cooling they were held at this temperature for 2min. Then they were also cooled at a rate of 10ºC/min.

An example of the thermogram obtained at the heating and cooling stages of the pipe-grade polyethylene sample is shown Figure 3.5. The characteristic points in the graph are described in Table 3.1.
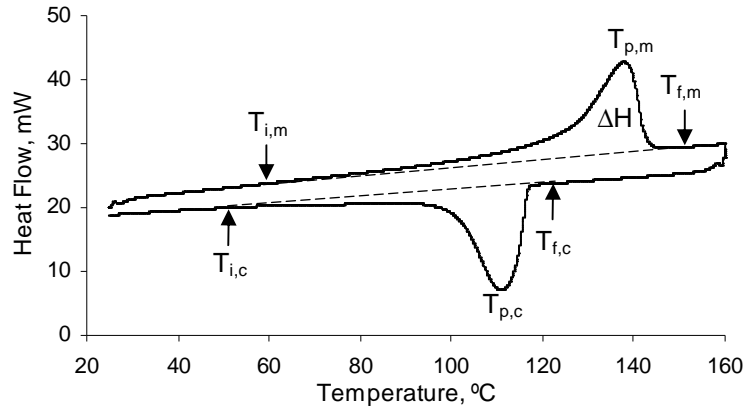
Figure 3.5 An example of the thermogram obtained in DSC at heating (top) and cooling (bottom) of pipe-grade polyethylene; dashed line – baseline. Note: the designations explained in the text below.

Table 3.1 Characteristic parameters obtained from the DSC thermogram.

Parameter	Definition/ description
ΔH	area between the melting endotherm and baseline, between $T_{i,m}$ and $T_{f,m}$ points; enthalpy of fusion of the specimen, kJ/kg
$T_{i,m}$	temperature at first detectable deviation of melting endotherm from baseline, start of melting, ℃
$T_{p,m}$	temperature at the greatest difference between melting endotherm and baseline, melting peak, ℃
$T_{f,m}$	temperature at last detectable deviation of melting endotherm from baseline, end of melting, ℃
$T_{i,c}$	temperature at first detectable deviation of crystallization exotherm from baseline, end of crystallization, ℃
$T_{p,c}$	temperature at the greatest difference between crystallization exotherm and baseline, crystallization peak, ℃
$T_{f,c}$	temperature at last detectable deviation of crystallization exotherm from baseline, start of crystallization, ℃

The temperatures of start and end of melting ($T_{i,m}$ and $T_{f,m}$) and start and end of crystallization ($T_{f,c}$ and $T_{i,c}$) are only estimated, while the melting and crystallization peak temperatures ($T_{p,m}$ and $T_{p,c}$) can be obtained directly from the graph as the endothermic and exothermic peaks, respectively.

In the method, it is assumed that the amorphous portion of the sample does not contribute to the melting endotherm. Thus, the degree of crystallinity is obtained by comparing the measured heat fusion with that estimated for 100% crystalline polyethylene. The value of 69cal/g is assumed (Peacock, 2000). As 1J is equal to 0.239cal, this gives 289J/g (kJ/kg). The crystallinity is obtained from Equation 3.4.

$$X_c = \frac{\Delta H}{289} \cdot 100\% \qquad\qquad \textbf{3.4}$$

where: X_c – percentage crystallinity, %

ΔH – enthalpy of fusion of the specimen, kJ/kg

3.2.4 Density

The density was determined using the immersion method (BSI, 2004). The immersion liquid used was 99% Heptane. The balance was calibrated before use. Then approximately 0.5g of the polymer sample was weighed in air as shown in Figure 3.6. The balance was tarred (zeroed) and the sample immersed in the liquid on the sample holder, and weighed again. The density of polymer was calculated using Equation 3.5 (BSI, 2004).

$$\rho = \frac{m \cdot \rho_H}{m - m_H} \qquad \textbf{3.5}$$

where: ρ_H – density of Heptane, g/cm³

m – mass of the specimen, g

m_H – mass of the specimen in Heptane, g

(a)

(b)
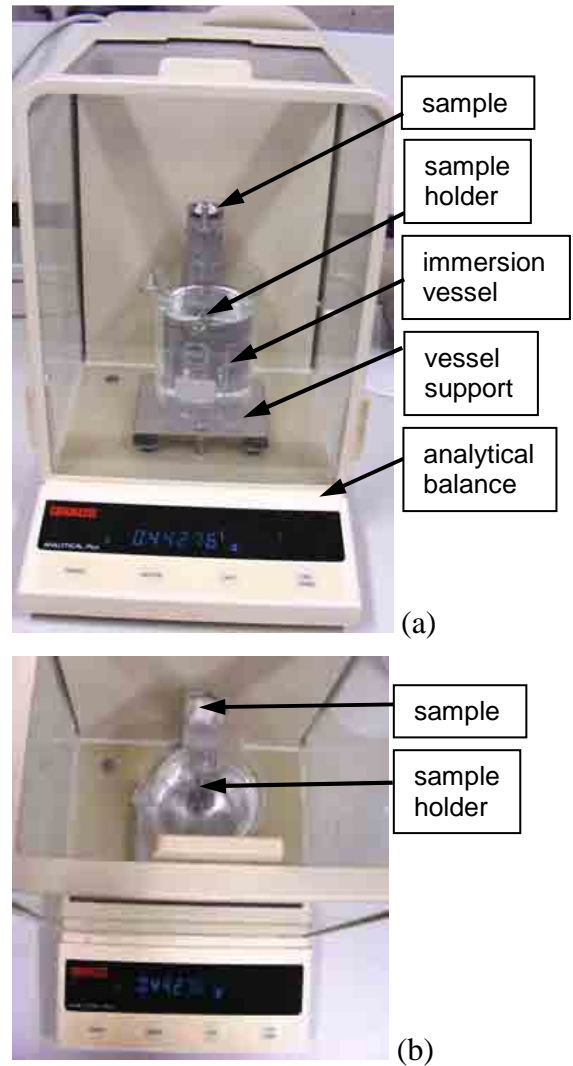
Figure 3.6 Density measurement arrangement; (a) front view, (b) top view.

Due to taring of the balance with a sample, the difference $'m - m_H'$ was read directly from the scale. The air and Heptane temperature was 25±1ºC. The density of Heptane at 25ºC is 0.684g/cm³ (Air Resources Board, 2010).

In the next section the results of the material characterization tests are introduced and analysed.

3.3 Results & discussion of material characterization

The aim of these tests was to investigate and characterise the materials and samples. Melt flow rate was only determined for two HDPE grades. Other parameters such as molecular weight (MW), molecular weight distribution (MWD), crystallinity, and density were determined for two HDPE grades and HMAs. The impact of the manufacturing conditions on the physical properties of pipe-grade HDPE and HMA2 is studied in the next chapter, where the production procedure and conditions of the samples are introduced.

3.3.1   Melt flow rate (MFR)

Due to the high MFR value for the off-the-shelf polyethylene the samples had to be collected every minute instead of the standard 10min intervals; however, the cut off polymer sample was still very long, as shown in Figure 3.7a. The weight of the '1-min samples' was multiplied by 10 to obtain the standard 10-min value. The average MFR of the off-the-shelf polyethylene

(a)   (b)

Figure 3.7 MFR samples of (a) the off-the-shelf and (b) pipe grade polyethylene.

was 7.62g/10min under a load of 2.16kg, with an SD of 0.15g/10min. The value for the pipe-grade polyethylene was 0.250g/10min under a load of 5kg, with an SD of 0.006g/10min, which is equal to the value specified by the manufacturer (Borealis, 2008).

There was a possibility of human error associated with cutting off the sample at the right time, (approximately ±5sec). The sample might also have been cut differently from sample to sample as it was done manually. The accuracy of the weight measurement was ±0.0001g. The experimental error in both cases was approximately 2%, which is less than the 5% accepted by BSI (2005b). The samples with air bubbles were discarded according to BSI recommendations (2005b).

The MFR of the HMA1 and HMA2 could not be measured as the material would stick to the metal cylinder. The values specified by the manufacturer are 2.1 and 3g/10min under 2.16kg load, at 190ºC, respectively (DSM Engineering Plastics, 2009a and 2009b).

3.3.2 Molecular Weight (MW) and Molecular Weight Distribution (MWD)

Due to a possible change in MW and MWD distribution as a result of the material processing, the original granules as well as the compression moulded samples were analyzed. The tests for each sample were repeated twice in accordance with the common practice of the experienced testing company in order to have confidence in the results. The results for the weight average (M_w), number average (M_n) and polydispersity index (PDI) are presented in Table 3.2 and the MWD is graphically illustrated in Figure 3.8. The sample name was dictated by Smithers Rapra with the first term indicating the number of run, the second is the description of the sample where 'C' stands for 'compression moulding', and the third term in the brackets is specific to the company's description.

Table 3.2 M_w, M_n and PDI of polymer samples. Note: averages (marked bold) based on the previous four values in the table (after Holding, 2010).

Sample	M_w	M_n	PDI
103 HMA1 8702 ES (SR3306/1)	109,000	26,800	4.1
113 HMA1 8702 ES (SR3306/1)	110,000	26,600	4.1
100 HMA1 1C (SR3306/2)	111,000	27,000	4.1
114 HMA1 1C (SR3306/2)	111,000	26,900	4.1
HMA1 average	**110,300**	**26,800**	**4.1**
101 HMA2 9403 (SR3306/3)	95,000	21,600	4.4
115 HMA2 9403 (SR3306/3)	94,200	21,800	4.3
102 HMA2 2C (SR3306/4)	94,900	21,800	4.3
116 HMA2 2C (SR3306/4)	95,100	21,800	4.4
HMA2 average	**94,800**	**21,800**	**4.4**
70 off-the-shelf (SR3306/5)	74,200	21,900	3.4
75 off-the-shelf (SR3306/5)	74,900	22,600	3.3
76 off-the-shelf 3c (SR3306/6)	73,600	22,600	3.3
87 off-the-shelf 3c (SR3306/6)	74,700	22,300	3.3
Off-the-shelf average	**74,400**	**22,400**	**3.3**
72 Pipe Grade (SR3306/7)	307,000	7,950	39
88 Pipe Grade (SR3306/7)	316,000	8,280	38
73 Pipe Grade 4c (SR3306/8)	309,000	8,040	38
89 Pipe Grade 4c (SR3306/8)	321,000	7,840	41
Pipe grade average	**313,300**	**8,000**	**39**
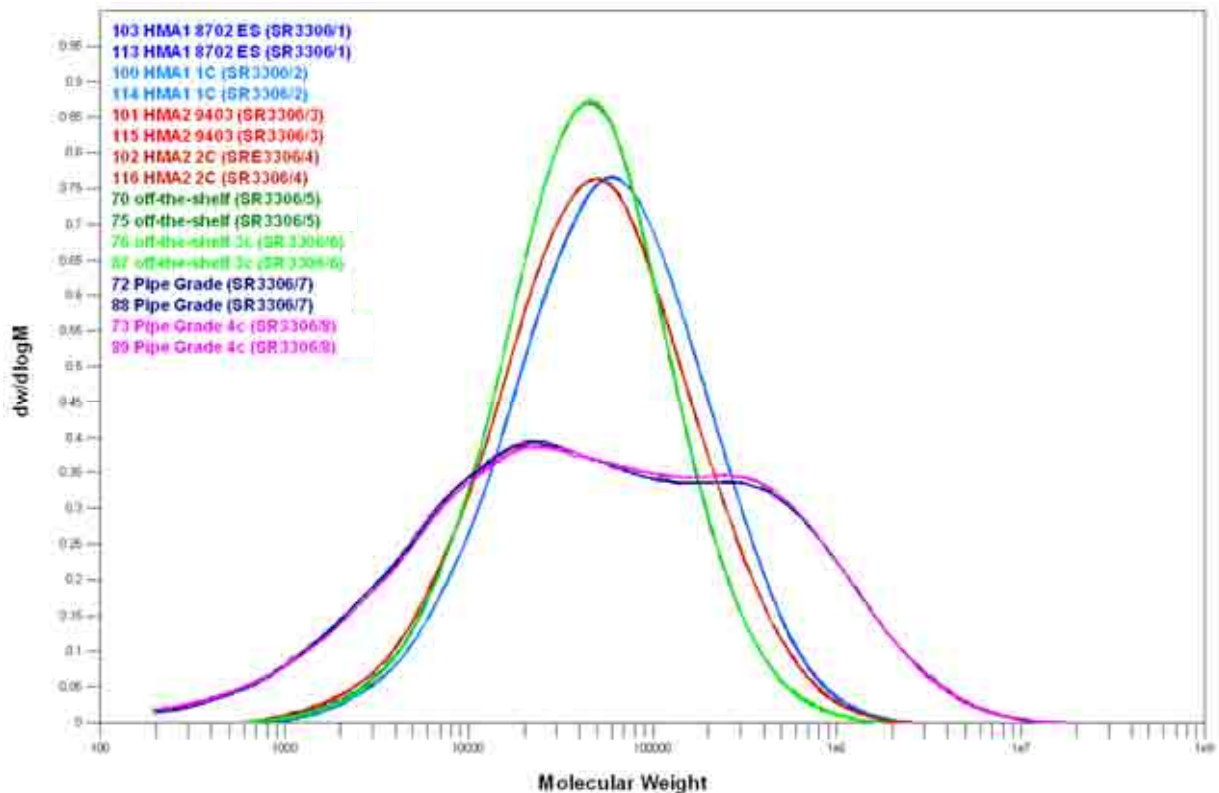
Figure 3.8 MWD of polymer samples. Note: the MW is plotted on logarithmic scale (Holding, 2010).

In Figure 3.8 the results for the duplicate samples overlap. The apparent symmetry of the curves is due to presentation of the data on a logarithmic scale. Bigger MW variation appears at high MWs for all samples. In the case of pipe grade polymer a slight flatting of the curve linking the two peaks of the bimodal MWD can be observed suggesting that the processing might cause a slight degradation and/or defects in some molecules. However, the differences are within the experimental error thus might be not real (Holding, 2010; Peacock, 2000). In general, the values for the original polymer granules and the compression moulded samples are in the same range (no considerable differences) for the same polymer in Table 3.2, thus their common averages were calculated. The results suggest that there is no noticeable influence of the polymers' processing on the MW and MWD with regards to the compression moulding.

It should be noted that for the analysis only a small amount of material (15mg) was used, therefore, the results might be not representative for a non-uniform material. However, as the data for the original and compression moulded samples of the same materials overlap, this suggests that the materials are uniform and thus, the results can be considered as representative. The Gel Permeation Chromatography (GPC) system is calibrated once at the start of testing the set of samples and hence the accuracy might drift with time. Therefore, the given values are not absolute and should be regarded in a comparative manner.

3.3.3 Crystallinity

First, the repeatability of the measurement was investigated by testing the samples cut from one compression moulded pipe-grade polyethylene sheet, from the vicinity. Table 3.3 presents the results.

Table 3.3 Crystallinity and characteristic temperatures of two pipe-grade polyethylene samples.

Sample	$T_{i,m}$	$T_{p,m}$	$T_{f,m}$	$T_{i,c}$	$T_{p,c}$	$T_{f,c}$	ΔH	X_c
	°C						kJ/kg	%
Pipe-grade 1	60	133.2	150	50	114.4	120	195.3	67.6
Pipe-grade 2	60	133.5	150	50	114.4	120	196.3	67.9

Most parameters obtained for both samples taken from one sheet from the vicinity are equal while the crystallinity values are very close. This suggests that the measurement is relatively accurate and it is enough to test one sample of each type. However, some small variations associated with the instrument/measurement accuracy can occur. In order to reduce them the instrument was calibrated from time to time.

An example of a graph for pipe grade polyethylene is presented and described in section 3.2.3, while Figure 3.9 presents the plots for remaining samples and Table 3.4 lists all numerical values.

(a)

(b)

(c)

(d)
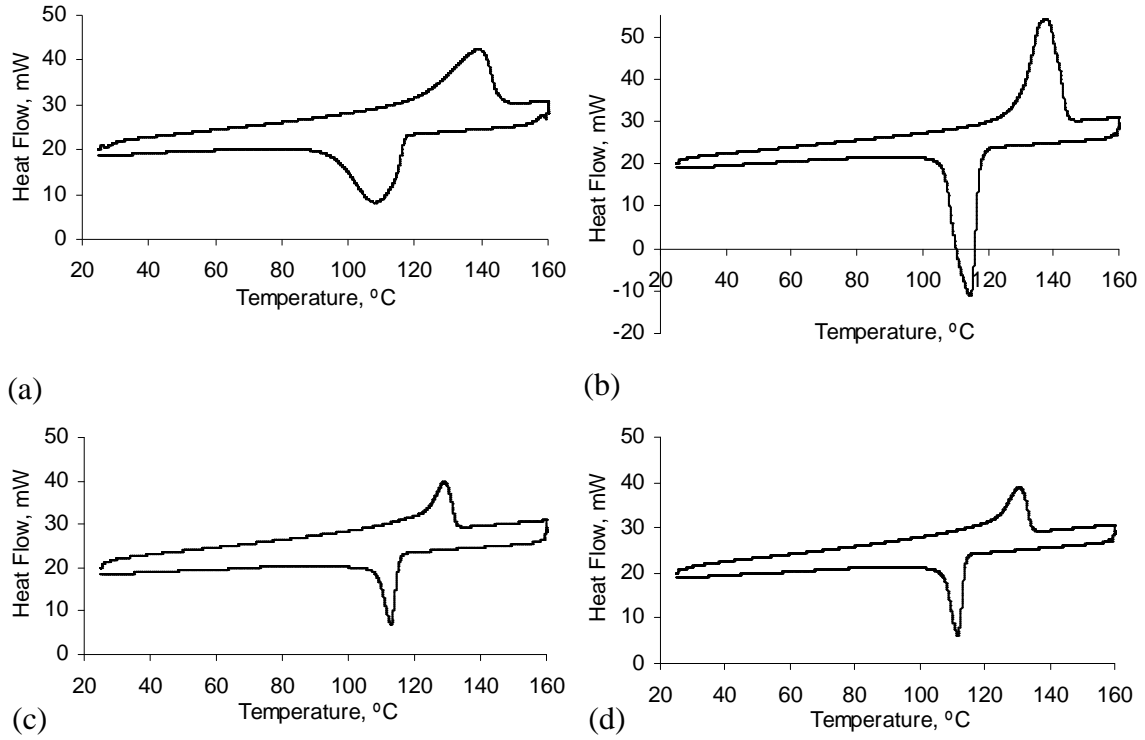
Figure 3.9 Thermogram of: (a) pipe grade granule, (b) off-the shelf polyethylene, (c) HMA1 and (d) HMA2.

Table 3.4 Density, crystallinity and characteristic temperatures of the samples heating and cooling cycles; C – compression moulded.

Sample	$T_{i,m}$	$T_{p,m}$	$T_{f,m}$	$T_{i,c}$	$T_{p,c}$	$T_{f,c}$	ΔH	X_c
	°C						kJ/kg	%
Pipe grade granule	60	138.8	155	60	108.1	120	175.2	60.6
Pipe grade C	60	133.2	150	50	114.4	120	195.3	67.6
Off-the-shelf C	60	137.6	150	60	114.5	125	229.0	79.2
HMA1 C	60	128.7	140	50	112.8	120	111.7	38.7
HMA2 C	60	130.5	140	60	111.6	120	130.2	45.1

The crystallization temperature is usually approximately 20ºC lower than the melting temperature (Peacock, 2000), which can be observed in the case of the tested materials. The $T_{p,m}$ ranges between 128 and 139ºC, which is close to the range for HDPE after Peacock (2000), 125-132ºC, while $T_{p,m}$ is in a range of 108-115ºC,

In most cases, the samples start to melt already at around 60ºC ($T_{i,m}$) but it requires a temperature of around 150ºC ($T_{f,m}$) at a heating rate of 10ºC/min to melt the complete sample. In the case of HMAs this temperature is a bit lower at 140ºC. Thus, the temperature of 190ºC applied and recommended by the manufacturer for compression moulding (Borealis, 2008) is definitely enough to ensure complete melting of all polymers used.

The cooling of the samples starts at approximately 120ºC ($T_{f,c}$) and continues until the temperature of around 50-60ºC ($T_{i,c}$) is reached. Therefore, the cooling of the moulds at this temperature range has an influence on the degree of the crystallinity of the produced samples.

The pipe grade granule had lower crystallinity than the compression moulded sample, which is associated with its production method and small size (quick cooling). When comparing different polymer grades the crystallinity reduced in the following order: off-the-shelf polyethylene > pipe grade polyethylene > HMA2 > HMA1.

Further, the density, which should reflect the crystallinity values, is discussed.

3.3.4   Density

The average density values were obtained on the basis of three samples produced under the same conditions. This is a minimal number of samples recommended by BSI (2004) and it was dictated by the fact that in some cases only three sheets were produced in the same conditions, so only three samples were available.

In order to determine the accuracy of the experiment, the density of samples cut from one compression moulded sheet from the vicinity was determined. The possible error associated with the weight measurement was ±0.0001g. The data are given in Table 3.5.

Table 3.5 Results from the density tests for samples cut from the same sheet.

	m, g	$m - m_H$, g	ρ, g/cm³
Sample 1	0.5509	0.3937	0.9571
Sample 2	0.6336	0.4531	0.9565
Sample 3	0.4490	0.3211	0.9564
Average			0.9567
SD			0.0004

The SD of the density for three samples taken from the same sheet was 0.0004g/cm³, thus, this is the accuracy of the measurement and has to be considered by analysing the results, while the maximum SD of the results for the samples cut out from different sheets was obtained for the off-the-shelf polyethylene and was equal to 0.0006g/cm³. Due to noticeable differences between the materials higher than the SDs and in accordance with BSI (2004), the values are presented with an accuracy of three decimal places.

The densities were 0.971 and 0.957g/cm³ for the off-the-shelf and pipe grade polymer, respectively. Only the latter falls within the standard HDPE density range of 0.941-0.960g/cm³ (ASTM, 2005). The HMAs composed mostly of the linear low density polyethylene (LLDPE) had values of 0.927 and 0.935g/cm³ for the HMA1 and HMA2, respectively, which is higher than the standard density range for the LDPE of 0.910-0.925g/cm³ (ASTM, 2005). The higher than expected densities of materials are due to the processing conditions, which is discussed in the next section.

The lower the cooling rate, the more time the polymer chains have to align resulting in a higher crystallinity and thus density. Therefore, the uniformity of the sheets with regards to the processing conditions needs to be also analysed and this is done in the next chapter where the sample production procedure is discussed.

In the next section the correlation between the material properties analysed in this chapter is discussed and their influence on the mechanical properties of the samples analysed/projected.

3.3.5 Summary of the material properties and their impact on the mechanical performance

Table 3.6 lists the key data for all tested polymers. The crystallinity (X_c) and density (ρ) are presented as rounded averages for compression moulded samples tested while the molecular weight (M_w) and the polydispersity index (PDI) associated with MWD are the averages for granules and compression moulded samples.

Table 3.6 The molecular weight (M_w), polydispersity index (PDI), crystallinity (X_c) and density (ρ) of the tested polymers.

Material	MFR g/10min	M_w	PDI	X_c %	ρ g/cm³
Pipe grade HDPE	0.25 under 5 kg	313,300	39	68	0.957
Off-the-shelf HDPE	7.62 under 2.16 kg	74,400	3.3	79	0.971
HMA1	2.1 under 2.16 kg	110,300	4.1	45	0.927
HMA2	3 under 2.16 kg	94,800	4.4	39	0.935

The MFR value is related to the molecular structure of polymer and it increases with decreasing M_W, which confirms the statements of the Plastic Pipe Institute (2007). In general M_W increases with MWD (expressed by PDI), however an exception are HMAs where for lower M_w (for HMA2) higher PDI is obtained. The highest M_W and MWD for pipe grade polyethylene is associated with its lowest MFR. For the off-the-shelf polymer the opposite

trend was observed suggesting that it has a simple molecular structure (very few side branches). This polymer is expected to have low long term strength, ductility and fatigue resistance but good processability. Therefore, it is expected to have the lowest mechanical properties such as tensile and impact strength, and stress crack and creep resistance. However, the flexural stiffness might be slightly larger than for the other polymers.

The pipe grade has a M_w of 313,300, which is over three times higher than for other polymers and PDI of 39, which is of an order larger than for other polymers. Without special modifications, HDPE and LLDPE (which is a major component of HMAs) have a relatively low PDI due to the molecular chains having not many side branches, which was observed for other materials. The bimodal MWD of pipe grade polyethylene (Figure 3.8), which is a result of material modification, indicates fractions of both, very high and very low MWs. It guarantees that the material will be strong in different failure modes and ensures good material processing, which is the requirement for a pipe material designed to last at least 50 years in service, in changing conditions (Plastics Pipe Institute, 2007).

From Table 3.6 it can be seen that the crystallinity increases when the density increases, which is in accordance with Peacock (2000). The off-the-shelf grade reaches the highest values. The low density of HMAs suggests they have some side branches which might be associated with a complex composition of these materials. Therefore, they are expected to be less strong but more ductile compared with HDPEs. As stated in section 2.2.2.3 lower crystallinity and density are associated with higher ductility, thus, higher resistance to crack propagation and impact forces but lower resistance to tensile and hoop stress and creep.

The specific properties of particular materials and their influence on the mechanical performance were already analysed and compared in the previous sections. These projections are summarized in Table 3.7.

83

Table 3.7 The projected mechanical performance of materials analyzed (relative to each other).

Material	Tensile strength & modulus	Ductility	Flexural stiffness	Impact strength	Stress crack resistance	Creep resistance	Process-ability
Pipe grade HDPE	High	High	High	High	High	High	High
Off-the-shelf HDPE	V.High	Low	V.High	Low	Low	Low	V.High
HMA1	Low	V.High	Low	V.High	V.High	V.High	-
HMA2	Low	V.High	Low	V.High	V.High	V.High	-

The results have shown that the properties of different polymers tested vary significantly and so does their mechanical performance projected on the basis of the literature. The tensile tests of all polymer grades analysed and the flexural, Charpy impact and flexural creep tests of pipe grade polyethylene will show if these projections are correct. As stated in section 2.3.3.7, the toughness of the matrix has also an influence on the mechanical performance of the samples with inclusions. It will be investigated how the samples with chips perform in comparison with the plain polyethylene samples. Further, the effect of different chip parameters, such as shape, size and orientation, on mechanical performance of the samples will be investigated. But first, the methods of sample production and the test procedures will be introduced in the next chapter.

Chapter 4   METHODOLOGY
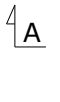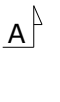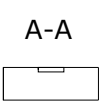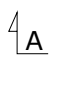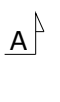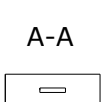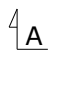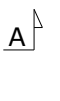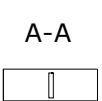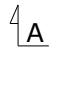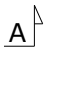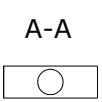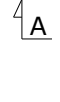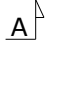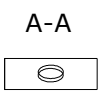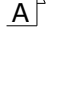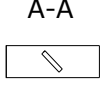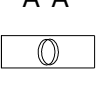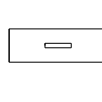
4.1 Introduction

It was evident from the literature review that there was no previously published work investigating the effect of inserting silicon chips into HDPE with respect to its mechanical properties. It was therefore decided to conduct a series of extensive mechanical tests using equipment available at the University and Exova to examine the fundamental behaviour of HDPE with chip inclusion. The tests conducted were tensile, bending, Charpy impact, flexural creep, and the adhesion pull-off test and are described in detail in this chapter together with a detailed description of the sample preparation and manufacture. The choice of chip and sample dimensions are also discussed. Preliminary testing was conducted as part of the methodology development and these results are presented in this chapter. The results of the main tests are presented in Chapters 5-7. The methodology as well as the results associated with the tensile tests of joints are included in Appendix A.

4.2 Coding used for the test samples

Due to many different chip orientations within the samples tested in the project it was decided to code them. This allowed test samples to be simply referenced. An example code is SC/0/90. The first term stands for the type of chip: SC – small circle (4mm²), LC – large circle (16mm²), SSQ – small square (4mm²), and LSQ – large square (16mm²) used in the preliminary experiments. The second and third term stand for the chip orientation towards the sample surface and edges, respectively. The possible angles are: 0, 45, and 90º. Thus SC/0/90 stands for: 4mm² circle parallel to the sample surface and perpendicular to the sample edges. Table 4.1 shows the codes of all samples tested as well as their schematic illustrations.

Table 4.1 Codes of the samples.

Code	Description	Schematic: plan & side elevation (not to scale)
SC/surf LC/surf SSQ/surf	4mm² circle, 16mm² circle, and 4mm² square on the sample surface	
SC/0/90 LC/0/90 SSQ/0/90	4mm² circle, 16mm² circle, and 4mm² square respectively parallel to the sample surface and perpendicular to the sample edges	
SC/90/0 LC/90/0 SSQ/90/0	4mm² circle, 16mm² circle, and 4mm² square respectively perpendicular to the sample surface and parallel to the sample edges	
SC/90/90 LC/90/90 SSQ/90/90	4mm² circle, 16mm² circle, and 4mm² square respectively perpendicular to the sample surface and perpendicular to the sample edges	
SC/45/90	4mm² circle at an angle to the sample surface and perpendicular to the sample edges	
SC/45/45	4mm² circle at an angle to the sample surface and at an angle to the sample edges	
SC/90/45	4mm² circle perpendicular to the sample surface and at an angle to the sample edges	
2SC/0/90 SC&SSQ/0/90	two 4mm² circles and 4mm² circle & 4mm² square, respectively, parallel to the sample surface and perpendicular to the sample edges	

86

4.3 Production of the test samples

The production of the samples involved manufacturing polyethylene plaques from which the samples were cut out. The silicon chips also required being cut to size and were coated in some cases. The methods of sample manufacture and cutting out as well as chip coating are described in this section.

4.3.1   Compression moulding

HDPE and HMA are thermoplastics. There are different ways in which they can be processed (see section 2.2.3.2, page 16). In this research, the polyethylene samples, as well as the HMA samples and coatings, were compression moulded using a hydraulic press available in the university laboratory. Flash picture-frame moulds of different thicknesses were used. The method and conditions of sample production influence the ultimate properties of the material. These are discussed in the following sections.

4.3.1.1 Construction of the hydraulic press

A hydraulically driven press was used to compression mould the samples. The platens of the press were electrically heated and cooled by water. The construction of the press is shown in Figure 4.1. The mould, with polymer placed between the platens, is shown schematically in Figure 4.2.
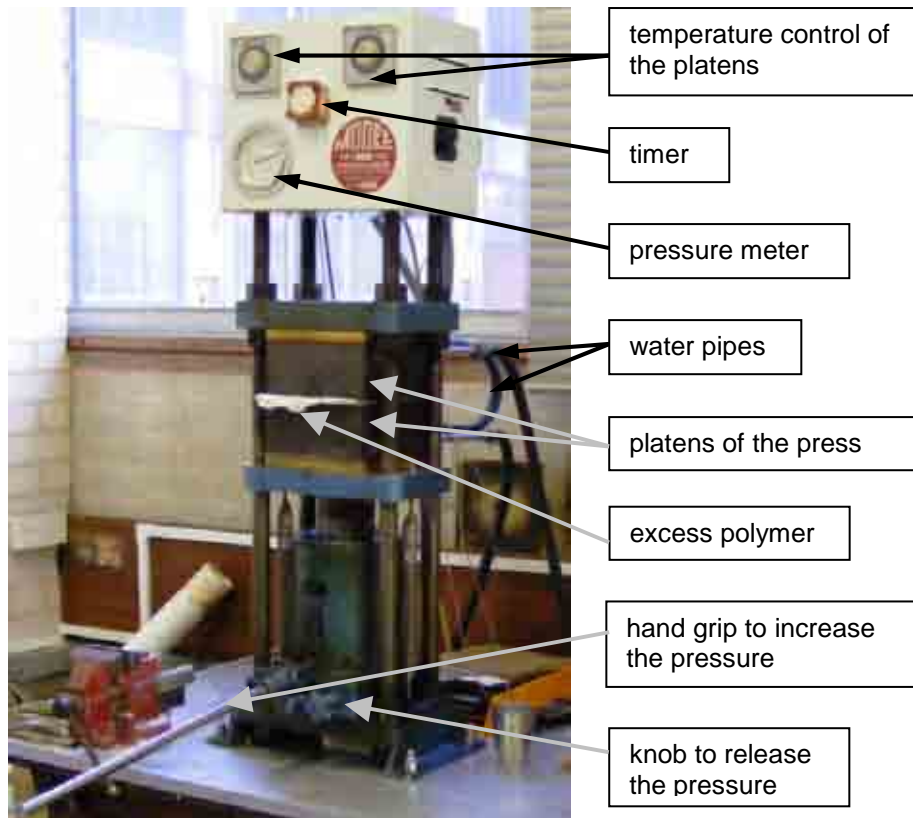
Figure 4.1 Hydraulic press used to produce the test samples.
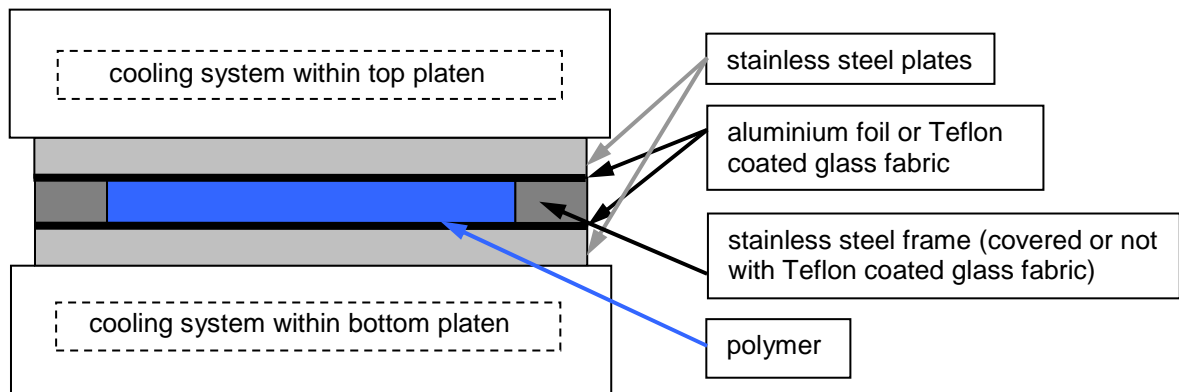
Figure 4.2 Schematic of the hydraulic-press platens showing the mould and the location of the polymer.

In the case of processing a HMA, which adheres easily to most surfaces in a molten state (Ames, 1978; Bentley, 2005), the mould and stainless steel plates were covered with Teflon coated glass fabric, as shown in Figure 4.3, in order to ensure a non-stick surface.
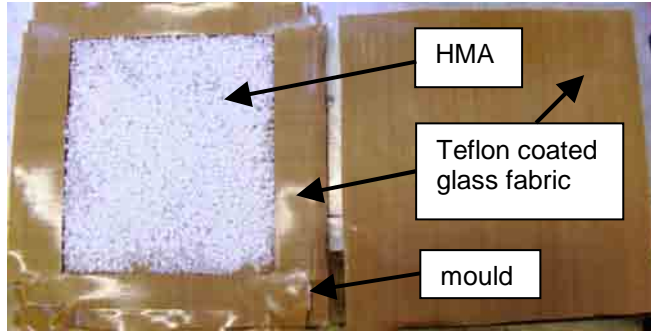
Figure 4.3 Stainless steel frame and plate coated with Teflon glass fabric to prevent the HMA sticking.

The pressure applied to the hydraulic press platens, and transferred to the polymer can be calculated on the basis of the load applied and the area of the platens. The maximum load capacity of the hydraulic press is 25 tons although up to 35 tons were reached in practice. The dimensions of the platens are: $20\text{cm} \times 20\text{cm}$. The pressure applied to the platens is obtained from Equation 4.1.

$$P_p = \frac{F_p}{A_p}$$
<div align="right">**4.1**</div>

where: P_p – pressure applied to the platens, Pa

F_p – force applied to the platens, N

A_p – area of the platens, $A_p = 20 \cdot 20 = 400\text{cm}^2 = 0.04\text{m}^2$

The force applied to the platens can be derived from Equation 4.2.

$$F_p = g \cdot L_p$$
<div align="right">**4.2**</div>

where: g – standard gravity, $g = 9.81\text{m/s}^2$

L_p – load applied to the platens, kg

By combining Equations 4.1 and 4.2, Equation 4.3 is derived.

$$P_p = \frac{g \cdot L_p}{A_p} \qquad\qquad \textbf{4.3}$$

Substituting the values for gravity and area into Equation 4.3, the pressure P_p can be expressed as:

$$P_p = 245 \cdot L_p \qquad\qquad \textbf{4.4}$$

Now assuming a maximum load applied to the platens of $L_p = 35$ tons ($35 \cdot 10^3 kg$), the pressure applied to the platens is $P_p = 8.6MPa$. The load is a more common parameter used in relation to polymer processing; therefore, it will be quoted in most cases.

4.3.1.2 Mould dimensions

Ten different moulds were used in the project for producing the various types and thicknesses of the samples. The moulds used for producing the HMA coating had internal dimensions of $9cm \times 9cm$ (external: $10.5cm \times 10.5cm$) and were permanently wrapped with Teflon coated glass fabric of thickness 0.15mm, with an adhesive layer. The thicknesses of these moulds were measured including the coating.

The moulds used for sample production had internal dimensions of $16cm \times 18cm$ (external: $21cm \times 23cm$). Various thicknesses were used, but the main samples were produced of 2.5 and 5mm thick moulds. When the HMA samples were produced of these moulds, they were covered with the Teflon coated glass fabric of thickness 0.25mm, without an adhesive layer.

The thickness of the square moulds for producing the HMA coating was measured in eight places, i.e. at two places along each side. The thickness of the rectangular moulds used for sample production was measured in ten places, i.e. at three places along both long sides, and at two places along both short sides. Their accuracy is influenced by the mould manufacturing process. Table 4.2 (page 93) lists the thicknesses of the moulds including mean values and the

standard deviations (SDs). The SD was calculated using a standard statistical Equation 4.5 (Taylor, 1982).

$$SD = \sqrt{\frac{\sum (x - \overline{x})^2}{n - 1}}$$

4.5

where: x – measured value

$\overline{x}$ – average (arithmetical mean)

n – number of measurements

Small SDs obtained (maximum value of 0.011mm) indicate that the thicknesses of the moulds were relatively uniform.

The stainless steel sheets, from which the moulds were obtained, were ordered from a steel manufacturer. The square moulds were laser cut and the rectangular moulds were wet died by experienced machine operators.

The process of the selection of sample and mould thicknesses and associated limitations are further explained in section 4.3.

4.3.1.3 Amount of material used for production of polyethylene sheet

Before polymer processing, the mould was filled with the polymer granules and introduced between the platens in the press. The amount of material to be used was calculated on the basis of the volume of each mould and the density of the polymer, plus a few extra grams were added based on experience. The required weight of polymer was estimated using Equation 4.6.

$$m_p = \rho_p \cdot V_m \qquad\qquad\qquad \textbf{4.6}$$

where: m_p – mass of the polymer, g

ρ_p – density of the polymer, $d_p \approx 1g/cm^3$ (see section 3.3.4, page 80)

V_m – volume of the mould, cm³

For the mould with internal dimensions of $0.5cm \times 16cm \times 18cm$, $V_m = 144cm^3$. Thus, the mass of the polyethylene used was 150g (including a few extra grams). When this mould was used for producing HMA samples, it was wrapped with Teflon coated glass fabric and a larger amount of polymer was used and proportionally thicker samples were produced. The weights of polymer used for particular moulds are listed in Table 4.2 (next section).

As from now the only mould dimension discussed will be thickness, the e.g. '5mm thick mould' will be described as '5mm mould' for simplification.

4.3.1.4 The compression moulding process

The compression moulding process was carried out in the following way. The platens of the press were electrically heated up to a temperature of 190ºC, which is the minimum processing temperature recommended by the manufacturer (Borealis, 2008). The mould with polymer granules sandwiched between the stainless steel plates was placed on the bottom platen. The platens were brought close together leaving a small space between the top plate and the top platen. The material was preheated without pressure for 5-15min, depending on the thickness of the mould as recommended by BSI (2007). The next stage involved applying a pressure. In the case of the thicker moulds (5 and 6mm) a low load of 10-15 tons was applied initially for 5min to make sure all the granules had melted. This was then increased up to 30-35 tons for 10min in order to release trapped air and excess material, which was squeezed out as shown in Figure 4.1. The choice of times and pressures for the thickest mould used is explained in

section 4.3.3. The times and pressures applied for specific moulds varied with regard to the mould thickness and are listed in Table 4.2.

Table 4.2 The parameters applied during compression moulding with regards to the mould thickness.

Thickness of the mould, mm			Weight of polymer, g	Heating up of polymer	Heating up of polymer under pressure	
Theoretical	Measured	SD		Time, min	Time, min	Load, tons
Moulds for HMA coating, internal dimensions: 9cm ×9cm						
0.8	0.834	0.008	8	5	5	10-15
0.9	0.929	0.004	9	5	5	10-15
1.2	1.188	0.003	11	6	5	10-15
1.5	1.481	0.008	13	7	5	10-15
Moulds for the polymers samples, internal dimensions: 16cm ×18cm						
1.5	1.469	0.009	45	8	5	12-17
2.5	2.414	0.006	74	9	5	18-23
3	3.016	0.001	91	10	5	18-23
4	4.032	0.011	121	12	10	25-30
5	4.906	0.007	146	15	5/10	15/30-35
6	5.894	0.006	175	15	5/10	15/30-35

The final stage involved switching off the heat supply and cooling water was released to pass through the platens of the press. The high pressure was maintained during the cooling stage. It took approximately 17min to reduce the temperature of the mould to 40-50ºC, depending on the platens, which did not cool uniformly. The parameters of the surrounding such as the temperature of the air and cooling water varied throughout the project and thus, might have influenced the cooling characteristics of the moulds. This is analysed in the next sections.

4.3.2 The effect of different cooling conditions

The changing cooling conditions need to be studied as the cooling process influences the degree of crystallinity of the polyethylene, which has a large effect on the mechanical properties of the material (Dusunceli & Colak, 2008). First, it was important to justify if the polymer sheet cools down uniformly across its width. However, the cooling rate could not be measured locally. Therefore, the density of the samples cut out from the middle and edges of the sheet was compared. Further, the influence of the air and cooling water temperature and also the impact of the platens' temperature and sample thickness on the cooling rate was determined by measuring the temperature of the top and bottom platen at specific time intervals. In each case, three experiments were carried out and the average was taken. The frequency of the measurement was higher at the beginning of the cooling process, i.e. when the temperature drop was faster. The average and maximum SDs of temperature measurement for the three experiments were 1 and 4ºC, respectively. Occasionally on the density of the samples produced under different cooling rate was compared.

4.3.2.1 The impact of the cooling system of the uniformity of polymer sheet across its width

Cawood (1980) suggests that in the picture-frame mould the material near the edge of the mould cools faster than the material in the centre as it looses the heat to the press platens as well as to the mould. As it solidifies first, the crystallinity and thus density of this material should be lower. However, the analysis of the samples taken from the middle and the edges of three moulded sheets produced under the same cooling rate indicated no considerable difference as the densities were 0.9566 and 0.9567g/cm³, respectively, with SDs of 0.0002 and 0.0004g/cm³. This suggests that the sheets are probably uniform. The way in which the moulds cool is related to the arrangement of the cooling system within the press platens. They

are probably more concentrated in the central part of the mould and thus the influence of the additional heat loss through the frame at the edges is balanced by the quicker heat lose through the press platens in the centre.

Further, the cooling characteristics for different cooling conditions were determined. Initially, the differences between the temperatures of the platens were investigated.

4.3.2.2 Cooling characteristics of the top and bottom platens

The cooling rates of the top and bottom platens were determined during cooling of the 5mm thick mould at a constant air temperature of 19ºC in order to justify the uniformity of cooling. Figure 4.4 shows the temperature-time relationship for both platens.
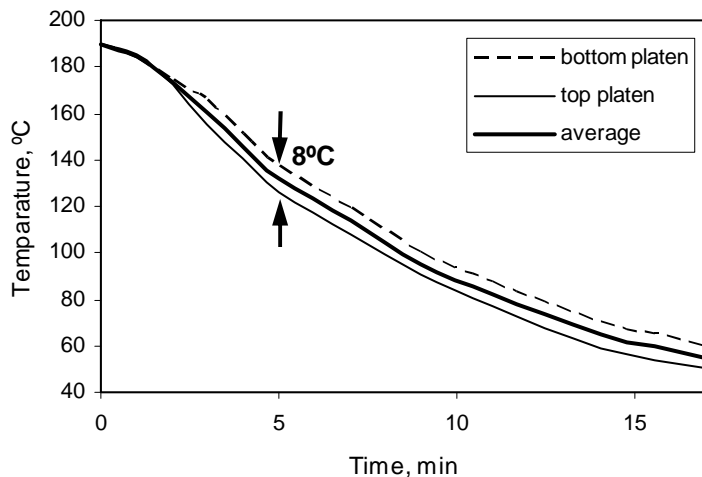
Figure 4.4 Cooling rate for a 19ºC air temperature.

From Figure 4.4 it can be seen that the cooling rate was equal to approximately 10°C/min, which is the same as used for the crystallinity determination in the DSC (section 3.2.3, page 70). There is a difference between the cooling rate of the top and bottom platen of around 8ºC. The difference is noticeable after 2min of cooling and increases slightly with time. Similar trends were observed for other temperature variations.

The heating and cooling water are supplied at the same rate to both platens. Therefore, this difference is attributed to the construction of the hydraulic press shown in Figure 4.1 (page 88). The bottom part under the platens has more metal elements to which the heat from the platens is transferred. Therefore, it takes longer to heat the bottom platen up and to cool it down. This slight difference in the cooling of the platens might have an impact on the uniformity of the properties throughout the thickness of the polymer in the mould.

In order to overcome this problem with the different temperatures, it was investigated whether starting with a higher temperature of the top platen would change the situation. Therefore, a test was carried out with an initial temperature of 200ºC for the top platen and 190ºC for the bottom platen at the same air temperature of 19ºC. The cooling rate for both platens is shown in Figure 4.5.
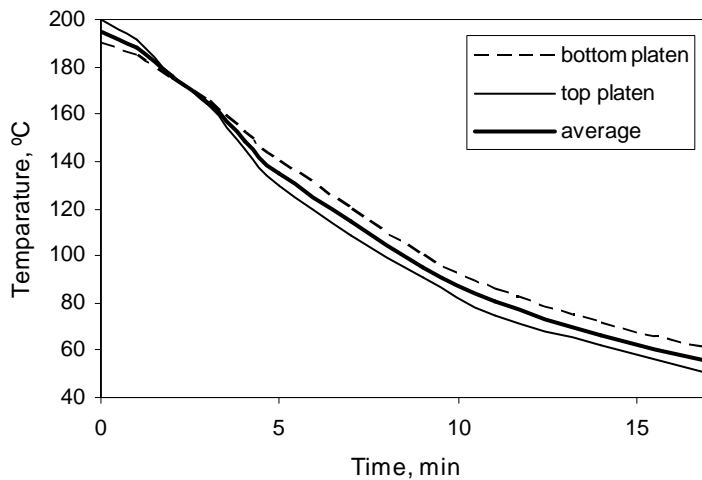
Figure 4.5 Cooling rate for a 19ºC air temperature when the top platen heated up to 200ºC and the bottom platen was at 190ºC.

From Figure 4.5 it can be seen that the top platen cools down more rapidly so after 2min both curves coincide and after 3min the temperatures start diverging again with the top platen still cooling down faster. After 5min there is no difference compared to when both platens started with the initial temperature of 190ºC (Figure 4.4). As the polymer starts to crystallize at

around 120ºC (section 3.3.3, page 78) achieved here after 6min, there is no benefit of using two different initial temperatures for the two platens when producing the polymer sheets. A platen temperature of over 200ºC was not considered as it was thought that the polymer might degrade when maintained at such a temperature for a long time.

In further analysis the cooling characteristic is presented as an average of the top and bottom platen.

As the air temperature varied between 16-25ºC during the production of the polymer sheets, its influence was analysed separately and is presented in the next section.

4.3.2.3 Effect of the air temperature

The air temperature could be controlled locally to some extent using an electric heater. The majority of the samples were produced in a temperature ranging from 19-22ºC.

The cooling characteristics for four different air temperatures were recorded and are shown in Figure 4.6. The temperature differences between the two extreme curves are marked on the graph in a few places.
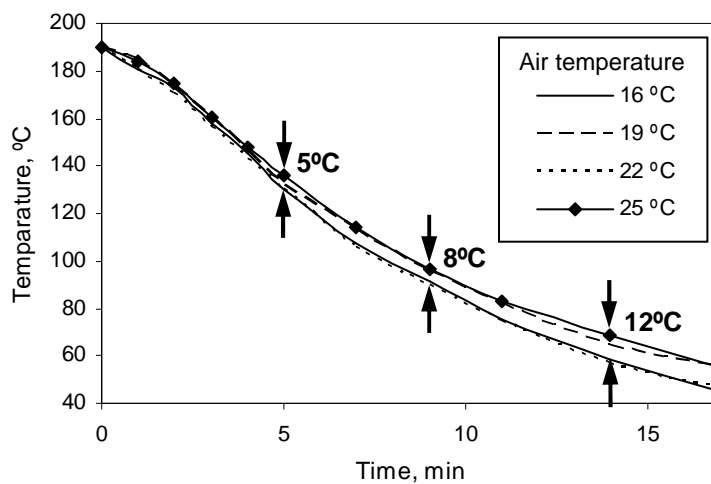
Figure 4.6 Cooling rate for varied air temperature.

97

Two groups of graphs can be distinguished in Figure 4.6. Faster cooling was characteristic for temperatures of 16 and 22ºC, while slower cooling was observed for temperatures of 19 and 25ºC. This is surprising as one would have expected the cooling characteristic to be similar for the two lower and the two higher air temperatures, respectively. Hence, this is suggesting that other parameters play a role in the cooling process. Therefore, the cooling water temperature was also investigated.

4.3.2.4 Effect of the cooling water temperature

Over a four month period (January to April) a temperature variation was recorded for the cooling water of between 8 and 14ºC. Figure 4.7 shows the cooling characteristics for two different cooling water temperatures (9 and 13ºC), and a constant air temperature of 22ºC.
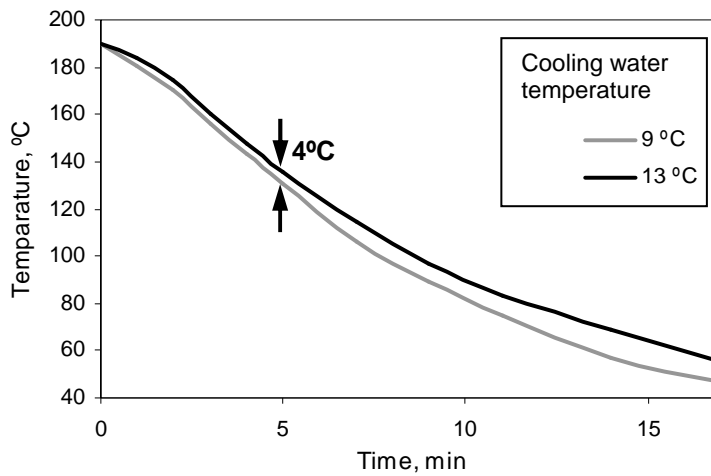
Figure 4.7 Cooling rate for different cooling water temperatures (9 and 13ºC) and constant air temperature (22ºC).

The curves for the two different cooling water temperatures are very close at the beginning and start to separate after 5min of cooling, at approximately 130ºC. This suggests that the variations in the cooling characteristics of the platens shown in Figure 4.6 are linked to the differences in the cooling water temperature. The impact of these differences on the density of the samples was determined. The densities were 0.9562 and 0.9566g/cm³ with SDs of 0.0003

and 0.0004g/cm³, for the samples cooled at 9 and 13ºC respectively, which is in agreement with the theory as the samples cooled slower reach higher density. However, due to the SD and measurement error (0.0004g/cm³) equal the difference between the results it is difficult to rely on them. Therefore, their impact on the tensile properties was also analysed and this will be discussed in section 5.2.1.

As temperature of cooling water cannot be controlled, some variations in the characteristics of samples due to the manufacturing conditions have to be accepted and considered when analysing the test results. In addition, it has to be noted that only two cooling water temperatures were compared, while it is possible that during the sample production the temperature reached even lower and/or higher values than recorded. Therefore, the resulting variations in cooling characteristics and thus, material properties might be even more significant.

In the case of HMA2 some samples were processed at the initial temperature of both platens of 210ºC, thus, the influence of the initial temperature on the cooling rate was also investigated.

4.3.2.5 Effect of the initial temperature of the platens

The cooling characteristics of the HMA2 samples processed at 190 and 210ºC were compared for a cooling water temperature of 9ºC. Figure 4.8 shows the results.
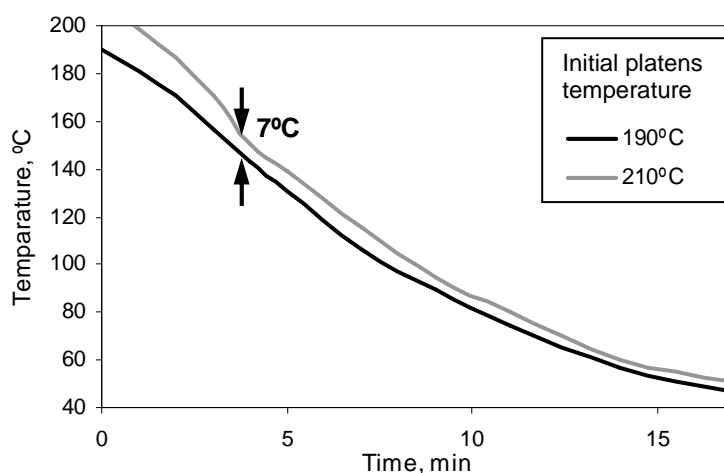
Figure 4.8 Cooling rate for the initial platen temperature of 190 and 210ºC with a cooling water temperature of 9ºC.

The cooling characteristics of the platens heated up to different temperatures differ. From the beginning, the curves come closer with time and after the first 4min the difference between them is significantly reduced (7ºC). As the HMA2 crystallizes in a temperature range of 60-120ºC (section 3.3.3), the difference between the cooling characteristics for both platen temperatures, even though small, might influence the crystallization process and thus the properties of the produced sheets. This was verified in the density test. The difference in the density of the samples taken from sheets moulded at these different conditions was small with values of 0.9350 and 0.9348g/cm³, for 190 and 210ºC respectively, with a SD of 0.0002g/cm³ equal the difference between the results what makes them unreliable. Although, the dependency is in accordance with the cooling rate results, i.e. the samples cooled at lower rate have greater density.

The influence of the mould thickness on the cooling characteristic was also studied.

4.3.2.6 Effect of the mould thickness

The cooling characteristics for the 5 and 2.5mm thick moulds were determined for the same cooling water temperature of 13ºC and at an air temperature of 22ºC. These results are shown in Figure 4.9.
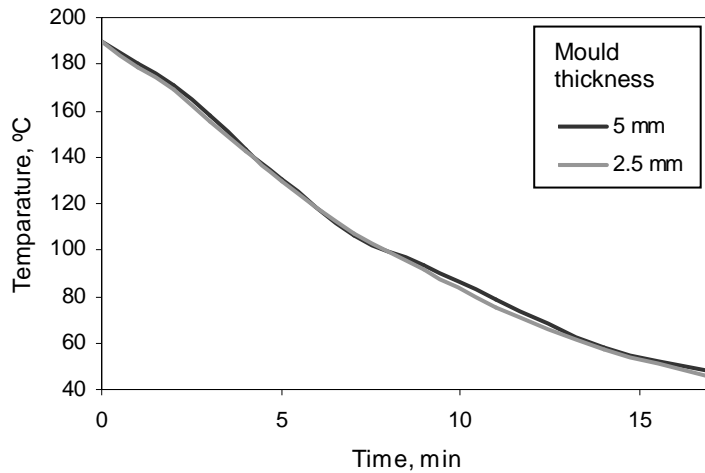
Figure 4.9 Cooling rate for the 5 and 2.5mm moulds for the cooling water temperature of 13ºC and air of 22ºC.

The curves for both moulds are very similar, which suggests that for these mould thicknesses they do not influence the cooling characteristics of the platens. This confirmed the density test, in which for both samples almost the same densities were obtained, being 0.9566 and 0.9565g/cm³, for the 4.2 and 2.2mm samples, respectively, with SDs of 0.0002 and 0.0004g/cm³ being larger than the small difference of 0.0001g/cm³.

4.3.3 Issues related to the sample thickness

It was important to investigate the parameters, which influence and limit the sample thickness used in the tests. Among them were polymer shrinkage due to the cooling process, delamination of the samples in the tests (lack of integrity), and the uniformity of sample thickness.

4.3.3.1 Shrinkage of polyethylene

During cooling of the polyethylene shrinkage occurs, which becomes increasingly important at thicknesses above 3mm (Cawood & Smith, 1980). As the thickness of the majority of the samples used in this project was above 3mm, determining the shrinkage rate was very important in order to judge the correct dimension for the mould as this is related to the sample thickness (ASTM, 2007b).

The shrinkage was calculated on the basis of the average thickness of the two moulds, 4 and 6mm thick, and the average thickness of two sheets produced from these moulds. The thickness of the frames and sheets is an average of ten measurements around the circumference, taken 15-20mm from the edges in the case of the sheets. The procedure for measuring the mould thickness was described in section 4.3.1.2. The dimensions are listed in Table 4.3.

Table 4.3 Dimensions of the sheets produced from two moulds.

	~ 4mm mould				~ 6mm mould			
	Mould	Sheet			Mould	Sheet		
		Sheet 1	Sheet 2	Average		Sheet 1	Sheet 2	Average
Thickness, mm	4.032	3.72	3.68	3.70	5.894	5.36	5.31	5.33
SD, mm	0.011	0.05	0.03		0.006	0.03	0.06	

Note: SD = standard deviation

The magnitude of the shrinkage can be calculated as:

$$S = \frac{h_m - h_s}{h_m}$$

4.7

where: S – shrinkage, %

h_m – thickness of the mould, mm

h_s – thickness of the sheet, mm

Thus, for the 4 and 6mm moulds the shrinkage is 8 and 10%, respectively. Cawood & Smith (1980) stated that the shrinkage is proportional to the mould thickness, and thus assuming a linear relationship the values for other mould thicknesses can be extrapolated.

It was considered appropriate to produce and test samples of two thicknesses, 3.32 and 6.64mm as these are typical for American Standards (e.g. ASTM, 2008a). The typical thickness for British Standards is 4mm (e.g. BSI, 2003b). On the basis of the shrinkage values obtained for 4 and 6mm moulds, the thickness of the moulds required to produce 3.32 and 6.64mm thick sheets could be estimated, as approximately 3.6 and 7.5mm, respectively.

Unfortunately, the stainless sheets from which the frames are manufactured are produced in limited standard thicknesses, i.e. in full millimetres for dimensions above 2.5mm. Therefore, it would be expensive, time consuming and probably impossible to mill the thicker sheets accurately to the desired thicknesses. Thus, it was decided to use the standard thicknesses available, i.e. 3 and 6mm. However, when the 6mm mould samples were tested in tension, problems with delamination and non-uniform sample thickness were observed.

4.3.3.2 Delamination of the samples

During preliminary tensile tests carried out on samples with chips, SC/0/90, delamination occurred. This suggested a lack of sample integrity and was attributed to the method of sample production, which is explained in detail in section 4.3.4.3. Basically, the chip was sandwiched between two thinner sheets, which were then reprocessed in the 6mm mould. The samples were cut out using a cutter available in the university laboratory (Figure 4.29b, page 121) and tested at 10mm/min.

The delamination started in the place of narrowing of the sample, usually before breaking (Figure 4.10). This phenomenon has also been observed by other researchers in reinforced polyethylene and polyethylene laminates (Argon & Bailey, 1974; Zhuang & Yan, 2006). They discovered that cracks emanated from fractures in reinforcing elements. However, in the current tests the chips did not break and it is speculated that the delamination occurred because the sheets did not remelt and did not bond properly during processing. Thus, the delamination was considered as the sample quality indicator. Delamination also occurred for different shapes of samples and testing speeds.

Figure 4.10 Delamination of the samples in tensile tests.

Beside the air and cooling water temperature, initial platens' temperature and mould thickness, the processing time and pressure have also an influence on the quality of the samples as indicated in the literature (BSI, 2007) and preliminary tests. The times and loads applied during the preliminary tests were: 10min of preheating and 8min of heating up under 15 tons. In order to prevent delamination and thus improve the quality of the samples, it was decided to reduce the maximum mould thickness to 5mm. To ensure complete remelting and bonding of the two sheets, the processing time was increased. The preheating was conducted for 20min and then the material was heated up for 10min under the same pressure of 15 tons.

The samples produced under these improved conditions, however, still delaminated. The temperature could not have been increased, as 190ºC is already 10ºC higher than recommended in the standard (BSI, 2007). In addition, heating the polymer for a long time at high temperature might cause its degradation. It was therefore decided to increase the load to 25 tons and keep the longer processing time. Under these conditions, the samples reached the

necessary quality and did not delaminate. However, there was another issue to investigate, the uniformity of the sample thickness.

4.3.3.3 Uniformity of sample thickness

The uniform thickness of the samples is important to draw meaningful conclusions from the different tests to be carried out. Reducing the mould thickness from 6 to 5mm and increasing the pressure from 15 to 25 tons not only eliminated delamination but also improved the quality of the sheets produced as can be seen in Figure 4.11.

(a)   (b)
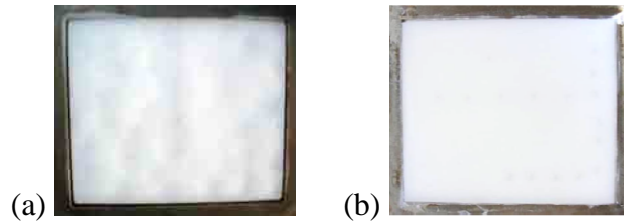
Figure 4.11 Wavy and smooth surface of the sheets produced from (a) 6 and (b) 5mm moulds.

As the maximum capacity of hydraulic press used in this project is ~35 tons, a few sheets were produced using this load. The differences between the sheets produced under 25 and 35 tons were not visible with the naked eye, therefore, the thicknesses of 20 samples cut out from these sheets were determined as an average of three measurements (Table 4.4).

Table 4.4 Thickness of the samples produced from 5mm mould under loads of 25 and 35 tons and width of the samples moulded under 35 tons.

Load, tons	25		35			
Dimension mm	Thickness		Thickness		Width	
	Average	SD	Average	SD	Average	SD
	4.41	0.01	4.28	0.01	12.59	0.02
	4.45	0.01	4.22	0.00	12.58	0.02
	4.46	0.02	4.23	0.02	12.55	0.03
	4.46	0.01	4.22	0.01	12.55	0.02
	4.5	0.02	4.30	0.03	12.58	0.03
	4.44	0.01	4.32	0.01	12.61	0.01
	4.47	0.01	4.14	0.05	12.61	0.01
	4.51	0.01	**4.22**	**0.05**	**12.62**	**0.04**
	4.42	0.01	4.18	0.04	12.60	0.01
	4.5	0.03	4.16	0.03	12.77	0.04
	4.54	0.02	4.12	0.01	12.62	0.01
	4.42	0.02	4.26	0.00	12.62	0.01
	4.56	0.08	4.16	0.00	12.62	0.02
	4.54	0.02	4.18	0.01	12.61	0.02
	4.46	0.01	4.30	0.00	12.64	0.01
	4.62	0.03	4.19	0.03	12.61	0.00
	4.37	0.03	4.23	0.01	12.61	0.01
	4.43	0.02	4.31	0.02	12.61	0.01
	4.52	0.02	4.24	0.02	12.61	0.01
	4.4	0.02	4.27	0.02	12.58	0.01
Average	4.47	0.02	4.23	0.02	12.61	0.02
SD	0.06		0.06		0.04	
Max SD		0.08		0.05		0.04

Note: marked bold – sample with maximum SDs of the thickness and width.

The uniformity of individual samples cut out from the sheets produced under different conditions was determined on the basis of the average and maximum SDs. The values were respectively 0.02 and 0.08mm for '25 tons sheet' and 0.02 and 0.05mm for '35 tons sheet'.

Due to better uniformity of latter samples, this load was applied in further tests when producing the sheets from the 5mm thick mould.

Some samples were also produced from a 2.5mm mould in order to investigate the thickness effect. The production of thinner sheets was more effective as the level of shrinkage and surface non-uniformity is smaller for thinner sheets (Cawood & Smith, 1980) and a lower load could be used.

4.3.4   Production of the samples with chips at different arrangements

In order to test the effect of an inclusion on the mechanical properties of polyethylene, there was a need to introduce the chips into the polyethylene. No examples were found in the literature where inclusions were introduced into polyethylene in the compression moulding process. A new technique therefore had to be developed. Three different types of procedures were developed depending on the required chip orientation, i.e. on the surface (surf), inside parallel (0/90) and perpendicular (90/0, 90/90, and 90/45) to the sample surface. These procedures are described in the following sections.

The sample codes are listed in Table 4.1, page 86.

4.3.4.1 Preliminary experiments related to sample production

Some preliminary experiments were carried out in order to determine the challenges related to producing compression moulded samples containing silicon chips. As a first step, the mould was filled with polymer granules and the LSQ chips were placed on the surface, as shown in Figure 4.12. It was noticed that due to processing the chips moved slightly. For example, some rotated (1, 2, 4), some moved towards the centre of the mould (4, 5), chip 3 moved towards the edges of the sheet, and some sunk into the polymer (1, 2, 5).
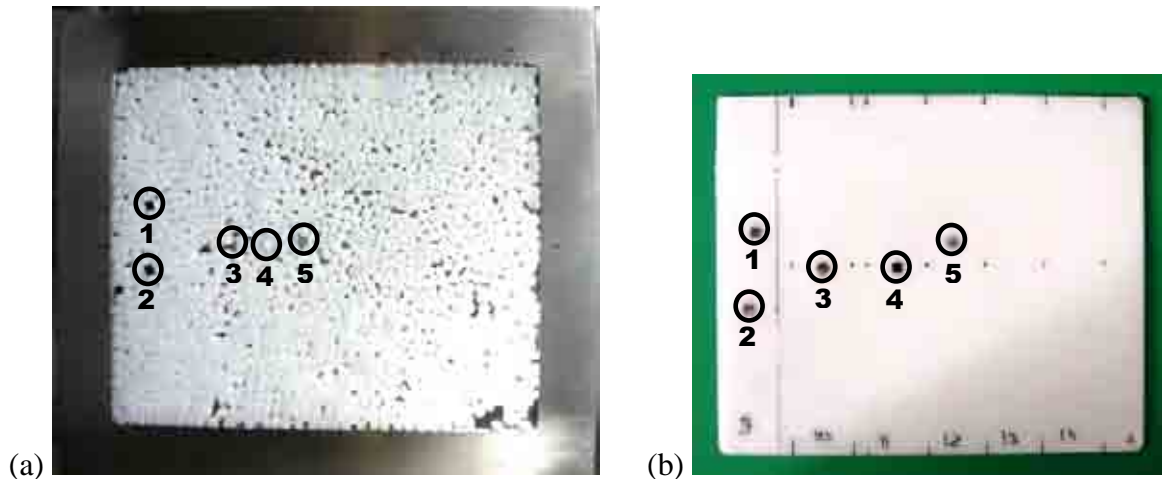
Figure 4.12 Polymer sheets with silicon chips on the top surface: (a) before and (b) after processing.

In the next experiment the mould was first filled with polymer and then the chips were placed on the bottom of the mould under the granules, however, still three out of eleven chips sunk, thus the method of sample production required improvement.

The square chips rotated, which was unavoidable and it could have an effect on the mechanical properties of the samples, therefore circular chips were considered for further tests. The choice of chip shapes and sizes is further discussed in section 4.3.6.

4.3.4.2 Samples with chips on the surface

The problem with the production method described in the previous section was that the chips were penetrating between the polymer granules. In the case when the polymer forms a smooth surface without any gaps, it is less likely that the chips will penetrate into the polymer and change its orientation. It was therefore decided to first produce a plain polymer sheet and then reprocess it with the chips on the surface. As the polymer shrinks during cooling, the plain sheet had to be from a mould thicker than the one from which the ultimate samples were made. Therefore, to produce 5mm mould samples, the 6mm mould was used for producing the initial plain polymer sheet (for the 2.5mm mould samples the 3mm mould was initially used).

The plain polymer sheet produced from the 6mm mould was placed in the 5mm mould. Due to the polymer shrinkage, the sheet was slightly smaller than the frame. The free space was filled with additional polymer granules (Figure 4.13a). The chips were put on the surface at a distance, which allowed samples to be cut from the sheet. In the case of tensile test samples their width was 25mm (see section 4.3.6.3), so the chips were placed approximately 28mm from each other. The safety margin was required as the chips could still move during polymer flow in the reprocessing procedure. The same rule was applied to other sample widths and chip orientations. Increasing the safety margin would have reduced the number of samples which could be made from one sheet. The arrangement used for the SC chips, before and after processing is shown in Figure 4.13.
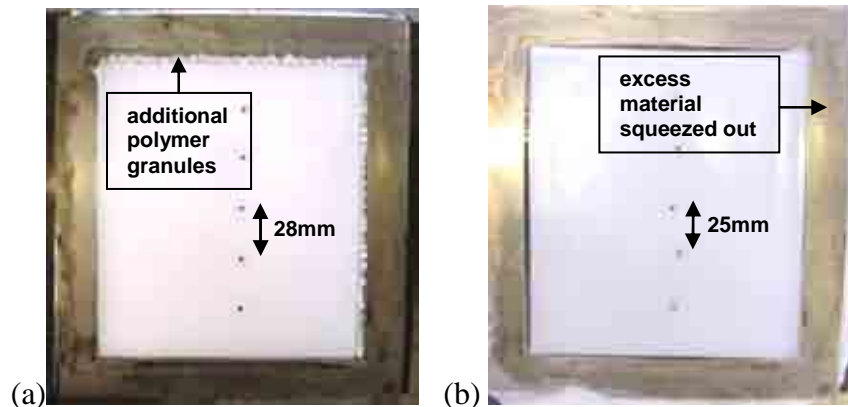
Figure 4.13 Production of the samples with chips on the surface: (a) before and (b) after processing.
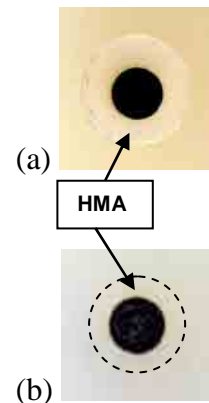
Figure 4.14 Chip coated with HMA, (a) before and (b) after processing.

There was a lot of excess material as the plain sheet was produced from a thicker mould. This excess was squeezed out once the pressure was applied (Figure 4.13b). It can be seen that the chips did not move significantly using this production process. However, the safety margin was useful as even though the distance between some chips reduced after processing, the planned number of samples could still be cut out from the sheet.

Some of the chips introduced into the polyethylene were coated. The techniques used to coat the chips are described in section 4.3.5. The polyethylene samples with the coated chips were produced in the same way as the samples with plain chips. When HMA was used as a coating to increase the bond between the polymer and the chip, it was hardly visible after processing, as shown/marked in Figure 4.14b.

The preliminary tests showed that there is no adhesion between the chip and the polyethylene unless the coating is used. The plain chip can be easily detached from the sample surface, where it remains only because it is tightly clamped within the matrix. The roughness of the chip, which is different on both sides, does not change this behaviour. This differs from the results of Zhang & Tanner (2008) and Joseph at al. (2002), who observed that the surface roughness of ceramic fillers influenced the interfacial bonding. However, the differences in the surface morphology of two compared particles were at the nanometre scale while here they are at the micrometer scale.

The production of the samples with chips inside posed new challenges. The procedures developed for these samples are described in the next section.

4.3.4.3 Samples with chips included inside parallel to the surface (0/90)

In order to produce the samples at the orientation 0/90, the chips were placed between two thin polymer sheets and reprocessed in a thick mould. The 5 and 2.5mm mould samples were made from two 3 and two 1.5mm mould sheets, respectively. Initially, the thin sheet was placed in the thick mould. The chips were then placed on top of this sheet at appropriate distances (Figure 4.15a), as explained in the pervious section, and covered with the second thin sheet (Figure 4.15b). Finally, this sandwich arrangement was reprocessed. This procedure is similar to the way in which polyethylene laminates are produced (Ingham, 2003).
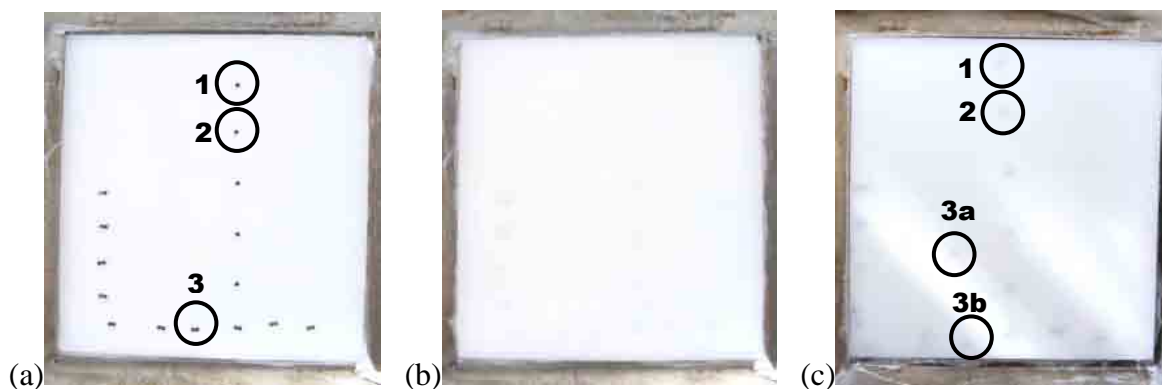
Figure 4.15 Production of the samples with chips at an orientation 0/90: (a & b) before and (c) after processing.

Pairs of chips were placed around the edges of the sheet to produce small square samples for X-ray scanning (Figure 4.15a). Due to polymer flow during the processing, chips 1 and 2 moved (Figure 4.15c). Most pairs of chips around the edges moved apart, e.g. chip 3a totally separated from its neighbour, chip 3b.

The majority of the chips moved to the left, which suggested that the press was not exactly horizontal. However, the level was measured with a spirit level and it turned out that the press was horizontal and hence could not have caused the observed movement of the chips, unless the deviation in level was too small to be detected by this measuring technique. The production of a sheet made from granules of two colours helped to determine the direction of polymer flow, and this is discussed in the next section.

4.3.4.4 Polymer flow during compression moulding

As the HMAs and HDPE matrix have the same colour, the optical observation of the interface and dispersion of HMA is very challenging (see Figure 4.14). Colouring of HMA might help but the required equipment was not available. Therefore, the hot press was utilized to mix it with the blue pipe-grade HDPE, as shown in Figure 4.16a. The mixing process was not effective, however, from the experiment it became clear in which direction the polymer flowed (Figure 4.16c).

(a)   (b)   (c)
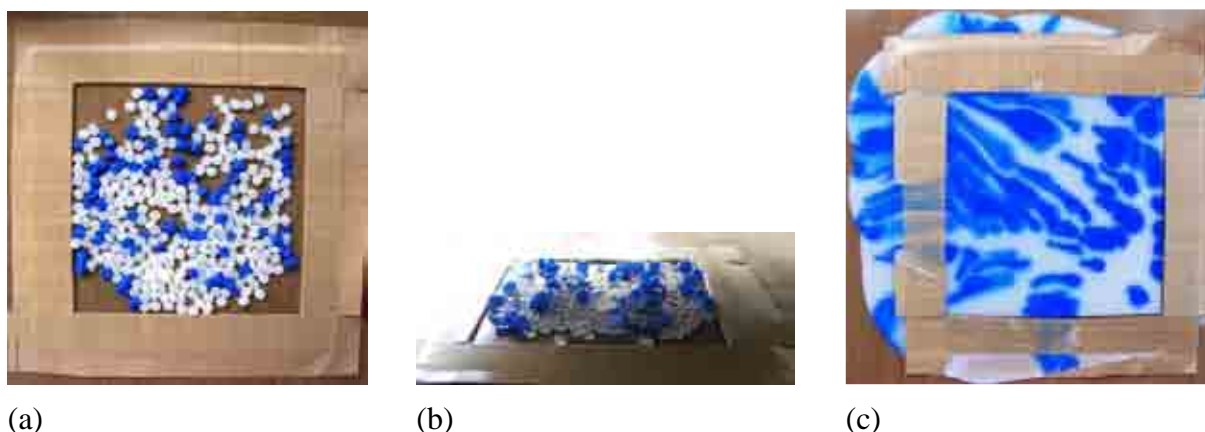
Figure 4.16 Polymer flow in the mould during compression moulding using a mixture of natural colour HMA and blue pipe-grade polyethylene: (a) granules before processing, (b) heated up granules in the press, (c) produced polymer sheet.

It can be seen that the polymers moved towards the top and left of the mould (Figure 4.16c). The granules in the centre moved less. As the chips for the test samples are placed centrally, they are not so affected by the polymer flow. However, due to the slight chip movement towards the left of the mould it was better to place them slightly on the right, as shown in see Figure 4.13a. The length of the test samples (maximum 12.5cm for the tensile test) is smaller than the width of the mould (16cm). Therefore, there is automatically a large safety margin for the movement of the chips along the length of the future test samples.

The polymer flow pattern was taken into account by arranging the chips in production of the samples with other chip orientations.

4.3.4.5 Samples with a chip inside perpendicular to the surface (90/0 and 90/90)

The production of test samples containing chips perpendicular to the surface was more complicated. In this case initially a plain sheet or sheets were also made. For 5mm mould samples with LC chips the initial sheet was made of 6mm mould. In the case of a 90/0 orientation, it was cut into pieces slightly wider than the intended width of the samples, using a band saw (Figure 4.17a and b, respectively). The cut edges were rough (Figure 4.17c) and the excess material was removed using a razor blade (Figure 4.17d).

The polymer pieces were then placed in the 5mm mould and the chips were vertically positioned between them, at the same level slightly right of the centre (Figure 4.17e), as the polymer moves to the left when it flows. The sheet was then reprocessed.
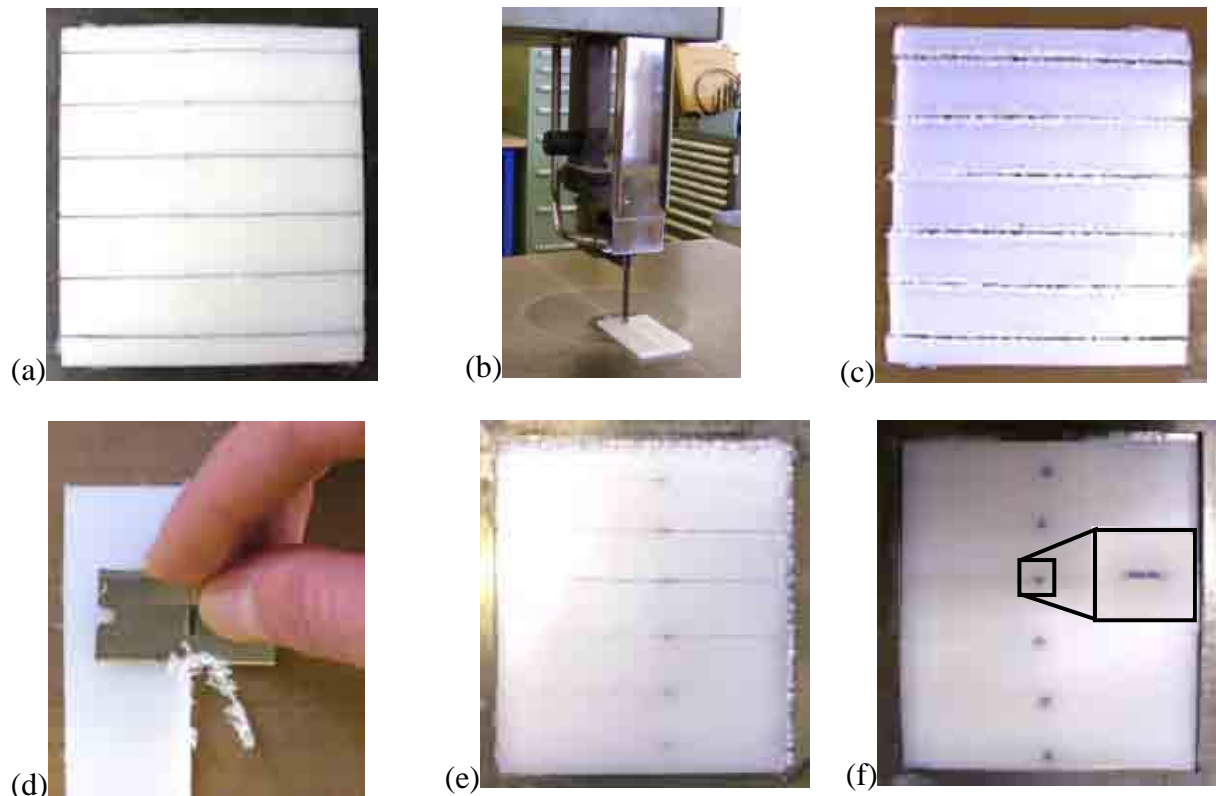
Figure 4.17 Production of the sheets with chips at the orientation 90/0: (a) marked up polymer sheet, (b) cutting the sheet using a band saw, (c) sheet cut into pieces, (d) removing the excess material from the edges, (e) pieces of polymer in the mould with chips in between, (f) the final processed sheet with zoomed in section of the smaller black square.

Unfortunately, producing samples using these procedures was very variable in terms of obtaining the correct chip orientation. Sometimes only one sample could be successfully obtained from a sheet, as shown in Figure 4.17f.

When producing the samples from the 2.5mm mould with SC chips at the same orientation, a sheet using the 3mm mould was produced, cut into pieces, and reprocessed with the chips included. In the case of 5mm mould samples with SC and SSQ chips, two plain polymer sheets were produced and reprocessed. The sheet from the 1.5mm mould was placed on the bottom of the final 5mm mould. The sheet from the 4mm mould was cut into pieces, which

were then placed on top of the sheet from the 1.5mm mould. The chips were placed between these pieces. This modification was required as it was hard to maintain the small chips in a vertical position between the pieces from the sheet from 6mm mould.

In order to produce the samples with LC chips at an orientation 90/90, the sheet from the 6mm mould was cut along into two pieces. The chips were placed in a vertical position, between these pieces, and the sheet was reprocessed in a 5mm mould. The procedure for small chips and thin samples was modified, i.e. thinner moulds were used for production of the samples. Figure 4.18 shows the SC chip arrangement before and after processing.

(a)   (b)
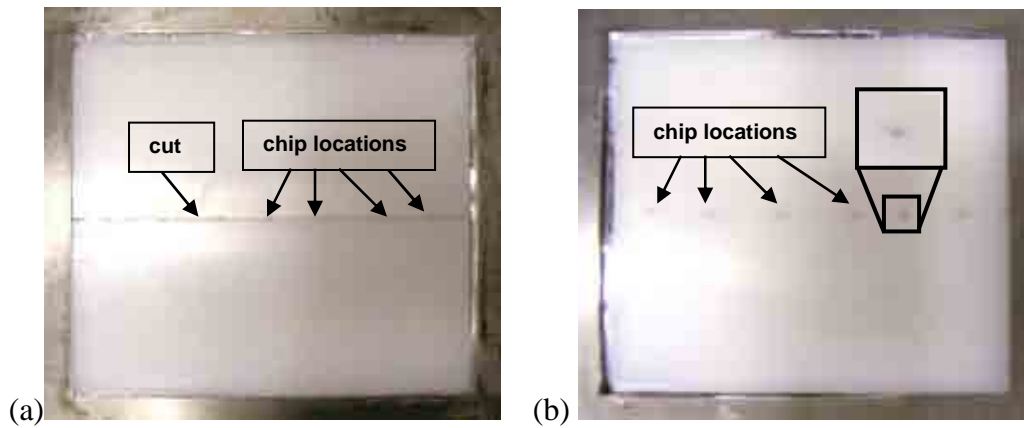
Figure 4.18 Production of the samples with chips at an orientation 90/90: (a) before and (b) after processing with zoomed in section of the smaller black square.

4.3.4.6 Samples with the chip at intermediate orientations

In the case of SC chips, intermediate orientations were also tested, for example 45/90, 45/45, and 90/45. The 45/90 orientation was achieved by cutting out the samples produced by a method described in the previous section, at a 45° angle, as shown in Figure 4.19. The 45/45 and 90/45 orientations were produced by using 'discarded' samples from the production of
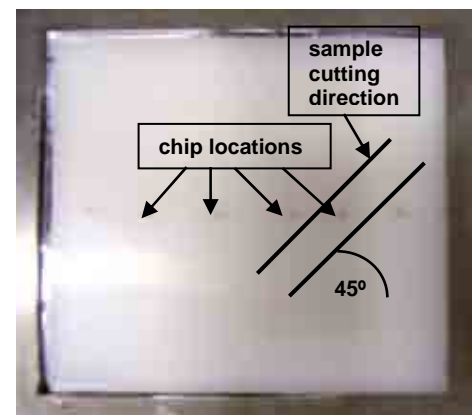
Figure 4.19 Sample cutting used for the 90/45 chip orientation.

the other chip orientations, i.e. where the chip had moved during production.

The chips with correct orientation were selected with the naked eye and the samples were cut out. In order to verify this selection the samples at different orientations were X-ray scanned and the examples are presented and discussed while analysing the data in Chapter 5.

4.3.5 Coating the chips

Three different types of coating were used in order to modify the adhesion between the silicon chip and the polyethylene, i.e. two HMAs, photoresist and Teflon. The techniques of coating the chips with different materials are described in this section.

4.3.5.1 HMA coating

In order to coat the samples with HMA, the chips were placed on or between two HMA sheets and processed in a similar way to the samples with the chips on the surface or inside (see sections 4.3.4.2 and 4.3.4.3). Different thicknesses of the coating were produced. The minimum thickness of the mould used was limited by the minimum thickness of the stainless steel sheets produced (0.5mm), including the Teflon coated glass fabric wrapping (0.15mm) to ensure a non-stick surface.

In the case of a coating only on one side, the HMA sheets were first produced from 0.9 and 1.5mm moulds. They were then placed in the 0.8 and 1.2mm moulds, respectively, with the chips on the surface and reprocessed (Figure 4.20).

(a)   (b)
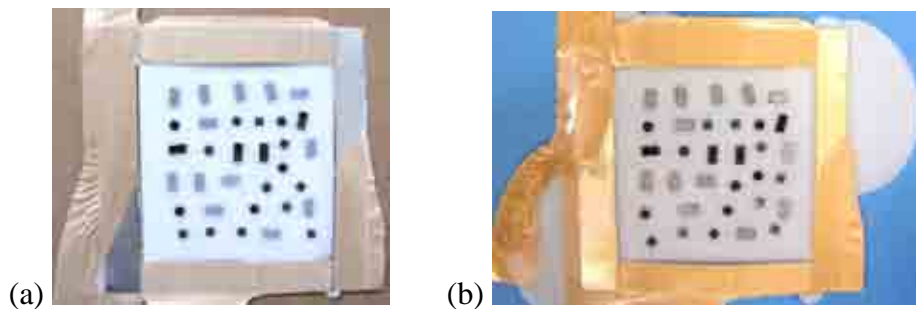
Figure 4.20 Chips with a coating of HMA on one side (a) before and (b) after processing.

As can be seen in Figure 4.20, the chips did not move much during the processing.

In the case of chips with a coating on two sides, the chips were placed between two sheets produced from 0.8 and 0.9mm moulds in order to produce the 1.2 and 1.5mm mould samples, respectively.

4.3.5.2 Photoresist coating

The photoresist coating was produced by a colleague using a MEMS manufacturing process called photolithography. The theoretical thickness of the photoresist layer should be $9\pm0.04\mu m$.

4.3.5.3 Teflon coating

The Teflon was manually sprayed over the samples. The chips were held by tweezers and the spray was applied from both sides. The chips were then left in a vertical position to allow the coating to set.

4.3.5.4 Thickness of the coating

The thickness of each type of coating was measured for five samples and the averages and SDs were calculated. The thickness of the coating on the surface of the chip was obtained by deducting the thickness of the chip (0.5mm) from the measured thickness of the chip with the coating. In the case of a coating on two sides, this value was divided by two. It has to be noted that the coated surface was usually uneven and due to the small size of the chip and measuring method (micrometer), the maximum thickness was recorded. Table 4.5 lists the thicknesses of different coatings on the chip surface.

Table 4.5 Thicknesses of different coatings on surface of the chip.

| Coating | Thickness of the chip with coating, mm | | Thickness of the coating, mm |
	Average	SD	Average
Coating on one side			
HMA1 thin	0.76	0.01	0.26
HMA1 thick	1.10	0.01	0.60
HMA2 thin	0.73	0.01	0.23
Coating on two sides			
HMA1 thin	1.05	0.02	0.27
HMA1 thick	1.35	0.04	0.42
HMA2 thin	1.04	0.03	0.27
Photoresist	0.536	0.004	0.018
Teflon	0.56	0.01	0.03

From Table 4.5 it can be seen that the 0.018mm photoresist coating had a thickness twice as large as the theoretical value of 9µm (section 4.3.5.2), however, it is in the thickest place.

The thickness of the coating on the side of the chip was obtained by deducting the diameter of the chip (2.26 and 4.52mm for SC and LC chips, respectively) from the measured value of the diameter of the chip with the coating, and dividing it by two. For each of the five samples, the diameter of the chip with the coating was measured in two places. The values are the same for chips coated with both HMAs as they were cut out using the same method (section 4.3.6.2). Table 4.6 lists the thicknesses of different coatings on side of the chip.

Table 4.6 Thicknesses of different coatings on the side of the chip.

Coating	Thickness of the chip with coating, mm		Thickness of the coating, mm
	Average	SD	Average
HMA on SC	4.75	0.05	1.25
HMA on LC	6.43	0.07	0.96
Photoresist	2.27	0.01	0.005
Teflon	2.26	0.01	-

From Tables 4.5 and 4.6 it can be seen that, on the side of the chip, the photoresist coating was very thin while the sprayed Teflon coating was not detected at all.

4.3.6   Choice of sample dimensions and methods of cutting them out

In this section the reasons behind the choice of sizes for the test samples and chips are discussed. In addition, different methods used to cut out the samples and silicon chips are described.

4.3.6.1 Silicon chips

The silicon chips were produced from 0.5mm thick wafers (Gad-el-Hak, 2002). Traditionally, these have a square shape and hence, initially chips of $4\text{mm} \times 4\text{mm}$ (LSQ) were produced. Preliminary experiments related to the sample production showed that the chips rotated during the processing procedure (section 4.3.4.1), which had an influence on the test results as illustrated in Figure 4.21. Beside the orientation, the chip size influenced the mechanical behaviour (see Figure 4.22). Therefore, for further test the circles of two sizes were used.
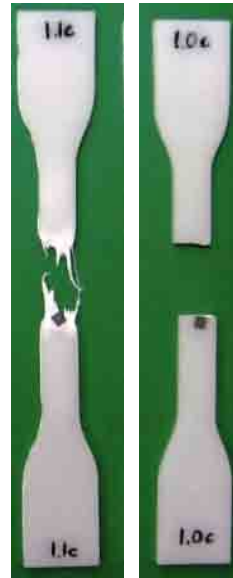
Figure 4.21 Broken tensile samples made from the off-the-shelf polyethylene with LSQ chips on the surface, at different orientations.
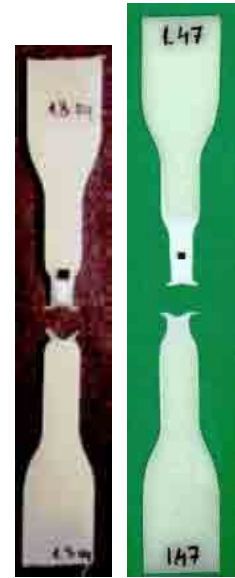
Figure 4.22 Broken tensile sample made from the pipe-grade polyethylene with LSQ and SSQ chips on the surface.

In order to investigate the chip shape effect a small square (SSQ) of size $2\text{mm} \times 2\text{mm}$ was also tested. The area of the square and the circle was kept constant, hence the resulting diameter of the small circle (SC) was 2.26mm. This allowed the same volume and contact area to be kept between the surface of the chip and the polymer. In addition, as the silicon chip is being used as a basis for a microsensor, the chips with the same surface area available for the construction of a sensor should be compared. The area of the large circular chip (LC) was four times larger, i.e. 16mm², with a corresponding diameter twice as large, i.e. 4.52mm.

The silicon chips were cut to size by colleagues using MEMS manufacturing techniques. The squares and rectangles were obtained by dicing the wafer with a diamond blade. The diced wafer is shown in Figure 4.23. The circles were obtained using an etching technique.

A special mask with circles marked on it was designed. The wafer was coated with a photoresist and exposed to UV light. Due to selective dissolution of the photoresist between UV exposed and un-exposed areas, the circles were separated from the wafer, as shown in Figure 4.24 (FSRM, 2003).

Figure 4.23 Wafer diced into square chips using a diamond blade.

Figure 4.24 The circles cut out from a wafer using an etching technique.

4.3.6.2 Chips coated with HMA

In order to cut out the coated chips, the intended cut lines were marked on the HMA sheet around the chips, as shown in Figure 4.25. The HMA envelope left around the chip was approximately 1-2mm (the exact dimension for the circles was given in Table 4.6). The accurate dimensions of different coatings were already listed and discussed in section 4.3.5.4.

The squares and rectangles were cut out using scissors, while the circles were cut out with punches (Figure 4.26). The punch was placed against the mark on the sheet and hit with a hammer as illustrated in Figure 4.27. The cut out chips surrounded by HMA are shown in Figure 4.28.
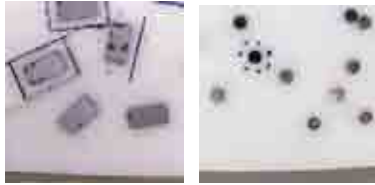
Figure 4.25 Intended cut lines marked around rectangular and circular chips.

Figure 4.26 Punches.

Figure 4.27 Cutting out the circular chip from the HMA sheet using a punch.

Figure 4.28 Chips surrounded by the HMA.

4.3.6.3 Tensile samples

The samples for the preliminary tests were produced using the dumbbell shape cutters available in the university laboratory. The preliminary tests on samples produced using cutter (a) indicated that they do not break (Figure 4.30), thus do not reach the strain at break (Figure 4.31) within the range of the tensile instrument.
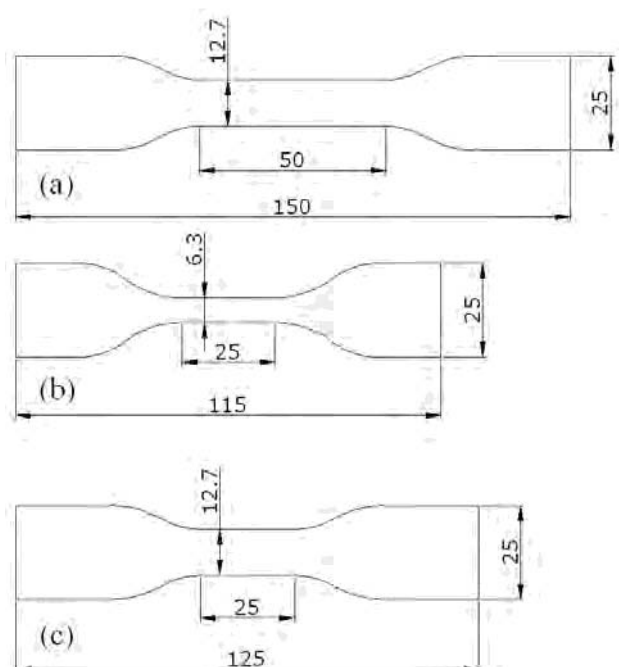
Figure 4.29 The dimensions of the dumbbell shape cutters/samples.
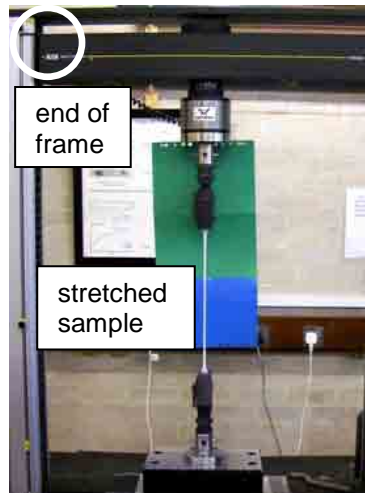
Figure 4.30 Stretching of the sample using cutter (a) shown in Figure 4.29, stopped due to limitations of the frame.
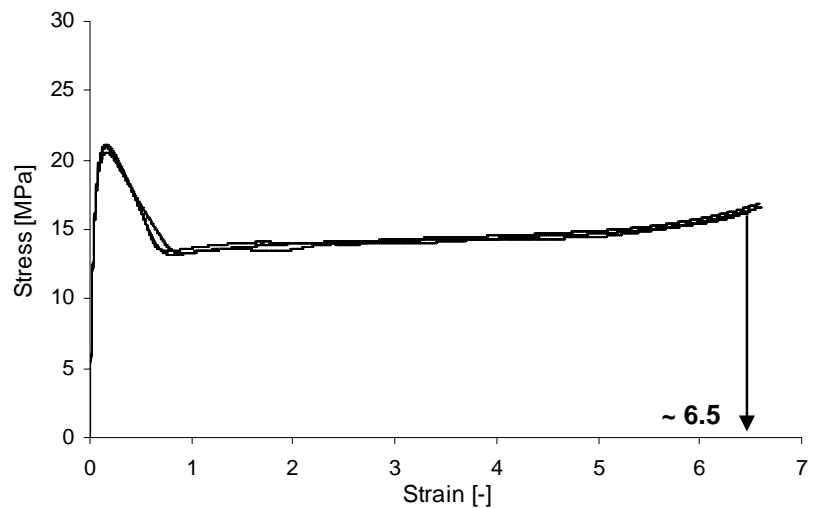
Figure 4.31 Example stress-strain relationships for tensile samples using cutter (a) in Figure 4.29.

The samples produced using cutter (b) (Figure 4.29b) broke; however, when they contained a chip, it moved out from the necked polymer during the test due to a too narrow gauge and thus neck of the sample. In consequence, the samples did not break in the vicinity of the chip and the strain at break was similar for the samples with and without a chip (Figure 4.32) even though the chip significantly affected the integrity of polyethylene.
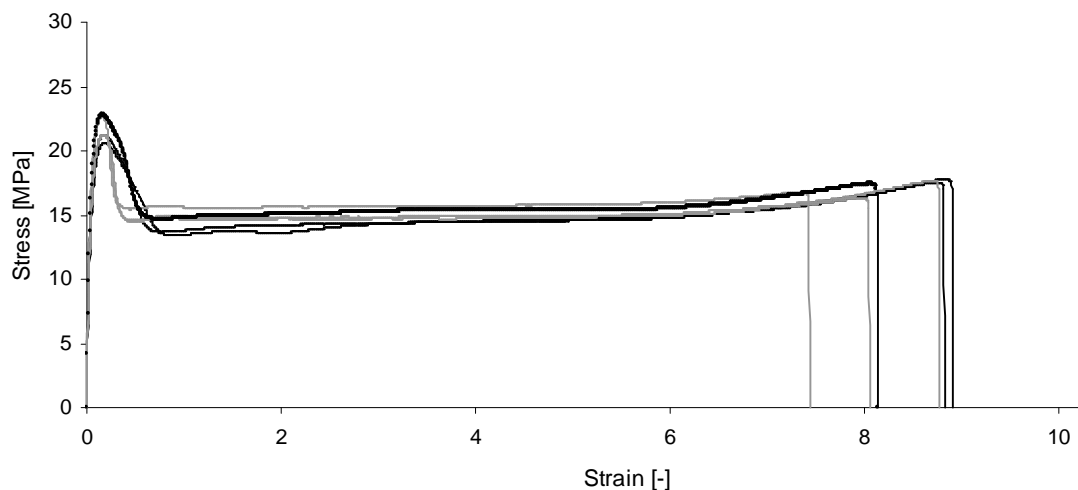
Figure 4.32 Example stress-strain relationships for 4.2mm thick samples produced using cutter (b) in Figure 4.29: (——) plain sample and (——) with a chip.

122

Beside the geometry of the sample this behaviour might have also been influenced by some edge irregularities, resulting from a blunt cutter, which might have dominated the chip effect.

It was decided to design a new cutter, which combines the advantages of both the existing cutters, i.e. a wide (Figure 4.29a) and short (Figure 4.29b) gauge region containing the chip even when the sample necks, and also ensuring that the sample would break within the range of the instrument. Its dimensions are presented in Figure 4.29c. The width of the gauge was limited by the width of the clamps of the Instron machine (25mm), so the gauge could not be wider than for the cutter (a), i.e. 12.7mm, which value is in accordance with ASTM (2008d). The proportion of the gauge width and length as in BSI (1996b) was maintained, where they recommend the values $25.4\text{mm} \times 50\text{mm}$. In addition, Hartest Precision Instruments Ltd. (2009) were consulted and they stated that the cutter dimensions are not critical.

Thus, the cutter based on the dimensions of cutter (a) (Figure 4.29), with a reduced gauge length of 25mm and thus total length of 125mm (Figure 4.29d), should allow for a maximum strain of the sample of 14. This value is based on the results for a sample from cutter (a) (strain at break of 6.5). The new cutter gauge length is half of that for cutter (a) gauge (50mm), thus, the strain at break should reach $2 \cdot 6.5 = 13$. In addition, the sample is 25mm shorter than a cutter (a) sample, which allows for an extra strain of 1. So the gauge length of 25mm should be enough considering that all the failed samples reached a maximum strain of 9.

In the cutting procedure a hydraulic press, similar to the one used for compression moulding was utilized to apply pressure to the cutter. To ensure the chip was centrally located in the sample, a ruler was used and the sample/cutter position marked clearly on the moulded sheet. The sheet with a cutter accurately positioned (Figure 4.33) was placed in the hydraulic press (Figure 4.34). The pressure was applied and the sample cut out.

Figure 4.33 Cutter positioned on the polymer sheet.   **Figure 4.34 Cutting process using the hydraulic press.**
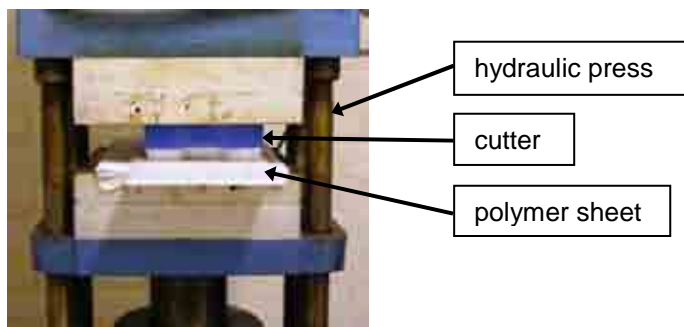
The edges of the samples cut from the off-the-shelf polyethylene sheets were rough and thus required smoothing with grading paper to obtain a uniform sample width. In Figure 4.35, the central parts of the pipe-grade polyethylene and off-the-shelf samples with rough and polished edges are shown.

(a)   (b)   (c)
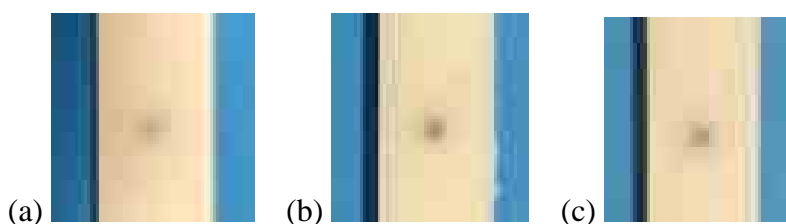
Figure 4.35 Edges of the polyethylene samples: (a) pipe-grade sample, (b) off-the-shelf sample with rough and (c) with polished edges.

4.3.6.4 Flexural, creep, and Charpy impact samples

Due to the rectangular shape of the samples used for the flexural, creep and Charpy impact tests, they can be cut out using many different techniques in contrast to the dumbbell shape tensile samples. The effectiveness of two available techniques was verified by comparing the theoretical width of the preliminary samples with their actual width obtained after cutting. The uniformity of the width and thickness of the sample is very important for the accuracy of the measurements.

The aim was to cut the samples so that the chip was in the centre of the sample. Figure 4.36a shows rectangular samples cut using a guided band saw and Figure 4.36b shows samples cut using a silicon carbide blade cutter with water cooling.

(a)   (b)
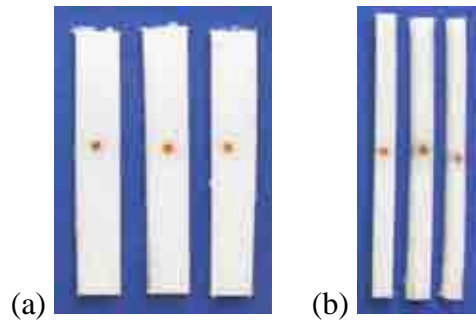
Figure 4.36 Samples cut using (a) guided band saw, (b) blade cutter using water cooling. Note: as the chips inside the samples were not visible in the picture, their approximate positions were marked on the sample surface.

sample in the holder
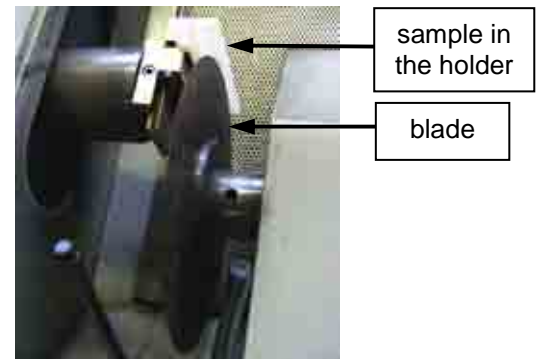
blade

Figure 4.37 Blade cutter with water cooling.

Table 4.7 shows the theoretical and actual widths of the samples. The widths were obtained as an average of three measurements along the sample. The SD therefore gives an indication of how uniform the samples were across their length.

Table 4.7 Theoretical and actual widths of the samples cut using different methods; all dimensions in mm.

Theoretical width	Actual width	SD	Difference between theoretical and actual width
Guided band saw			
12.7	13.29	0.14	0.59
12.7	12.48	0.21	0.22
12.7	12.99	0.46	0.29
	Average: 0.27		0.36
Wet blade cutter			
7	6.01	0.03	0.99
6.5	5.79	0.05	0.71
5	4.62	0.08	0.38
	Average: 0.05		0.39

From Table 4.7 it can be concluded that cutting with a wet blade cutter (SD of 0.05mm) produced much more uniform samples than cutting with a band saw (SD of 0.27mm). Although the difference between the theoretical and actual widths was slightly larger when using the wet blade cutter, this method was considered the most effective. Appropriate adjustments of the sample arrangement would reduce this difference. In addition, in this technique the chips were more centrally located. The disadvantage of this method was the time required to cut one sample, which was around 40min. Each sample had to be fixed in a holder separately. In addition, there was extra material required (around 10mm) to set the sample deeply.

Due to the shortcomings of both methods it was decided to order the type of cutter and utilize the method, which was used to produce tensile samples and produced even more uniform samples than the wet blade cutter. Due to cost issues, only one cutter could be ordered and thus the dimensions of the rectangular samples had to be unified. The width of the samples was chosen to be equal to the width of the gauge in the tensile samples (12.7mm). This is also a typical sample width recommended in the American Standards on flexural (ASTM, 2007c), creep (ASTM, 2001), and Charpy impact tests of plastics (ASTM, 2008b). The length of the cutter was 120mm so any sample up to 120mm long could be obtained. The choice of length of the samples associated with the testing procedures and other parameters is explained further in sections 4.4.2.1 (for the bending mode) and 4.4.4.1 (for the impact mode).

Some of the rectangular samples for the Charpy impact test were additionally notched. This was done using a Charpy notch machine (Figure 4.38). Figure 4.39 shows an example of a rectangular sample with a notch.
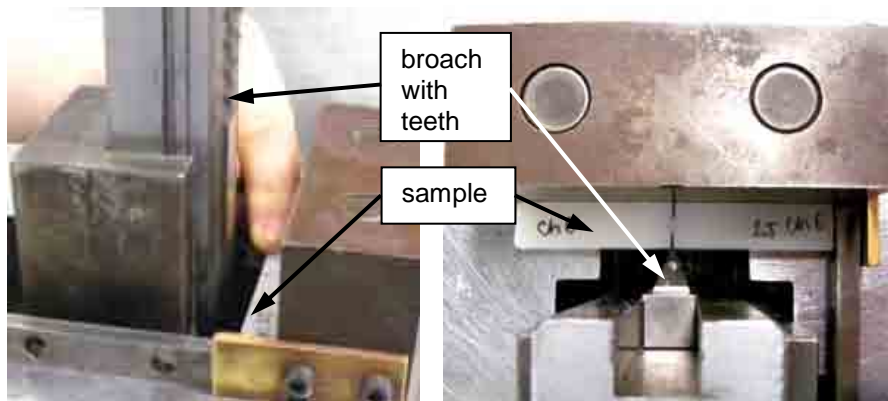
Figure 4.38 Hand operated Charpy notch machine (side and plan view).

Figure 4.39 Notched sample for the Charpy impact test.

4.3.6.5 Pull-off test samples

In the pull-off test, non-standard equipment and sample dimensions were used. The length of the sample used in the test was equal to the thickness of the 4.2mm moulded sheet. The area of the chip became the cross-section of the sample. The dimensions were limited by the grips of the Instron machine. Two sizes of chip were considered: $4mm \times 4mm$ and $4mm \times 8mm$.

Initially, a range of samples were cut with an excess margin around them from a polyethylene sheet using a flexural cutter (Figure 4.40a). Individual samples were then separated using a Stanley knife. It was noticed that when cutting along the long side of the rectangle, close to the chip, the pressure generated during cutting was transferred to the brittle silicon chip resulting in small defects on the chip. This caused stress concentrations and the chip broke during testing. It was therefore necessary to cut the sample with a sufficient excess margin from the chip to prevent this (Figure 4.40b). The excess material was then peeled off using a knife in small steps. The thin polymer skin on the edges of the chip was milled using grinding paper.
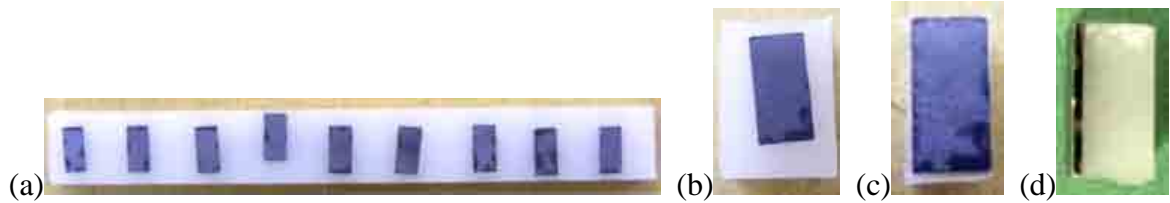
Figure 4.40 Stages of cutting out the pull-off test samples. (a) samples separated from the polyethylene sheet using a flexural cutter, (b) individual sample separated using a knife, (c) excess material removed from around the sample using a knife, (d) final milled sample (side view).

Square samples were used in the main tests as it was noticed that the square chip was less susceptible to failure resulting from defects formed during the sample preparation.

4.4 Tests

The main tests aimed to investigate the effect of including chips on the mechanical performance of polyethylene and to characterize the materials. They included tensile, bending, flexural creep, Charpy impact and pull-off tests and were carried out at ambient temperature, 23±2ºC, as recommended by the standards (ASTM, 2008c; BSI, 2008; UK Water Industry, 2001). The samples were conditioned for at least 24hrs before testing in the same temperature range in accordance with UK Water Industry (2001). The test procedures, data processing and error calculations, where applicable, are discussed in this section. The implication of these errors is discussed later, while analyzing the results.

4.4.1 Tensile test

In the tensile test the behaviour of material under axial tensile loading is investigated and the tensile properties such as Young's modulus, yield stress, strain at break and energy at break are determined.

4.4.1.1 Experimental procedure

The test was carried out using an Instron 5566 testing machine (Figure 4.41), with a maximum load (force) capacity of 10kN and a maximum cross-head speed of 500mm/min.

The dumbbell shape samples were tested at a speed of 10mm/min, which is one of the values recommended by BSI (1996c). The speed of 1mm/min is recommended for Young's modulus specification; however, only three
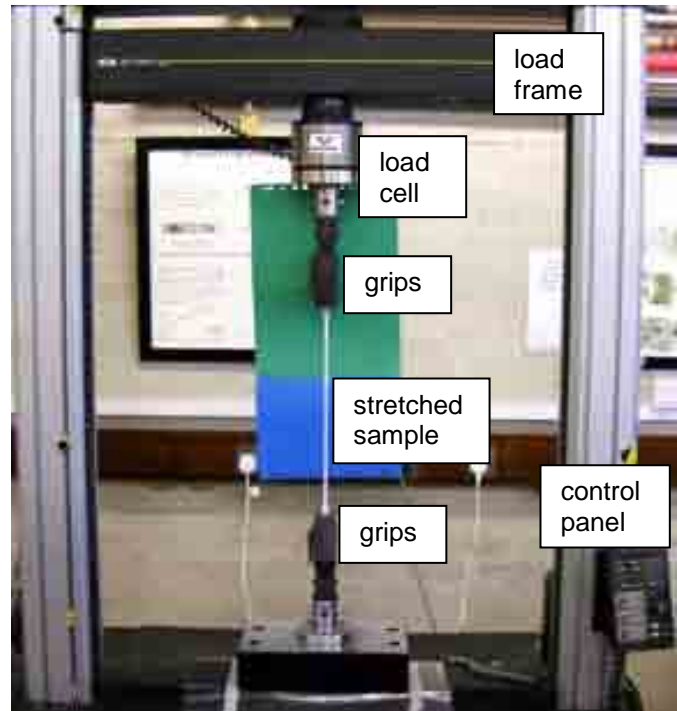
Figure 4.41 Instron 5566 testing machine.

samples were tested at this speed and were only stretched up to a strain of 1 as the full test would take around 6hrs due to the geometry of the samples (Figure 4.29c, page 121) and ductile properties of polymer. One test at 10mm/min takes up to 35min, which is a reasonable time and allows for an accurate observation of the sample during stretching. The effect of the strain rate on the mechanical performance of the samples with and without a chip was investigated for the speeds 5, 10, 20, and 100mm/min. Two sample thicknesses, 2.2 and 4.2mm, were tested.

The Instron 5566 was calibrated every day before starting the testing. The load applied was automatically recorded every second. The repeatability of the results was verified in the initial tests and at least five samples of each type were tested. In cases where the results were more variable, additional tests were carried out, as explained further in section 5.2.2 (page 155).

4.4.1.2 Data analysis

With the application of an external tensile force, a specimen responds with a change in dimensions: an increase in length and a decrease in area. In the nominal (engineering) stress calculation, the change of the specimen area is not considered, and the tensile stress is defined as (BSI, 1996a):

$$\sigma = \frac{F}{A_0} \qquad\qquad 4.8$$

where: σ – tensile stress, MPa

F – load (force), N

A – specimen initial cross-sectional area (initial), mm²

The tensile strain is defined as:

$$\varepsilon = \frac{l - l_0}{l_0} \qquad\qquad 4.9$$

where: ε – axial strain, –

l_0 – gauge length of the test specimen, mm

l – extension of the specimen, mm

The speed (of the Instron cross-head motion), gauge length, sample thickness and width values were input into the software before each test. The strain rate and extension were measured indirectly based on the speed and displacement as the functions of the initial gauge length.

The values were automatically converted, and the stress-strain response was obtained. The stress-strain response in tension was briefly introduced in sections 2.2.4.1 and 2.2.4.2 (pages 19 and 22) and an example of the graph for plain polyethylene was shown in Figure 2.15 (page 25).

The gauge length was assumed to be the length of the narrow parallel section of the sample (see Figure 4.29) in accordance with common practice (Peacock, 2000). However, the material outside the gauge length also stretched non-uniformly. Therefore, the strain measurement was not accurate and unreastically high values up to 14 were obtained (which is the limit instrument range for the geometry of tested samples). It could be done more precisely using an extensometer, e.g. strain gauge or video extensometer; however, they are normally only used for small strains due to their limited range (Caddell et al., 1972) and the specialized equipment was not available. Therefore, the strain related values, such as Young's modulus and strain at break were only indicative and mainly used for comparative purposes.

According to BSI (1996a) the Young's modulus (E) should be calculated as a slope of the stress-strain curve between the strains 0.0005 and 0.0025:

$$E = \frac{\sigma_{0.0025} - \sigma_{0.0005}}{0.002} \qquad \textbf{4.10}$$

where: $\sigma_{0.0025}$ – stress value at strain 0.0025

$\sigma_{0.0005}$ – stress value at strain 0.0005

0.002 – strain difference between the strains: 0.0025 and 0.0005

However, in practice the first two strain values recorded were approximately 0 and 0.0067, thus the modulus was calculated for two first strain values and corresponding stresses.

4.4.2 Flexural bending

The flexural bending test allows the flexural properties of the material to be determined, such as flexural modulus and strength. Due to the material ductility and flexibility, the samples were not expected to break; hence the flexural strength could not be obtained. The theoretical peak stress value was also recorded.

4.4.2.1 Experimental procedure

The test was also carried out using an Instron 5566, but with different fixtures compared to the tensile test, as shown in Figure 4.42. Initially, 4-point bending tests were performed on rectangular samples; however, this was further changed to 3-point bending. The reasons for it and the results of the tests are discussed in section 5.3.1 (page 222). The radius of the supporting and loading noses in both tests was 5mm, in accordance with BSI (2003b).

A span to depth ratio of 16 was used, giving the spans of 70 and 35mm for the 4.2 and 2.2mm thick samples, respectively. In the case of the 4-point bending test, a load span to support span ratio of ½ was used. According to the ASTM recommendations (2007c), the sample should be overhanging on each end at least 10% of the support span and no less than 6.4mm. Therefore, the length of the 4.2 and 2.2mm thick samples was 86 and 48mm, respectively, which is at least 20 times the thickness.
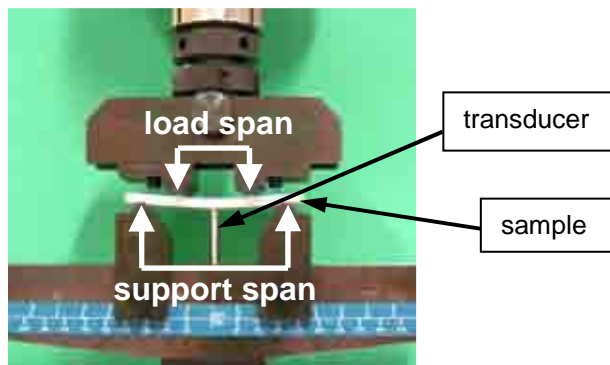
Figure 4.42 4-point bending fixture.   **Figure 4.43 3-point bending fixture.**
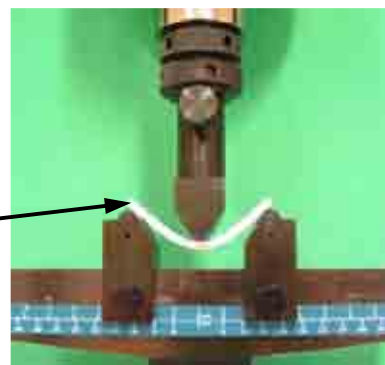
A strain rate of 0.01min^{-1} was used as recommended by the American and British Standards (ASTM, 2007c; BSI, 2003b). The speed was calculated on the basis of Equation 4.11.

$$r = \frac{zL^2}{6h}$$

<div align="right">**4.11**</div>

where: r – rate of cross-head motion, mm/min

L – support span, mm

h – specimen thickness, mm

z – strain rate, min^{-1}

Equation 4.11 yields a speed of approximately 2mm/min for the 4.2mm thick samples and 1mm/min for the 2.2mm thick samples. The strain rate effect was also investigated for a speed of 20 and 80mm/min (strain rate of 0.1 and 0.4min^{-1}). The short term flexural modulus obtained at 20mm/min was also used to determine the force/load value for the creep test, as further explained in 4.4.3.1.

Similarly as in the case of tensile test, the Instron 5566 was calibrated every day before starting the tests and the load applied was automatically recorded every second. The load was measured only above a trigger threshold by applying a preload of approximately 0.1N. This removed the initial curved region of the graph (toe), which has to be compensated for anyway in the data analysis to give the corrected zero point on the strain or extension axis (ASTM, 2007c; BSI, 2003b). At least five samples of each type were tested.

4.4.2.2 Data analysis

With the application of an external force in the flexural test, the specimen bends and the strain increases. The bending speed was set and incorporated into the software and the load and extension were measured. In the case of the 3-point bending test, the extension was based on the cross-head displacement as a function of the initial gauge length. Initially, the displacement was also measured by a transducer, which was the only displacement measuring device in the case of the 4-point bending test. The pressure and voltage were measured and

133

converted into the force and displacement, respectively. The data obtained from the Instron and the transducer were then converted into the strain and stress values. The flexural stress in 3-point bending is defined as (ASTM, 2008a; BSI, 2003b):

$$\sigma_f = \frac{3FL}{2bh^2}$$

4.12

In the 4-point bending test the flexural stress is given by Equation 4.13 (for load span ½ of the support span).

$$\sigma_{f4} = \frac{3FL}{4bh^2}$$

4.13

where: σ_f – flexural stress in 3-point bending, MPa

σ_{f4} – flexural stress in 4-point bending, MPa

F – load (force), N

L – support span, mm

b – specimen width, mm

h – specimen thickness, mm

The strains in 3- and 4-point bending are defined by Equations 4.14 and 4.15, respectively (ASTM, 2008a; BSI, 2003b).

$$\varepsilon_f = \frac{6sh}{L^2}$$

4.14

$$\varepsilon_{f4} = \frac{4.36sh}{L^2}$$

4.15

where: ε_f – flexural strain in 3-point bending

ε_{f4} – flexural strain in 4-point bending

s – deflection, mm

All the equations concerning the flexural properties of the materials apply only to the linear stress-strain behaviour and thus to small deflections. However, outside this region they can be used for comparative purposes (BSI, 2003b).

Figure 4.44 shows the stress-strain relationship for 3- and 4-point bending tests for a plain polyethylene sample. The 3-point bending values were measured by both, the Instron and displacement transducer. As the flexural strength cannot be determined for the materials that do not break within the 5% strain limit (ASTM, 2007c), the peak flexural stress obtained in 3-point bending was analysed for comparative purposes. The peak value of the stress-strain curve is associated with the sample rotating and slipping off the supports, which causes a change in test geometry, thus the value is only theoretical.
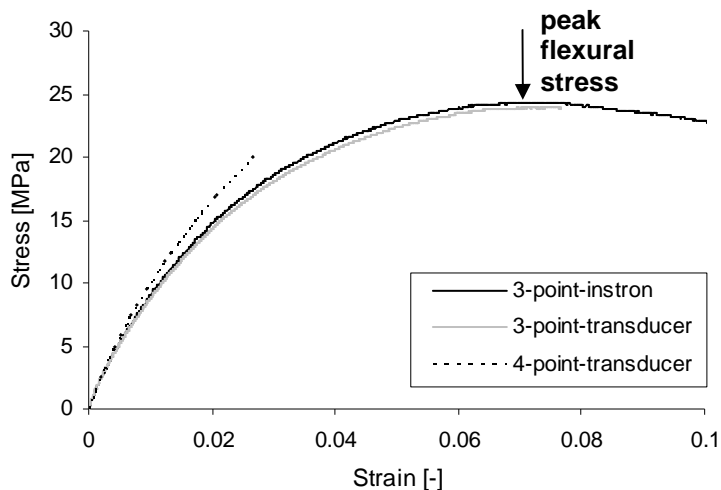
Figure 4.44 Example of a stress-strain relationship for a plain polymer sample associated with 3- and 4-point bending with the displacements measured by the Instron and transducer in 3-point bending, and by the transducer in 4-point bending.

Figure 4.44 shows that the graphs for 3-point bending, obtained from the Instron and the transducer overlap suggesting that the Instron measurement is accurate and thus the strain rate (speed) measurement is also accurate, not just surrogate as in the case of a tensile test. The transducer measurement was stopped earlier due to the limited capacity of the device. The 4-

point bending test was stopped earlier due to the limitations of the loading fixture (Figure 4.42).

The flexural modulus (E_f) was calculated according to BSI (2003b) for the strains of approximately 0.0005 and 0.0025, and the corresponding stresses (see Equation 4.10).

4.4.3 Creep test

The flexural creep test is carried out in order to determine the long term properties of materials. The samples are subject to different constant loads over a period of time, the creep curves are obtained and the creep modulus at specific time and/or load is extrapolated. The tests were performed using the equipment available at Exova and the specimens were set up by their experienced technicians.

4.4.3.1 Experimental procedure

The same dimensions of the samples and the same span to depth ratio as in the flexural bending test were used, in accordance with American and British Standards (ASTM, 2009a; BSI, 1997). The stress, and thus the applied load, was calculated as 0.0025 of the flexural modulus on the basis of the flexural test results for a strain rate of 0.1min^{-1} (speed 20mm/min), in accordance with the recommendations of Hesketh (2009) and Ferry (2007), who proposed a guideline for creep testing of liner materials based on the British and American standards (ASTM, 2001; BSI, 2002). These recommendations were used in this case as pipes are considered as one of the applications for microsensors.

Another British Standard (BSI, 2003c) recommends that the stress should not cause a deflection greater than 0.1 times the support span, which is impossible to follow in the case of ductile and flexible polyethylene as it does not break in flexural creep mode and hence was not appropriate in this case. The ASTM (2001) recommends the application of a stress, which

causes 1% strain within 1000hrs of testing, for material comparison purposes. However, to determine this stress might require many preliminary tests, which could not be afforded in this project. The stress applied in the creep test depends ultimately on the material working conditions and can vary.

As the flexural modulus was 1322MPa at 20mm/min (see section 5.3.3), the stress applied was: $0.0025 \cdot 1322 = 3.25$MPa. The additional stresses tested were 6.5 and 13MPa.

The force to be applied was obtained from Equation 4.12 for every sample separately due to small differences in the sample dimensions. The force was converted into load using Equation 4.16.

$$F_0 = g \cdot L_0 \qquad \qquad \textbf{4.16}$$

where: g – standard gravity, g = 9.81m/s²

$\qquad$ L_0 – load maintained constant, kg

Some samples were tested in the air and some in a wet environment to simulate plastic pipe conditions. Water and random air bubbles were contained in a sealed low density polyethylene (LDPE) bag, as shown in Figure 4.46. The quantity of water used was enough to immerse most of the sample, but avoided water between the sample and the loading and supporting noses.

For the smallest stress (3.25MPa) special loading fixture had to be made (Figure 4.45) as the standard fixtures at Exova (Figure 4.47) are designed for higher loads. Therefore, a smaller number of samples were tested at this stress.
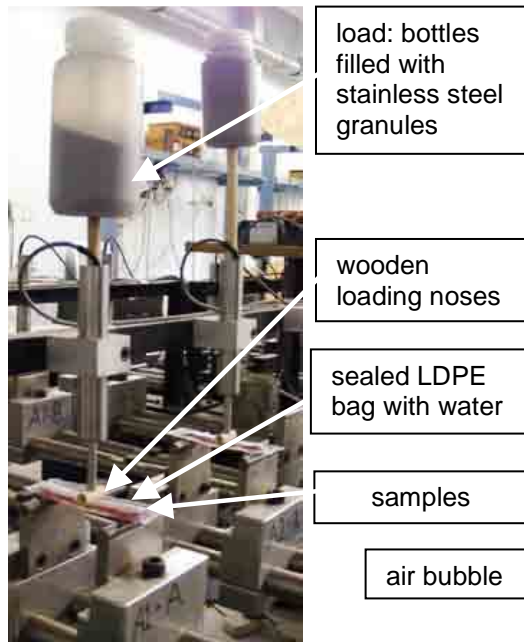
Figure 4.45 Flexural creep test apparatus with special loading fixture for the stress of 3.25MPa.

Figure 4.46 Flexural creep test sample.
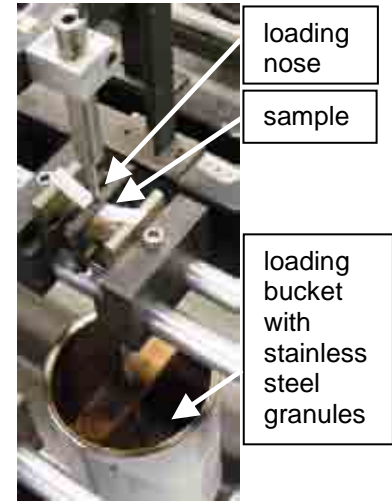
Figure 4.47 Flexural creep test apparatus with standard loading fixture for the stresses of 6.5 and 13MPa.

4.4.3.2 Data analysis

For the creep test, the change in flexural creep modulus over time was plotted on a logarithmic scale. The deflection values were collected automatically, initially at a higher rate and then at a lower rate, in accordance with BSI (1997). On the basis of the data collected for over 1000hrs, the values for longer periods can be extrapolated (ASTM, 2001). This extrapolation is useful for materials used for long term applications, e.g. pipes, which are designed for 50 years. In practice, the data were collected for approximately 2000hrs. The flexural creep modulus was calculated for each deflection (s) on the basis of parameters assumed as constant over the duration of the test, using Equation 4.17 (BSI, 1997).

$$E_{fc} = \frac{FL^3}{4bh^3 s} \qquad\qquad \textbf{4.17}$$

E_{fc} (flexural creep modulus) is expressed in MPa while other parameters are defined as in Equations 4.12 and 4.14.

For each sample a power law curve fit was plotted on the basis of the data points, from which the creep modulus at 50 years was extrapolated.

4.4.4 Charpy impact test

This test was used to investigate the behaviour of the specimen under impact conditions.

4.4.4.1 Experimental procedure

In the non-instrumented impact test only the total energy absorbed by the specimen is recorded. The Zwick 5102 pendulum (hammer) type non-instrumented impact machine was used and was capable of measuring energy in the range 0.5 to 4.0J (giving a speed of a falling pendulum of 2.93m/s). A schematic of the Charpy impact test is presented in Figure 4.48.
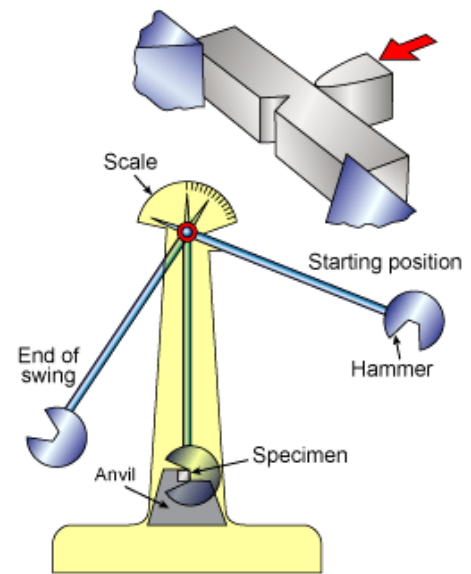
Figure 4.48 Schematic of Charpy impact test (TWI, 2009).

Only the 4.2mm thick samples were used. They were tested edgewise (on their edge) so the previous width became the depth of a sample. Ten unnotched and notched samples were tested, which is the minimum number recommended by BSI (2001a).

The notch depth of 25% was applied, which represented the critical notch size over which most materials experience brittle failure (Ingham, 2003). The radius of the sharp notches was around 10µm.

The span to depth ratio of approximately six was used, which is recommended by BSI (2001a) and this is necessary to accommodate for shear effects that might occur in the

breakdown (Ingham, 2003). This gave a span of 76mm for the sample depth of approximately 12.6mm (which was assigned as a 'width' for the purpose and arrangement of other tests).

The brittleness or toughness of the samples with and without a chip was investigated on the basis of the data obtained and an examination of the failure surfaces.

4.4.4.2 Data analysis

The impact energy was obtained from the test. By definition, this is the energy required to break a sample (BSI, 2001a). However, due to the ductile characteristics of the polyethylene, the samples did not totally break (Krishnaswamy et al., 2006). Therefore, the value obtained is not absolute. The impact strength of the unnotched samples was calculated using Equation 4.18 (BSI, 2001a).

$$a_U = \frac{E_a}{hb} \times 10^3$$

4.18

where: a_U – impact strength of the unnotched sample, kJ/m²

E_a – energy absorbed, J

h – specimen thickness, mm

b – specimen width, mm

Due to the ductility of polyethylene the notched samples broke only partially, thus, the impact strength calculated for these samples using Equation 4.19 is also not absolute.

$$a_N = \frac{E_a}{hb_N} \times 10^3$$

4.19

where: a_N – impact strength of the notched sample, kJ/m²

b_N – remaining specimen width (under the notch), mm

4.4.5   Pull-off test

The pull-off test aimed to investigate the bonding between the silicon chips and polyethylene created by the HMA and other interlayers in a direct way. These types of test are used for testing the strength of coatings (ASTM, 2009b). The test was carried out using the Instron machine with a modified fixture. The standard pull-off test equipment could not have been used as the polyethylene would not have bonded to the metal surface of the rig.

4.4.5.1 Experimental procedure

The test arrangement was specifically developed as part of this research to cope with the particular requirements of the samples. Two shapes of the chip were considered in these tests: square (4mm×4mm) and rectangle (4mm×8mm). An example sample is shown in Figure 4.40d. The side of the sample with a chip on the surface was stuck using super glue to a metal block (Figure 4.49) and a load was applied to the metal block and chip for 10-20min in order to ensure uniform adhesion (Figure 4.50). The square sample was loaded with 423g and the rectangular sample was loaded with 710g as these loads were available in the lab and the weights appeared reasonable. When too high loads (over 1kg) were applied, the chip broke.

After the block with the chip was installed in Instron with the upper side of the sample loose, the instrument was zeroed (calibrated).

The polyethylene side of the sample had to be installed in a different way, in the upper grip of the Instron, as polyethylene does not stick to metal using any glue cured at room temperature. The pull-off test fixture is shown in Figure 4.51. The clamps were closed in such a way that a gauge of approximately 1mm was left.

Figure 4.49 The pull-off test sample with polished edges glued to the metal block.

Figure 4.50 Samples glued to metal blocks were temporarily loaded to ensure uniform adhesion.
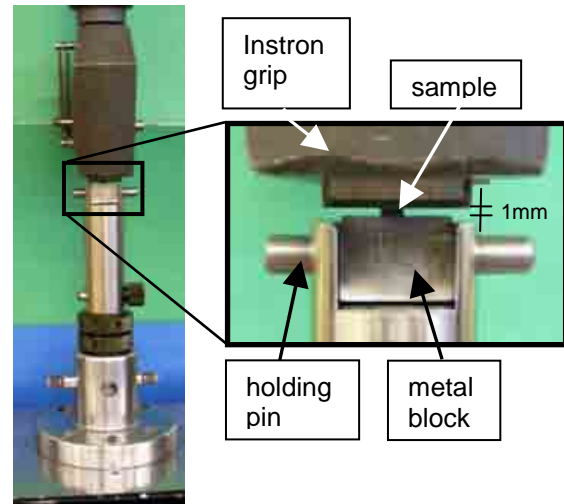
Figure 4.51 Pull-off test arrangement.

Tension was applied to the sample at a very low speed of 0.1mm/min. It had to be ensured that the bond between the chip and the glue was stronger than the bond between the chip and polyethylene formed by the HMA. Therefore, different types of impact glues and super glues were tested.

It was noticed that if the superglue activator was applied to both bonded surfaces before the glue this improved the adhesion. Additionally, the dried glue from around the edges of the chip had to be removed/peeled off with knife and grinding paper used to improve the effectiveness of the bond.

As indicated in section 3.1.2 there is a difference in roughness of both sides of a silicon wafer. In some cases it could be seen with the naked eye, in other not and both sides of the chip seemed to be equally smooth. When the rough side could be distinguished, the HMA was applied between the smooth side and the polyethylene matrix. On the rough side the superglue was applied to attach the sample to the metal block. However, the preliminary experiments on the samples with chips arranged in the opposite way indicated that there are large variations in

142

the results for the same type of sample arrangement. The difference between two chip sides/ sample arrangements could not be picked up due to other more dominating factors, which determine the effectiveness of the silicon-polyethylene bond formed by the HMAs discussed further in section 6.2.

4.4.5.2 Data analysis

The force applied to the sample was measured. The gauge length and dimensions of the sample were incorporated into the software. The results were automatically converted into the stress and strain values on the basis of Equations 4.8 and 4.9. The strain measurement was not accurate and therefore, only the peak stress value was analysed and compared for different types of samples. The value for the chip-polyethylene interface without any additional interlayer or with some coatings tested was equal to zero, as the chip did not adhere to polyethylene at all.

Chapter 5 RESULTS & DISCUSSION OF THE SHORT TERM TESTS

5.1 Introduction

Chapters 3 and 4 described the results of the material characterization tests and the methodology, respectively. It was evident from the experiments that the materials used, even though all based on polyethylene, have different structural and physical properties and thus their different mechanical performance is expected. Further, it was shown that the manufacturing conditions influence some of the properties of polymers. In this chapter the results of the short term tests such as tensile, flexural and Charpy impact are analyzed.

As stated in section 2.3.3 the mechanical properties of polymers with inclusions depend on many parameters and most of them will be investigated here. Table 5.1 lists the parameters analysed in particular tests. The adhesion between the silicon chip and the polyethylene matrix is studied in Chapter 6.

Table 5.1 Parameters investigated in particular tests.

Parameter	Test			
	Tensile	Flexural bending	Charpy impact	Flexural creep
Manufacturing conditions	√	√		
Strain rate	√	√		
Matrix material	√			
Chip effect	√	√	√	√
Chip shape	√	√		
Chip size	√	√		
Chip orientation	√	√		
Number of chips	√			
Chip-matrix interface	√	√		

The polyethylene with the inclusion of silicon chips can be related to the polymer composites when comparing with other research results. As indicated in section 2.3.3, there is a lot of literature written on this topic; however, it has to be noted that the fillers often have much smaller size (few micrometers) than the tested chips and often various irregular shapes. The most alike silicon chips are mica and glass flakes and platelets, which have similar shape, composition and density of $2.8g/cm^3$ (Xanthos, 2010) in comparison with $2.3g/cm^3$ for silicon (Gad-el-Hak M., 2002). Their aspect ratio (proportion of the greatest to the smallest dimension) is usually larger than for the silicon chips that have been considered here. The circular silicon chips can also be compared to glass beads, which have regular shape and comparable composition. With regards to the polymer matrix, different materials were tested by the researchers and the most alike polyethylene (PE) is polypropylene (PP) as it is also a thermoplastic polyolefin, having similar composition and properties.

The term plain is used for the material/sample without the inclusion of a chip. The thickness of the samples tested is approximately 4.2mm unless stated otherwise. For explanation of the chip orientation in particular samples refer to section 4.2 (page 85).

Table 5.2 summarises the number of samples tested in particular tests with regards to the sample type.

Table 5.2 Number of samples tested in particular tests.

Sample	Thickness mm	Test		
		Tensile	Flexural bending	Charpy impact
plain	4.2	10[+] (plus 6 off-the-shelf)[++]	10[+]	10 notched & 10 unnotched
	2.2	10	5	-
SC/surf	4.2	6	-	-
	2.2	9	-	-
LC/surf	4.2	10	10 (5 in and 5 out)*	-
SSQ/surf	4.2	10 (5 at 0° and 5 at 45°)**	-	-
SC/0/90	4.2	10[+] (plus 6 off-the-shelf)[++]	10	10 notched & 10 unnotched
	2.2	5	5	-
LC/0/90	4.2	6	5	-
SSQ/0/90	4.2	6	-	-
SC/90/0	4.2	5	5	-
LC/90/0	4.2	6	5	-
SSQ/90/0	4.2	8	-	-
SC/90/90	4.2	8	5	-
LC/90/90	4.2	7	5	-
SSQ/90/90	4.2	7	5	-
SC/45/90	4.2	8	-	-
SC/45/45 (SC/90/0 slanted)	4.2	5	-	-
SC/90/45	4.2	5	-	-
2SC/0/90	4.2	5	-	-
SC&SSQ/0/90	4.2	7	-	-
Total number of samples		186	80	40

[+] In the tensile and flexural bending tests the strain rate effect was investigated, thus 3 extra plain samples were tested at the speeds of 1, 5, 20, and 100mm/min and 3 extra SC/0/90 samples at the speeds 5, 20 and 100mm/min in tension, and 5 extra plain samples at the speeds 20 and 80mm/min in bending.

++ In the tensile test the material effect was investigated and so the extra plain and SC/0/90 off-the-shelf polyethylene samples were analysed.

* LC/surf samples were tested in the flexural bending test with the LC chip on the inner and outer fibres of the beam/sample

** SSQ/surf samples were tested in the tensile test with the SQ chip at two angles towards the sample edges, 0° and 45°

First, the results of the tensile test are presented and discussed. The pictures are not to scale unless stated otherwise.

5.2 Tensile test

This chapter focuses on tensile tests conducted using an Instron machine (see section 4.4.1) in which the stress-strain curves as well as the tensile values such as Young's modulus, yield stress and strain at break were obtained for the samples. As indicated in Table 5.1 the complete series of tests is carried out in this stress mode.

Initially, five samples of each type were tested as recommended by BSI (1996a). In the next section the influence of the manufacturing conditions is analysed. Further, the minimum number of samples ensuring good repeatability is determined for plain polyethylene and samples with a chip for which a higher variation of the results is expected.

5.2.1 The effect of sample manufacturing conditions on plain polyethylene samples (reference samples)

As indicated in section 4.3.2 the cooling rate of the samples produced in compression moulding varied depending on the conditions, especially the cooling water temperature. The density tests have shown that it slightly influenced the properties of the final product as for the samples cooled at 9 and 13ºC the densities were 0.9562 and 0.9566g/cm³, respectively (section 3.3.4, page 80). Even though the difference was within the SD (0.0004g/cm³), thus insignificant, its influence on the mechanical performance was further investigated in tension.

Five samples were cut out from different sheets produced under these two conditions. Figure 5.1 shows the data while Tables 5.3 and 5.4 list the numerical values.
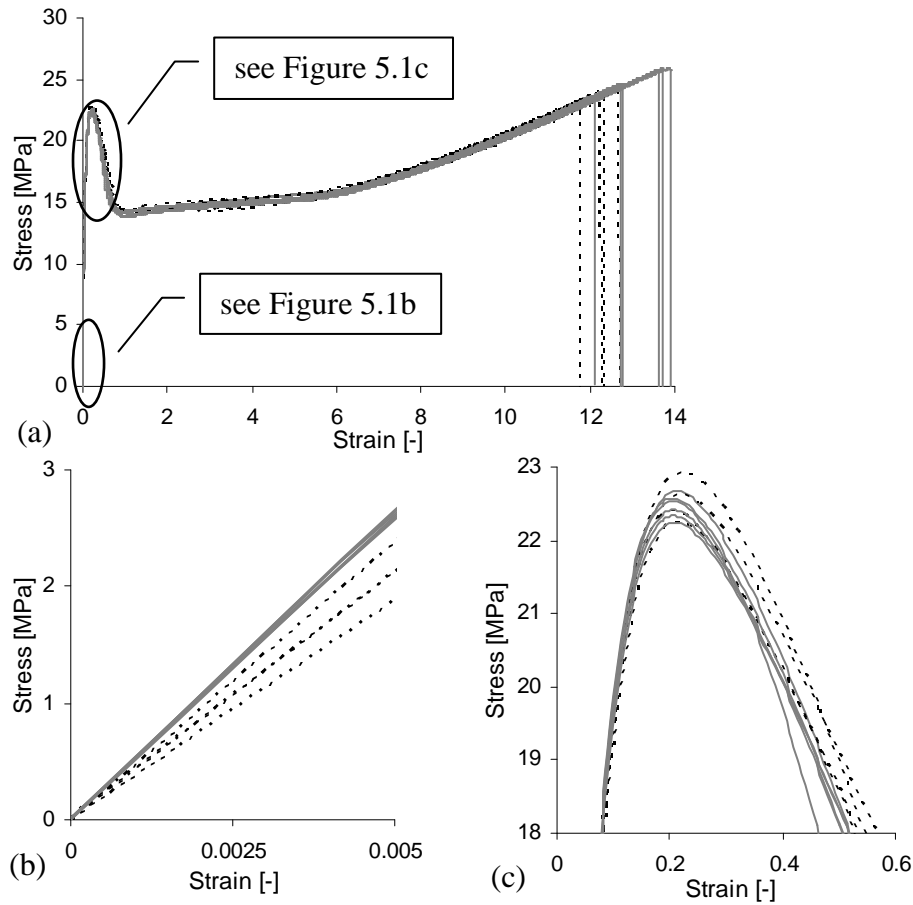
Figure 5.1 (a) Stress-strain curves for the samples produced at different cooling water temperatures: (——) 9ºC and (- - -) 13ºC; (b) enlarged elastic region, (c) enlarged peak region.

Table 5.3 Tensile values for the samples produced at a cooling water temperature of 9ºC. Note: the marking lines explained further in the text.

Sample	Young's modulus MPa	Yield stress MPa	Strain at break
t349	520	22.2	13.7
t350	516	22.5	12.7
t351	502	22.3	13.6
t352	513	22.6	12.8
t353	509	22.4	13.9
Average	512	22.4	13.3
SD	7	0.2	0.6

Table 5.4 Tensile values for the samples produced at a cooling water temperature of 13ºC. Note: the marking lines are explained further in the text.

Sample	Young's modulus MPa	Yield stress MPa	Strain at break
t6	421	22.2	12.7
t7	503	22.7	12.1
t8	424	22.6	12.3
t9	377	22.9	11.7
t15	477	22.4	12.2
Average	440	22.6	12.2
SD	50	0.3	0.3

The shape of the curves in Figure 5.1 is characteristic for HDPE (Powell, 1983) and was described in section 2.2.4.2 (page 22).

The SDs express the variations among the samples associated with their different properties or variations in the measurements. Therefore, in order to estimate the reliability of the results it is important to justify the accuracy of the measurement for a sample influenced by both, the measurement of the sample dimensions and the instrument precision. The sample thickness and width were measured with a digital micrometer with an error of 2µm (Squires, 1988) in three places along the gauge length. The area calculated on the basis of the average values was then used for the stress calculation. The average dimensions and SDs of 20 samples were listed in Table 4.4 (page 106). The maximum SDs of the thickness and width among these samples were 0.05 and 0.04mm, respectively.

In order to see how these variations influenced the results, the stress-strain graphs were plotted for the sample with the maximum SDs, i.e. for the minimum and maximum cross-sectional areas (A_{min} and A_{max}) obtained on the basis of the minimum and maximum thicknesses and widths measured for the sample ($A_{min} = 4.174 \cdot 12.578 = 52.501 \text{mm}^2$ and $A_{max} = 4.277 \cdot 12.657 = 54.134 \text{mm}^2$). The average area was: $A = 4.22 \cdot 12.62 = 53.26 \text{mm}^2$. The average values have lower accuracy limited by the magnitude of SD. The influence of the different cross-sectional areas on the stress-strain relationship is shown in Figure 5.2.
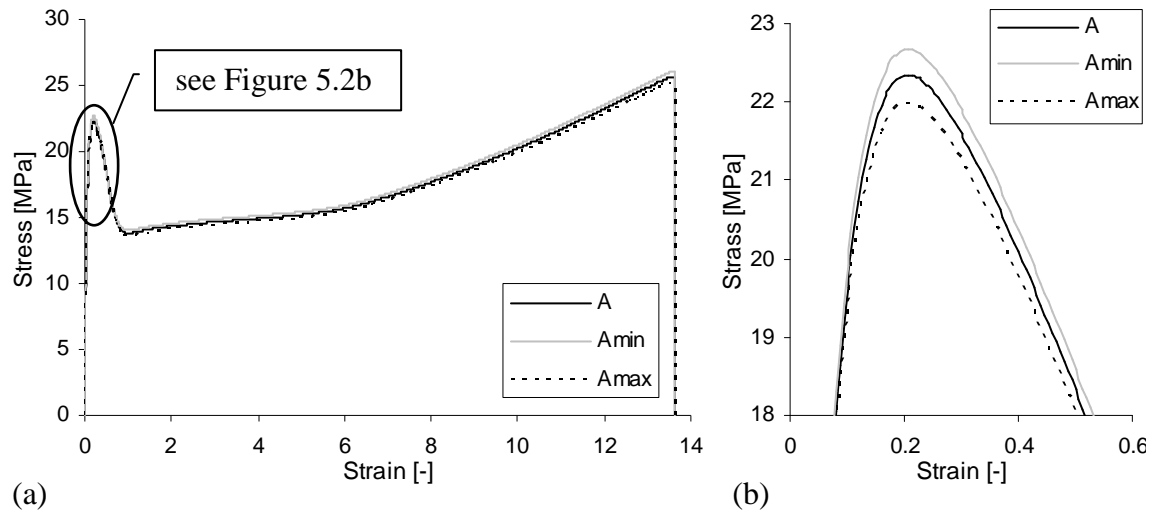
Figure 5.2 (a) Stress-strain relationship for a range of cross-sectional areas, (b) enlarged peak region.

Figure 5.2 shows that the effect on the stress-strain relationship for different cross-sectional areas is small. However, the yield stresses differ slightly and are 22.35, 22.67, and 21.99MPa, for A, A_{min}, and A_{max}, respectively, with a maximum difference of 0.68MPa. Thus the error can be assumed as half of this difference, i.e. ±0.34MPa. The Young's moduli are 502, 510, and 494MPa, respectively, with a maximum difference of 16MPa.

Another more common and complex way of estimating the possible deviation of the results is by applying special error calculation equations (Squires, 1988; Taylor, 1982). The equations take into account the errors of all the components, which contribute to a particular quantity Z. In the case of adding or subtracting quantities X and Y, the error ΔZ is calculated as:

$$(\Delta Z)^2 = (\Delta X)^2 + (\Delta Y)^2 \qquad \textbf{5.1}$$

where ΔX and ΔY are the errors of the quantities X and Y. In the case of multiplying or dividing quantities X and Y, the error ΔZ is calculated as:

$$\left(\frac{\Delta Z}{Z}\right)^2 = \left(\frac{\Delta X}{X}\right)^2 + \left(\frac{\Delta Y}{Y}\right)^2 \qquad \textbf{5.2}$$

Equation 5.2 can be used to determine the error in the cross-sectional area of the sample (ΔA). The calculation is done for the sample with maximum SDs in the thickness and width, i.e. 0.05 and 0.04mm, respectively, giving ΔA as:

$$\left(\frac{\Delta A}{53.26}\right)^2 = \left(\frac{0.05}{4.22}\right)^2 + \left(\frac{0.04}{12.62}\right)^2 \rightarrow \Delta A = 0.65 \text{ mm}^2$$

The errors associated with instrument accuracy are specified by the manufacturer (Instron, 2005). The load measurement accuracy is $\pm 0.5\%$ of the reading down to 1/250 of the load cell capacity ($10\text{kN}/250 = 40\text{N}$). The strain measurement accuracy is $\pm 0.5\%$ of the reading down to 1/50 of the full instrument range ($1/14 = 0.7$). It means that for the load and strain values below 40N and 0.07, respectively, there is no guarantee that the data obtained are accurate and the error cannot be estimated.

As the E is calculated for very low loads and strains (see Equation 4.10), it is impossible to rely on these data. However, the values are obtained and used for comparative purposes between different types of samples and materials.

The error for the yield stress ($\Delta \sigma_y$) is calculated on the basis of the area and load measurement errors. The load applied at yield was $F_y = 1190\text{N}$, which is over 40N, thus the relative load error $\Delta F_y/F_y$ was 0.005 in accordance with the instrument manufacturer specifications (Instron, 2005). The A and ΔA values used in the calculation were 53.26 and 0.65mm², respectively.

$$\left(\frac{\Delta \sigma_y}{22.34}\right)^2 = \left(\frac{0.65}{53.26}\right)^2 + \left(0.005\right)^2 \rightarrow \Delta \sigma_y = 0.29 \text{ MPa}$$

The $\Delta \sigma_y$ of ± 0.29MPa gives the difference between the largest and the smallest σ_y of around 0.58MPa. This is 0.1MPa smaller than the difference between the maximum and minimum σ_y of 0.68MPa, calculated on the basis of the minimum and maximum cross-sectional areas

(without considering the load measurement error). The values differ due to the different approaches used in the error calculations. The average $\Delta\sigma_y$ is assumed as approximately 0.3MPa. This value is applied for all the samples, as it was obtained for the specimen with the largest variation in the dimensions taken from 20 samples.

The values are overestimated, as the load is applied to the whole sample and it is reasonable to use the average thickness and width values in the calculation.

The strain at break in this experiment is only an estimate as the gauge length is estimated, as discussed previously. Additionally, the ultimate sample failure may be accelerated by random sample defects formed during sample preparation (compression moulding and cutting out) (Peacock, 2000).

From the data obtained in the initial experiments it can be seen that the higher density samples (cooled at 13ºC) reach lower modulus of 440MPa in comparison with 512MPa obtained for the lower density samples, which is in contrast to the theory (Peacock, 2000). A high SD of 50MPa suggests non-uniformity of the samples and/or low accuracy of the measurement. As already indicated, there is no guarantee of the accuracy of the strain measurement at the strains at which the Young's modulus was obtained (between 0 and 0.0067), therefore, there is some uncertainty in Young's modulus value, which has to be remembered while analysing the results.

The average yield stress of the samples with the higher density is slightly higher (22.6MPa) than for the lower density samples (22.4MPa), however, the difference is smaller than the experimental error associated with obtaining the yield stress value (0.3MPa). Therefore, this difference appears insignificant, although, it is in accordance with the research of Meinel & Peterlin (1971) who tested quenched (rapidly cooled) and annealed (slowly cooled) HDPE

samples at a speed of 1mm/min obtaining a higher yield stress (peak) for higher density

samples (Figure 5.3). Their results for both samples differ more due to greater differences in

the manufacturing conditions.
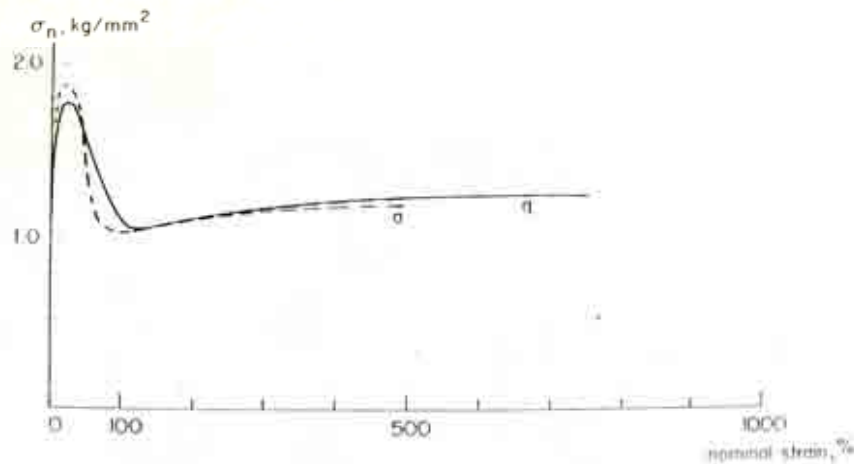
Figure 5.3 Nominal stress-strain curve of (——) quenched and (- - -) annealed polyethylene samples (Meinel & Peterlin, 1971).

The strain at break is lower in the case of the higher density (and thus crystallinity) samples

(12.2) as the material is more brittle. The lower density samples reach the strain at break of

13.3 as they have more amorphous regions and thus chain entanglements holding the

crystallites and the whole structure together (Mitchell, 2004). This dependency is also in

accordance with Meinel & Peterlin (1971).

It can be concluded that the samples cooled at a higher water temperature having higher

density exhibited lower ductility (elongation at break) and higher yield stress. However, the

latter one was measured with an accuracy equal to the difference between the results, thus

cannot be relied on. The Young's modulus measurement did not allow for any certain

conclusions to be made. The effect of the cooling water temperatures in the range investigated

in these tests appears very small; however, it has to be noted that some samples might have

been processed under more extreme conditions and their performance might differ more from

these analysed here.

The plain samples (without chips) will be used as a reference in order to identify the influence of the chips. Due to variations in the sample manufacturing conditions over the duration of the project, averages and SDs for all ten samples produced at two different cooling water temperatures were calculated (Table 5.5).

However, not only the numerical values are important, but also the shape of the curves. Hence, three representative curves were identified: the curve with strain at break and yield stress closest to the calculated averages (t350), the curve with the minimum strain at break, usually associated with the maximum yield stress (t349) and the curve with the maximum strain at break, usually associated with the maximum yield stress (t9). The last two represent the extremes, i.e. the envelopes of all the curves.

In the selection process of the average and extreme data the strain at break value is considered first. In the case of multiple samples with strain at break values close to the average, the yield stress value is also considered. As the Young's modulus cannot be specified accurately due to inaccuracy of the strain measurement, especially at very low strains, this value is not considered in the curve selection process.

The samples are marked in Tables 5.3 and 5.4 and the same marking scheme is applied when required throughout the whole section on the tensile tests.

Table 5.5 Average tensile values with SDs obtained for ten plain polyethylene samples.

	Young's modulus MPa	Yield stress MPa	Strain at break
Average	476	22.5	12.8
SD	50	0.2	0.7
SD as % of the average	11	1	6

Due to limited accuracy of the measurements the obtained values, especially Young's moduli and strains at break, cannot be compared with values found in the literature. However, as the objective of these tests is to determine the influence of including silicon chips in polymer, the measurements can be used for comparison within this set of experiments.

In the next section the minimum number of samples to be tested is determined on the basis of samples with and without a chip.

5.2.2 Determining a minimum number of samples with and without a chip to be tested

As indicated in the previous section the variations in the tensile values among the same type of samples can be attributed to material non-uniformity due to varying production conditions of samples, variations in sample dimensions, and limited instrument accuracy. Therefore, the minimum number of samples to be tested has to be specified. In the case of samples with a chip, in addition, the position of the chip can deviate from the intended as indicated in section 4.3.4. Therefore, the repeatability of the tests for samples with a chip has to be also investigated.

The SDs of the tensile values for the plain polyethylene samples presented in the previous section show that testing ten (Table 5.5) instead of five samples (Tables 5.3 and 5.4) does not improve the repeatability significantly. Normally, lower SDs would be expected for more samples; however, ten samples were produced under different conditions, while the five samples from each group were produced under the same conditions, thus are more uniform. In order to verify this the SDs for six samples produced under different conditions are calculated (three first from each group, from Tables 5.3 and 5.4). The values for the Young's modulus, yield stress and strain at break are 46MPa, 0.2MPa and 0.7, respectively, which is almost the same as for ten samples (Table 5.5). This suggests that testing a smaller number of plain

155

polymer samples, i.e. six or five, which is the minimum number recommended by BSI (1996a) is appropriate as increasing the number of samples does not improve the repeatability significantly but increases the sample preparation and testing time.

Although testing six samples provided a reasonable repeatability for plain polymer, this conclusion might not be valid for samples including a chip. Therefore, ten SC/0/90 samples were tested and the minimum number ensuring good repeatability of the results was determined. It has to be noted that the sheets from which the samples were cut out might have been produced under different conditions, which were not recorded for every sheet and sample. Figure 5.4 presents the plots for the samples with chips and selected plain polyethylene samples while Table 5.6 gives the numerical values. The averages and SDs are calculated for first five and for all ten samples.
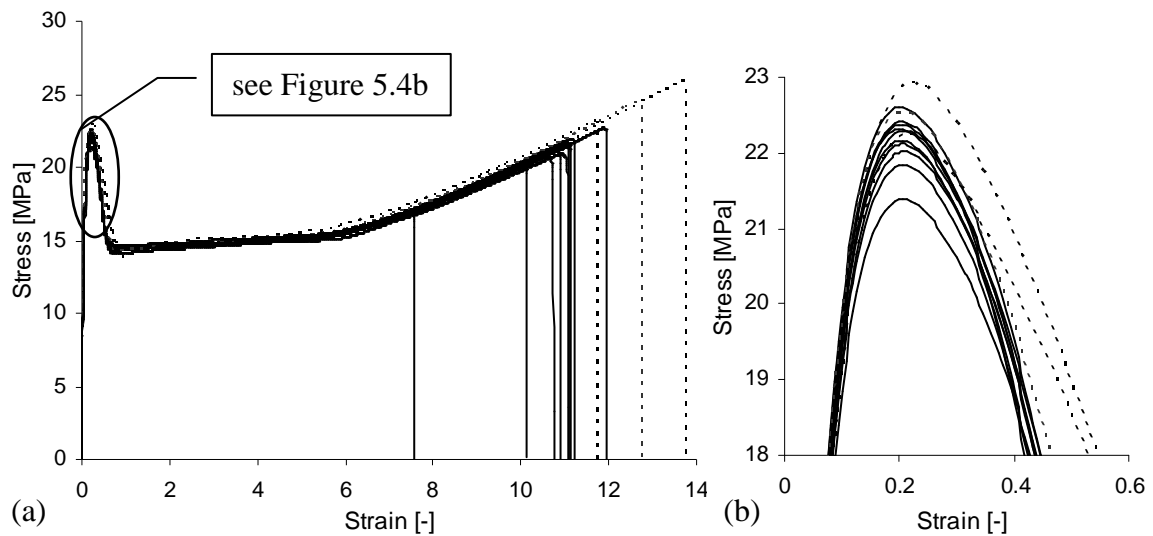
Figure 5.4 (a) Stress-strain curves for (——) the SC/0/90 samples and (- - -) the selected plain polyethylene samples; (b) enlarged peak region.

Table 5.6 Tensile values for the SC/0/90 samples with the averages and SDs calculated for five and ten samples.

Sample	Young's modulus MPa	Yield stress MPa	Strain at break
t50	524	21.8	11.1
t51	516	22.0	11.1
t52	527	22.1	11.1
t53	526	22.3	10.7
t54	535	22.4	7.6
Average of five samples	526	22.1	10.3
SD of five samples	7	0.2	1.5
t67	526	22.4	10.1
t355	526	22.6	11.2
t356	535	22.3	11.1
t357	514	22.2	10.9
t358	505	21.4	11.9
Average of ten samples	523	22.2	10.7
SD of ten samples	9	0.3	1.2

From Figure 5.4 and Tables 5.5 and 5.6 it can be seen that the spread of the curves for ten samples with chips is slightly larger than in the case of plain polyethylene samples concerning the strain at break values for which the SD is 1.2 compared with 0.7 for ten plain samples. This might be due to a slight variation in chip positioning in each sample as the chip is the reason for an accelerated sample failure. However, the X-ray scans of the samples shown in Figure 5.5 indicate that the chip positioning at this orientation is very accurate. The Young's modulus values are more consistent in the case of the samples with a chip (SD of 9MPa in comparison with 50MPa for ten plain samples). The SDs of the yield stress are similar.

When analysing the repeatability of results for the samples with a chip, the SDs of the tensile values are comparable for five and ten samples. There appears to be one line out of character with a much lower yield stress unusually associated with low strain at break (t358). This relationship might be due to the chip position in the sample, which accelerated its failure. When excluding this sample in the calculation of the averages and SDs of nine remaining samples, the values presented in Table 5.7 are obtained.
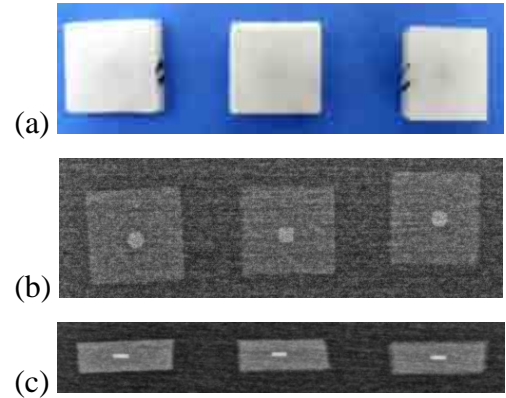
Figure 5.5 (a) Picture of the SC/0/90 samples and their X-ray scans: (b) top view and (c) front view (cross-section).

Table 5.7 Average tensile values with SDs obtained for nine SC/0/90 samples, excluding the extreme t358 sample.

	Young's modulus MPa	Yield stress MPa	Strain at break
Average of nine samples	525	22.2	10.5
SD of nine samples	7	0.2	1.2

The differences between averages and SDs calculated for ten (Table 5.6) and nine samples (Table 5.7) are not significant and the relationships between the values for the samples with and without a chip discussed previously remain similar.

The similar values of SDs for five and for ten samples suggest that it is appropriate to test five samples. For certain chip arrangements more than five and up to ten samples were tested in order to achieve an acceptable repeatability and distinguish the characteristic trends.

In the next section the results for the samples with and without a chip are compared.

5.2.3 Chip effect

In this section the plain polyethylene samples and the samples with a chip (SC/0/90) are compared in order to determine how the inclusion of a chip of much larger size than standard polymer reinforcement influences polyethylene mechanical behaviour. Figure 5.4 shows the plots while Table 5.8 lists the key numerical values.

Table 5.8 Average tensile values with SDs obtained for plain and SC/0/90 samples.

Sample	Young's modulus MPa	Yield stress MPa	Strain at break
plain			
Average	476	22.5	12.8
SD	50	0.2	0.7
SC/0/90			
Average	523	22.2	10.7
SD	9	0.3	1.2

From Table 5.8 it can be seen that the Young's modulus of the samples with a chip is higher than for the plain polyethylene; however, the difference is within the maximum SD (50MPa), thus it is hard to rely on it. The yield stress is higher for the plain samples; however, the difference is again insignificant. Only the strains at break differ by a significant value of 2.1, which is greater than the maximum SD of 1.2.

Even though the first two quantities cannot be justified due to the limited accuracy of their measurement, these dependencies are in accordance with the observations of other researchers testing composites. They also noticed a reinforcing effect of fillers such as glass beads (Liang, 2007; Liang & Li, 1998; Lu et al., 1992; Yang et al., 2008), glass flakes (Majeed, 2001), and mica flakes (Liang & Yang, 2007) on the polymer matrix. The details of their research were given in section 2.3.3.1. The examples of the results obtained by some researchers for different filler contents are given in Figures 5.6 and 5.7.
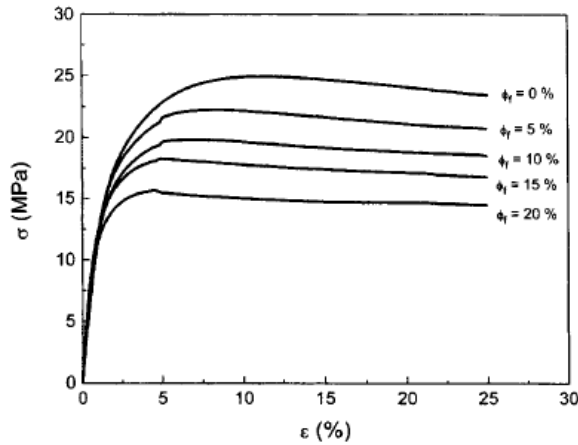
Figure 5.6 Stress-strain curves of PP reinforced with different content of glass beads (Φ_f) of average diameter 4μm tested at speed 1mm/min (Liang & Li, 1998).
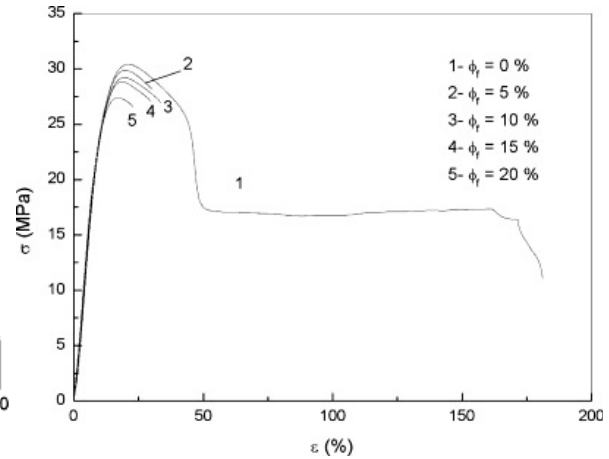
Figure 5.7 Stress-strain curves of PP reinforced with different content of glass beads (Φ_f) of average diameter 70μm tested at speed 50mm/min (Liang, 2007).

It has to be noted that the polymer grades they studied varied from the pipe-grade HDPE analysed in this research and the fillers they used had different composition, size, shape, and concentration than the silicon chips. In addition, the geometry of their samples and the speed of testing differed; however, the results presented here seem to be consistent with their observations. In general, the fillers improved stiffness (Young's modulus) but reduced strength (yield stress) and ductility (strain at break) with increasing filler content. Only Liang & Yang (2007) noticed an increase in strain at break for up to 5% filler content and then drop; however, in the tested composite the matrix-filler interface was improved due to the use of a silane coupling agent.

The tensile values for the samples with a chip can also be obtained from Equations 2.10-2.12 (page 39); however, it has to be remembered that the theoretical calculations are practically not appropriate for the case of a single chip considered here, as they are designed for small filler particles uniformly distributed within polymer.

When applying Equation 2.10 for theoretical calculation of Young's modulus of a composite (E_C) the modulus for plain polyethylene (476MPa) and the volumetric content of the chip (V_F)

are considered. V_F is calculated on the basis of the volume of the SC chip $(0.5 \cdot 4 = 2 \text{mm}^3)$ and the volume of the polyethylene within the gauge region (approximately: $4.2 \cdot 12.6 \cdot 25 = 1323 \text{mm}^3$), which gives $V_F = 0.15\%$ (one chip per sample). Thus $E_C = 476\,(1 + 2.5 \cdot 0.0015) = 478 \text{MPa}$, which is much smaller than the value obtained in the experiments. The potential difference of 2MPa between the value for the samples with and without a chip obtained from the calculation is smaller than the practical difference of 47MPa.

The theoretical yield stress can be obtained from Equation 2.11, $\quad _{yC} = 22.5\,(1 - 0.0015^{2/3}) = 22.2 \text{MPa}$. This time the value is in agreement with the experimental result. The strain at break of a composite can be projected using Equation 2.12, $\quad _C = 12.8\,(1 - 0.0015^{1/3}) = 11.3,$ which gives a value a bit greater than the experimental value of 10.7.

The last two equations consider a reduction of the effective available load bearing area of the matrix due to the inclusion of the filler. The yield stress can be adequately estimated by considering a direct reduction in the sample cross-section due to the inclusion of a chip. Initially, the cross-section of the sample is approximately 54mm² while the cross-section of the SC chip is 1.13mm² in the widest place, which is approximately 2% of the sample. As the stress is equal to the load divided by the cross-sectional area, the yield stress of the SC/0/90 sample reduces theoretically to: $\quad '_{yC} = 22.5\,(1 - 0.02) = 22.1 \text{MPa}$, which is also relatively close to the experimental value obtained.

In the stress calculations the constant cross-sectional area of the sample is considered (nominal stress); however, when the neck develops the cross-section of the sample reduces. The chip does not deform and constitutes an even higher percentage of the reduced sample cross-section. Therefore, the chip effect becomes theoretically more severe with increased duration of the test, but it is difficult to estimate how the proportion of chip to the polymer

area changes throughout the test. However, this applies only to the small part of the sample, where the chip is placed. With increased duration of the test, the sample elongates and the chip effect becomes more local and does not have much influence on the shape of the graph.

More complex equations for the modulus calculation (e.g. Halpin & Kardos, 1976) consider also the aspect ratio and the orientation of the filler. The best reinforcing effect is observed when the volume fraction and the aspect ratio are fairly large, and there is a minimum misalignment of fibres or flakes from the axis or plane of application of the stress (Xanthos, 2010). In this case the aspect ratio (4.5) and volumetric content (0.15%) are very small, although the orientation of the chip is advantageous.

Further, the deformation of the samples with and without a chip is analysed and compared on the basis of the specimen profiles (Figures 5.9 and 5.11) at different stages of the tensile test marked in Figures 5.8 and 5.10. As the profiles of both samples were similar, only selected photographs of the sample with a chip showing differences between both samples are shown.

The chips and cracks could be seen with the naked eye during the test; however, they are not clearly visible in the photos, therefore the crack area and chip are occasionally marked, by an ellipse and a circle to highlight these areas, respectively.
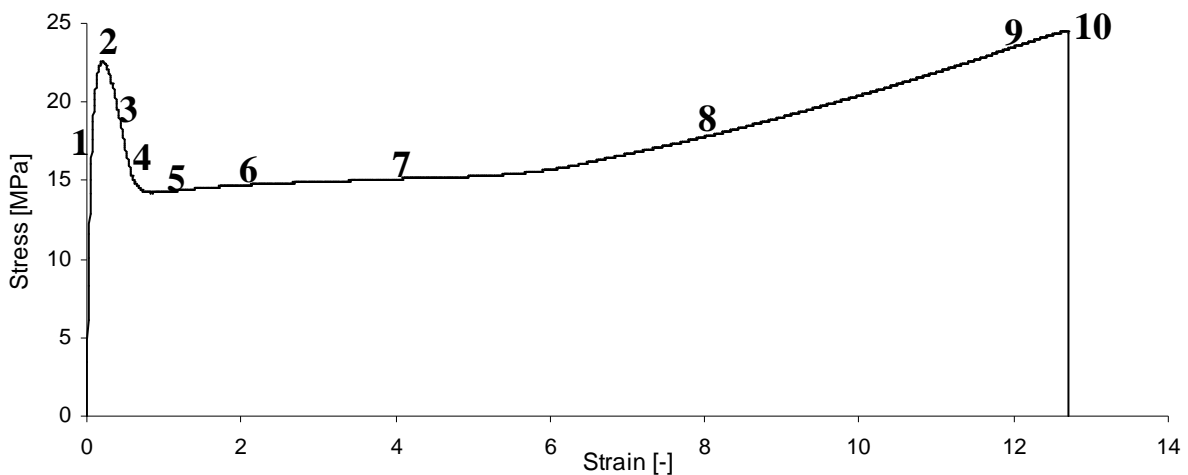
Figure 5.8 Stress-strain curve for the plain polyethylene sample with characteristic stages marked and shown in the photographs in Figure 5.9.

162
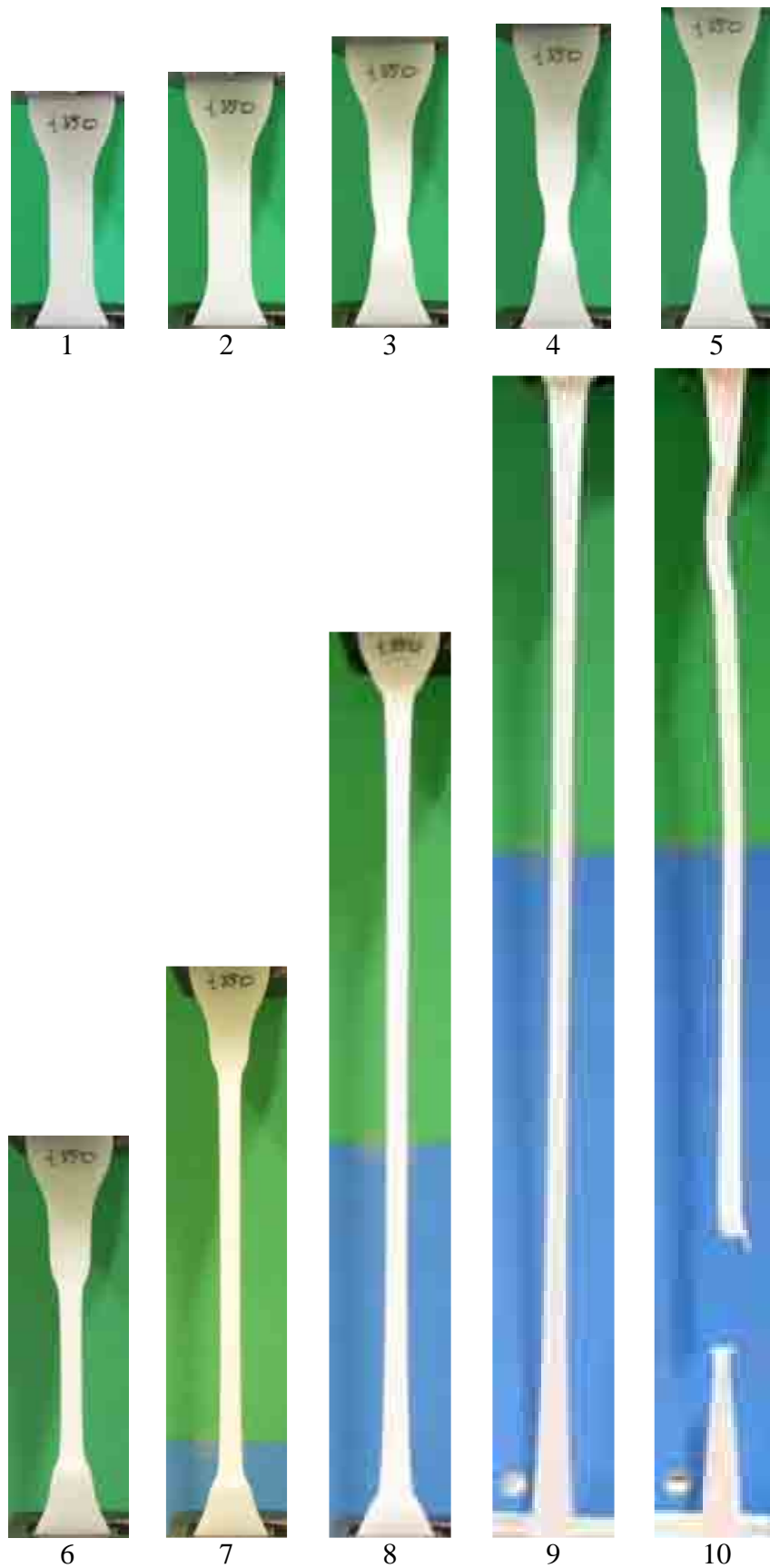
Figure 5.9 Profiles of the plain polyethylene sample during characteristic stages (see Figure 5.8) of the tensile test.
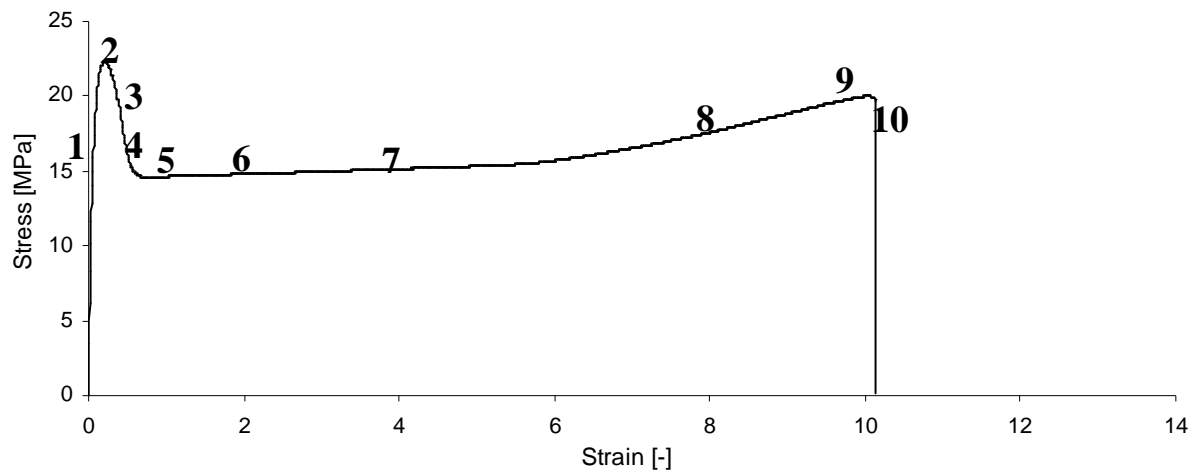
Figure 5.10 Stress-strain curve for the SC/0/90 sample with characteristic stages marked and shown (only selected) in the photographs in Figure 5.11.
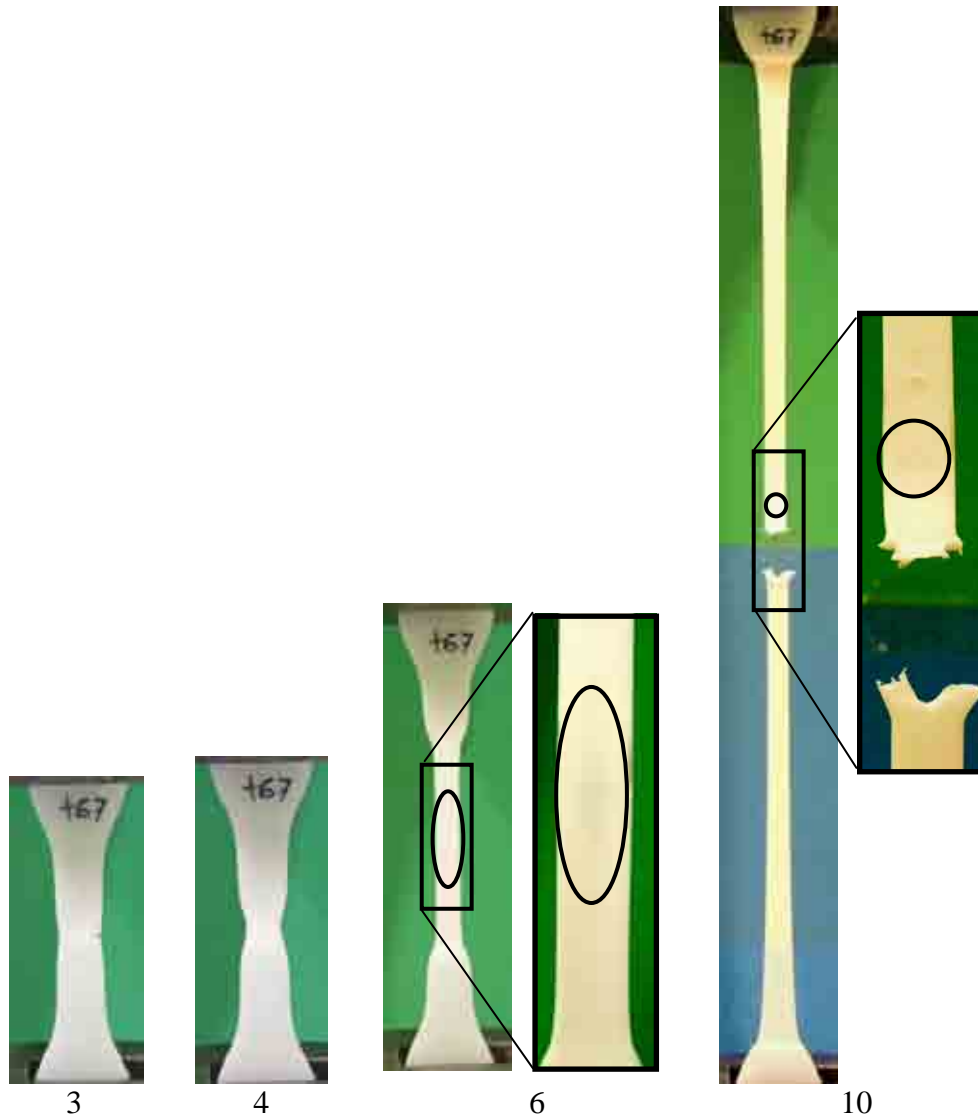
Figure 5.11 Profiles of the SC/0/90 sample during selected characteristic stages (see Figure 5.10) of the tensile test. Note: the crack region is marked in stage 6 (ellipse) while the chip is identified in stage 10 (circle), and the central part of the sample is enlarged in both stages.

The tensile deformation of plain polyethylene samples on a molecular level was described in section 2.2.4.2, where the characteristic test stages are also named (Figure 2.15). When analysing the macroscopic behaviour of the samples in Figures 5.9 and 5.11 it can be seen that initially they stretch homogenously within the gauge region until they reach a yield point (stage 2) at which one cross-sectional slice yields independently of the rest of the specimen. From this local narrowing of the sample the neck starts to form. Initially, the thinning is not visible with the naked eye but with time the neck becomes more distinct as it narrows down (stage 3) until a strain of approximately 0.6 is reached (stage 4).

In the case of the sample with a chip, the separation of the chip from the matrix causes a reduction of the area undergoing an external stress load concentration and hence the matrix around the chip (central) yields first (Figure 5.11, stage 3). In the case of the plain polyethylene sample the neck starts to form in a more random place, which depends on the structural material/sample characteristic and/or defects. After the yield point the stress-strain curve of the sample with a chip goes down steeper as the neck narrows down quicker than in the case of the plain polyethylene (see Figure 5.4 for comparison). In further stages the curves are identical and overlap.

Further, the neck propagates to encompass the entire length (cold drawing process) and the sample elongates. The force required for the neck propagation is almost constant resulting in a 'plateau' in the stress-strain curve in a strain range of approximately 1-6 (see Figures 5.8 and 5.10). Thus the 'natural draw ratio' is approximately 6.

Then, the 'strain hardening' stage proceeds until the sample breaks at the weakest point.

In the case of the chip in the sample it is constrained within the polyethylene and causes a continuous stress concentration, which increases with the neck development as the ratio of the

chip to the reduced cross-sectional area of the sample (turning into neck) increases. As the crack increases, the chip gets looser due to lack of adhesion between the chip and the polyethylene matrix. A crack opening displacement and thus a microstrain at a crack tip can be relatively large and can reflect two extreme deformation behaviours: shear yielding (formation of yield zone) and/or crazing (formation of fibrous zone), both associated with plastic deformation. In plain polyethylene samples this phenomena also occurs and is described as stress whitening (American Society of Metals, 2003).

The crack expands along the chip plane in the tensile direction during sample elongation. This could be seen during the test with the naked eye; however, the photographs do not show it clearly and therefore the region encompassing the crack is marked in Figure 5.11, stage 6. The crack development can be better seen in the photographs of the sample with a chip on the surface presented further, in section 5.2.6.1. Similar behaviour was observed by Zhuk et al. (1992) (Figure 5.12) and Lu et al. (1992) who tested glass bead filled polyethylene. First, the matrix in the polar region of the particles yielded and they debonded from the matrix;
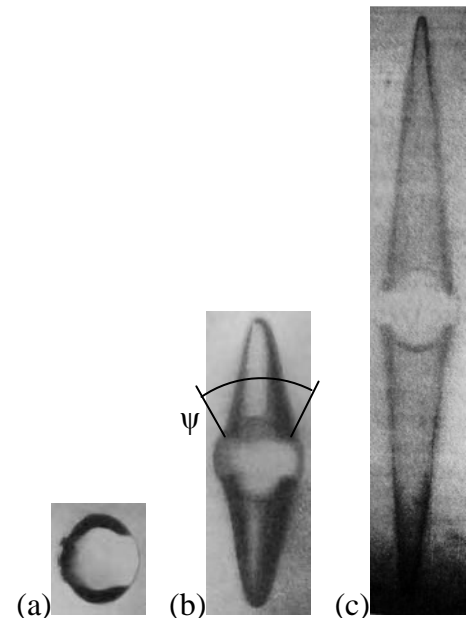
Figure 5.12 Void formation around the glass bead in PE: (a) initiation of debonding (dark region), (b) void formation during debonding, (c) a void in the neck region; ψ – debonding angle (Zhuk et al., 1992).

then the voids appeared in the polar zone of the particles and grew along the tensile direction. The extensive plastic deformation at the crack tip is ultimately the point of sample failure.

The results showed that inserting an SC chip at the orientation 0/90 has little impact. However, the importance of other factors such as chip shape, size, number and orientation

166

need to be further investigated. Other parameters such as sample thickness, matrix material and speed of testing also require investigation and the last one is studied in the next section.

5.2.4 Strain rate effect

The plain polyethylene and SC/0/90 samples were tested at additional speeds (5, 20, and 100mm/min) besides standard 10mm/min in order to determine the effect of strain rate on material performance. Exceptionally, only three samples of each type were tested as the differences between the plots were clear enough to draw general conclusions and the data are not used for comparison with other tests later in the project.

In addition, three plain polyethylene samples were tested at 1mm/min, which is the speed recommended by BSI (1996c) for Young's modulus measurement. The test was stopped at a strain of 1.0 as it would take around 18hrs to test three samples to the end and for the Young's modulus calculation only the initial elastic part of the stress-strain curve is required.

Figures 5.13 and 5.14 show the data for the selected samples with the yield stress and strain at break values closest to the average are presented for each speed.
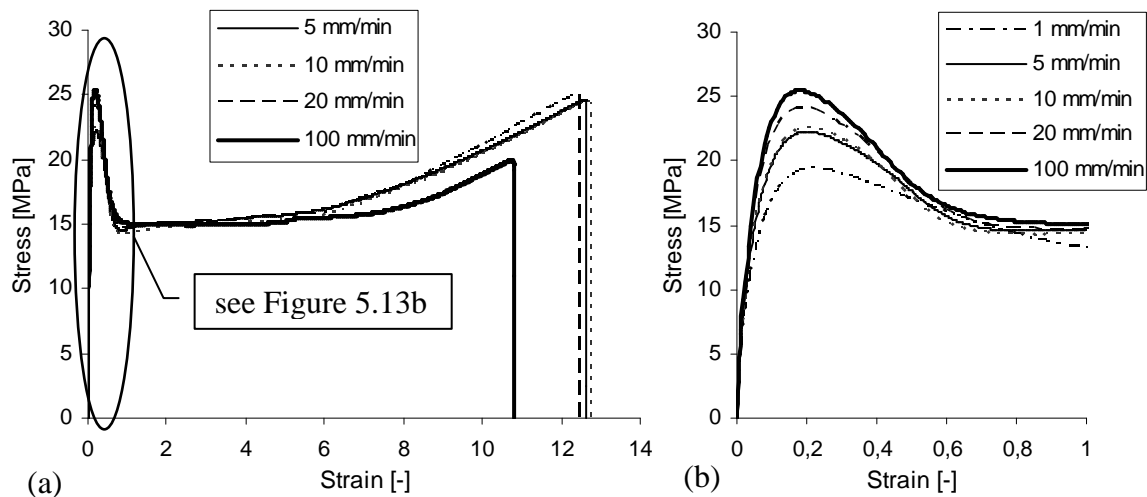
Figure 5.13 (a) Stress-strain curves for the selected plain polyethylene samples tested at speeds 5, 10, 20, and 100mm/min; (b) enlarged initial section of (a). Note: 1mm/min presented only in (b).
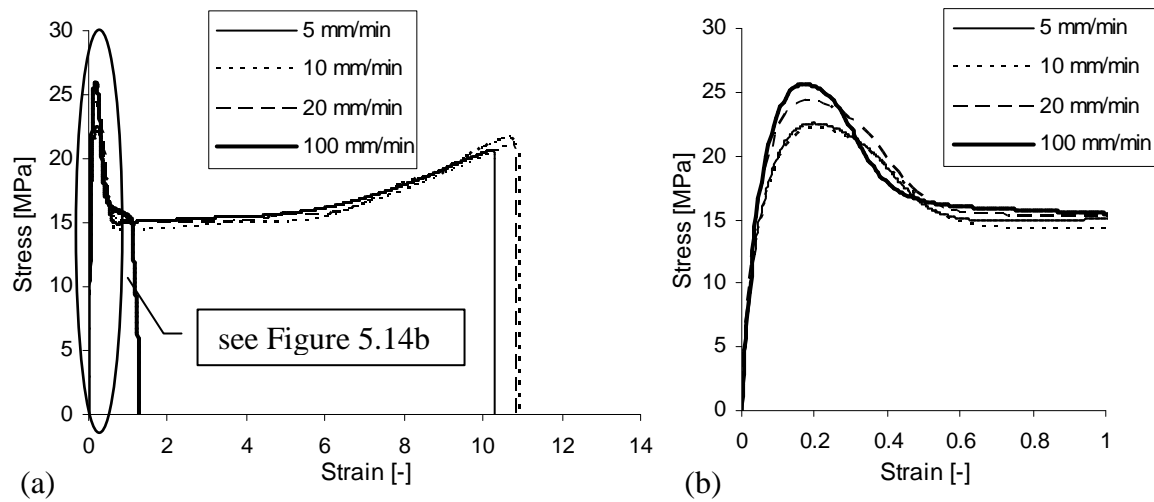
Figure 5.14 (a) Stress-strain curves for the selected SC/0/90 samples tested at speeds 5, 10, 20, and 100mm/min; (b) enlarged initial section of (a).

When comparing the shapes of the curves for samples with and without a chip for each speed a similar tendency can be observed as for the samples tested at 10mm/min and analysed in section 5.2.3 (page 159). For SC/0/90 samples, after the yield point is reached, the curve goes down steeper (larger negative gradient) than in the case of the plain polyethylene. After this point the curves are identical and overlap and finally the plain samples reach larger strain at break values than the samples with a chip.

Tables 5.3, 5.4 and 5.6 presented the results for the samples tested at 10mm/min, while Tables 5.9-5.15 list the results for other speeds. Table 5.16 summarizes the key numerical values.

Table 5.9 Tensile values for the plain polyethylene samples tested at 1mm/min.

Sample	Young's modulus MPa	Yield stress MPa
t408	513	19.6
t409	490	19.4
t412	474	19.1
Average	492	19.4
SD	20	0.3

168

Table 5.10 Tensile values for the plain polyethylene samples tested at 5mm/min.

Sample	Young's modulus MPa	Yield stress MPa	Strain at break
t391	515	21.4	12.7
t392	545	22.4	14.0
t393	535	22.3	12.7
Average	532	22.0	13.1
SD	15	0.5	0.8

Table 5.11 Tensile values for the SC/0/90 samples tested at 5mm/min.

Sample	Young's modulus MPa	Yield stress MPa	Strain at break
t396	579	23.1	9.7
t399	548	22.5	10.3
t416	516	21.2	10.9
Average	548	22.3	10.3
SD	32	1.0	0.6

Table 5.12 Tensile values for the plain polyethylene samples tested at 20mm/min.

Sample	Young's modulus MPa	Yield stress MPa	Strain at break
t381	505	23.9	13.6
t382	501	24.1	12.4
t383	499	23.7	12.4
Average	502	23.9	12.8
SD	3	0.2	0.7

Table 5.13 Tensile values for the SC/0/90 samples tested at 20mm/min.

Sample	Young's modulus MPa	Yield stress MPa	Strain at break
t386	516	24.4	10.6
t387	520	24.4	10.8
t388	501	23.5	10.8
Average	512	24.1	10.7
SD	10	0.5	0.1

Table 5.14 Tensile values for the plain polyethylene samples tested at 100mm/min.

Sample	Young's modulus MPa	Yield stress MPa	Strain at break
t413	430	25.0	12.2
t414	423	25.4	10.8
t415	414	25.6	9.3
Average	422	25.3	10.8
SD	8	0.3	1.5

Table 5.15 Tensile values for the SC/0/90 samples tested at 100mm/min.

Sample	Young's modulus MPa	Yield stress MPa	Strain at break
t389	428	25.6	1.3
t390	442	25.9	1.3
t400	433	25.9	1.2
Average	434	25.8	1.3
SD	7	0.2	0.1

Table 5.16 Average tensile values and SDs for the plain and SC/0/90 samples tested at speeds of 1, 5, 10, 20, and 100mm/min.

Speed of testing mm/min	Average Young's modulus MPa	SD of Young's modulus MPa	Average yield stress MPa	SD of yield stress MPa	Average strain at break	SD of strain at break
plain						
1	492	20	19.4	0.3	-	-
5	532	15	22.0	0.5	13.1	0.8
10	476	50	22.5	0.2	12.8	0.7
20	502	3	23.9	0.2	12.8	0.7
100	422	8	25.3	0.3	10.8	1.5
SC/0/90						
5	548	32	22.3	1.0	10.3	0.6
10	523	9	22.2	0.3	10.7	1.2
20	512	10	24.1	0.5	10.7	0.1
100	434	7	25.8	0.2	1.3	0.1

When analysing the chip effect at different speeds, for the Young's modulus and strain at break the same dependency as at 10mm/min is noticed (lower moduli and higher strains at break for the plain samples). The yield stresses are slightly higher for the samples with a chip, which contradicts the observations of other researchers (e.g. Liang & Yang, 2007) and is assigned to non-uniformity of the samples and low accuracy of the measurement as for 5mm/min the SD of 1.0MPa was recorded.

The Young's modulus obtained at 1mm/min is 492MPa while the value measured by the material manufacturer at the same speed is 1000MPa (Borealis, 2008). This difference might be due to possibly a different geometry and production procedure of the samples, and different test equipment and measurement methods used.

When analysing the strain rate effect for the samples with and without a chip, the yield stress increases while the strain at break decreases with increasing speed (with some exceptions

assigned to the variations among the samples with a chip), which is in agreement with the research of Meinel & Peterlin (1971) and Ting et al. (2006a) who also tested polyethylene at various speeds ranging from 0.005 to 50mm/min.

The chip has the greatest impact at the highest speed of 100mm/min reducing strain at break to only 1.3 in comparison with 10.8 for the plain samples, which confirms observations of Kobayashi et al. (1996) who analysed the strain rate effect in glass beads reinforced HDPE.

Concerning Young's modulus no certain conclusion can be drawn as the limited accuracy of the measurement even reduces with increasing speed of testing plus the sample tested at high speeds might slip from the grips due to a very dynamic start of the test.

The results have shown that the speed of testing has an impact on the mechanical performance of the samples in tension; however, the other samples are tested using one speed (10mm/min), therefore this differences do not have an impact on further analyses.

In the next section the material effect is studied for two different grades of polyethylene with and without a chip.

5.2.5 Material effect

The influence of the material type on the mechanical behaviour of the samples with and without a chip is studied here. As an alternative to the pipe-grade HDPE analysed in section 5.2.3 the off-the-shelf HDPE is investigated. Figure 5.15 presents the plots and Tables 5.17 and 5.18 list the tensile values for the plain and SC/0/90 samples, respectively.
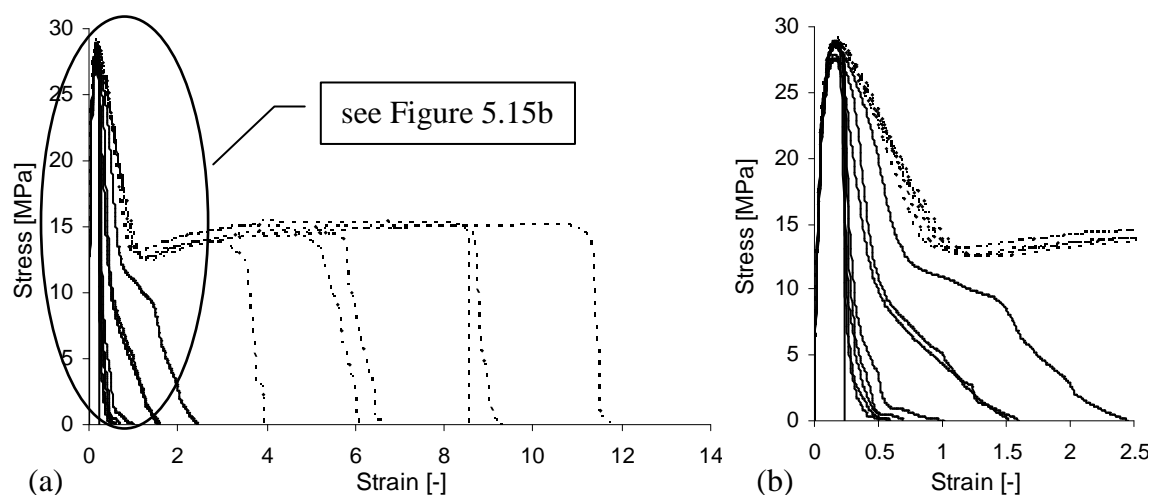
Figure 5.15 (a) Stress-strain curves for (- - -) the plain and (——) SC/0/90 off-the-shelf polyethylene samples; (b) enlarged initial section of (a).

Table 5.17 Tensile values for the plain off-the-shelf polyethylene samples.

Sample	Young's modulus MPa	Yield stress MPa	Strain at break
t165	740	28.3	9.3
t166	722	28.6	11.8
t167	748	28.7	8.5
t169	665	28.7	6.1
t335	723	28.8	6.7
t336	686	29.1	3.9
Average	714	28.7	7.7
SD	32	0.3	2.8

Table 5.18 Tensile values for the SC/0/90 off-the-shelf polyethylene samples.

Sample	Young's modulus MPa	Yield stress MPa	Strain at break
t170	757	28.7	0.6
t305	717	27.9	0.7
t306	741	28.9	0.6
t307	698	28.8	0.5
t308	725	28.5	2.4
t309	689	27.5	1.5
Average	727	28.3	1.0
SD	23	0.5	0.7

The stress-strain curves for the plain off-the-shelf HDPE samples have also a shape typical for HDPE with characteristic regions: elastic, yielding, necking, and cold drawing (Powell, 1983). However, the strain hardening stage (raising of the curve), which follows the cold drawing stage (plateau) observed in the case of pipe-grade HDPE (Figure 5.1) cannot be distinguished here. After Callister (2007) the precise shape of a force versus elongation curve

172

is determined by the initial morphology and molecular characteristics of the material, which differ for both polymer grades as indicated in section 3.3.5, page 82.

The off-the-shelf polyethylene has a very sharp peak and a much higher yield stress (28.7MPa) and Young's modulus (714MPa) than the pipe-grade material (22.5 and 476MPa, respectively), while its strain at break is noticeably lower (7.7 in comparison with 12.8 for the pipe grade). It has relatively high SD of 2.8, which is 36% of the average value while the SD for the pipe grade is only 0.7 (5%). This suggests that the off-the-shelf polymer might have more internal defects such as air voids, which accelerate sample failure. Its strength at break (ultimate strength) which is the stress before failure is also significantly lower in comparison with the value for the pipe-grade polymer (15 and 24MPa, respectively).

These differences are due to variations in the morphology of both samples indicated in section 3.3.5. The relatively high MFR and low MW and MWD of the off-the-shelf polymer contribute to a high crystallinity and density (79% and 0.971g/cm³, respectively) and are the signs of a simple structure of molecular chains with few branches. The low MW contributes to a low number of tie molecules connecting the lamellae (crystallites) and thus the elongation (ductility) and resistance to crack propagation are small (Nielsen, 1974; Ting et al., 2006b). The pipe grade polymer has different structural and physical properties (crystallinity and density equal to 67% and 0.956g/cm³, respectively), thus is much more ductile. In general, the higher the crystallinity and density of the material, the higher the yield stress and modulus and the lower the strain at break (Peacock, 2000), which the obtained results confirm.

The performance of the samples with chips also differs significantly. The chip in the case of already more brittle off-the-shelf polymer causes even more embrittlement reducing the strain at break to 1.0 compared with 10.7 for the pipe-grade polymer. This is in accordance with the

theory described by Nielsen (1974) that the composites with a ductile matrix have a higher elongation.

The visual analysis of the sample profiles and fracture might be useful by comparing the sample performance in tension. Figures 5.16-5.19 show the graphs with marked test stages and the photographs of sample profiles.
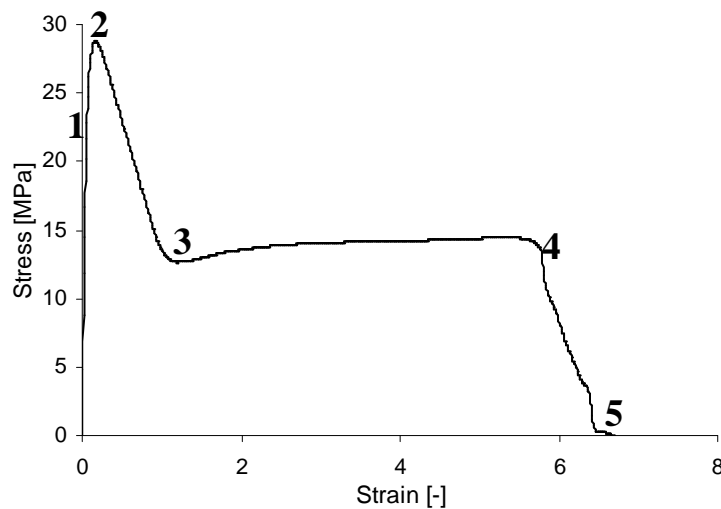
Figure 5.16 Stress-strain curves for the plain off-the-shelf polyethylene sample with characteristic stages marked and shown in the photographs in Figure 5.18.
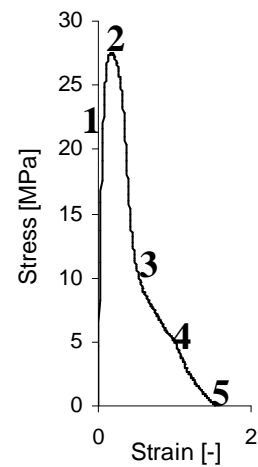
Figure 5.17 Stress-strain curve for the SC/0/90 off-the-shelf polyethylene sample with characteristic stages marked and shown in the photographs in Figure 5.19.
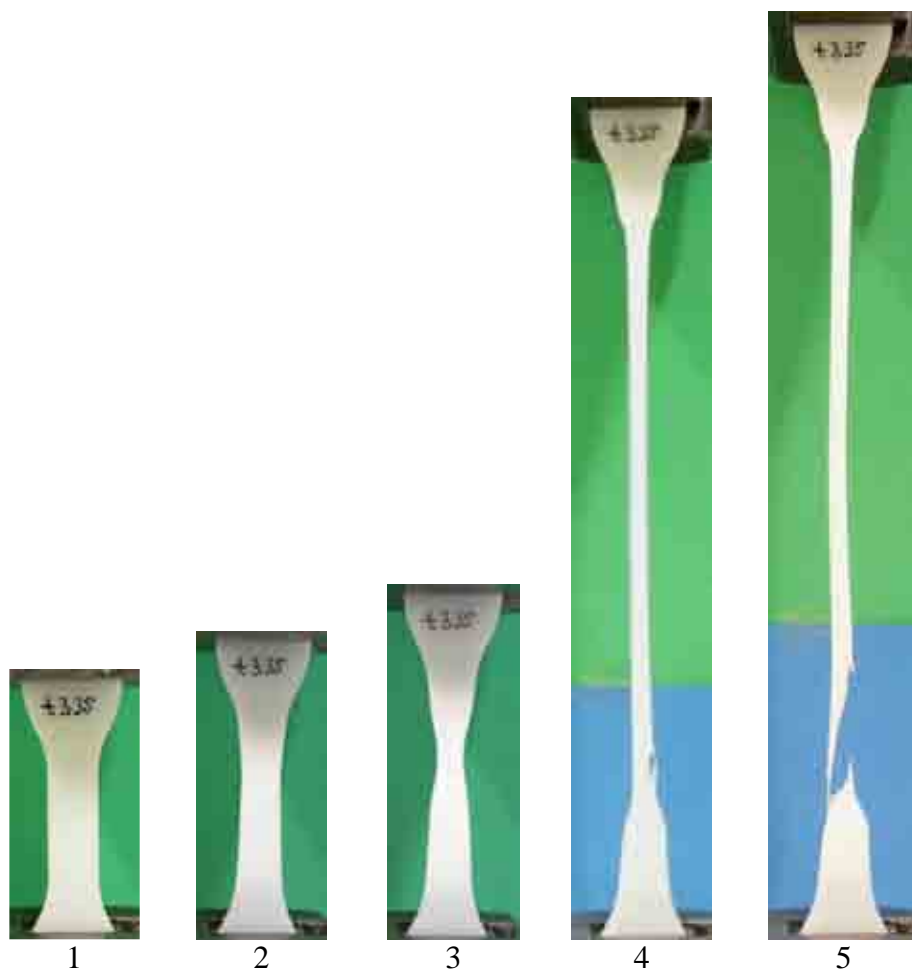
Figure 5.18 Profiles of the plain off-the-shelf polyethylene sample during characteristic stages (see Figure 5.16) of the tensile test.
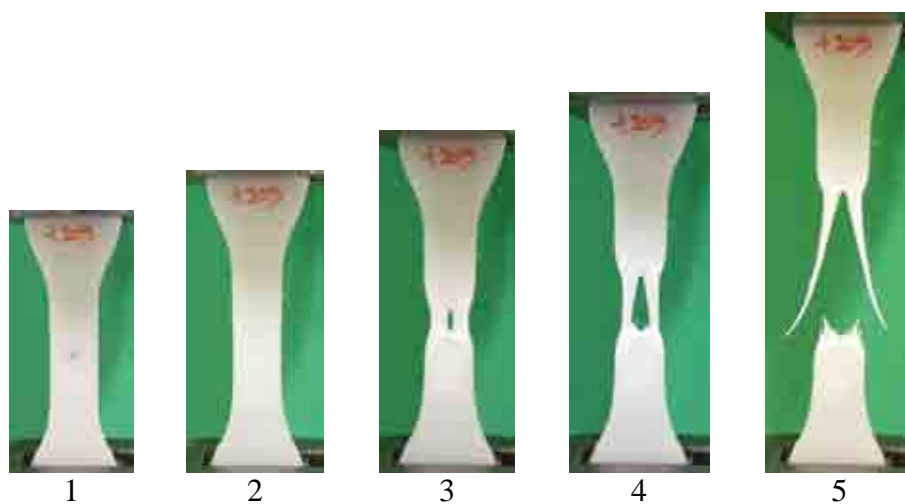
Figure 5.19 Profiles of the SC/0/90 off-the-shelf polyethylene sample during characteristic stages (see Figure 5.17) of the tensile test.

In the case of plain samples after the yield stress is reached the neck forms slower (curve goes down gentler) and is narrower in the off-the-shelf samples compared with the pipe-grade polymer (Figures 5.8 and 5.9, section 5.2.3). The cracks nucleate at random locations and propagate with very little ductility (Figure 5.18, Stages 4 and 5). The sample reaches a lower strain at break and the fibres break in stages in contrast to the pipe grade where the crack propagates horizontally across the sample cross-section.

In the case of the sample with a chip in both polymer grades the neck starts in the centre around the chip, which causes a stress concentration. In the case of pipe-grade polymer (Figures 5.10 and 5.11, section 5.2.3) the neck develops and encloses the entire gauge length. The crack develops within the neck without preventing sample elongation and the sample fails at the crack tip at a high strain. In the case of the off-the-shelf polymer the crack generates and penetrates through the sample thickness before the full neck is developed. It divides the sample into two parts causing formation of two separate thin necks (Figure 5.19, stage 3) which immediately narrow down and fail at their thinnest points. There is no cold drawing and strain hardening stage characteristic for ductile materials and the failure is considered as rather brittle.

The tests showed that the off-the-shelf HDPE is more susceptible to failure with and without a chip, when tested in tension. Pipe-grade HDPE is a very ductile material and therefore has a good stress crack resistance. However, this is dependent on the chip orientation, size, and shape, which are studied in the next sections.

5.2.6 Orientation effect on the basis of SC chip

This section aims to determine the influence of the chip orientation on sample performance in tension. The orientation SC/0/90 was already introduced. The data are initially compared with

other orientations of the SC chip and further, the effects of the chip shape and size are studied with respect to the orientation.

As the literature review indicated the important aspects associated with the chip orientation are position in relation to the direction of the applied load and the boundary conditions (the volume of the matrix surrounding the chip) (see section 2.3.3.2). These are especially important, when the proportion of the chip size to the sample size is relatively large like here. Therefore, the chip orientation towards the tension direction was varied. The position of the chip in relation to the sample surface influences the boundary conditions, thus it was investigated as well. Further, the test was also carried out for thinner (2.2mm thick) samples with an SC chip, where the proportion of the chip size to the sample size was even greater.

The tests indicated that the orientation of the chip has a great impact on the way in which the crack develops, therefore, first the plots and profiles of the samples during the tensile test are studied and compared. Further, the numerical data are presented and analysed.

5.2.6.1 Analysis of the profiles of the samples with an SC chip at various orientations

In this section the development of the crack in the samples with an SC chip at various orientations is studied. When the chip is located on the surface, there is no matrix cover from one side of the chip, thus this extreme orientation is studied first (Figure 5.21) and compared with the orientation 0/90 (Figure 5.11, page 164) where in both cases the chip is aligned parallel to the sample surface. As the neck developed similarly like in the SC/0/90 sample in most cases, only the central part of the sample with a chip is usually presented, like it was done in Figure 5.11, stages 6 and 10. The numbers assigned to the stages in different figures (samples) do not usually correspond to each other unless stated otherwise.
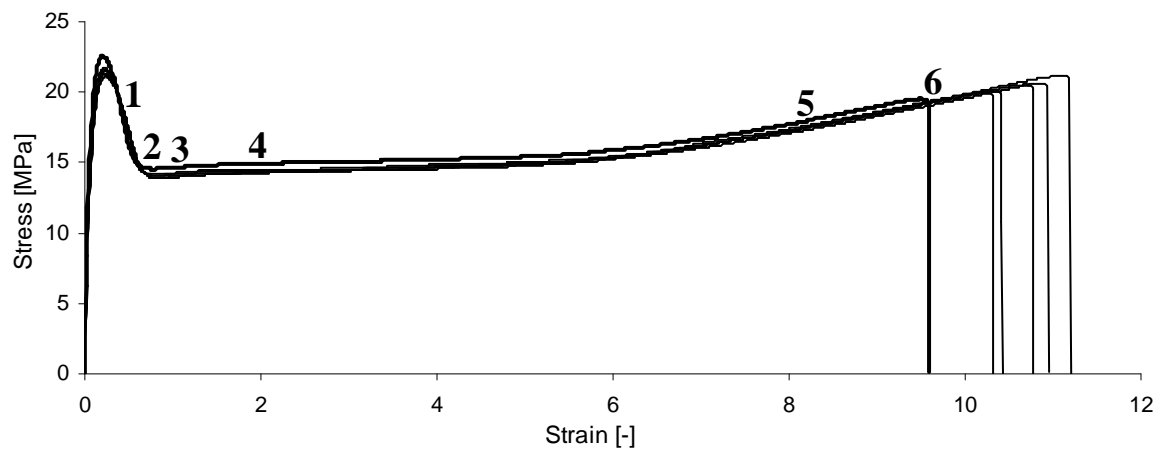
Figure 5.20 Stress-strain curve for the SC/surf samples with characteristic stages marked for the sample marked bold and shown in the photographs in Figure 5.21.

| 1 | 2 | 3 | 4 | 5 | 6 |
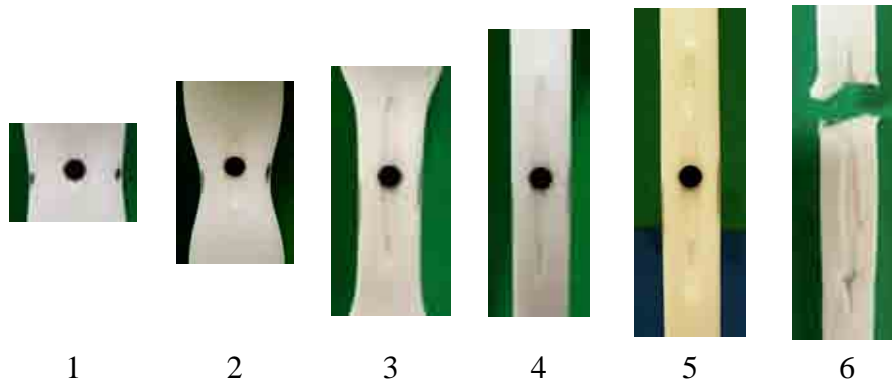
Figure 5.21 Central part of the SC/surf sample during characteristic stages of the tensile test.

From Figure 5.21 it can be seen that the crack starts to form simultaneously with the neck (stage 1). The approximate debonding angle (ψ) (for the definition see Figure 5.12) at this stage equals to approximately 45°. When the neck narrows down the crack expands (stage 2) and ψ increases to 68°. The crack also narrows down while expanding (compare stages 2 and 3). The width of the crack in the widest place in stage 3 is smaller than the diameter of the chip, which suggests that the chip is slightly pushed out of the crack. Further, the crack expansion and narrowing slows down and no significant difference in the shape of the crack can be seen between stages 4 and 5 when the sample elongates significantly (see Figure 5.20).

Similar observations were made by Zhuk et al. (1992) who studied the debonding of glass beads within the PP and PE matrix and concluded that it is terminated at an angle of 68° when

it becomes energetically disadvantageous due to friction. However, they investigated glass beads inside the matrix, thus the inclusions could not be pushed out of the crack. No literature was found on the mechanical properties of the samples with inclusion on the surface.

The upper crack tip expands more (Figure 5.21, stage 5), which suggests a higher stress concentration in this part of the crack. Finally, the sample fails at the upper crack tip after it penetrates through the whole sample thickness and width (stage 6).

Further, the orientation of the chip towards the sample surface and edges is varied maintaining the parallel orientation towards the direction of the applied load. In Figure 5.22 the shapes of all stress-strain curves for orientations 45/45 and 90/0, and selected SC/0/90 samples are compared.
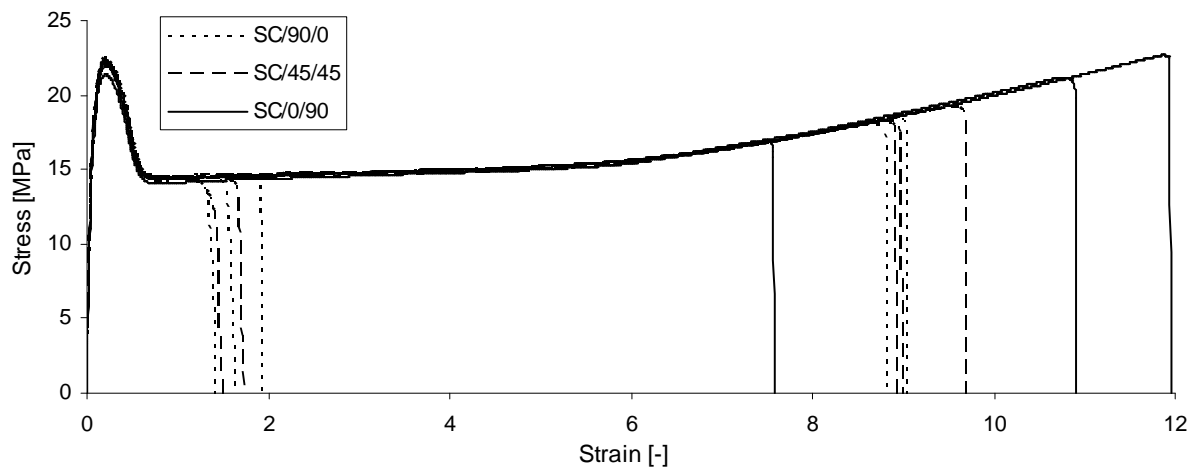
Figure 5.22 Stress-strain curves for the SC/90/0 and SC/45/45 samples and the selected SC/0/90 sample.

When analysing the plots for the SC/45/45 and SC/90/0 samples two groups of graphs can be distinguished with regards to the strain at break values, below 2 and approximately 9 (on average). These variations are assigned to the chip position, which is further studied on the basis of the X-ray scans of a few samples at both orientations (Figure 5.23).

(a)   (b)
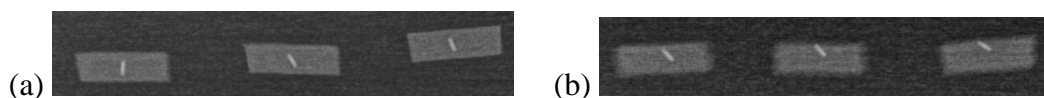
Figure 5.23 X-ray scans through the cross-sections of the (a) SC/90/0 and (b) SC/45/45 samples.

The X-ray scans indicate that there can be some slight deviation from the theoretical chip arrangement. At the orientation 90/0 (Figure 5.23a) only in the first sample the actual chip position is in accordance with the intended position. Other chips slanted slightly towards the sample edges. At the orientation 45/45 (Figure 5.23b) all the chips are approximately at the angle of 45º towards the sample surface; however, they are placed in the upper part instead of the middle of the sample, touching its surface. As the differences between actual chip positions for both orientations are greater than the differences between the samples from the same group, it indicates that something else in the chip position governs the pattern of crack development influencing the strain at break. This is studied on the basis of the profiles of the selected samples from both discrete groups, with high and low strains at break.

| 1 | 2 | 3 | 4 |
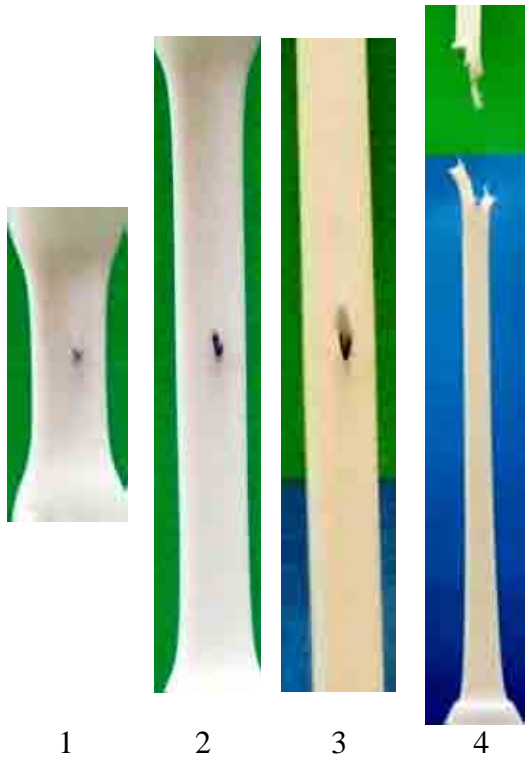
Figure 5.24 Central part of the theoretical SC/90/0 sample with a high strain at break during characteristic stages of the tensile test. Note: in stage 4 the profile of the sample down from the chip is shown, in a smaller scale.

| 1 | 2 | 3 | 4 |
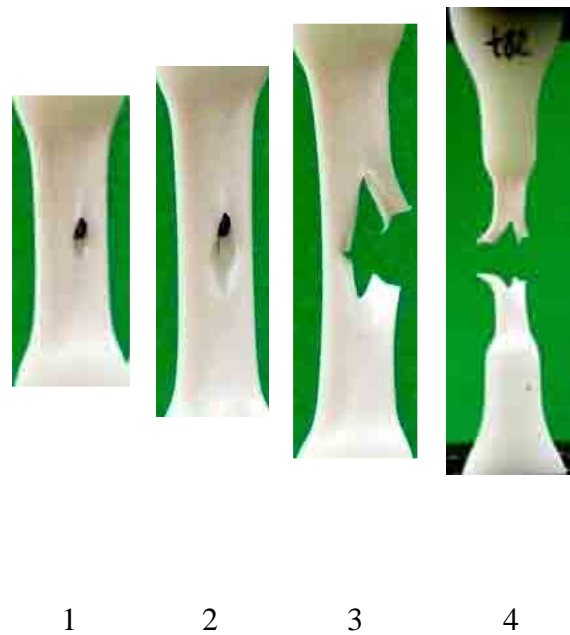
Figure 5.25 Central part of the theoretical SC/90/0 sample with a low strain at break during characteristic stages of the tensile test. Note: in stage 4 the whole profile of the sample is shown, in a smaller scale.

In both samples, with high and low strain at break, the neck forms at the level of the chip, which causes stress concentration. In the first sample (Figure 5.24) the neck elongates and encompasses the whole gauge length like in the plain polyethylene (Figure 5.9), SC/0/90 (Figure 5.11) and SC/surf samples (Figure 5.21). The crack develops slowly in the vicinity of the chip, in the chip plane along the neck and through the sample thickness, which contributes to sample failure, while in the SC/0/90 and SC/surf samples the crack developed mostly in the chip plane along the neck and the failure originated at the crack tip.

Once the crack increases the chip gets looser and it realigns within the crack and positions itself along the neck/crack in the tension direction (Figure 5.24, stage 3) causing much smaller stress concentration. This is similar to the chip placed on the sample surface (Figure 5.21), which is not totally constrained within the polymer matrix and therefore causes less stress concentration.

In the second sample (Figure 5.25) the chip seems to be positioned at a small angle towards the tension direction, which imposes a different pattern and direction of crack development. The crack is definitely wider and has a rhombus shape in contrast to the crack developed in the sample presented in Figure 5.24, which has a more ellipsoidal, oval shape and is narrower. Due to the large size of the rhombus crack the local thinning forms in the middle of the crack and it penetrates through the sample thickness. First, the neck is split by the crack into two narrower necks and then one of them breaks (Figure 5.25, stage 3). This is followed immediately by the sample failure at a relatively small strain (Figure 5.25, stage 4), before the neck encompasses the whole gauge length.

The first type of samples (with high strain at break) can be classified as 90/0 as the chip orientation is very close to the intended. The second type of samples (with low strain at break) can be classified as 90/0 slanted, as the chip orientation deviated slightly from the intended.

181

Therefore, as the chip does not form any regular angles with the sample surface and/or edges, it should not be classified as 45/45.

These analyses show that a slight deviation from the orientation parallel to the tension direction has a significant influence on the structural integrity of the polymer. Therefore, the performance of the samples with varied orientation towards the tension direction is further studied.

The samples at the orientations SC/90/90 (the chip perpendicular to the tension direction) as well as SC/45/90 and SC/90/45 (intermediate orientation towards the tension direction) were tested and compared. The shapes of the obtained stress-strain curves were very similar and are shown in Figures 5.26-5.28. The profiles of the samples were also very similar, thus only one (for the orientation 90/90) is shown in Figure 5.29 with the characteristic stages marked in Figure 5.26.
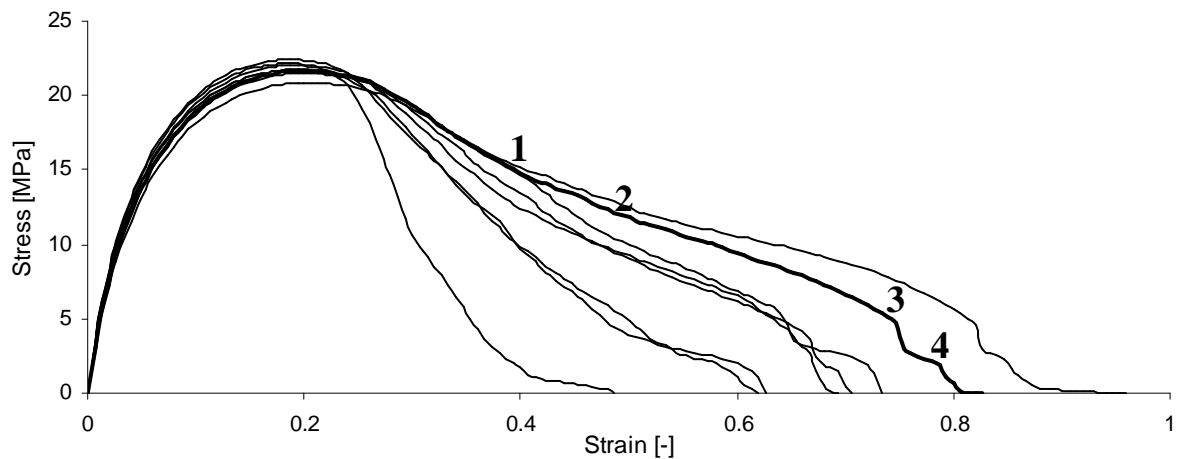
Figure 5.26 Stress-strain curves for the SC/90/90 samples with characteristic stages marked for the sample marked bold and shown in the photographs in Figure 5.29.
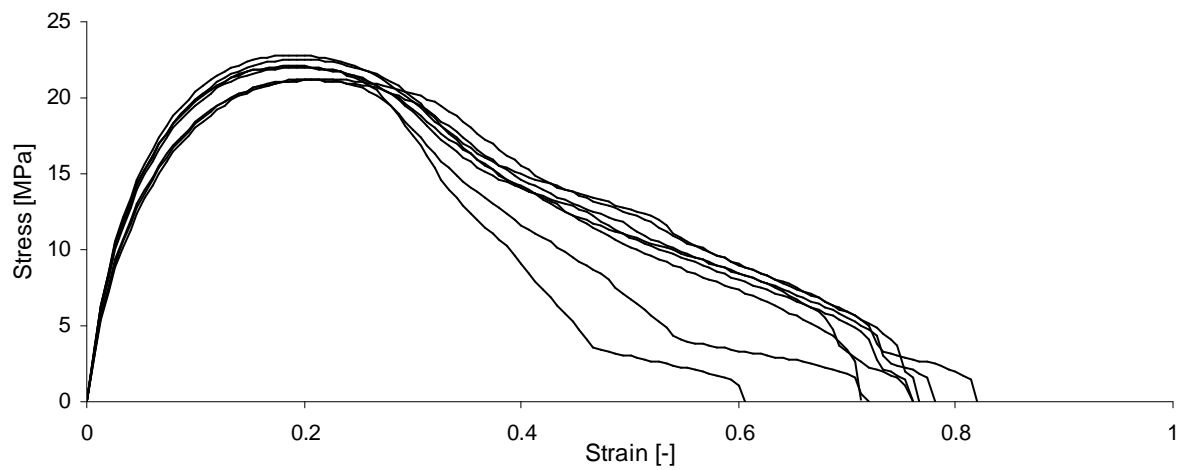
Figure 5.27 Stress-strain curves for the SC/45/90 samples.
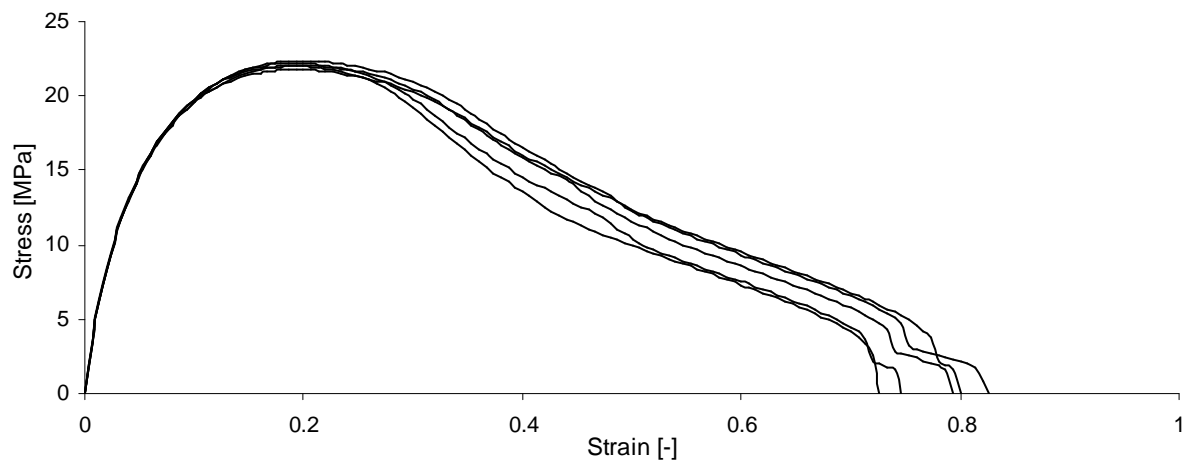
Figure 5.28 Stress-strain curves for the SC/90/45 samples.
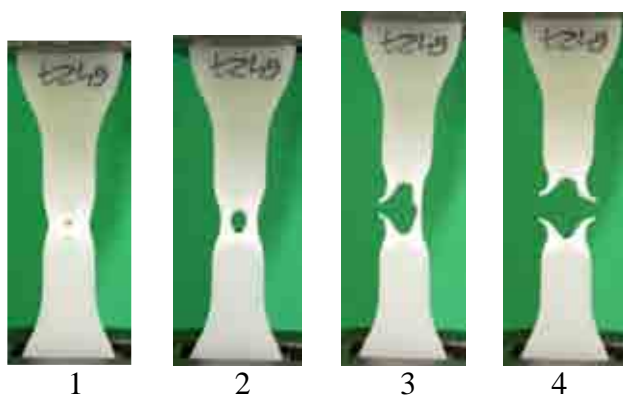
Figure 5.29 Profiles of the SC/90/90 sample during characteristic stages (see Figure 5.26) of the tensile test.

At the orientation SC/90/90 the chip area (4mm²) amounts to 7% of the sample cross-section, reducing the area of the load bearing polymer matrix, thus the crack formed in the vicinity of

the chip penetrates quickly through the sample thickness. It expands immediately and the sample is split by the crack into two narrow 'necks' and when the first one fails this is immediately followed by the failure of the second. After the first 'neck' breaks (Figure 5.29, stage 3), the load (nominal stress) reduces (Figure 5.26, stage 3). In the sample stretching process no cold drawing or strain hardening stages typical for plain polyethylene can be observed and the failure is close to brittle as the neck does not develop properly.

In addition, at the orientation 90/90 the chip has a minimum polymer cover (1mm on both sides of the sample, on average); however, the same applies to the sample 90/0, which reached much greater strain at break, thus this is not the only cause of accelerated sample failure.

These tests confirm previous observations that once the chip's position deviates from the orientation parallel to the tension direction, the failure is significantly accelerated, which is in agreement with other researchers, who studied polymer composites. However, they investigated the impact of the filler orientation on the stiffness of the composite (Liang & Yang, 2007; Xanthos, 2010). The impact of an SC chip at various orientations on the stiffness and other parameters is studied in the next section on the basis of the tensile data.

5.2.6.2 Analysis of the results obtained for the samples with an SC chip at various orientations

In this section the results obtained in the tensile test for different samples with an SC chip are analysed.

Tables 5.19-5.24 list the tensile values for the samples with an SC chip at the orientations: 90/0, 90/0 slanted, 90/90, 45/90, 90/45 and surface. The data for the plain and SC/0/90 samples were listed in Tables 5.3, 5.4 and 5.6 (pages 148 and 157). Figure 5.30 shows the

plots for the samples at each orientation, with the values closest to the calculated averages. The plots for two extreme plain polyethylene samples are also shown in order to justify the potential influence of the sample manufacturing conditions on their mechanical performance. Table 5.25 summarizes the tensile values.

Table 5.19 Tensile values for the SC/90/0 samples.

Sample	Young's modulus MPa	Yield stress MPa	Strain at break
t76	413	22.2	8.8
t79	478	22.3	9
t81	465	21.8	8.9
t83	517	22.1	9
t84	504	22.0	9.7
Average	475	22.1	9.1
SD	40	0.2	0.4

Table 5.20 Tensile values for the SC/90/0 slanted samples.

Sample	Young's modulus MPa	Yield stress MPa	Strain at break
t77	415	22.2	1.6
t78	493	21.9	1.4
t80	526	22.5	1.9
t82	519	22.2	1.5
t85	525	22.3	1.7
Average	496	22.2	1.6
SD	47	0.2	0.2

Table 5.21 Tensile values for the SC/90/90 samples.

Sample	Young's modulus MPa	Yield stress MPa	Strain at break
t103	531	22.1	0.5
t104	532	22.4	0.6
t216	505	21.7	0.7
t217	479	22.2	0.7
t218	464	21.7	0.8
t219	418	20.9	1.0
t220	477	22.0	0.7
t251	515	21.7	0.6
Average	490	21.8	0.7
SD	39	0.5	0.2

Table 5.22 Tensile values for the SC/45/90 samples.

Sample	Young's modulus MPa	Yield stress MPa	Strain at break
t28	475	21.2	0.7
t29	474	21.2	0.8
t107	492	21.1	0.8
t108	542	22.8	0.8
t109	530	22.5	0.7
t248	542	22.1	0.8
t249	520	22.0	0.8
t250	538	22.1	0.6
Average	514	21.9	0.7(5)
SD	29	0.6	0.1

Table 5.23 Tensile values for the SC/90/45 samples.

Sample	Young's modulus MPa	Yield stress MPa	Strain at break
t242	540	22.0	0.7
t243	527	22.2	0.7
t244	532	22.3	0.8
t245	528	22.0	0.8
t246	530	21.8	0.8
Average	531	22.1	0.8
SD	5	0.2	0.1

Table 5.24 Tensile values for the SC/surf samples.

Sample	Young's modulus MPa	Yield stress MPa	Strain at break
t30	471	21.7	10.4
t31	481	21.6	10.3
t32	476	21.3	10.9
t33	352	21.5	10.8
t39	376	21.1	11.2
t68	537	22.6	9.6
Average	449	21.6	10.5
SD	70	0.5	0.6
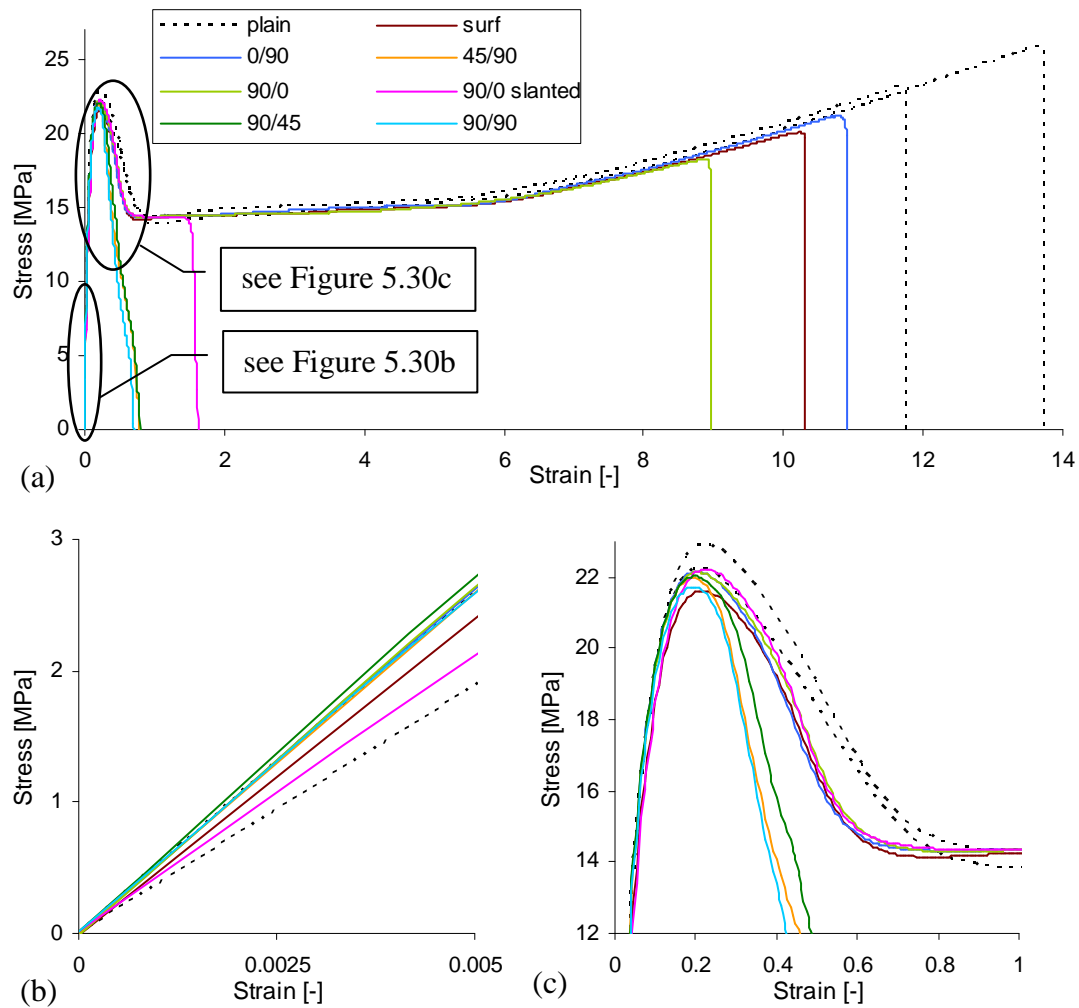
Figure 5.30 (a) Stress-strain curves for the samples with an SC chip at various orientations, (b) enlarged elastic region, (c) enlarged peak region. Note: the legend in (a) applies also to (b) and (c).

Table 5.25 Average tensile values with SDs for the samples with an SC chip at various orientations.

Orientation	Young's modulus MPa		Yield stress MPa		Strain at break	
	Average	SD	Average	SD	Average	SD
plain polymer	476	50	22.5	0.2	12.8	0.7
surf	449	70	21.6	0.5	10.5	0.6
0/90	523	9	22.2	0.3	10.7	1.2
90/0	475	40	22.1	0.2	9.1	0.4
90/0 slanted	496	47	22.2	0.2	1.6	0.2
90/45	531	5	22.1	0.2	0.8	0.1
45/90	514	29	21.9	0.6	0.7(5)	0.1
90/90	490	39	21.8	0.5	0.7	0.2

When looking at the slope of the stress-strain curves in Figure 5.30b reflecting Young's moduli it can be seen that the plots for most samples fit within the range determined for the plain polyethylene produced under different conditions, thus, the variations in the values might be due to different properties of the matrix. The average values range between 449MPa for the SC/surf samples and 531MPa for the SC/90/45 samples. The large SDs for some types of samples (maximum value of 70MPa for SC/surf samples) might also be associated with varying properties of the matrix and with the low accuracy of the modulus measurement.

After Xanthos (2010), in the oriented composites the largest modulus is obtained when the filler is aligned parallel to the tension direction, which is theoretically also the case here as the Young's modulus for the SC/0/90 samples is 523MPa (only for the SC/90/45 samples a slightly higher value was obtained). Composite modulus decreases rapidly when the filler deviates even slightly from this orientation and the transverse modulus (filler oriented perpendicular to the tension direction) is the smallest (Xanthos, 2010). Even though these findings were determined for fibres and flakes they should still be applicable to some extent

for other types of reinforcement, i.e. the silicon chips, which can be classified as platelets or flakes. Here, the value for the SC/90/90 samples (490MPa) was also in the lower range; however, this is not certain due to the limited accuracy of the measurements.

The average yield stresses for the samples with an SC chip are usually below the values obtained for the plain polyethylene produced under various conditions (see Figure 5.30c), for which the average yield stress equals to 22.5MPa. For the SC/surf samples the smallest value of 21.6MPa was recorded; however, this might be associated with low stiffness of the matrix as for these samples the lowest modulus was also obtained. In the case of other chip orientations it is suspected that the chip causes the reduction in the yield stress, especially in the samples where the modulus is larger than for the plain polymer, which applies to most of the samples. This might be due to the fact that the chip reduces the cross-section of the load bearing polymer matrix by maximum 7% in the SC/90/90 samples, as was mentioned in the previous section. For these samples the theoretical stress obtained on the basis of the value measured for plain polyethylene can be calculated as: $\sigma'_{yC} = 22.5\,(1-0.07) = 20.9\text{MPa}$, which is almost 1MPa lower than the value obtained experimentally. This difference might be due to the fact that the reduction in the sample cross-section is only local, at the length of 0.5mm, which is the thickness of the chip. Therefore, this calculation is not accurate.

The tensile values can also be obtained from the equations designed for composites, based on the measured values for the plain polyethylene and the volumetric content of the SC chip. The values were already calculated and discussed in section 5.2.3; however, the equations used do not consider the chip orientation. The theoretical yield stress was 22.2MPa, which is equal or very close to the values obtained for the orientations 0/90, 90/0, 90/0 slanted and 90/45. The actual strains at break are smaller than calculated.

Anyway, it is evident from the experiments that the chip reduces the yield stress of the samples and this effect is most significant for the orientations 90/90 and 45/90 for which the Young's moduli are larger than for the plain polyethylene while the yield stresses reached only 21.8 and 21.9MPa, respectively. Thus, the low yield stress is assigned to the presence of a chip. At other orientations the yield stress was also reduced; however, this will be further investigated and compared for other shape and size of a chip.

The chip has also a significant effect on the ductility of the samples. At the orientations 90/90, 45/90 and 90/45 it caused the embrittlement of the samples and they reached the strains at break of only 0.7-0.8 (in comparison with 12.8 for the plain polymer). The results were almost the same for all three types of samples even though at the orientations 45/90 and 90/45 the chip was at approximately 45° towards the tension direction, while in the SC/90/90 samples it was perpendicular. At the orientation 90/0 the strain at break reduced to 9.1; however, when the chip was slanted (deviated slightly from the intended orientation), the crack developed much quicker reducing the strain at break to 1.6 on average. Thus, the numerical data confirm the conclusions based on the observations of sample profiles (see previous section), that even small deviation from the orientation parallel to the tension direction causes significant embrittlement of the samples.

For the SC/0/90 and SC/surf samples the highest strain at break values among the samples with a chip were obtained (10.7 and 10.5, respectively). However, as for the latter samples the lowest Young's modulus was recorded, it can be concluded that the chip on the surface has only a negative effect on the mechanical performance of the samples in tension, as it reduces both the stiffness and the ductility.

The relatively high Young's modulus of the SC/0/90 samples means that the chip causes a slight polymer reinforcement, while the relatively small reduction in the yield stress and strain

at break means that it does not have any significant impact on the structural integrity. Thus, this orientation is considered as the most advantageous, which confirms the already mentioned findings of other researchers (e.g. Liang & Yang, 2007).

As the results indicate, the orientation of the chip influences the performance of the samples in tension, therefore, the chip shape and size effects are studied for different orientations separately.

5.2.7 Chip shape and size effects

In this section the chip shape and size effects are investigated for various orientations of the SSQ and LC chips and compared with the SC chip in order to find out how the individual chips influence the integrity of polymer and at which orientation the differences are greatest. The basic orientations, i.e. surf, 0/90, 90/0, and 90/90, are analysed. The intermediate orientations such as 45/90, 90/45 and 90/0 slanted could not have been investigated for the SSQ and LC chips due to the time constraints.

As for the SC chip, first the crack development in the samples is studied.

5.2.7.1 Analysis of the profiles of the samples with SSQ and LC chips at the basic orientations

Initially, development of a crack for the orientation on the surface is explored. In the case of square chips two extreme positions are investigated, with chip sides at angles of 0º and 45º towards the tension direction. Figure 5.31 shows the plots for the samples with an SSQ chip, while Figure 5.32 shows the plots for the samples with an LC chip and the selected samples with an SC chip on the surface.
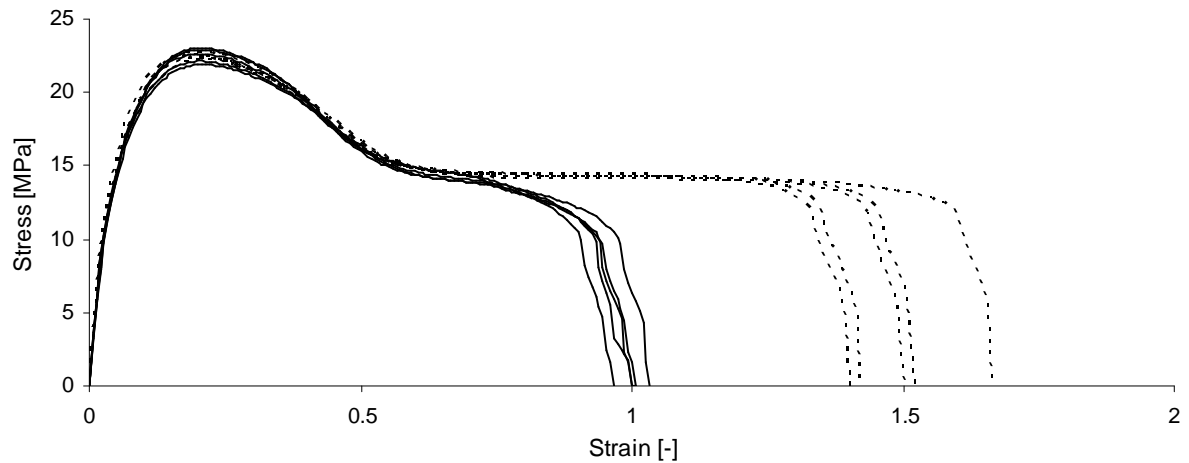
Figure 5.31 Stress-strain curves for the SSQ/surf samples with sides of a chip at (- - -) 0º and (——) 45º towards the tension direction.
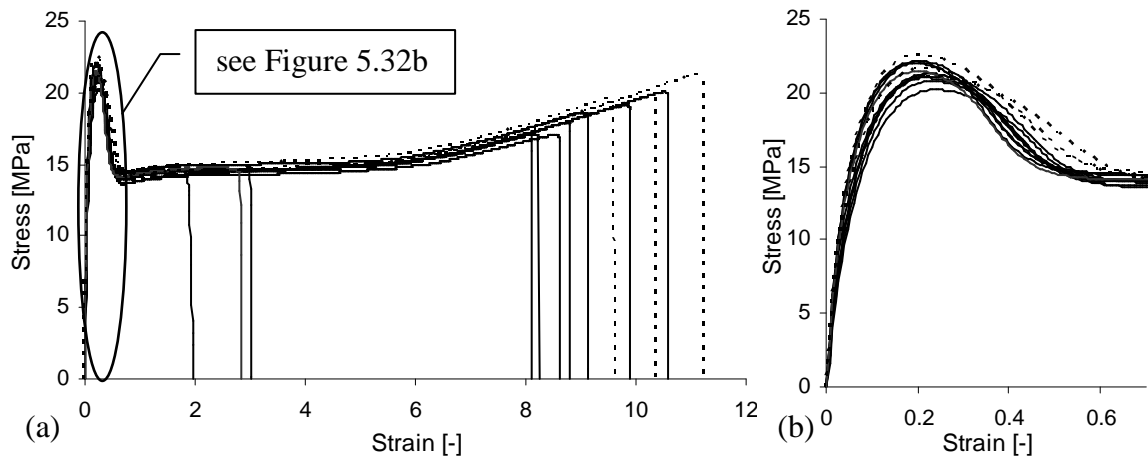
Figure 5.32 (a) Stress-strain curves for (——) the LC/surf samples and (- - -) the selected SC/surf samples; (b) enlarged initial section of (a).

From Figure 5.31 it can be seen that the SSQ chips at two orientations reach relatively close strain at break values, slightly larger for the chip with the sides at an angle of 0° to the tension direction. This might be due to a greater stress concentration formed by the chip positioned at an angle of 45°. After Mirza & Ansari (1974) the highest stress concentration in the case of square inclusions occurs at the corners and reaches a maximum when the sides are oriented at 45° towards the tension direction, with the most advantageous orientation occurring at 0° and 90°. This might be partly associated with the fact that the distance between the chip and the edge of the sample is smallest for this worst orientation.

191

This is further studied on the basis of specimens' profiles during the tensile test.

| 1 | 2 | 3 | 4 |
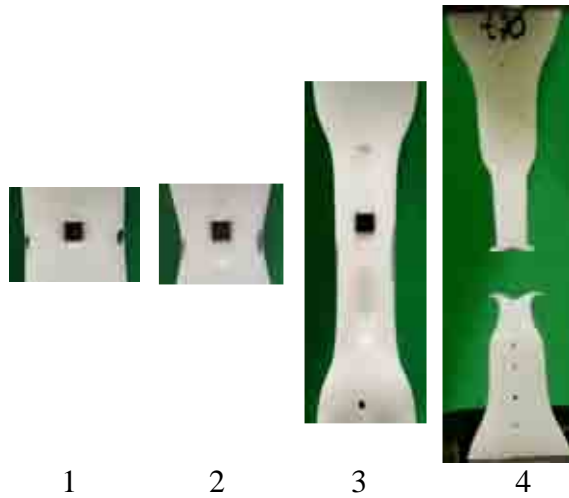
Figure 5.33 Central part of the SSQ/surf sample with sides of the chip at 0º towards the tension direction, during characteristic stages of the tensile test. Note: in stage 4 the whole profile of the sample is shown, in a smaller scale.
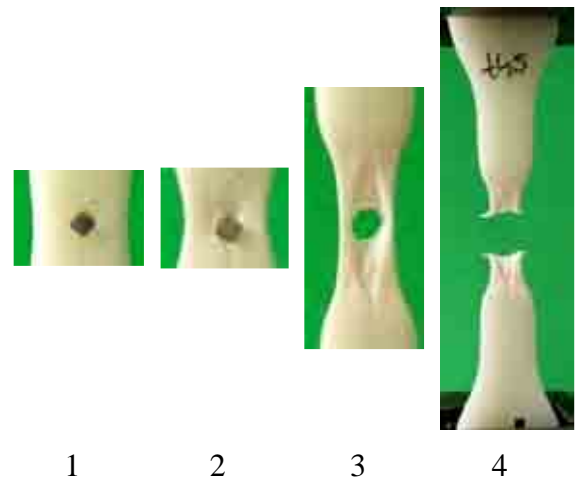
Figure 5.34 Central part of the SSQ/surf sample with sides of the chip at 45º towards the tension direction, during characteristic stages of the tensile test. Note: in stage 4 the whole profile of the sample is shown, in a smaller scale.

It can be seen from Figures 5.33 and 5.34 that the way in which the crack develops and propagates and the mechanism of sample failure differ depending on the position of the SSQ chip. In the case of the chip alignment at an angle of 0º to the tension direction the crack formation and development are similar to that in the sample with an SC chip (Figure 5.21, page 178). However, the shapes of the cracks differ and in the SSQ chip sample it is almost rectangular (with a width equal to approximately the width of the chip) while in the SC sample it is initially ellipsoidal (with a width equal to the diameter of the chip in the widest place), and during extension its ends become sharper and narrower. The SC chip is pushed out of the crack at some point (Figure 5.21, Stage 3). In both cases the samples break at the crack tip; however, in the case of the SSQ sample the tip expands more through the sample width before the sample fails at a much smaller strain (Figure 5.33).

When the SSQ chip is positioned at an angle of 45º towards the tension direction, the crack develops a bead shape with a maximum width equal to the diagonal of the chip, and having

sharp ends. The sample fails in the middle of the crack where it penetrates through the sample thickness and forms a hole (Figure 5.34, stage 3).

Further, the crack development in the sample with an LC chip is studied.

1   2   3   4   5   6
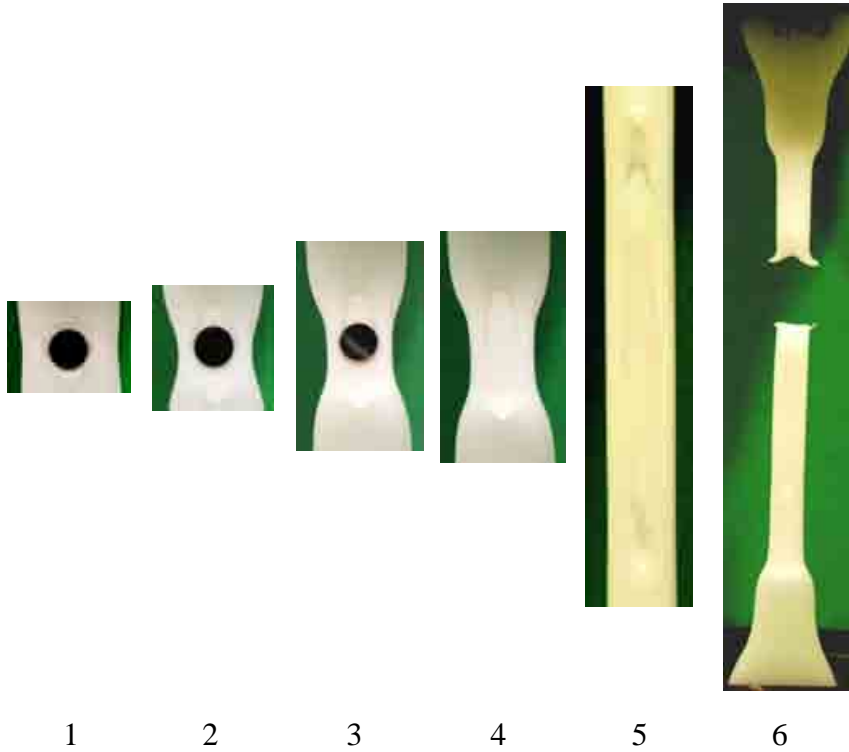
Figure 5.35 Central part of the LC/surf sample during characteristic stages of the test. Note: in stage 6 the whole profile of the sample is shown, in a smaller scale.

In the case of the LC/surf sample (Figure 5.35) the crack develops in the same way as in the SC/surf sample (Figure 5.21). However, the width of the crack formed is larger as the diameter of the chip is greater. The crack expands with the neck and it breaks due to expansion of the crack tip through the sample width and thickness in a similar way as in the SC sample, but at a lower average strain. At a certain point as the crack develops the LC chip is also displaced from the crack, which can be clearly seen in Figure 5.35, stages 3 and 4. The debonding angle changes with the crack and neck development, being 45º at stage 1, reaching the highest measured values of 61º at stage 2 and decreasing to 58º by stage 3 after the chip is pushed out. Pushing out the chip has a positive affect on the sample performance as the chip

does not force a large width to the crack and without the chip it can narrow down and expand with the neck.

The debonding angle in the case of the LC chip is smaller than in the case of the SC chip, which is inconsistent with the observations of Schűller (2002) who stated that it does not depend on the inclusion radius. However, this tendency might be associated with the boundary conditions in the samples tested. First, the chip is located on the surface, thus, it is constrained only from one side by the matrix. Second, the distance between the chip and the sample edges is significantly smaller for the LC chip, which might influence the geometry of the crack, e.g. by reducing its expansion across the sample width.

The next orientation investigated is 0/90.

As the chip at this orientation is immersed in the polymer matrix, the position of the sides of the SSQ chip cannot be determined for each sample. Figure 5.36 shows the X-ray scans of three SSQ/0/90 samples. Only the chip in the middle has the sides aligned parallel to the sample edges and, thus, tension direction. The other two chips rotate and have sides at an angle (between 0º and 45º) to the sample edges.

(a)

(b)

Figure 5.36 (a) Picture of the SSQ/0/90 samples and (b) their X-ray scans (top view).

In Figure 5.37 the shapes of the stress-strain curves for the samples tested at the orientation 0/90 are compared. For the complete data for the samples with an SC chip see Figure 5.4.
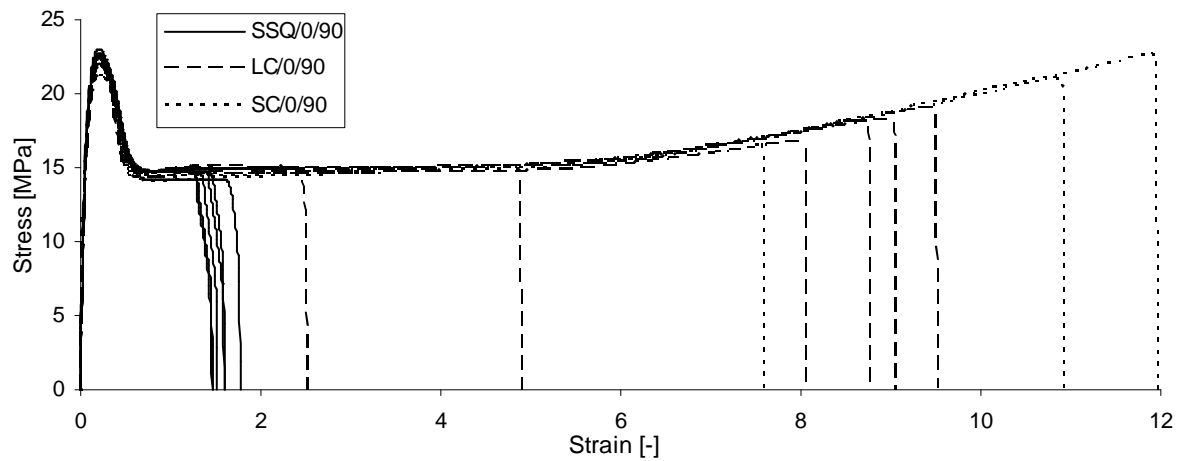
Figure 5.37 Stress-strain curves for the SSQ/0/90 and LC/0/90 samples and the selected SC/0/90 samples.

From Figure 5.37 it can be seen that the samples reach different strain at break values, which are in a very wide range for the LC chip. These variations are assigned to the way in which the crack develops, which is presented in Figures 5.38 and 5.39 for both chips.

1   2   3   4
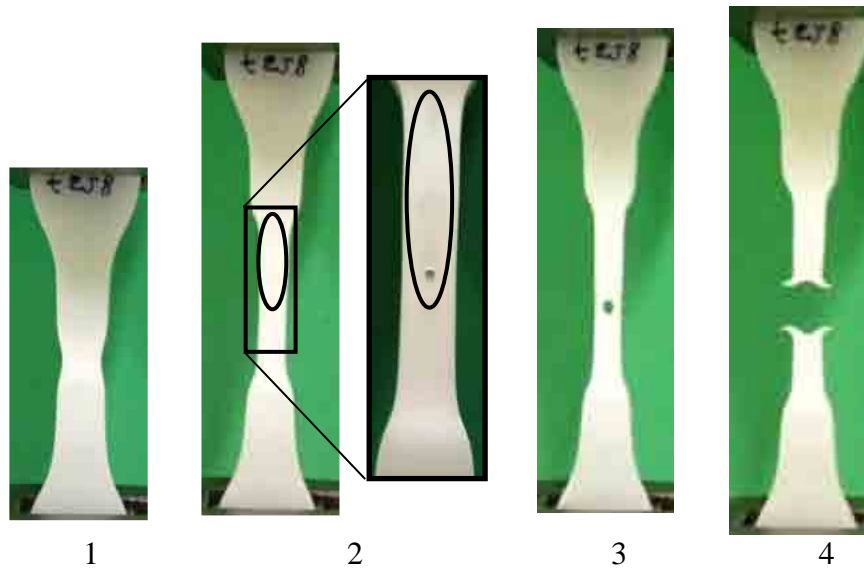
Figure 5.38 Profiles of the SSQ/0/90 sample during characteristic stages of the tensile test. Note: the crack region is marked in stage 2 (ellipse), and the central part of the sample is enlarged.
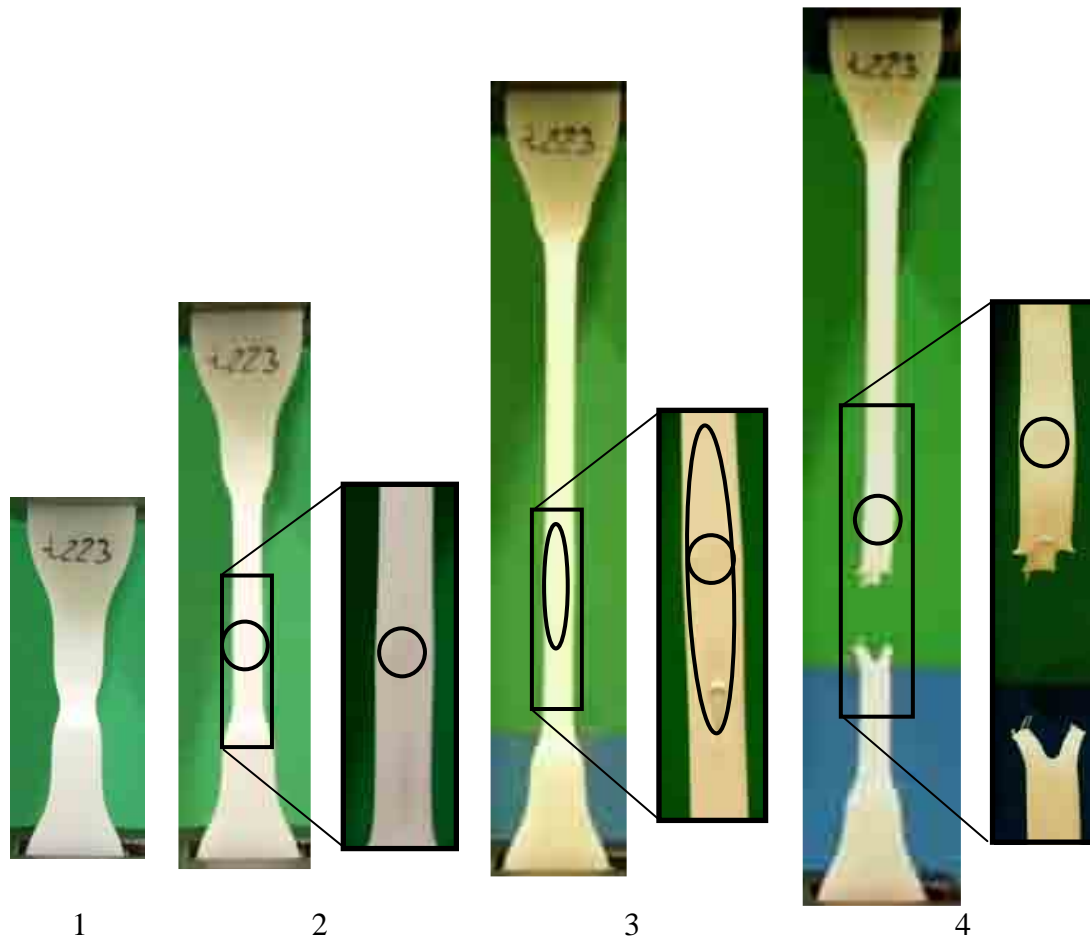
Figure 5.39 Profiles of the LC/0/90 sample during characteristic stages of the tensile test. Note: the crack region is marked in stage 3 (ellipse) while the chip is identified in stages 2-4 (circle), and the central part of the sample is enlarged in these stages.

The failure patterns are comparable for all the samples including SC/0/90 presented in Figure 5.11 (page 164). The neck starts to form at the level of the chip, which causes stress concentration (Figures 5.35 and 5.36, stage 1). The crack forms around the chip and it propagates along the neck. However, the SSQ chip is moved to the top and the LC chip is moved to the bottom of the neck, in contrast to the SC chip, which is centrally located throughout the test. In the case of the SSQ chip the sample fails before the neck encompasses the whole gauge length. All the samples break at the crack tips. In the case of the SSQ chip, the tip expands in such a way that a rhombus shaped hole forms that penetrates through the sample thickness, leading to immediate sample failure. The LC sample fails in a similar way as the SC sample, although at a lower average strain.

Further, the 90/0 orientation is investigated.

Figure 5.23a indicated that the actual orientation of the chips in the SC/90/0 samples varied from the intended. Therefore, the cross-sections of the samples with the SSQ and LC chips were also scanned in order to investigate their actual positions (Figure 5.40).

(a) (b)
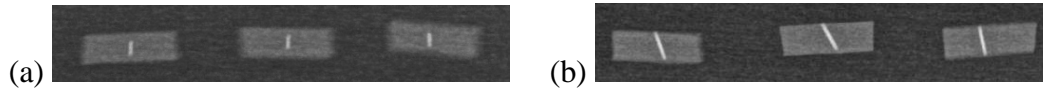
Figure 5.40 X-ray scans through the cross-sections of the (a) SSQ/90/0 and (b) LC/90/0 samples.

The X-ray scans show that the SSQ chips (Figure 5.40a) tend to align in accordance with the intended orientation, while the LC chips (Figure 5.40b) are not exactly perpendicular to the sample surface, which might be due to their diameter (4.52mm), which is slightly larger than the thickness of the samples (4.2mm).

Figure 5.41 presents the shapes of the stress-strain curves for the samples tested at the orientation 90/0. For the data for the samples with an SC chip see Figure 5.22 (page 179).
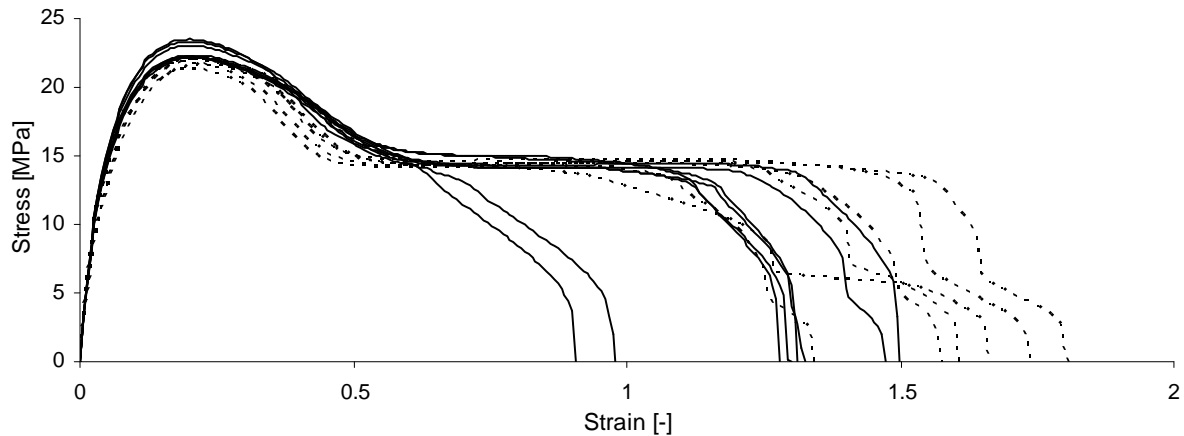
Figure 5.41 Stress-strain curves for the (——) SSQ/90/0 and (- - -) LC/90/0 samples.

From Figure 5.41 it can be seen that the samples with the SSQ and LC chips reach much smaller strain at break values than the samples with the SC chip. This means that the crack in

the first two samples develops much quicker, which is studied on the basis on the photographs of the samples during the tensile test, presented in Figures 5.42 and 5.43.
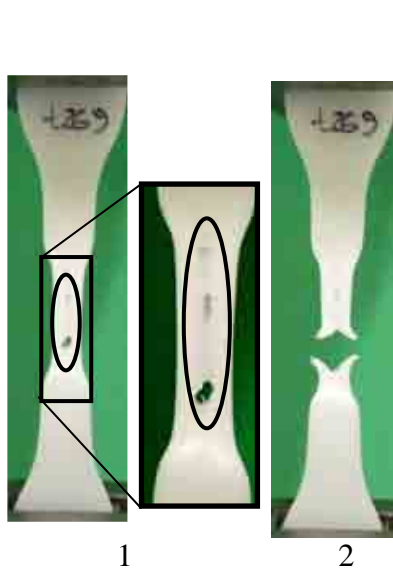
Figure 5.42 Profiles of the SSQ/90/0 sample during characteristic stages of the tensile test. Note: the crack region is marked (ellipse) in stage 1, and the central part of the sample is enlarged.
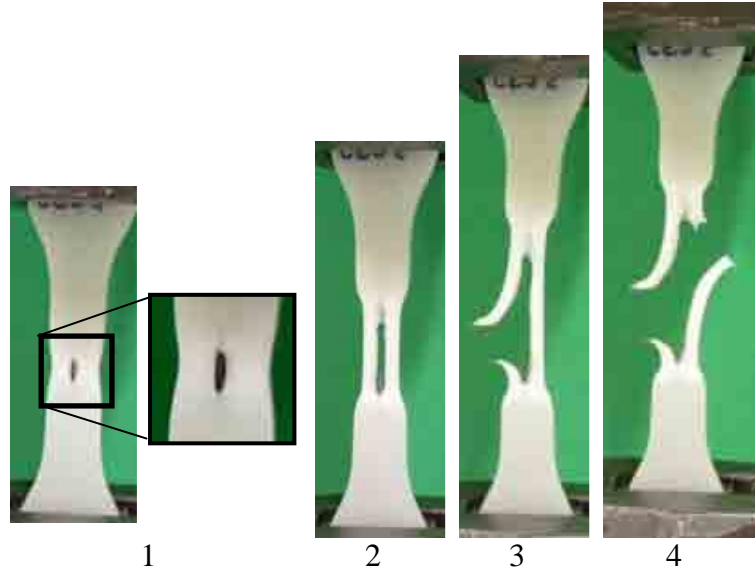
Figure 5.43 Profiles of the LC/0/90 sample during characteristic stages of the tensile test. Note: the central part is enlarged in stage 1.

The SSQ/90/0 sample fails at the crack tip in a similar way to the samples with the orientation 0/90 (Figure 5.38). The crack tip expands through the sample thickness and width causing immediate failure before the neck encompasses the whole gauge length.

In the case of the LC chip, a narrow crack forms around the chip and it expands splitting the neck into two parts (Figure 5.43, stage 2). After one part fails (stage 3), the second part also fails immediately and the whole sample breaks (stage 4). This failure is similar to the one observed for the SC chip (Figure 5.24, page 180); however, in the case of the SC/90/0 sample it takes longer for the crack to penetrate through the sample thickness and the neck is split into two parts only locally just before the sample fails.

The last orientation investigated is 90/90.

Again, the accurate position of the SSQ chips was investigated on the basis of the X-ray scans (Figure 5.44) in order to see how the sides align in relation to the sample surface.
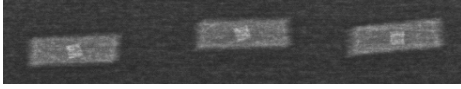
Figure 5.44 X-ray scans through the cross-sections of the SSQ/90/90 samples.

The X-ray scans show that the edges of the SSQ chips tend to align parallel to the sample surface during sample production.

Figures 5.45 and 5.46 show the shapes of the stress-strain curves for the samples with an SSQ and LC chips, respectively, tested at the orientation 90/90, while the data for the SC chip were presented in Figure 5.26.
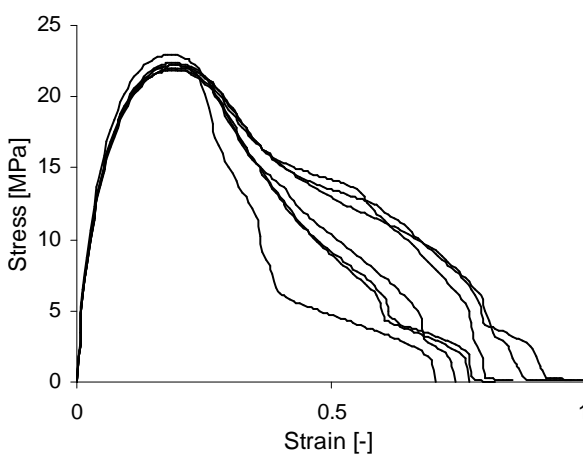
Figure 5.45 Stress-strain curves for the SSQ/90/90 samples.
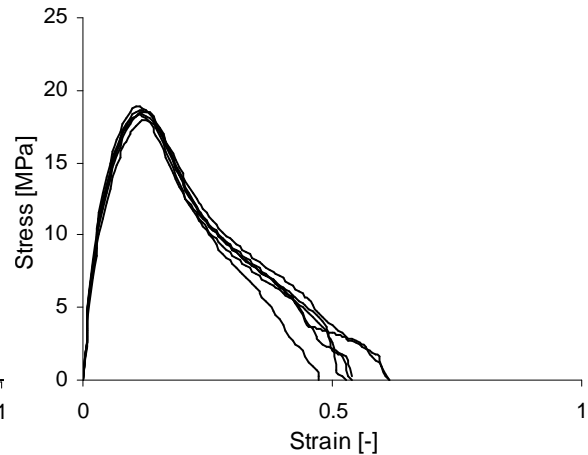
Figure 5.46 Stress-strain curves for the LC/90/90 samples.

The failure pattern of all the samples was similar, like for the SC/90/90 sample (see Figure 5.29, page 183).

In the next section the numerical results are analysed and the effects of chip shape and size are discussed.

5.2.7.2 Analysis of the results obtained for the samples with SC, SSQ and LC chips at the basic orientations

The tests indicated that the differences between the SC, SSQ and LC chips depend on their orientation. Tables 5.26-5.34 list the tensile data for the samples with SSQ and LC chips. For the complete set of data for the samples with an SC chip see Table 5.6 (page 157) section 5.2.6.2. and Tables 5.19-5.24 (page 185). Table 5.35 lists the average results for all the compared orientations.

Table 5.26 Tensile values for the SSQ/surf samples with sides of a chip at 0° towards the tension direction.

Sample	Young's modulus MPa	Yield stress MPa	Strain at break
t41	542	22.4	1.5
t42	544	22.4	1.7
t43	511	22.2	1.5
t44	536	22.8	1.4
t70	533	22.5	1.4
Average	533	22.5	1.5
SD	13	0.2	0.1

Table 5.27 Tensile values for the SSQ/surf samples with sides of a chip at 45° towards the tension direction.

Sample	Young's modulus MPa	Yield stress MPa	Strain at break
t45	539	22.6	1.0
t46	511	21.9	1.0
t47	530	22.1	1.0
t48	486	22.9	1.0
t49	534	23.0	1.0
Average	520	22.5	1.0
SD	22	0.5	0

Table 5.28 Tensile values for the LC/surf samples.

Sample	Young's modulus MPa	Yield stress MPa	Strain at break
t34	469	21.3	8.2
t35	337	21.1	9.9
t36	253	20.2	10.6
t37	319	20.8	8.1
t38	426	21.3	8.8

Sample	Young's modulus MPa	Yield stress MPa	Strain at break
t69	479	21.0	8.6
t153	521	22.1	3.0
t312	528	22.0	9.1
t313	534	22.1	2.0
t314	521	21.5	2.8
Average	439	21.3	7.1
SD	101	0.6	3.2

Table 5.29 Tensile values for the samples SSQ/0/90.

Sample	Young's modulus MPa	Yield stress MPa	Strain at break
t110	525	22.4	1.6
t111	539	22.5	1.6
t112	546	22.6	1.5
t113	590	22.9	1.5
t114	533	22.7	1.5
t258	524	22.0	1.8
Average	543	22.5	1.6
SD	24	0.3	0.1

Table 5.30 Tensile values for the samples LC/0/90.

Sample	Young's modulus MPa	Yield stress MPa	Strain at break
t21	384	21.8	8.8
t23	396	22.0	9.5
t101	487	21.3	8.1
t102	498	21.9	2.5
t222	437	21.9	9.0
t223	450	22.0	4.9
Average	442	21.8	7.1
SD	46	0.3	2.8

Table 5.31 Tensile values for the SSQ/90/0 samples.

Sample	Young's modulus MPa	Yield stress MPa	Strain at break
t86	543	23.0	1.3
t87	544	23.5	0.9
t88	523	22.2	1.0
t89	547	23.3	1.3
t90	526	22.3	1.5
t267	530	22.2	1.3
t268	537	22.2	1.5
t269	523	22.2	1.3
Average	534	22.6	1.3
SD	10	0.6	0.2

Table 5.32 Tensile values for the LC/90/0 samples.

Sample	Young's modulus MPa	Yield stress MPa	Strain at break
t72	442	22.0	1.7
t73	458	22.1	1.7
t74	413	21.6	1.8
t75	525	21.9	1.6
t221	459	21.3	1.3
t252	550	21.8	1.6
Average	475	21.8	1.6
SD	52	0.3	0.2

Table 5.33 Tensile values for the SSQ/90/90 samples.

Sample	Young's modulus MPa	Yield stress MPa	Strain at break
t91	556	22.9	0.7
t92	520	22.2	0.7
t93	518	22.0	1.0
t94	528	22.4	0.9
t95	522	22.2	1.0
t256	517	21.9	0.8
t257	526	21.9	0.8
Average	527	22.2	0.8
SD	14	0.4	0.1

Table 5.34 Tensile values for the LC/90/90 samples.

Sample	Young's modulus MPa	Yield stress MPa	Strain at break
t60	507	18.6	0.5
t61	516	18.4	0.5
t62	479	18.4	0.5
t63	445	17.9	0.6
t64	505	18.3	0.5
t65	528	18.9	0.7
t66	517	18.1	0.5
Average	500	18.4	0.5
SD	28	0.3	0.1

Table 5.35 Summary of tensile values for the SC, SSQ and LC chips at different orientations.

Chip	Tensile values	Orientation							
		surf		0/90		90/0		90/90	
		Average	SD	Average	SD	Average	SD	Average	SD
SC	Young's modulus, MPa	449	70	523	9	475	40	490	39
	Yield stress, MPa	21.6	0.5	22.2	0.3	22.1	0.2	21.8	0.5
	Strain at break	10.5	0.6	10.7	1.2	9.1	0.4	0.7	0.2
SSQ	Young's modulus, MPa	533	13	543	24	534	10	527	14
	Yield stress, MPa	22.5	0.2	22.5	0.3	22.6	0.6	22.2	0.4
	Strain at break	1.5	0.1	1.6	0.1	1.3	0.2	0.8	0.1
LC	Young's modulus, MPa	439	101	442	46	475	52	500	28
	Yield stress, MPa	21.3	0.6	21.8	0.3	21.8	0.3	18.4	0.3
	Strain at break	7.1	3.2	7.1	2.8	1.6	0.2	0.5	0.1

Note: For the SSQ/surf samples the tensile values are given for the chip positioned at an angle of 0° towards the tension direction. For the angle of 45° the average Young's modulus, yield stress and strain at break equal to 520(±22)MPa, 22.5(±0.5)MPa and 1.0(±0), respectively.

When analysing the effects of chip shape and size for all orientations, it can be seen from Table 5.35 that the highest Young's modulus and yield stress values are obtained for the SSQ chip. The strain at break is the lowest for this chip for all orientations except 90/90. In general, this means that the samples with the SSQ chip are the strongest and stiffest, and also the most brittle; however, it has to be remembered that some differences (especially when they are within SDs) might be due to different properties of the matrix and/or the limited accuracy of the measurement.

This observation might be explained by the research carried out by Pukánszky (1990) who investigated the effect of filler type/shape on the tensile properties of polymers and observed that the platelets had a better reinforcing effect than spheres. The spheres can be compared to the circular chips due to their regular shape, while the platelets are comparable with the square chips as they also have sharp edges and corners causing stress concentration (Feingold et al., 1972). However, the fillers tested were only a few micrometers in size and their volumetric content was up to 30%, which is different from the individual chips few millimetres large.

Savin (1961) designed a 2D model on which basis he calculated that the stress concentration is four times larger for the rectangle at 30° towards the tension direction than for the circle. Even though in the 2D model the stress around the circular hole concentrates at the equator (Timoshenko & Goodier, 1951), while in the 3D models the highest stress concentration is detected at the poles (Lu et al., 1992) and the other parameters of his model also differ significantly from those applied in this project, this provides an indication of the scale of difference between both shapes of a chip.

Concerning the chip size effect, doubling of the diameter of the circular chip seems to not have any noticeable influence on the Young's modulus, which is consistent with the

observations of Nielsen (1974). Only at the orientation 0/90 the value for the SC chip is significantly larger (523MPa) than for the LC chip (442MPa). However, large SDs, especially for LC/surf samples (101MPa), do not allow any certain conclusions to be drawn.

The yield stress and strain at break values are lower for the LC chip at each orientation and this is mostly associated with the reduction of the cross-section and thus volume of polymer to sustain the load and strain, which is more significant for the LC chip (29% at the orientation 90/90 and 4% at other orientation) than for the SC chip (7% at the orientation 90/90 and 2% at other orientations). Kousourakis et al. (2008) who studied the influence of thin and long holes (galleries) on the tensile and compressive properties of aerospace carbon/epoxy laminates also noticed that the galleries reduce the load bearing area of the structure. Schűller (2002) also observed that the load the bond can sustain depends largely on the ratio between the particle diameter and the cross-section of the sample, and the larger the sample the smaller the debonding stress. Large inclusions also have a more detrimental effect than small ones because after dewetting (debonding) from the matrix, the larger the particle the larger the void/crack which forms around it (Nielsen, 1974). A large particle has a similar effect to an agglomeration of smaller particles, which was also found to reduce the strain at break of the material. These theories suggest that the LC chip debonds quicker and a larger crack forms around the chip which weakens the sample.

In addition, the smaller distance between the chip and the sample edges in the case of an LC chip additionally increase the stress concentration factor after Durelli and Murray (1943) and Durelli et al. (1966). The higher stress concentration, which increases with defect size, accelerates sample failure (Callister, 2007; Griffith, 1920; Williams, 1984).

The parameters for the samples with an LC chip can be projected on the basis of the experimental results for the plain polyethylene and the volumetric content of the chip within a

sample (0.6%) using Equations 2.10-2.12, as it was explained for the SC chip in section 5.2.3. The theoretical Young's modulus, yield stress and strain at break values are 483MPa, 21.8MPa and 10.5, respectively. The theoretical yield stress is in agreement with the measured value for the orientations 0/90 and 90/0, while the strains at break obtained experimentally are much smaller than calculated. The same was observed for the samples with an SC chip (see section 5.2.6.2). The measured strain at break values for the LC chip are very inconsistent, especially at the orientations on the surface and 0/90 for which the SDs of 3.2 and 2.8, respectively, were obtained.

In the next section the performance of the samples with two SC chips and SC & SSQ chips is analysed for the orientation 0/90.

5.2.8   The effect of number of chips

In this section the influence of two chips on the performance of the polyethylene in tension is determined. The tests were carried out for two adjacent chips, 2SC and SC&SSQ.

As explained in section 4.3.4.3 (page 110), it is difficult to produce samples with two chips attached, as they tend to split due to polymer flow. Figure 5.47 shows the X-ray scan of the samples with two SC chips. It can be seen that the two chips are located in a line, along the sample edge, in accordance with the intended position, however a small gap between the chips appeared in some cases (left and right sample). In addition, the SSQ chip in the SC&SSQ sample tends to rotate in
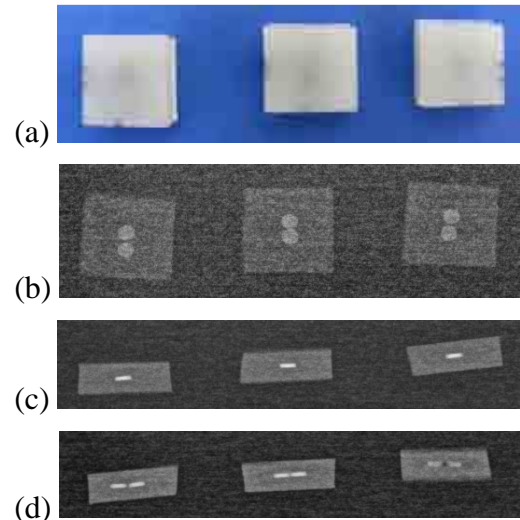
Figure 5.47 (a) Picture of the 2SC/0/90 samples and their X-ray scans: (b) top view, (c) front view, and (d) side view.

205

relation to the sample edges as it was presented in Figure 5.36 (page 194).

The effect of single SC and SSQ chips at the orientation 0/90 was studied in the previous sections.

Figures 5.48 and 5.49 show the plots for the samples with 2SC and SC&SSQ chips and selected samples with SC and SSQ chips at the orientation 0/90.
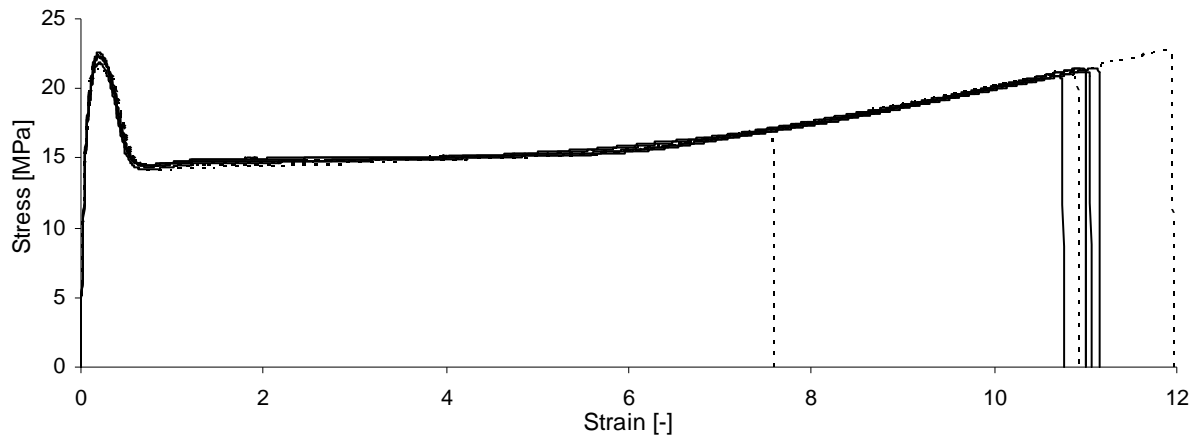
Figure 5.48 Stress-strain curves for (——) the 2SC/0/90 samples and (- - -) the selected SC/0/90 samples.
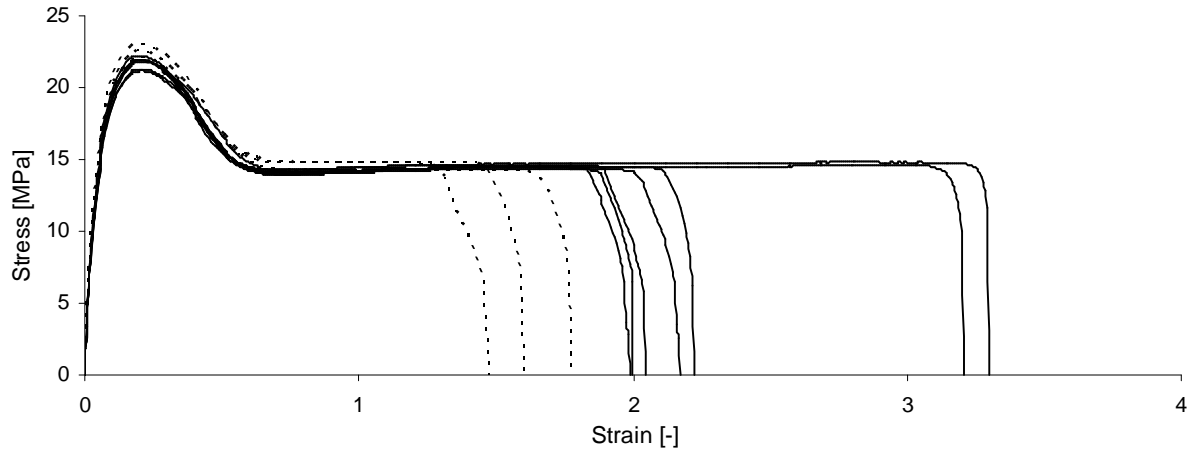
Figure 5.49 Stress-strain curves for (——) the SC&SSQ/0/90 and (- - -) the selected SSQ/0/90 samples.

The shapes of the curves for the two chips are similar to the plots for the single chips and differ mostly by the strain at break values. Figures 5.50 and 5.51 show the crack development in the samples with two chips.
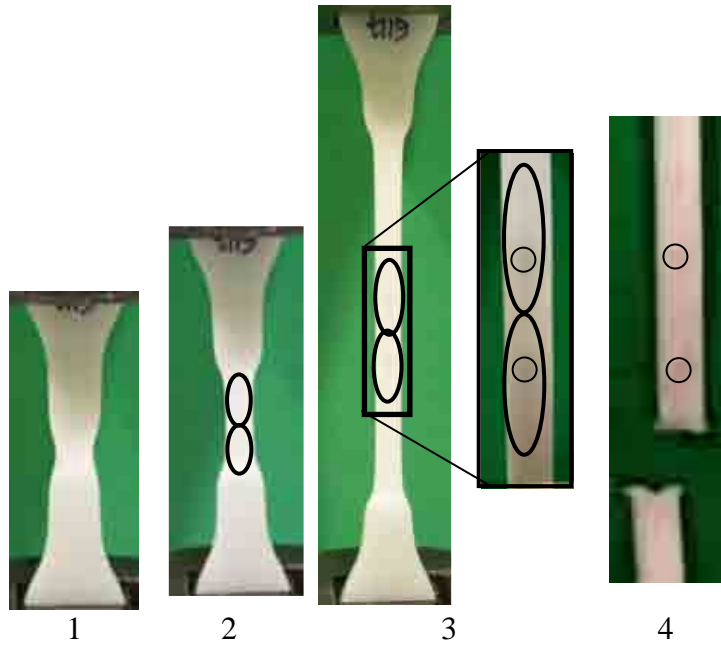
Figure 5.50 Profiles of the 2SC/0/90 sample during characteristic stages of the tensile test. Note: the crack region is marked in stages 2 and 3 (ellipse) while the chip is identified in stages 3 and 4 (circle), and the central part of the sample is enlarged in stages 3 and 4.

Figure 5.51 Profiles of the SC&SSQ/0/90 sample during characteristic stages of the tensile test.

It can be seen in Figure 5.50, stage 2 that the chips separate at the beginning of the stretching and separate cracks form around them. The cracks expand along the neck as the test continues. They seem to arrest each other in the direction towards each other, thus are not symmetrical on both sides of the chip. On the sides of the chips further from the sample centre the expansion of the cracks and crack tips is more extensive (see Figure 5.50, stage 3). The sample breaks at the crack tip, which expands more, which is the bottom tip of the bottom chip in these cases; the SSQ chip tip in the case of the SSQ&SC sample (Figure 5.51). This is understandable as the SSQ chip causes higher stress concentration thus the crack and crack tip around it expand quicker.

Tables 5.36 and 5.37 list the tensile values for the samples with two chips, while in Table 5.38 the key numerical data for the samples with single chips are recalled.

Table 5.36 Tensile values for the 2SC/0/90 samples.

Sample	Young's modulus MPa	Yield stress MPa	Strain at break
t115	531	22.6	10.8
t116	526	21.8	11.1
t117	548	22.4	11.0
t118	542	22.3	11.2
t119	532	22.3	11.0
Average	536	22.3	11.0
SD	9	0.3	0.1

Table 5.37 Tensile values for the SC&SSQ/0/90 samples.

Sample	Young's modulus MPa	Yield stress MPa	Strain at break
t254	539	22.2	2.0
t255	514	22.0	2.2
t295	527	21.9	2.0
t296	510	21.3	2.2
t297	518	21.9	3.3
t298	508	21.8	3.2
t299	507	21.1	2.0
Average	518	21.7	2.4
SD	12	0.4	0.6

Table 5.38 Average tensile values with SDs for the SC/0/90 and SSQ/0/90 samples.

Sample	Young's modulus MPa	Yield stress MPa	Strain at break
SC			
Average	523	22.2	10.7
SD	9	0.3	1.2
SSQ			
Average	543	22.5	1.6
SD	24	0.3	0.1

The effect of the number of chips can be best investigated on the basis of the results for the samples with one and two identical chips. Thus, first the SC and 2SC samples are compared. The samples with SC and SSQ chips were already introduced in sections 5.2.3 and 5.2.7.2. It is evident that the tensile values are slightly greater for two chips, which could mean that the higher chip content improves both the stiffness and the ductility of the samples. However, the obtained differences are within the SDs of the values, therefore it is difficult to draw any meaningful conclusion. Many other researchers, e.g. Liang (2007), observed usually an increase in Young's modulus and a decrease in yield stress and strain at break with the

addition of filler, as discussed in detail in section 5.2.3. However, Nicolais & Narkis (1971) discovered that there are cases where fillers promote craze formation (characteristic for ductile failure) that cause an increase in elongation to break with filler addition. As the energy is used for chip debonding and crack propagation in the case of more chips/cracks, more energy is required to cause ultimate failure.

In addition, the strain at break values for two chips were more consistent (SD of 0.1) than for one (SD of 1.2). It is thought that this might be due to more consistent stress distribution in the case of two chips in the samples so the cracks form and propagate at similar stresses.

The theoretical tensile values for two chips can be calculated on the basis of Equations 2.10-2.12 and the values obtained are 490MPa for the Young's modulus, 22.0MPa for the yield stress and 12.8 for the strain at break. The values should theoretically be the same for the 2SC and SC&SSQ samples; however, practically it is not the case. They also do not coincide with the experimental results, which is not surprising as the equations have been derived for uniformly dispersed micro size particles and the few millimetre sized chips give the effect of a filler agglomeration, accelerating failure plus in the case of poor adhesion between the chips and the polymer there is a higher reduction in strain at break in comparison to the value calculated from the equation (Nielsen, 1974).

When comparing all the samples the highest yield stress was obtained for the SSQ chip (22.5MPa) while the lowest value was recorded for the SC&SSQ sample (21.7MPa). For one and two SC chips the similar middle values of 22.2 and 22.3MPa, respectively, were obtained.

Concerning the strain at break values, the highest was recorded for the 2SC samples (11.0) being only slightly higher than the value for one SC chip (10.7). The lowest strain at break was obtained for one SSQ chip (1.6), which is also smaller than the value for the SC&SSQ

sample (2.4). This might suggest that the stress concentration caused by the SSQ chip is reduced due to the presence of another SC chip. Other reasons for higher ductility of the samples with two chips have already been explained.

On the basis of the results obtained it can be assumed that the optimum sample performance at the orientation investigated is when more than one SC chip is present. However, this requires further research.

In the next section the effect of sample thickness is investigated.

5.2.9   Effect of sample thickness

This section aims to investigate the effect of the thickness of polyethylene samples on their performance with a chip. Initially, plain polyethylene samples of two thicknesses, 2.2 (thin) and 4.2mm (thick), are compared. Subsequently, the samples with an SC chip at orientations surf, 0/90, 90/0, and 90/90, are investigated.

The sample profiles were similar for both thicknesses, thus only the numerical data analysed. The 4.2mm thick samples were introduced in section 5.2.1.

First the plain polyethylene samples of two thicknesses are compared.

5.2.9.1 Effect of sample thickness for the plain polyethylene samples

The densities of the samples of two thicknesses produced under the same conditions was almost equal being 0.9566 and 0.9565g/cm³, for the 4.2 and 2.2mm samples, respectively, thus similar tensile properties are expected. However, as the samples analysed used in the tensile test were produced under varied conditions their properties might differ as indicated in section 5.2.1. Figure 5.52 shows the plots for the 2.2mm thick and selected 4.2mm thick samples. Table 5.39 lists the numerical data for the 2.2mm thick samples and Table 5.40 list

the key numerical data for the 4.2mm thick samples (for the complete data see Tables 5.3 and 5.4, page 148). The '+' after the strain at break value means that the tests of some samples were not completed, i.e. the samples did not break due to the limited range of the tensile machine, and the last recorded values (e.g. 14.1+) were taken into account in the calculation of the average.
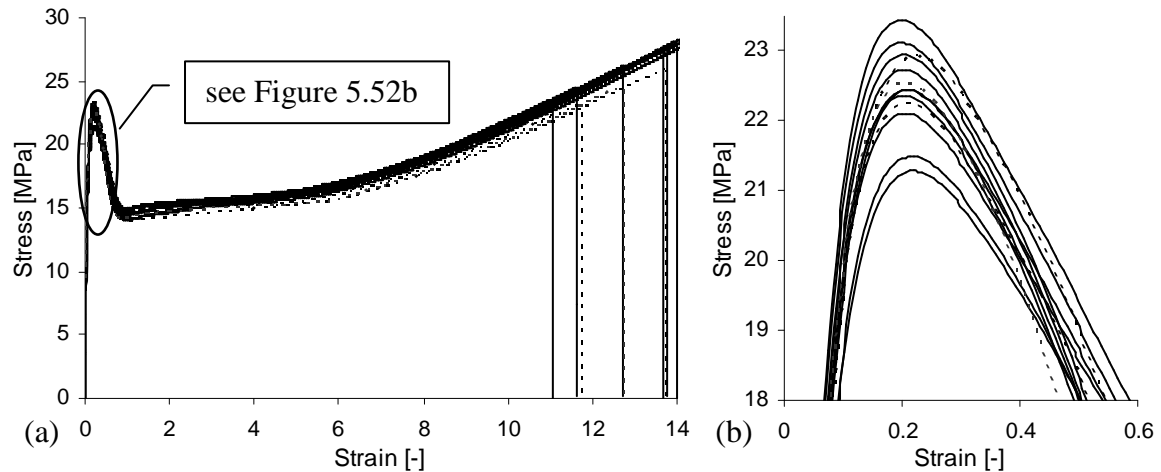
Figure 5.52 (a) Stress-strain curves for (——) the 2.2mm thick and (- - -) the selected 4.2mm thick plain polyethylene samples; (b) enlarged peak region.

Table 5.39 Tensile values for the 2.2mm thick plain polyethylene samples.

Sample	Young's modulus MPa	Yield stress MPa	Strain at break
t125	508	21.5	14.1+
t126	550	22.9	11.6
t127	564	23.1	11.1
t128	518	22.4	12.7
t129	502	21.3	14.3+
t132	536	22.1	13.8
t133	569	23.4	13.7
t134	543	22.4	14.0
t135	550	22.7	14.1+
t136	513	22.4	14.0+
Average	535	22.4	13.3+
SD	24	0.7	1.1

Table 5.40 Average tensile values with SDs for the 4.2mm thick plain polyethylene samples.

Sample	Young's modulus MPa	Yield stress MPa	Strain at break
Average	476	22.5	12.8
SD	50	0.2	0.7

The yield stresses of the thin and thick samples are almost equal, 22.4 and 22.5MPa, respectively, while the Young's moduli differ; however, the difference of 59MPa is only slightly larger than the maximum SD of 50MPa, thus can be mostly due to the measurement error and different properties of the matrix.

Even though the thin samples have slightly larger modulus on average, they also reach very high strain at break values sometimes exceeding the machine capacity, thus are more ductile. This might be associated with the plane stress and plane strain effect explained briefly in Figure 5.53. In general, in thinner samples there is a higher
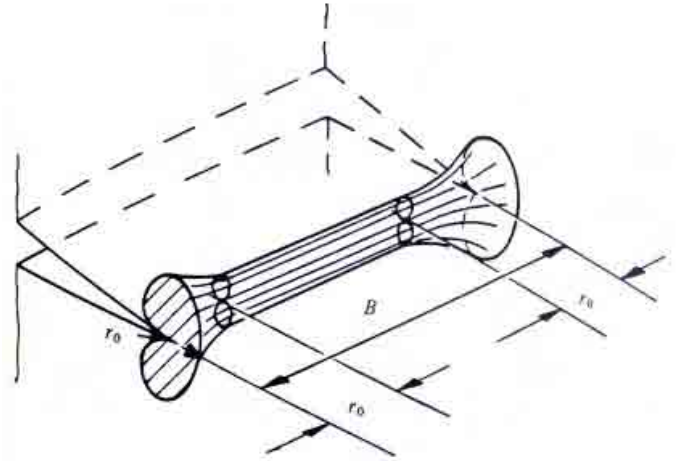
Figure 5.53 Plane stress and plane strain region in the sample; B – sample thickness, r_0 – plane stress region, B - $2r_0$ – plane strain region (Williams, 1984).

percentage of the external plane stress region contributing to more extensive plastic deformation and thus higher ductility. In very thin samples the plane strain conditions theoretically do not exist (Griffith, 1920; Ingham, 2008; Williams, 1984).

Further tests aim to investigate the impact of sample thickness on the performance of the samples with chips.

5.2.9.2 Effect of sample thickness for the samples with chips

In this section the samples of two thicknesses with circular chips are studied.

There was a similar problem with positioning SC chips especially at the orientations 90/0 and 90/90 within 2.2mm thick samples as with LC chips included in 4.2mm thick samples and the chips were slightly slanted in relation to the sample surface deviating from the theoretical

orientation due to their diameter (2.26mm) slightly exceeding the thicknesses of the sample, as illustrated in Figure 5.54.

(a)   (b)
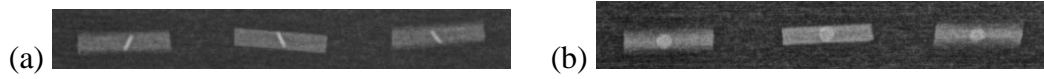
Figure 5.54 X-ray scans through the cross-sections of the 2.2mm thick (a) SC/90/0 and (b) SC/90/90 samples.

The results for the 2.2mm thick samples with an SC chip are compared with the results for the 4.2mm thick samples with an SC chip and also with an LC chip in order to investigate if the same proportion of the chip cross-section to the sample cross-section gives the same results. Figures 5.55-5.58 show the plots for the 2.2mm thick samples with an SC chips and selected 4.2mm samples with SC and LC chips at various orientations, while Table 5.45 summarizes the key numerical data. Tables 5.41-5.44 list the tensile values for the 2.2mm thick samples. The 4.2mm thick samples with SC and LC chips were already introduced in sections 5.2.2 and 5.2.7.2.
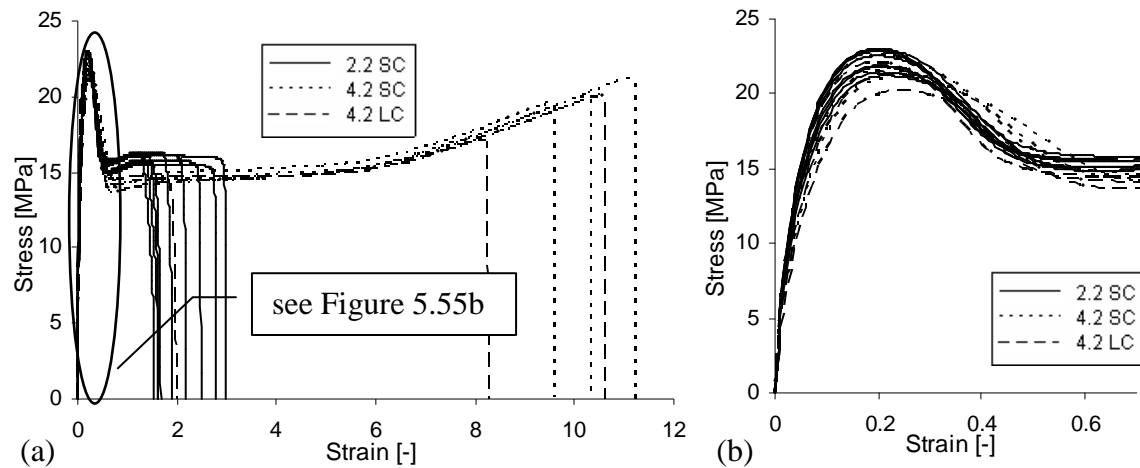
Figure 5.55 (a) Stress-strain curves for the 2.2mm thick SC/surf samples and the selected 4.2mm thick SC/surf and LC/surf samples; (b) enlarged initial section of (a).
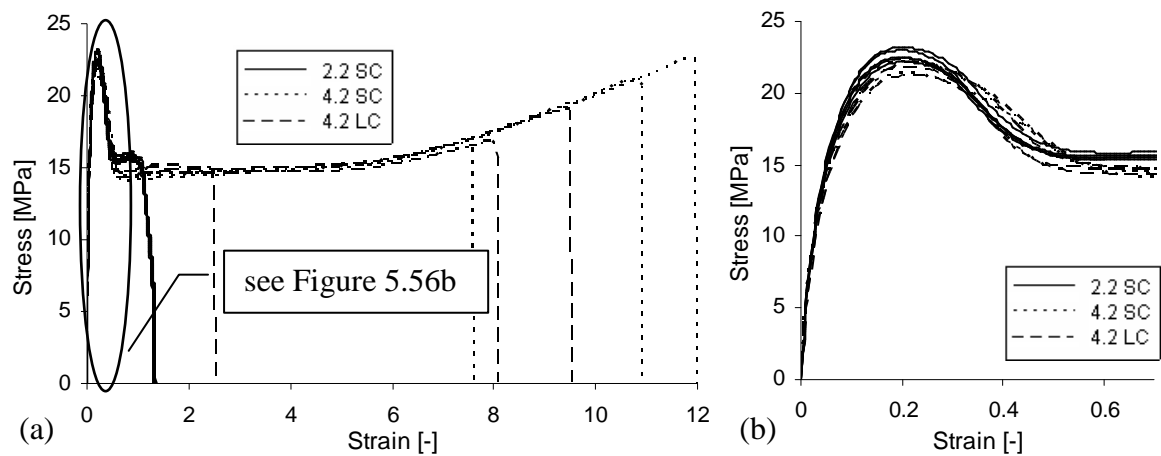
Figure 5.56 (a) Stress-strain curves for the 2.2mm thick SC/0/90 samples and the selected 4.2mm thick SC/0/90 and LC/0/90 samples; (b) enlarged initial section of (a).
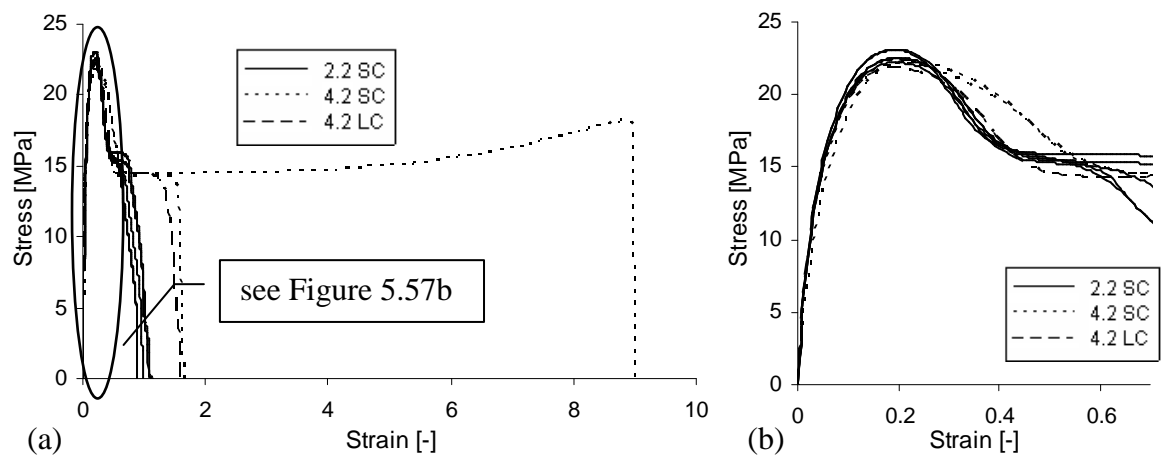
Figure 5.57 (a) Stress-strain curves for the 2.2mm thick SC/90/0 samples and the selected 4.2mm thick SC/90/0 and LC/90/0 samples; (b) enlarged initial section of (a).
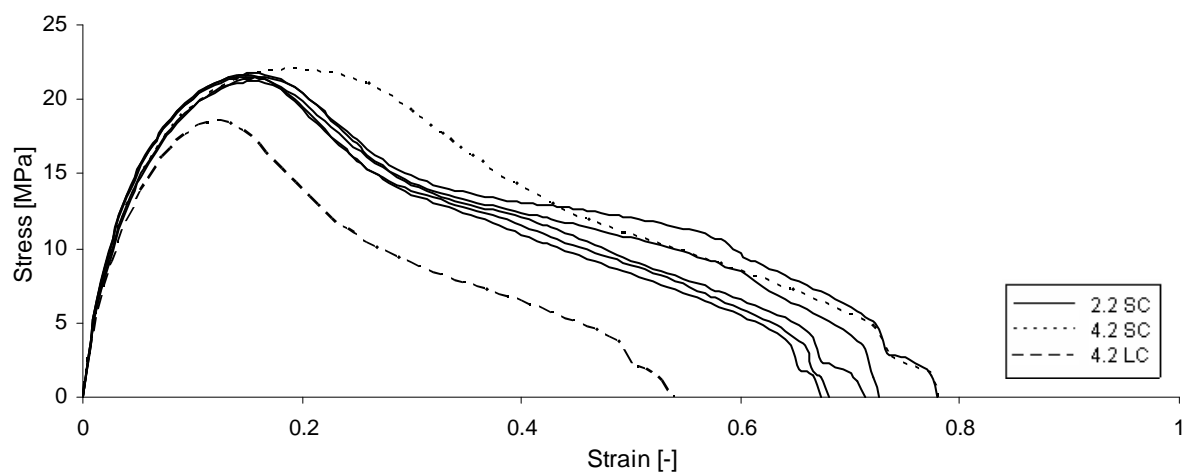
Figure 5.58 Stress-strain curves for the 2.2mm thick SC/90/90 samples and the selected 4.2mm thick SC/90/90 and LC/90/90 samples.

214

Table 5.41 Tensile values for the 2.2mm thick SC/surf samples.

Sample	Young's modulus MPa	Yield stress MPa	Strain at break
t120	491	21.2	1.7
t121	524	21.8	2.5
t122	522	21.5	2.8
t123	532	21.9	1.6
t148	578	22.8	1.9
t149	566	23.0	2.2
t150	571	23.0	1.6
t151	553	22.5	3.0
t152	563	22.8	1.5
Average	545	22.3	2.1
SD	29	0.7	0.6

Table 5.42 Tensile values for the 2.2mm thick SC/0/90 samples.

Sample	Young's modulus MPa	Yield stress MPa	Strain at break
t55	530	22.5	1.3
t56	536	22.2	1.4
t57	549	23.2	1.4
t58	504	22.5	1.3
t59	554	23.0	1.3
Average	535	22.7	1.3
SD	20	0.4	0.1

Table 5.43 Tensile values for the 2.2mm thick SC/90/0 samples.

Sample	Young's modulus MPa	Yield stress MPa	Strain at break
t143	554	22.2	1.0
t144	545	22.5	1.1
t145	563	23.0	1.1
t146	560	23.1	0.9
t147	546	22.5	0.9
Average	553	22.7	1.0
SD	8	0.4	0.1

Table 5.44 Tensile values for the 2.2mm thick SC/90/90 samples.

Sample	Young's modulus MPa	Yield stress MPa	Strain at break
t138	572	21.5	0.7
t139	520	21.4	0.7
t140	530	21.2	0.7
t141	559	21.7	0.8
t142	560	21.6	0.7
Average	548	21.5	0.7
SD	22	0.2	0.0

Table 5.45 Summary of the key tensile values for the 2.2mm thick samples with and without an SC chip and 4.2mm samples with and without SC and LC chips at different orientations.

Sample	Tensile values	Orientation							
		surf		0/90		90/0		90/90	
		Average	SD	Average	SD	Average	SD	Average	SD
2.2mm SC	Young's modulus, MPa	545	29	535	20	553	8	548	22
	Yield stress, MPa	22.3	0.7	22.7	0.4	22.7	0.4	21.5	0.2
	Strain at break	2.1	0.6	1.3	0.1	1.0	1.0	0.7	0.0
4.2mm SC	Young's modulus, MPa	449	70	523	9	475	40	490	39
	Yield stress, MPa	21.6	0.5	22.2	0.3	22.1	0.2	21.8	0.5
	Strain at break	10.5	0.6	10.7	1.2	9.1	0.4	0.7	0.2
4.2mm LC	Young's modulus, MPa	439	101	442	46	475	52	500	28
	Yield stress, MPa	21.3	0.6	21.8	0.3	21.8	0.3	18.4	0.3
	Strain at break	7.1	3.2	7.1	2.8	1.6	0.2	0.5	0.1

When comparing the results in Table 5.45 it can be concluded that for each orientation the Young's modulus and yield stress values are the highest while the strain at break values are the lowest (excluding the 90/90 orientation) for the thin samples with an SC chip. These observations are in an agreement with Nielsen (1974) and Xanthos (2010), who state that the smaller filler provides a better reinforcement for the polymer. However, as the Young's modulus was also higher for the thin plain samples, this dependency might be associated with different properties of the matrix and/or geometry of the sample. The yield stress was similar for the plain samples of both thicknesses, thus the variations in the values for the samples with chips are, at least to some extent, assigned to the presence of a chip.

The thin SC/0/90 and SC/90/0 reach greater yield stress (22.7MPa) than the plain samples (22.4MPa), which might mean that the chip has a reinforcing effect in these samples. However, in this case the difference between the values is smaller than the SD of 0.4MPa, thus might not be real and/or might be due to higher crystallinity of the matrix. This is not the case for the thick samples with an LC chip at these orientations for which the yield stress gets reduced (from 22.5 to 21.8MPa). Thus, the difference between the samples with and without a chip is greater (0.6MPa), even though the proportion of the chip cross-section to the sample cross-section for thin samples with an SC chip and thick sample with an LC chip is the same at these orientations (4%).

The SC chip makes up a higher percentage of the volume and cross-section of the thin samples than of the thick samples, thus the yield stress should be rather reduced for thin samples as it was for the thick samples. This is the case for the orientations on the surface and 90/90 where the chip causes the largest reduction in the sample cross-section. When calculating the yield stress on the basis of this reduction for the thin SC/90/90 (14%), thick SC/90/90 (7%) and thick LC/90/90 samples (30%) the yield stress values of 20.8, 18.7 and 15.8MPa, respectively, are obtained. However, this reduction is only local, at the distance equal or slightly greater than the thickness of a chip (0.5mm). The experimental values for the thin and thick samples with an SC chip are noticeably higher (21.5 and 21.8MPa, respectively) than the theoretical values, while the yield stress obtained for an LC chip in the thick sample (18.4MPa) is close to the calculated value.

The strain at break value in every case, except the plain samples, is also associated with the reduction in the sample cross-section and thus a reduced volume of polymer to stretch and sustain the load. This reduction is highest for the thin SC/90/90 and thick LC/90/90 samples, so the strains at break reach only 0.5 and 0.6, respectively.

At other orientations the reduction in the sample cross-section is almost the same in the case of the thin samples with an SC chip and the thick samples with an LC chip. However, a much lower strain at break is reached by the thin samples as the polymer cover is much thinner in these samples and as the neck develops this covering becomes even thinner making it easier for the crack to penetrate through the sample thickness and cause it to fail.

After applying Equations 2.10-2.12 (page 39) to estimate the theoretical tensile values on the basis of the experimental results for the plain polymer samples and the volumetric content of the chips, the results listed in Table 5.46 are obtained.

Table 5.46 Theoretical tensile values obtained on the basis of Equations 2.10-2.12 for the 2.2 and 4.2mm thick samples with the SC and LC chips.

Sample	Volumetric content of the chip in a sample, V_f	Young's modulus, MPa Equation 2.10	Yield stress MPa Equation 2.11	Strain at break Equation 2.12
2.2mm, SC chip	0.003	539	21.9	11.4
4.2mm, SC chip	0.0015	478	22.2	11.3
4.2mm, LC chip	0.006	483	21.8	10.5

The theoretical and experimental results do not overlap; however, in both cases the highest Young's modulus was obtained for the thin samples. Concerning the thin samples, the actual yield stress is higher for the orientations 0/90 and 90/0 and lower for the orientations on the surface and 90/90, than calculated. The actual stain at break (between 2.1 for the SC/surf samples and 0.6 for the SC/90/90 samples) is much lower than calculated.

In the case of the thick samples with SC and LC chips at the orientations 0/90 and 90/0 the yield stresses obtained in the experiments are equal or very close to the theoretical values (as already mentioned in previous sections) and also lower than calculated for the orientations on the surface and 90/90. The strains at break are also lower than calculated.

This shows that it is hard to rely on the theoretical calculations, which do not consider the orientations of the chip and were developed for the composites with small filler particles uniformly distributed within the matrix. However, it is interesting to see that in some cases the theoretical and experimental values overlap.

The strain at break values are so low due to the large proportion of the chip size to the sample size. In the case of a larger sample an SC chip would cause a smaller reduction in the area of the load bearing polymer matrix, thus the orientation effect might be less significant. However, in larger samples the crack development would be more difficult to observe and thus analyse and another method of crack monitoring than photographical would have to be developed. In order to compare the influence of a silicon chip on larger structures the pipe joints with and without a chip are investigated in Appendix A.

Further, the chapter on the tensile tests is summarized.

5.2.10 Summary of the tensile test

The data were already introduced in the previous sections and due to their large number they are not listed here again. In this section the findings are summarized without referring to the specific values.

The manufacturing conditions had an impact on the tensile properties of the samples. The actual alignment of a chip was not always in accordance with the intended, which also had an influence on the results. The effect of a chip depended on the polymer toughness and the chip caused more significant embrittlement in the less tough off-the-shelf polyethylene. In further tests, the tougher pipe grade polyethylene was investigated.

The SC chip did not cause any significant changes in the sample stiffness (modulus), while the LC chip caused its reduction. The SSQ chip had a small reinforcing effect on the samples

(improved Young's modulus and yield stress), which is probably due to the corners, which 'clamp' in the matrix, and confirms the results of Pukánszky (1990) who observed that the platelets have a better reinforcing effect than round beads. It is interesting to see that the results confirm the discoveries related to fillers, which have different character than a chip as have much smaller size and are added at high concentrations and uniformly distributed within the matrix.

All chips caused a reduction in ductility, which was most significant for the SSQ chip due to the high stress concentration at the corners leading to cracking.

The impact of the chips depended on their orientation. A slight deviation from the alignment parallel to the tension direction caused a significant reduction in the ductility, so the performance of the samples with the SC chip reduced as follows: $0/90 > \text{surf} > 90/0 > 90/0 \text{ slanted} > 90/45 > 45/90 > 90/90$. The samples at the last three orientations behaved like brittle as no proper neck developed.

It was observed that the reduction in the yield stress and strain at break due to the inclusion of a chip is a consequence of the reduction in the sample cross-section thus in the volume of polymer, which deforms and sustains the load. This effect was especially observed for the LC chip and the SC chip in the thin (2.2mm) samples, at the orientation 90/90, for which the lowest yield stress and strain at break values were recorded in comparison with other samples of the same thicknesses.

At other orientations the strain at break reduced more significantly in the thin SC chip samples due to thinner polymer cover, which breaks quicker accelerating the crack propagation. The yield stress values were larger for the thin than for the thick samples with the SC chip. This is explained by the fact that in these samples the chip makes up a higher

volume, thus its reinforcing effect is higher. Two SC chips in a thick sample had a similar effect. Thus, it can be concluded that small chips at greater number (concentration) give a better reinforcing effect, which is a typical trend for most fillers (Xanthos, 2010). In addition, the samples with two chips were slightly more ductile, which is in contrast to the typical behaviour of the composites (Xanthos, 2010). However, only a 0/90 orientation was investigated for two chips.

When there was no chip present in the samples, the thin one (2.2mm) was more ductile (sometimes exceeding the instrument range) than the thick one (4.2mm) even though the crystallinity and yield stress values were similar. This is probably due to the thin samples being more dominated by the plane stress conditions leading to more extensive plastic deformation and thus energy absorption of the samples (Williams, 1984).

The tensile test has shown that the chip has a significant influence on the performance of polyethylene samples and this depends on different parameters of a chip and of a sample. Further, it will be investigated if the chip also changes the mechanical behaviour in the bending mode.

5.3 Flexural bending test

In this section the results of the bending tests carried out on the compression moulded samples are presented and discussed. The intention was to carry out these tests using all variations investigated in the tensile test. However, it soon turned out that some variations do not produce significantly different results. Thus, fewer variations with respect to size, shape and orientation of the chips were tested in flexural bending listed in Table 5.1 (page 144). This is explained in detail in the following sections.

The majority of the samples were 4.2mm thick and were tested at the speed of 2mm/min. Occasionally, other parameters were applied and are stated when appropriate.

Initially, 3- and 4-point bending tests were compared in order to choose the most appropriate bending mode for further samples.

5.3.1   Comparison of 3- and 4-point bending

Initial test were first carried out in both bending modes for the samples with and without a chip. Figures 5.59-5.61 show the data and Tables 5.47-5.50 list the numerical values. First the plain samples are compared, further the chip effect is investigated in both bending modes.
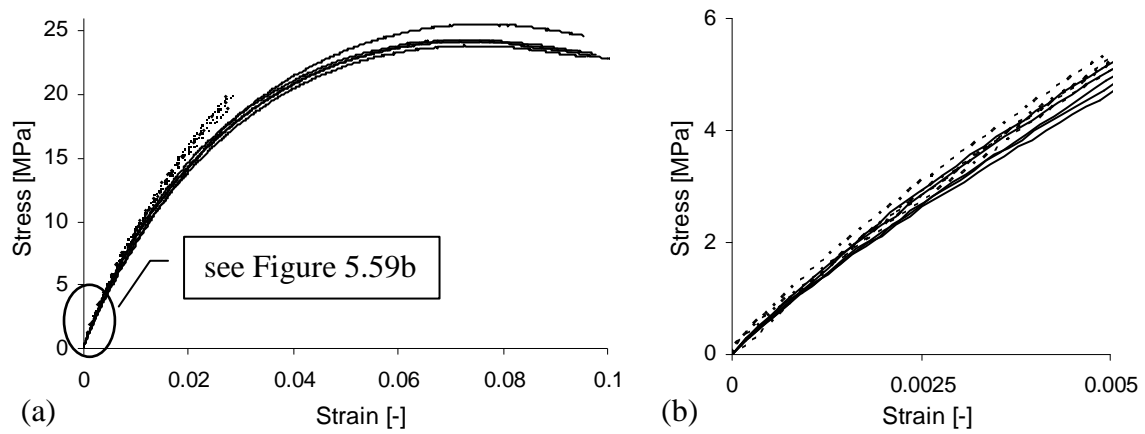
Figure 5.59 (a) Stress-strain curves for plain samples tested in (——) 3-point and (- - -) 4-point bending; (b) enlarged elastic region.
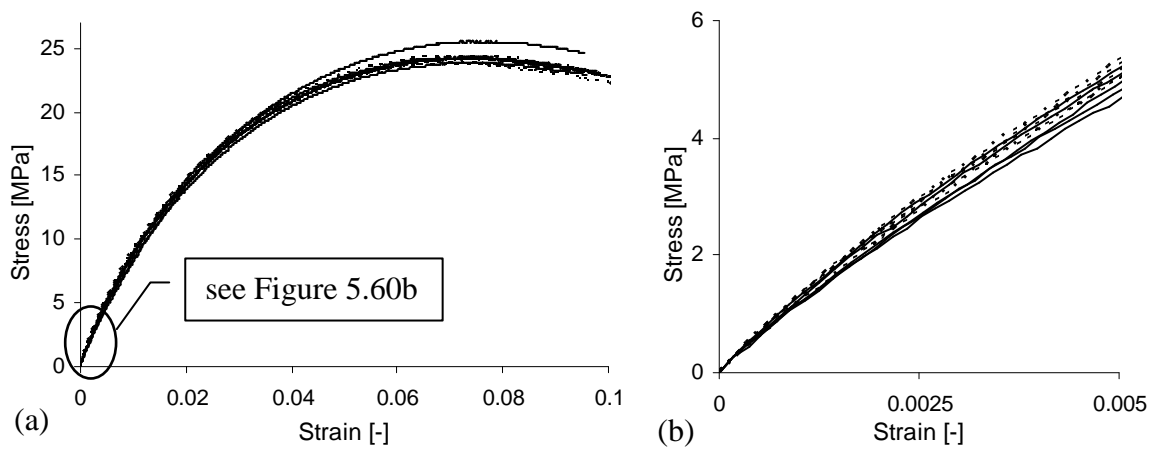
Figure 5.60 (a) Stress-strain curves for (——) plain and (- - -) SC/0/90 samples tested in 3-point bending; (b) enlarged elastic region.
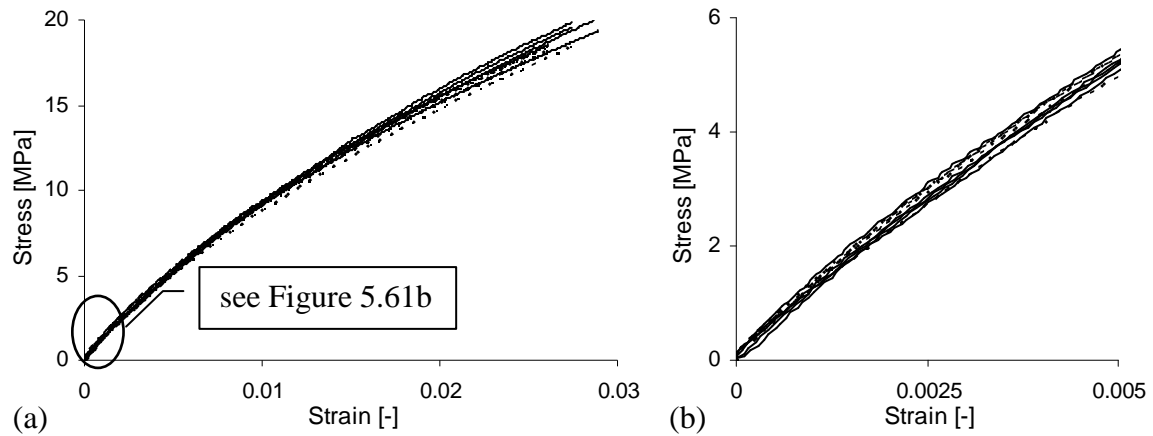
Figure 5.61 (a) Stress-strain curves for (——) plain and (- - -) SC/0/90 samples tested in 4-point bending; (b) enlarged elastic region.

Table 5.47 Flexural values for the plain polyethylene samples tested in 3-point bending.

Sample	Flexural modulus MPa	Peak stress MPa
86	992	25.5
87	1011	24.3
88	1093	24.2
89	1128	24.3
90	1014	23.9
Average	1048	24.5
SD	59	0.6

Table 5.48 Flexural values for the plain polyethylene samples tested in 4-point bending.

Sample	Flexural modulus MPa
81	1092
82	1134
83	1122
84	1016
85	1075
Average	1088
SD	46

Table 5.49 Flexural values for the SC/0/90 polyethylene samples tested in 3-point bending.

Sample	Flexural modulus MPa	Peak stress MPa
66	1128	24.4
67	1139	23.9
68	1084	24.2
69	1094	23.8
70	1090	24.1
Average	1107	24.1
SD	25	0.3

Table 5.50 Flexural values for the SC/0/90 polyethylene samples tested in 4-point bending.

Sample	Flexural modulus MPa
71	1133
72	1101
73	1159
74	1139
75	1009
Average	1108
SD	59

The samples did not break, which is typical behaviour for polyethylene (Peacock, 2000). The samples in 4-point bending deformed only up to a strain of approximately 0.03 as shown in Figure 5.59a due to the limitations of the fixture as illustrated and explained in section 4.4.2.1 (page 132).

In order to know the reliability of the numerical values it is important to estimate the measurement errors. Similarly as in the case of tensile test, the accuracy of the data obtained in the flexural test is influenced by the sample dimensions, the instrument precision and also the actual span value. The variations in dimensions of the flexural samples are the same as for the tensile specimens due to identical methods of manufacture and cutting out of the samples. The stress-strain relationship of the plain polyethylene sample with maximum SDs for the thickness (Δh) and width (Δb) of 0.05 and 0.04mm, respectively, was also plotted for the average (A), the minimum (A_{min}), and the maximum (A_{max}) cross-sectional areas. The average, minimum, and maximum thicknesses and widths of the sample were 4.29, 4.244, 4.343mm, and 12.65, 12.607, 12.693mm, respectively.
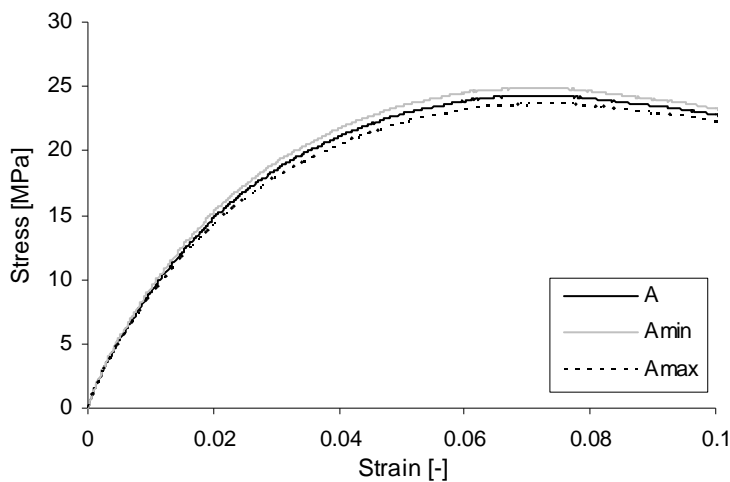
Figure 5.62 Stress-strain relationship obtained from the 3-point bending for plain polymer with a range of different cross-sectional areas.

Figure 5.61 shows that the curves for different sample dimensions almost coincide. The peak flexural stress values are 24.92, 24.32, and 23.64MPa for A, A_{min}, and A_{max}, respectively. The difference between the maximum and minimum values is 1.28MPa.

The flexural moduli (E_f) calculated from these results are 904, 936, and 867MPa, respectively, giving a maximum range of 69MPa and thus an error of 35MPa (assumed as half of the maximum range). The E_f was calculated in the same way as Young's modulus for very low forces and strains (see Equation 4.10, page 131), and thus the results are inaccurate and only used for comparative purposes between different types of samples.

The error of the peak flexural stress can also be calculated using Equation 5.2 (page 150), taking into consideration the width, thickness, span and load (force) errors. The span was measured with a vernier digital caliper, giving a span error (ΔL) of 0.05mm (Squires, 1988). The load measurement accuracy specified by the manufacturer (Instron, 2005) is ±0.5% of the reading down to 1/250 of the load cell capacity (10kN/250 = 40N).

Referring to Equations 4.12 (page 134) and 5.2 (page 150) the peak flexural stress error ($\Delta \sigma_{fp}$) can be calculated from Equation 5.3.

$$\left(\frac{\Delta_{fp}}{\sigma_{fp}}\right)^2 = \left(\frac{\Delta F}{F}\right)^2 + \left(\frac{\Delta L}{L}\right)^2 + \left(\frac{\Delta b}{b}\right)^2 + 2 \cdot \left(\frac{\Delta h}{h}\right)^2 \qquad \textbf{5.3}$$

where $\Delta \sigma_{fp}$, ΔF, ΔL, Δb, and Δh are the load (force), support span, specimen width, and thickness errors, respectively. Equation 5.3 yields a peak flexural stress error of:

$$\left(\frac{\Delta_{fp}}{24.32}\right)^2 = (0.005)^2 + \left(\frac{0.05}{70}\right)^2 + \left(\frac{0.04}{12.65}\right)^2 + 2 \cdot \left(\frac{0.05}{4.29}\right)^2 \rightarrow \Delta_{fp} = 0.43\text{MPa}$$

The $\Delta \sigma_{fp}$ of ±0.43MPa gives the difference between the largest and the smallest σ_{fp} of approximately 0.86MPa. This is 0.42MPa smaller than the difference between the maximum and minimum σ_{fp} of 1.28MPa, calculated on the basis of the minimum and maximum cross-

sectional areas without considering the load and span errors. The average $\Delta\sigma_{fp}$ is approximately 0.5MPa and this error value is assumed for all other samples, as it was obtained for the specimen with the highest dimension variations of 20 samples.

The strain measurement accuracy is ±0.5% of the reading down to 1/50 of the full instrument range (Instron, 2005). Thus, for the load and strain values below 40N and 0.07, respectively, there is no guarantee that the data obtained are accurate and the error cannot be estimated.

When comparing the results for two bending modes, it can be seen in Figure 5.59b that the plots almost overlap at the initial stage of the test curves, however, a small difference of 40MPa in the average modulus values is obtained from the calculations. When comparing with the maximum SD of 59MPa and the measurement error of ±35MPa the difference is not big, although, it was also observed by other researchers. Brancheriau et al. (2002) and Mujika (2006) stated that such variations in moduli might be due to rotating and slipping of the samples off the support spans in a different way in both tests as illustrated in Figure 5.63. In the case of the 4-point bending the contact between the specimen and the loading noses also changes, thus the loading span is increased during the test.
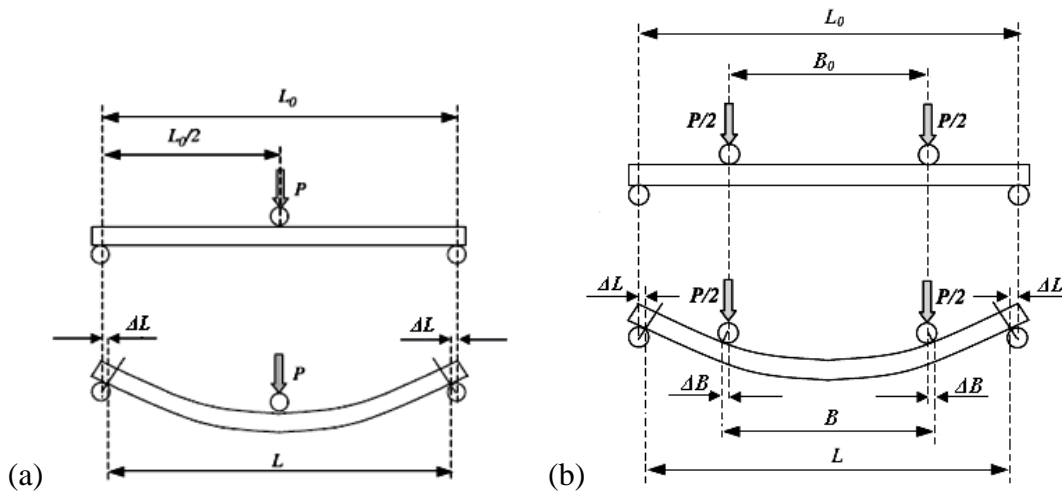
Figure 5.63 Undeformed and deformed (a) 3-point and (b) 4-point bending test configurations, where: L_0, B_0 – dimensions in the undeformed configuration (m), L, B – dimensions in the deformed configuration (m), ΔL, ΔB – change in dimensions (m), P – load (N) after Mujika (2006).

With regards to the chip effect in both bending modes a slight difference between the results for the samples with and without a chip is observed (Tables 5.47-5.50). The flexural modulus is larger by 59MPa and 20MPa for the samples with a chip tested in 3- and 4-point bending, respectively, suggesting their higher stiffness. However, the difference is within the range of SDs, which suggests low accuracy of the measurement and/or varying properties of the matrix among the same type of samples.

The peak stress was only recorded for the 3-point bending and the value is larger for the plain samples (Table 5.47). This is a bit surprising as for a higher flexural modulus a higher peak stress is expected as both reflect the material stiffness. This might be again due to slipping of the samples off the support noses and thus inaccurate measurement. As the difference between samples with and without a chip is slightly larger for 3-point bending and in addition in this mode the sample can de deformed up to a larger strain so the theoretical peak stress value can be obtained and the chip-matrix response at larger deformations can be investigated this bending mode is chosen for further tests. The chip effect is analysed further in detail in section 5.3.4.

In order to analyse the influence of the matrix on the material properties associated with the manufacturing conditions and to specify the optimal number of the samples to be tested the already presented five plain samples are compared with an additional five samples cut out from a different sheet and the optimal number of the samples to be tested is determined.

5.3.2 The effect of manufacturing conditions on plain polyethylene samples (reference samples) and the minimum number of samples to be tested

Figure 5.64 shows the results for the plain polymer samples produced under different conditions (classified as conditions A and B) and Tables 5.51 and 5.52 list the flexural values.
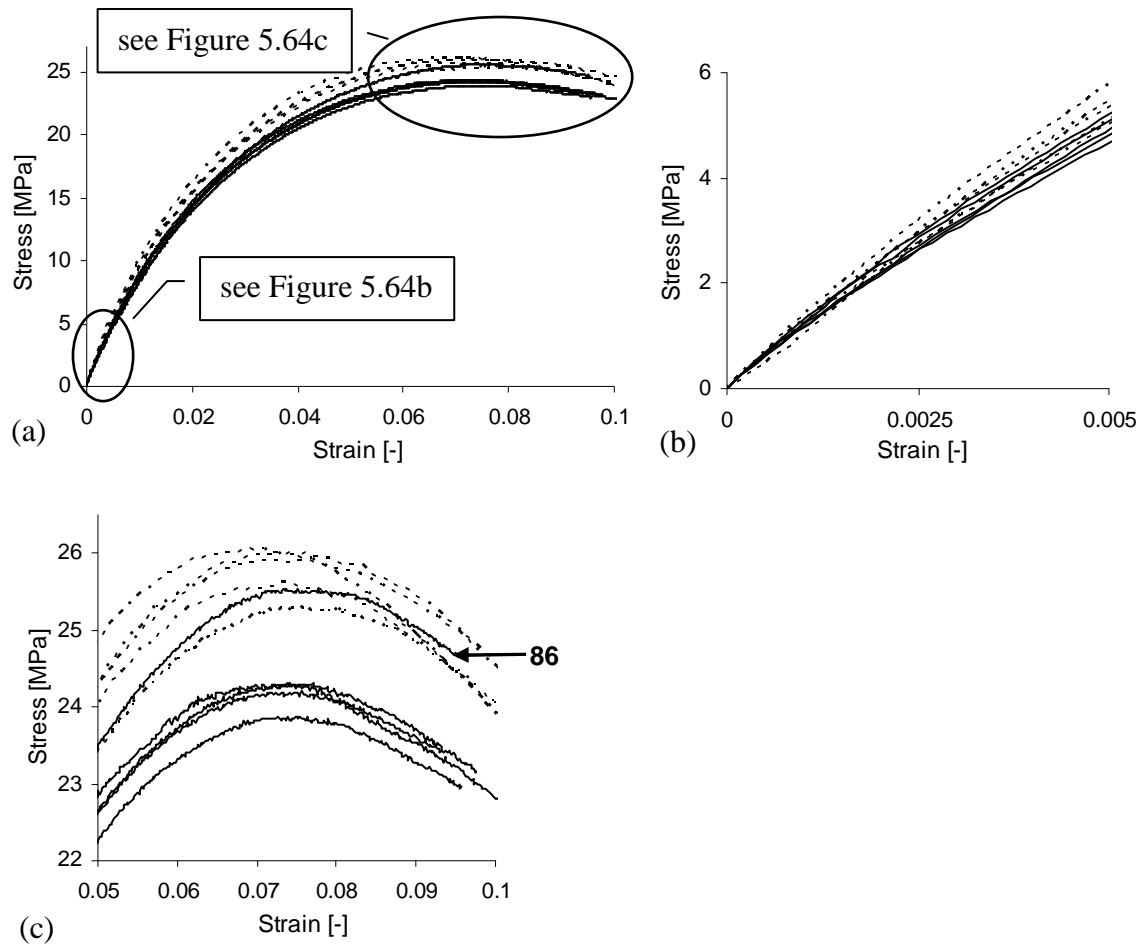
Figure 5.64 (a) Stress-strain curves for the plain samples produced under different conditions: (——) A and (- - -) B; (b) enlarged elastic region; (c) enlarged peak stress region.

Table 5.51 Flexural values for the plain samples produced under condition A. Note: the marking lines explained further in the text.

Sample	Flexural modulus MPa	Peak stress MPa
86	992	25.5
87	1011	24.3
88	1093	24.2
89	1128	24.3
90	1014	23.9
Average	1048	24.5
SD	59	0.6

Table 5.52 Flexural values for the plain samples produced under condition B. Note: the marking lines explained further in the text.

Sample	Flexural modulus MPa	Peak stress MPa
176	1070	25.3
177	1215	26.1
178	1110	25.6
179	1164	26.0
180	1155	25.9
Average	1143	25.8
SD	55	0.3

The flexural moduli and peak stresses of the samples produced under condition B reached higher values, 1143 and 25.8MPa, respectively, as compared with the samples produced under condition A. The differences in moduli (95MPa) and peak stresses (1.3MPa) are larger than the maximum SDs (59 and 0.6MPa, respectively), therefore they can be relied on. Higher flexural modulus is associated with higher peak stress, which was expected as both values are related and should increase with increasing sample stiffness. Therefore, it is assumed that the samples produced under condition B have higher crystallinity and thus were produced under a lower cooling rate associated with higher cooling water temperature.

The difference in the peak stresses for both types of samples can also be clearly seen in Figure 5.64 as the curves group depending on the material properties imposed by the manufacturing conditions. Sample 86 stands out from the group as it has an exceptionally high peak stress of 25.5MPa while the modulus for this sample is exceptionally low (992MPa). Normally, as already mentioned, the opposite tendency would be expected. However, it has to be noted that the shape of the curve after exceeding the elastic region is also associated with slipping and repositioning of the sample on the support noses, which might have been different in the case of sample 86.

For the comparison between the samples three representative curves were identified: the curve with a peak stress closest to the calculated average (178), and/or the extreme curves (the envelopes) with the minimum (90) and maximum peak stress (177). In the case of multiple samples with peak stress values close to the average, the flexural moduli is also considered. The samples are marked in Tables 5.51 and 5.52. This marking scheme is used when required throughout the whole section on the flexural bending test and the associated Appendices.

In order to justify the repeatability of the results the SDs for five samples produced under conditions A and B (Tables 5.51 and 5.52) and for all ten samples (Table 5.53) are compared.

Table 5.53 Average flexural values with SDs obtained for ten plain polyethylene samples produced under different conditions.

Sample	Flexural modulus MPa	Peak stress MPa
Average	1095	25.1
SD	74	0.8
SD as % of the Average %	7	3

Higher SDs obtained for ten samples reflects a larger variation in the results, which is assigned to different manufacturing conditions, which could not be measured nor controlled for every sample. This suggests that at least ten samples should be tested to ensure a reasonable reproducibility. Not withstanding this, only five samples were tested in accordance with the standards (ASTM, 2008a; BSI, 2003b) due to the lack of time.

However, in order to get an appreciation of the potential variation due to the varied manufacturing conditions, the extreme results for samples 90 (Table 5.51) and 177 (Table 5.52) are used for comparison with the samples with chips. For the numerical comparison the averages obtained for all ten samples produced under different conditions are used.

Whenever possible, additional plain samples were cut out from the same sheet as the specific samples with chips and tested in order to eliminate the variations in the matrix properties. However, it has to be noted that only a limited number of samples can be produced from one sheet, which depends on the chip orientation. In the case of some orientations, especially when the chip is placed perpendicularly to the sheet surface, the effectiveness of the sample production is very low and only a few samples can be obtained from one sheet (see section 4.3.4.5, page 112), thus the full set of samples is cut out from various sheets having various properties.

As the peak stress is obtained for strains between 0.06 and 0.08 (Figure 5.64c) it is enough to present the data up to a strain of 0.08.

Before the main tests for the samples with chips were carried out the strain rate effect was investigated for the plain samples.

5.3.3   Strain rate effect

The strain rate effect is analysed for the speeds 2, 20, and 80mm/min, which represent the strain rates of 0.01, 0.1 and 0.4min^{-1} (Equation 4.11, page 133). The strain rate of 0.01min^{-1} is recommended in the standards for unreinforced and reinforced plastics and also used in most tests for the determination of flexural modulus (ASTM, 2007c and 2008a; BSI, 2003b) while the strain rate of 0.1min^{-1} can be used for materials, which undergo large deflections during testing (ASTM, 2007c). Figure 5.65 shows the plots for each speed and Tables 5.54 and 5.55 list the flexural values for the speeds of 20 and 80mm/min. The data for 2mm/min were summarized in Table 5.53.
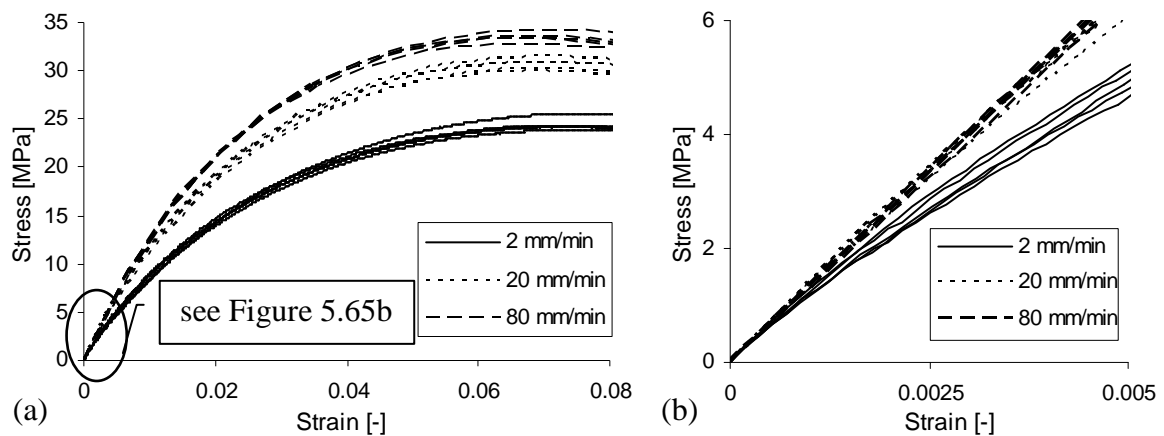
Figure 5.65 (a) Stress-strain curves for the plain samples tested at different speeds; (b) enlarged elastic region.

Table 5.54 Flexural values for the plain polyethylene samples tested at a speed of 20mm/min.

Sample	Flexural modulus MPa	Peak stress MPa
91	1269	30.3
92	1342	30.9
93	1314	30.9
94	1345	31.4
95	1341	29.9
Average	1322	30.7
SD	32	0.6

Table 5.55 Flexural values for the plain polyethylene samples tested at a speed of 80mm/min.

Sample	Flexural modulus MPa	Peak stress MPa
96	1329	33.3
97	1344	33.4
98	1286	34.2
99	1314	32.8
65	1329	33.6
Average	1320	33.5
SD	22	0.5

Concerning the peak stress, the differences between different speeds are significant and reduce with increasing speed being the lowest (24.5MPa) for 2mm/min. A similar tendency is observed for the flexural modulus values, which is also the lowest (1048MPa) for the lowest speed; however, the values for higher speeds are almost equal (the difference of 2MPa is much lower than the SDs). These results are mostly in line with the theory (Plastic Pipe Institute, 2007).

The data obtained for the speed of 20mm/min were used for the determination of the stress levels to be applied in the flexural creep test (Chapter 7).

Further, the chip effect is analysed.

5.3.4 Chip effect for an SC chip

The chip effect is studied first on the basis of SC/0/90 samples. As they were cut out from different sheets than the plain polyethylene samples, exceptionally ten samples were tested.

Tables 5.56 and 5.57 list the numerical data for two sets of SC/0/90 samples produced under different conditions, C and D. The data for the plain samples were listed in Tables 5.51 and

5.52. Figure 5.66 shows the plots for the extreme samples and Table 5.58 summarised the key numerical data for ten samples with and without a chip produced under different conditions.

Table 5.56 Flexural values for the SC/0/90 samples produced under condition C.

Sample	Flexural modulus MPa	Peak stress MPa
66	1128	24.4
67	1139	23.9
68	1084	24.2
69	1094	23.8
70	1090	24.1
Average	1107	24.1
SD	25	0.3

Table 5.57 Flexural values for the SC/0/90 samples produced under condition D.

Sample	Flexural modulus MPa	Peak stress MPa
200	975	25.1
201	960	24.9
202	991	24.9
203	982	24.8
204	891	24.4
Average	960	24.8
SD	40	0.2
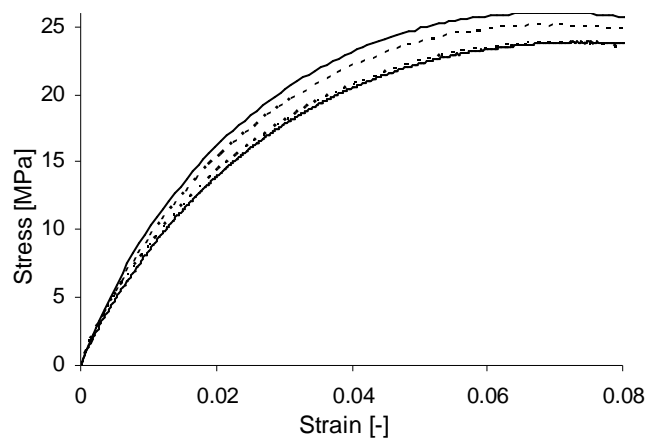
Figure 5.66 (a) Stress-strain curves for the extreme (——) plain samples (produced under conditions A and B) and (- - -) SC/0/90 samples (produced under different conditions C and D).

Table 5.58 Average flexural values with SDs obtained for ten plain and SC/0/90 samples.

Sample	Flexural modulus MPa	Peak stress MPa
plain		
Average	1095	25.1
SD	74	0.8
SC/0/90		
Average	1033	24.5
SD	84	0.4

The flexural values for the SC/0/90 samples (modulus and peak stress equal to 1033 and 24.5MPa, respectively) are lower than for the plain polyethylene (1095 and 25.1MPa, respectively), which gives a different pattern than observed by other researchers.

In general, the typical fillers improve the flexural properties of the material (Xanthos, 2010). Liang & Yang (2007) who tested mica reinforced HDPE and Kromminga & Van Esche (2001) who tested talk particles as reinforcement observed linear dependency between filler content and flexural strength and modulus. Shucai et al. (1996) who investigated PP reinforced also with mica, Adhikary et al. (2008) who tested wood flour HDPE composites, Yang et al. (2008) who studied PP filled with glass bead particles (which are similar to circular chips due to their regular shape and low aspect ratio) all observed an increase in flexural strength and modulus with increasing filler content.

However, their research differed significantly from current research as the particles were much smaller (micrometers scale) and they were added at higher contents (over 5%). In addition, there was no bond between the chip and the polyethylene while the mentioned fillers were usually treated with silane coupling agents for improved adhesion between the filler and the matrix, which improves the reinforcing effect (Borup & Weissenbach, 2010). Adur & Flynn (1987), who tested wood flour reinforced plastics, observed that when the adhesion is poor the reinforcement can even reduce the tensile and flexural strengths of composite. A loose chip might act as a hole reducing the volume of the matrix, which sustains the load and causes a stress concentration as demonstrated by Savin (1961) (Figure 2.35, page 52).

However, it has to be noted that the differences between the plain and SC/0/90 samples are smaller than the SDs, thus unreliable and are probably due to the variations in the manufacturing conditions and limited accuracy of the measurement. Therefore, the chip effect is further studied for larger chip size. First, the LC/0/90 and LC/surf orientations are

investigated, while in section 5.3.6 additionally the 90/0 and 90/90 orientations are studied and the results for both chip sizes are compared.

5.3.5 Chip effect for an LC chip

As explained in section 5.3.2 there are variations in the properties of the samples due to varied manufacturing conditions. In order to exclude these variations, the LC/0/90 samples are compared with plain polyethylene samples cut out from the same sheet (produced under condition B) to ensure the possible differences between the results are only due to the inclusion of a chip. Tables 5.59 and 5.60 list the flexural values for the plain and LC/0/90 samples produced under conditions B. In Figure 5.67 the extreme curves are compared.

Table 5.59 Flexural values for the plain samples produced under condition B.

Sample	Flexural modulus MPa	Peak stress MPa
176	1070	25.3
177	1215	26.1
178	1110	25.6
179	1164	26.0
180	1155	25.9
Average	1143	25.8
SD	55	0.3

Table 5.60 Flexural values for the LC/0/90 samples produced under condition B.

Sample	Flexural modulus MPa	Peak stress MPa
181	1151	24.9
182	1201	25.2
183	1146	24.7
184	1092	25.0
185	1125	24.4
Average	1143	24.8
SD	40	0.3
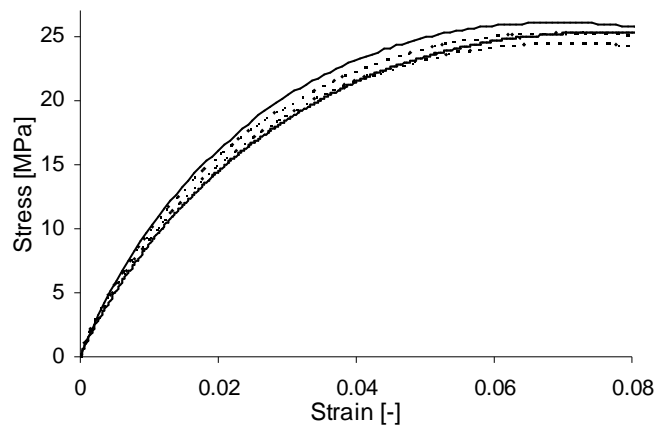
Figure 5.67 Stress-strain curves for the plain (——) and (- - -) LC/0/90 samples from the same sheet produced under conditions B.

The results indicate that there is no difference between the flexural moduli of the samples with and without an LC chip being equal to 1143MPa. Thus, the differences in the moduli recorded for the samples with and without an SC chip (Table 5.58) are then probably due to variations in the properties of the matrix.

The peak stress is higher for the plain polyethylene being 25.8MPa in comparison with 24.8MPa for the LC/0/90 samples. The difference of 1MPa is larger than the SD of 0.3MPa and the measurement error of 0.5MPa (section 5.3.1). In the case of the SC samples the peak stress was also greater for the plain polymer, however the difference of 0.6MPa was smaller than the SD of 0.8MPa, thus it is hard to conclude if the SC chip has any effect on the samples. This will be further studied for other orientations.

As the stress is proportional to the load (Equation 4.12, page 134) it means that it requires more load to deform the plain sample to the same degree (strain) as compared with the sample with an LC chip. The easier deformation of the sample with a chip might be associated with the fact that the chip breaks at some point.

The point of breaking of silicon chips in the samples was acoustically detected as the brittle material makes a noticeable sound as it happens. In some cases the sound was recorded twice,

236

which meant the chip had broken in two places and/or two stages. In Table 5.61 the strains recorded, at which the sound of the chip breaking occurred, are listed. In Figure 5.68 the breaking points are marked for each sample.

Table 5.61 The strains recorded at which the first and second sound of the chip breaking occurred.

Sample	1st breaking point	2nd breaking point
181	0.021	0.026
183	0.036	0.088
184	0.057	-
185	0.041	-
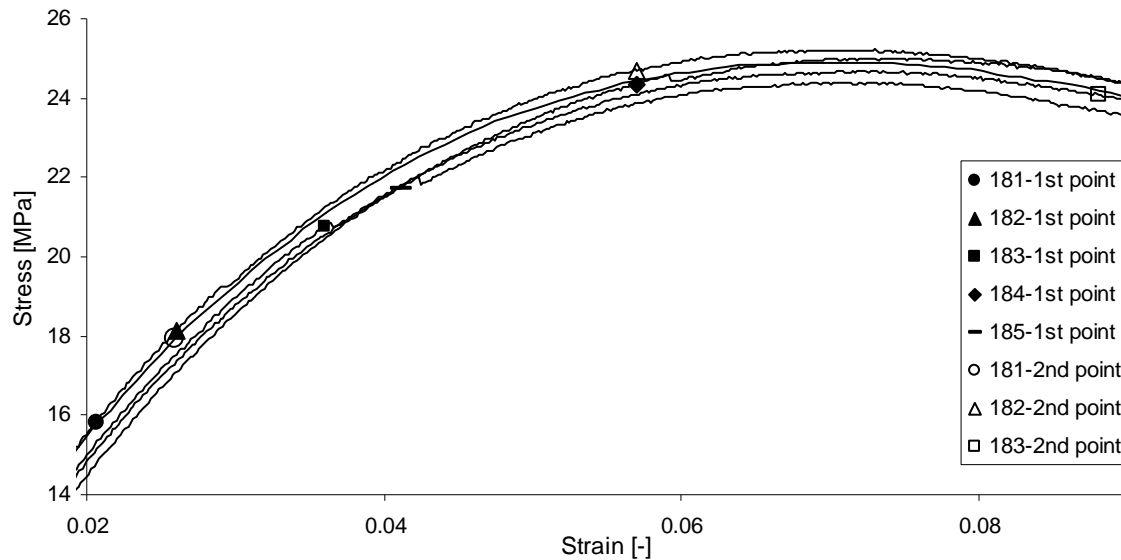
Figure 5.68 Stress-strain curves for the LC/0/90 samples with points marked at which the breaking (1st and 2nd) of the chip was recorded.

From Figure 5.68 and Table 5.61 it is difficult to see any relationship between the strain at which the first break of the chip occurs and the flexural modulus and peak stress values. This might need to be studied in more detail and it would be worthwhile to find the association between the breaking point and the actual chip orientation. For each sample the first breaking point was before the peak stress was reached. The earliest and the latest points were obtained for samples 181 and 184, respectively, for the strains approximately 0.02 and 0.06 and the

extensions associated of 4 and 11mm, respectively. The bending angles for such extensions can be estimated (10º and 40º) as illustrated in Figure 5.69.

(a)   (b)
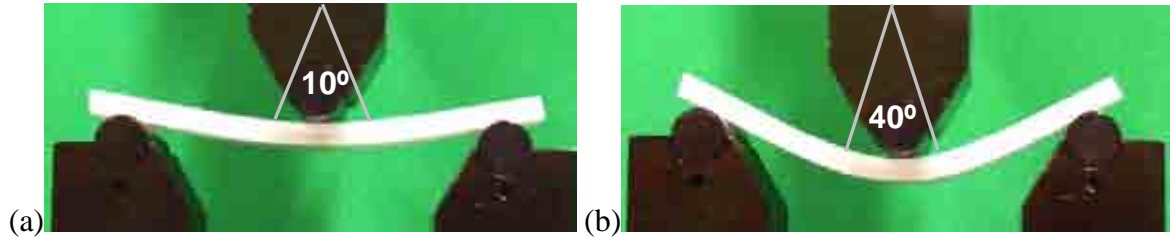
Figure 5.69 The bending angles at which first breaks of the chips occurred for samples (a) 181 and (b) 184.

The lowest angle is probably achieved for the chip orientation exactly as desired. The X-ray scans of a few samples shown in Figure 5.70 indicate slight variations in the chip distance and orientation towards the sample surface and edges. Therefore, different angles are likely to occur. Another reason for these variations might be the location of the chip in relation to the loading nose.
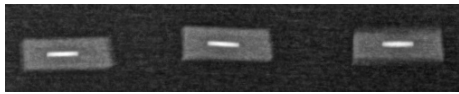
Figure 5.70 X-ray scans through the cross-section of the LC/0/90 samples.

In order to investigate the way in which the chips break a few samples with an LC chip were melted, as in the molten state the polymer is transparent because there are no crystals present, thus the crack in the chip could be seen. Figure 5.71 shows the example samples.

(a)   (b)
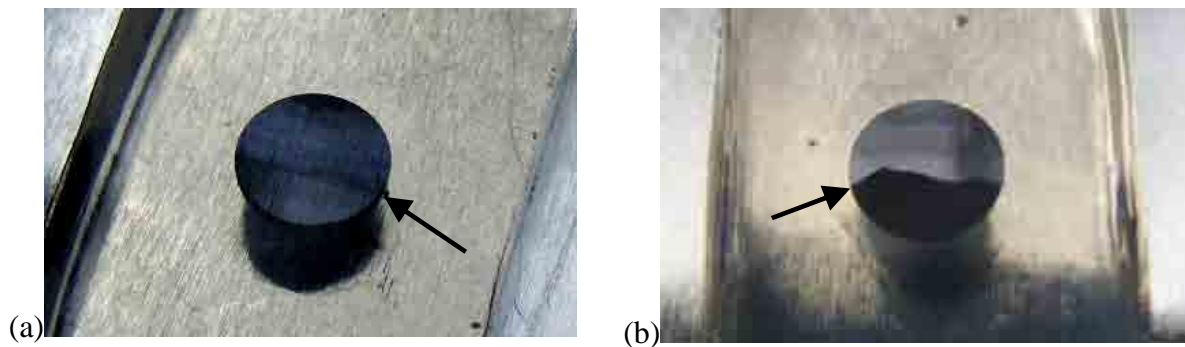
Figure 5.71 The broken chips in a molten polymer; the start of a crack marked by an arrow.

The visual analysis indicated that the cracks have different shapes and positions but are usually straight and go across the chip close to the equator along the sample width as illustrated in Figure 5.71a. The crack in Figure 5.71b has an unusual shape and probably formed in stages at different strains.

As at the orientation 0/90 the variations in the actual positions of the chips might have influenced the results, the LC chips on the surface were investigated, as their position can be better controlled at this orientation.

The chip on the outer side of the beam is subject to tension and the chip on the inner side of the beam is subject to compression (Yu & Zhang, 1996), while the chip placed in the middle of the sample (orientation 0/90) is not stretched or compressed in the initial stage of the test as it is on the neutral axis (centre line of the beam). Both cases were analysed in order to see if the side at which the chip is located has any influence on the sample performance. The samples were produced from the same sheet, however, the plain samples were produced from different sheet, thus in Figure 5.72 the plots for the extreme samples of each type are presented. Tables 5.62 and 5.63 list the numerical values for the samples with LC chips on the surface while the data for the plain samples were summarized in Table 5.53 (page 230).
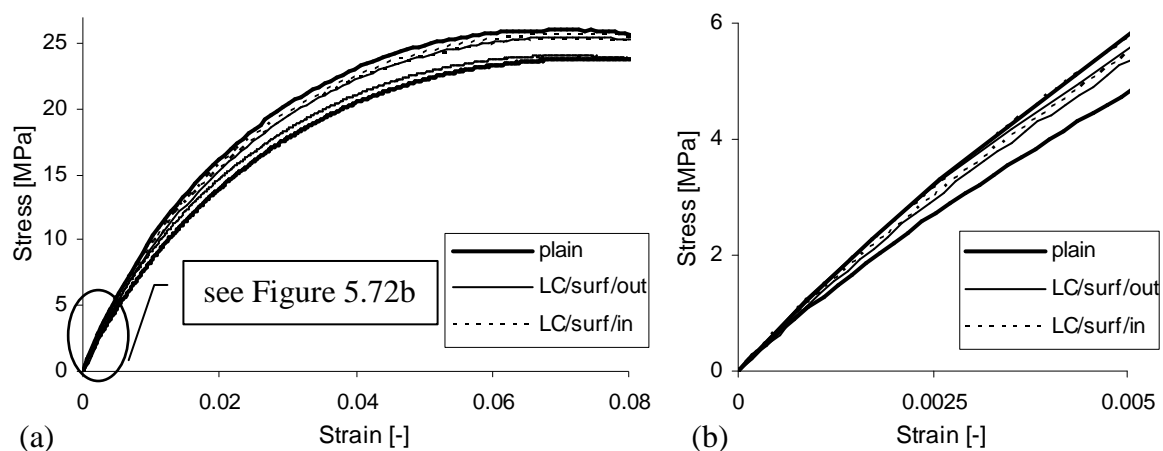
Figure 5.72 (a) Stress-strain curves for the samples with an LC chip on the inside and outside surface fibres; (b) close up of the elastic region.

Table 5.62 Flexural values for the LC/surf/out (outer surface) samples.

Sample	Flexural modulus MPa	Peak stress MPa
147	1256	24.4
148	1142	24.3
149	1178	24.1
186	1240	25.5
187	1183	25.0
Average	1200	24.7
SD	47	0.6

Table 5.63 Flexural values for the LC/surf/in (inner surface) samples.

Sample	Flexural modulus MPa	Peak stress MPa
150	1182	25.6
151	1231	25.4
152	1254	25.3
189	1199	25.7
190	1147	25.4
Average	1203	25.5
SD	42	0.2

From Figure 5.72 it can be seen that the plots are between the envelopes obtained for the plain samples produced under various conditions, thus, the highest average modulus obtained among the samples tested up to now might be due to the highest stiffness of the matrix.

The peak stress for the samples with an LC chip on the outer fibres (24.7MPa) is close to the value obtained for the orientation 0/90 (24.8MPa). These values are lower than for the plain samples (25.1MPa). In contrast, the peak stress obtained for the chip on the internal fibres is highest (25.5MPa), which might be associated with the phenomena that the chip on the internal fibres resists bending force and more energy is required to deform the sample to the same strain in comparison with other types of samples.

The LC chips on the surface did not break due to sample bending.

Further, the impact of the SC and LC chips at the orientations perpendicular to the sample surface is compared.

5.3.6 Chip size effect

In this section the 90/0 and 90/90 orientations are investigated for the SC and LC chips. The samples with these orientations had to be cut out from different sheets due to the low effectiveness of their production. As indicated in section 4.3.4.5 sometimes only one appropriate sample was achieved from a sheet.

Tables 5.56 and 5.57 (page 233) list the data for the SC chip and Table 5.60 (page 235) – for the LC chip, at the orientation 0/90. Tables 5.64-5.67 list the data for the orientations 90/0 and 90/90. The key flexural values for both chips are summarized in Tables 5.68 and 5.69.

Table 5.64 Flexural values for the SC/90/0 samples.

Sample	Flexural modulus MPa	Peak stress MPa
154	1009	24.7
155	1021	24.6
156	986	24.4
157	1026	23.9
158	1044	24.1
Average	1017	24.3
SD	21	0.3

Table 5.65 Flexural values for the SC/90/90.

Sample	Flexural modulus MPa	Peak stress MPa
159	1063	24.2
160	957	23.5
161	1043	24.4
162	1034	24.0
163	1028	24.5
Average	1025	24.1
SD	40	0.4

Table 5.66 Flexural values for the LC/90/0 samples.

Sample	Flexural modulus MPa	Peak stress MPa
131	1075	23.6
132	1050	23.6
133	1067	23.3
134	1064	24.1
135	1033	23.2
Average	1058	23.5
SD	16	0.3

Table 5.67 Flexural values for the LC/90/90.

Sample	Flexural modulus MPa	Peak stress MPa
126	1078	22.7
127	1053	22.9
128	1053	22.5
129	1056	22.8
130	1037	22.7
Average	1055	22.7
SD	14	0.2

Table 5.68 Flexural values for the samples with an SC chip at different orientations.

Orientation	Flexural modulus MPa	Peak stress MPa
0/90		
Average	1033	24.5
SD	84	0.4
90/0		
Average	1017	24.3
SD	21	0.3
90/90		
Average	1025	24.1
SD	40	0.4

Table 5.69 Flexural values for the samples with an LC chip at different orientations.

Orientation	Flexural modulus MPa	Peak stress MPa
0/90		
Average	1143	24.8
SD	40	0.3
90/0		
Average	1058	23.5
SD	16	0.3
90/90		
Average	1055	22.7
SD	14	0.2

From Table 5.68 it can be seen that for the SC chip the flexural moduli and peak stresses are very close for all tested orientations, slightly lower than for the plain polyethylene (1095 and 25.1MPa, respectively), however the differences are smaller than the SDs, thus insignificant.

When comparing the flexural moduli of samples with an LC chip the highest value was recorded for the orientation 0/90; however, this is due to the properties of the matrix as for the plain sample from the same sheet the same value was obtained (Table 5.59). The peak stress for the LC/0/90 samples was lower (24.8MPa) than for the plain samples from the same or from other sheets (25.8MPa and 25.1MPa, respectively), thus its reduction was assigned to the break of the chip (see previous section). At other orientations the peak stresses were further reduced following the pattern: $0/90 > 90/0 > 90/90,$ and the differences between the values are greater than the SDs. At the orientations 90/0 and 90/90 the chip did not break, thus the peak stress reduction might be due the hole formed between the chip and the matrix and uneven position of the chip indicated in the X-ray scans (Figure 5.40b, page 197).

The flexural moduli for a sample with an LC chip are in general larger than for an SC chip when comparing the same orientations, which is in accordance with the results of other researchers, e.g. Lusis et al., 1973 and Yang et al., 2008, who observed an improvement in flexural properties with particle size and aspect ratio. However, no relevant literature was found on the orientation effect in the flexural test of composites or materials with inclusions or holes.

It can also be concluded that the chip reduces the peak stress of polyethylene, and this reduction increases with the chip size. However, the bending test is normally carried out up to much lower deformations and thus there is no relevant literature with which the results can be compared. Thus, the variations in the peak stress values can also be a result of slipping off the samples and their rearrangement during the test, besides breaking of the chip in the LC/0/90 samples.

As the largest chip effect (a reduction in the flexural peak stress) was observed for the chip orientation 90/90, this orientation is used to study the chip shape effect.

5.3.7 Chip shape effect

Table 5.70 list the flexural data for the SSQ chip at the orientation 90/90. Tables 5.65 and 5.67 listed the data for the SC and LC chips, respectively, while Table 5.53 (page 230) summarized the values for the plain polymer. Figure 5.73 shows the plots for the samples with SSQ, SC and LC chips at the orientation 90/90. The samples were produced from different sheets, thus the plots for the extreme samples of each type are presented. Table 5.71 lists the key numerical values.

Table 5.70 Flexural values for the SSQ/90/90 samples.

Sample	Flexural modulus MPa	Peak stress MPa
192	1100	26.3
193	1172	26.4
194	1193	26.3
195	1184	26.5
196	1200	26.2
Average	1170	26.3
SD	40	0.1

(a)

(b)

(c)
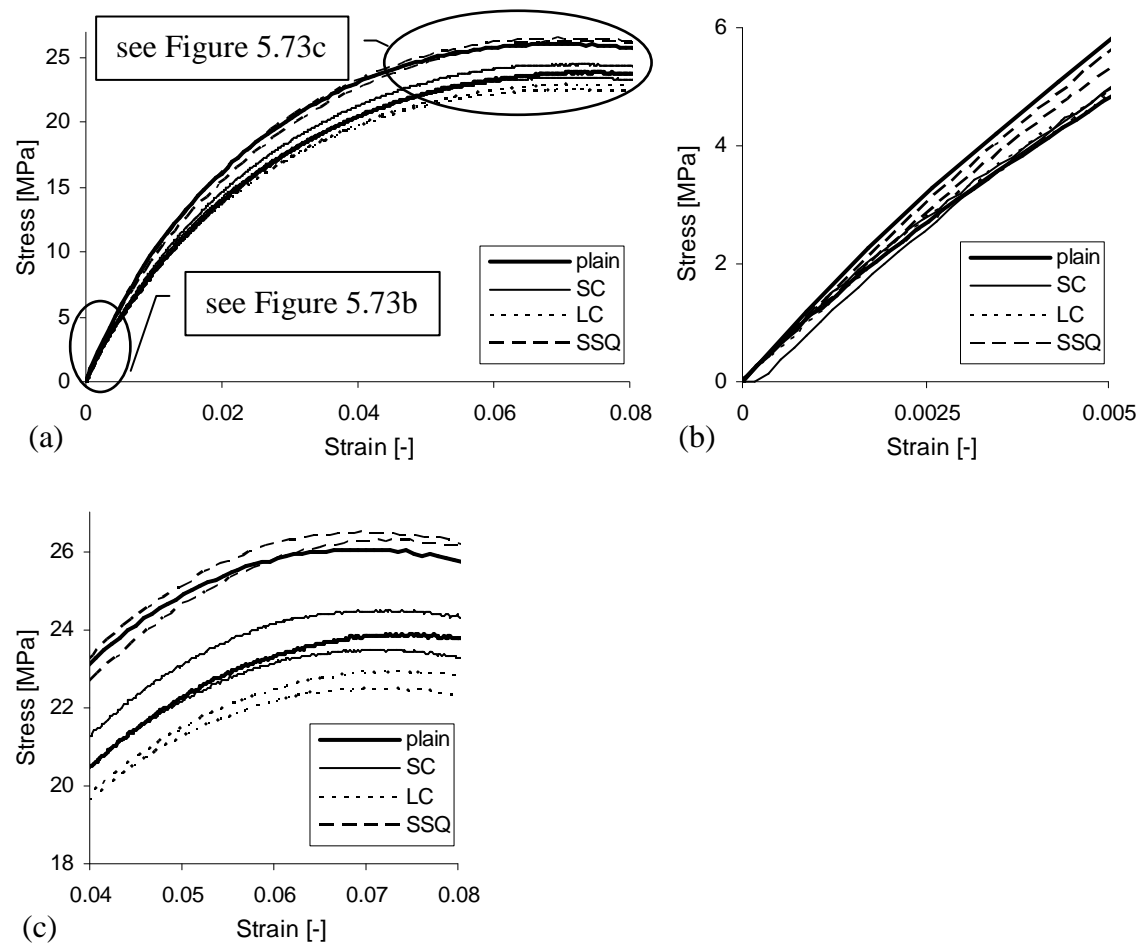
Figure 5.73 (a) Stress-strain curves for the samples with SC, LC, and SSQ chips at the orientation 90/90 and selected plain polyethylene samples; (b) enlarged elastic region; (c) enlarged peak stress region.

Table 5.71 Average flexural values with SDs for the samples with SSQ, SC and LC chips at the orientation 90/90.

Chip	Flexural modulus MPa	Peak stress MPa
SC		
Average	1025	24.1
SD	40	0.4
LC		
Average	1055	22.7
SD	14	0.2
SSQ		
Average	1170	26.3
SD	40	0.1

The flexural moduli of the samples are probably associated with the properties of the matrix as for most of the samples they are in the range between two extreme plain polyethylene samples (Figure 5.73). The peak stresses for the samples with an LC chip are lower (22.7MPa on average) and for the SSQ samples they are higher (26.3MPa on average) than for the plain and SC/90/90 samples (25.1 and 24.1MPa, respectively) and the differences are larger than the SDs, thus significant. This means that the LC chip reduces while the SSQ chip increases the sample stiffness, especially at large deformations.

Further, the thickness effect is studied on the basis of the samples approximately two times thinner (2.2mm) with and without an SC chip.

5.3.8 Thickness effect

As the previous tests indicated the SC chip does not have any significant influence on the performance of polyethylene in bending, while the LC chip reduces sample stiffness, at high deformations. In this section it is investigated how the reduction of sample thickness

influences the chip effect. This is studied for the SC/0/90 samples of two thicknesses and also compared with the LC/0/90 4.2mm thick samples.

As the manufacturing conditions influence the results the samples with and without a chip were cut out from the same sheet. The test was carried out at the speed of 1mm/min to maintain the same strain rate of approximately 0.01min^{-1}, and the support span was twice as small. Tables 5.72 and 5.73 list the data for the thin samples, plain and SC/0/90, respectively, while Table 5.58 summarized the flexural values for the thick samples with and without a chip. Figure 5.74 shows the data for both sample thicknesses. The plots for the thin (2.2mm) and thick (4.2mm) samples differ significantly and all thin samples were cut out from the same sheet, thus only the average curves are shown for these samples. For the thick samples the extreme curves are presented. Tables 5.72 and 5.73 list the key numerical values for the thin and thick samples with and without a chip.

Table 5.72 Flexural values for the 2.2mm thick plain polyethylene samples.

Sample	Flexural modulus MPa	Peak stress MPa
164	1169	31.2
165	1199	31.0
166	1158	31.4
167	1173	31.7
168	1069	31.6
Average	1154	31.4
SD	50	0.3

Table 5.73 Flexural values for the 2.2mm thick SC/0/90 samples.

Sample	Flexural modulus MPa	Peak stress MPa
169	1106	30.6
170	1079	30.9
171	1175	31.3
172	1138	30.5
173	1160	30.4
Average	1132	30.7
SD	39	0.4
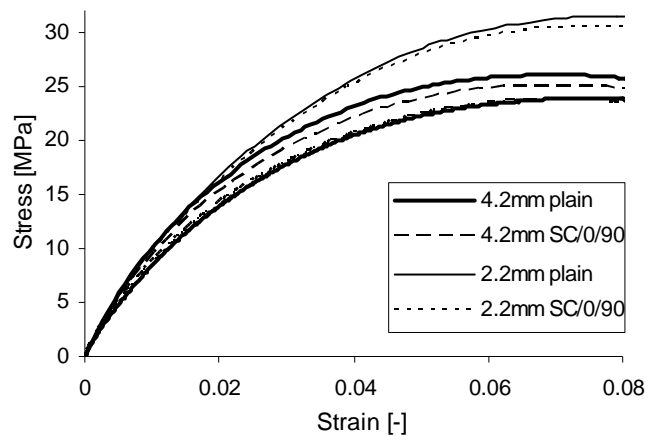
Figure 5.74 Stress-strain curves for the 2.2 and 4.2mm thick samples with and without a chip.

Table 5.74 Average flexural values with SDs for the 2.2mm thick plain and SC/0/90 samples.

Sample	Flexural modulus MPa	Peak stress MPa
plain		
Average	1154	31.4
SD	50	0.3
SC/0/90		
Average	1132	30.7
SD	39	0.4

Table 5.75 Average flexural values with SDs for the 4.2mm thick plain and SC/0/90 samples.

Sample	Flexural modulus MPa	Peak stress MPa
plain		
Average	1095	25.1
SD	74	0.8
SC/0/90		
Average	1033	24.5
SD	84	0.4

The thin samples with and without a chip were cut out from the same sheet and in consequence have similar moduli (Table 5.74), however the values for the plain sample are slightly higher. The peak stress of the plain samples is higher by 0.7MPa, which is more than the maximum SD of 40MPa. A similar trend was observed for the thick samples with SC (Table 5.75) and LC chips (see section 5.3.5).

When comparing the two thicknesses of the samples, the moduli are slightly higher while the peak stresses are significantly higher for the thin samples. This might be associated with the smaller support span, which limited the deformation of the sample at high strains as illustrated

in Figure 5.75. Therefore, a higher load was required to bend the sample to the same relative strain obtained from Equation 4.14 (page 134).

(a)   (b)

Figure 5.75 The test arrangement in 3-point bending for (a) 4.2mm and (b) 2.2mm thick samples.

In the next section the results of the bending test are summarized.

5.3.9   Summary of the results of the flexural bending test

Similar values of the flexural modulus were obtained in the 3- and 4-point bending modes and for further tests the 3-point bending was chosen mostly because the samples in this mode could be deformed to a larger degree and the theoretical flexural peak stress could be obtained.

The results for the plain polyethylene samples produced under different conditions varied, and for the stiffer samples higher flexural moduli and peak stresses were obtained. In order to eliminate the impact of varying matrix properties on the variations in the results, whenever possible, the samples produced from the same sheet were compared.

With an increasing rate of testing the flexural modulus and peak stress increased, which is in accordance with the theory (Plastics Pipe Institute, 2007).

Table 5.76 lists the key numerical results.

Table 5.76 Summary of the flexural values.

Sample		Flexural modulus MPa	Peak stress MPa
thick			
plain (ten samples)		1095	25.1
SC/0/90 (ten samples)		1033	24.5
SC/90/0		1017	24.3
SC/90/90		1025	24.1
LC/0/90	the same sheet	1143	24.8
plain		1143	25.8
LC/90/0		1058	23.5
LC/90/90		1055	22.7
LC/surf/out		1200	24.7
LC/surf/in		1203	25.5
SSQ/90/90		1170	26.3
thin			
plain	the same sheet	1154	31.4
SC/0/90		1132	30.7

The analysis indicated that the flexural moduli are usually associated with the properties of the matrix as for different samples from the same sheet similar values were obtained. The values for the thick and thin samples were also similar.

Among the flexural peak stresses greater variations were recorded. The values for the plain samples were usually greater than for the samples with chips. An exception was the SSQ/90/90 sample for which a very high peak stress (26.3MPa) was obtained, which suggests a reinforcing effect of the square chip at large deformations. When the LC chip was placed on the inner surface of the sample (compressed fibres) it also caused an increase in the sample stiffness as the rigid chip resists bending of the sample and therefore a higher load must be applied to overcome this (peak stress of 25.5MPa).

In contrast, the LC chip at other orientations caused a reduction in the peak stress and the lowest value (22.7MPa) was recorded for the LC/90/90 sample. In general, the effect of the orientation on the peak stress reduced with the following: $0/90 > 90/0 > 90/90$. The differences in the results for the samples with an LC chip at different orientations are more significant than among the samples with an SC chip.

The flexural moduli for the samples with an LC chip were in general larger than for the SC chip when comparing the same orientations, which is in accordance with the results of other researchers (e.g. Yang et al., 2008), while the peak stresses were lower for the LC chip for the orientations 90/0 and 90/90. This might be associated with an uneven position of the chip and the possible hole formed around the chip at large deformations.

At the orientation 0/90 the LC chip broke, due to the brittleness of the silicon, at different strains 0.02-0.06 associated with different bending angles (10-40°). It reduced the peak stress by 1MPa as compared with the plain samples produced from the same sheet.

When analysing different thicknesses of the samples, for the 2.2mm thick samples with and without a chip the same pattern as for the 4.2mm thick samples was observed and higher flexural values were recorded for the plain samples. The peak stresses were much larger for the 2.2mm thick samples, which is probably due to the limitations of the fixtures (bending prevented by the supporting noses), which required more energy (load) to deform these specimens to particular strains.

The influence of a chip on the mechanical performance of the polyethylene samples in bending was very small while this effect was significant in the tensile stress mode. In the next section the chip effect in the impact stress mode is investigated.

5.4 Charpy impact test

The Charpy impact test was carried out for the notched and unnotched 4.2mm thick samples. As the test was carried out at Exova, it was done only for one orientation (SC/0/90), for which the sample production is most consistent and which is theoretically optimal for the improvement of the fracture toughness by some fillers (see section 2.4). The impact strength was calculated on the basis of Equations 4.18 and 4.19 (page 140). The width and the width under the notch were measured for each sample and the notch depth was expressed as a percentage of the width. The aim was to achieve a notch depth of 25%. Ten samples of each type were tested to gain confidence in the results, which is the minimum number recommended by the British Standard (BSI, 2001a). Table 5.77 lists the key numerical data.

Table 5.77 Charpy impact test results for notched and unnotched samples with and without a chip. Note: the averages are presented with the resolution of magnitude of SD.

Unnotched				Notched					
Without chip		With chip, SC/0/90		Without chip			With chip, SC/0/90		
Sample	Impact strength a_U kJ/m²	Sample	Impact strength a_U kJ/m²	Sample	Notch depth %	Impact strength a_N kJ/m²	Sample	Notch depth %	Impact strength a_N kJ/m²
Ch1	57.2	Ch11	61.7	Ch21	24	29.8	Ch31	27	41.8
Ch2	59.1	Ch12	59.9	Ch22	26	31.4	Ch32	22	42.8
Ch3	60.2	Ch13	62.1	Ch23	25	29.4	Ch33	25	42.6
Ch4	58.5	Ch14	58.8	Ch24	25	30.4	Ch34	23	43.0
Ch5	60.5	Ch15	58.5	Ch25	25	31.4	Ch35	26	44.1
Ch6	57.9	Ch16	58.2	Ch26	25	30.6	Ch36	27	42.2
Ch7	57.5	Ch17	59.0	Ch27	24	29.7	Ch37	27	44.8
Ch8	59.1	Ch18	61.1	Ch28	25	31.5	Ch38	26	44.1
Ch9	59.1	Ch19	59.9	Ch29	25	30.9	Ch39	27	42.2
Ch10	59.4	Ch20	60.3	Ch30	24	29.8	Ch40	27	44.8
Average	59		60		25	30		25	43
SD	1		1		1	1		1	1

Before the results are analysed, the error in the data measurement is estimated to know their reliability. It is associated with the dimension of the samples, the actual support span value and the energy measurement. The span was measured with a vernier digital caliper, giving an error of 0.05mm (Squires, 1988). It was set only once and thus kept constant. The span is not considered in any calculations, thus, it is also excluded in the error calculation.

The energy was measured with an accuracy of 0.001J and the dimensions of the sample were measured in the centre of the sample only, according to the standard recommendations (BSI, 2001a). Therefore, the thickness error is associated with micrometer measurement error of 2µm (Squires, 1988). As the deviation in width for different samples is associated with the uneven edges (section 4.3.6.3, page 121), the error remains the same as described for the other tests, i.e. 0.04 mm, which is the maximum SD of the width obtained from 20 samples. The width under the notch was measured with a special device, shown in Figure 5.76.

Figure 5.76 Device used to measure the sample width under the notch.

The impact strength error for a notched sample is calculated on the basis of Equations 4.18 (page 140) and 5.2 (page 150) as:

$$\left(\frac{\Delta a_N}{a_N}\right)^2 = \left(\frac{\Delta E_a}{E_a}\right)^2 + \left(\frac{\Delta h}{h}\right)^2 + \left(\frac{\Delta b_N}{b_N}\right)^2 \qquad \textbf{5.4}$$

where Δa_N, ΔE_a, Δh, and Δb_N are the impact strength, energy, specimen width under the notch, and specimen thickness errors, respectively. From Equation 5.4 the error for a specific sample with dimensions h = 4.370mm and b_N = 9.44mm, absorbed energy E_a = 1.256J, and impact strength 30.45kJ/m², is:

252

$$\left(\frac{\Delta a_N}{30.45}\right)^2 = \left(\frac{0.001}{1.256}\right)^2 + \left(\frac{0.002}{4.370}\right)^2 + \left(\frac{0.04}{9.44}\right)^2 \rightarrow \Delta a_N = 0.13 \text{kJ/m}^2$$

From Table 5.77, the 1kJ/m² difference between the average impact strength of the unnotched samples without (59kJ/m²) and with a chip (60kJ/m²) is larger than the measurement error of ±0.13kJ/m² but still very small and equal to the SD of the results for both types of samples, thus insignificant.

For the notched samples, the impact strength of the samples with a chip is significantly higher (43kJ/m²) than for the plain polyethylene samples (30kJ/m²) and the difference is much bigger than the SD. The chip might act as a binder holding two halves of the sample together and the extra energy might be required for pulling out one half of the chip of the polyethylene matrix as illustrated in Figure 5.78b. In addition, the chip arrests the crack to some extent and it propagates less as the remaining ligament connecting the two halves of the sample is thicker (Figure 5.78b). This is further evidence that the energy required to break the sample including a chip would be even higher, thus suggesting that the difference in the impact strength between the samples with and without a chip is even bigger than shown in Table 5.77.

(a)   (b)

Figure 5.77 (a) Unnotched and (b) notched Charpy impact samples after failure.

(a)   (b)

Figure 5.78 Partly broken notched Charpy impact samples (a) without and (b) with a chip.

The majority of Charpy impact tests on polymers and polymer composites were carried out by other researchers for the notched samples. However, Liang & Yang (2007) tested both notched and unnotched mica reinforced HDPE and in both cases they observed that the

impact strength decreases with increasing filler content, with the effect most significant for a filler content of up to 5%. Shucai et al. (1996) and Vu-Khanh et al. (1985) who studied mica reinforced PP also observed that the inclusion of a filler reduces the impact strength, especially in the case of tough polymers. However, the chips tested here are circular and thus have smooth and regular edges, therefore the stress concentrations created by the chip and around the chip are small, which might be one of the reasons why the results differ. In addition, the mentioned researchers studied different polymer grades, and the particles were much smaller than the silicon chips, added at larger concentrations, dispersed and oriented randomly, and treated with silane coupling agent for improved adhesion between the filler and the matrix. While the samples tested here included individual chips orientated parallel to the impact loading direction. There was no adhesion between the chips and the matrix, and the concentration of the chips was very small, around 0.05% (one chip per sample), which is calculated on the basis of the volume of the SC chip (2mm³) and the volume of the polyethylene between the supports (approximately 4022mm³). Therefore, the differences in the results might be due to varying test conditions.

After Piggott (1980), the reduced impact strength due to the filler might be due to the sharp corners and irregularities of flakes and platelets, which cause stress concentration. Another source of stress concentration might be the air bubbles squeezed between the filler and the matrix (Nielsen, 1974). Therefore, the silicon chips can be better compared to glass beads for which Liang & Li (1998) observed that the impact strength of the composite is up to 1.4 times higher than of the PP matrix itself for the highest investigated filler content of 20%. This is explained by the mechanism in which the inclusions contribute to the formation of crazes around their surface due to the stress concentration occurring after application of the load. The crazes increase the surface area to absorb the impact fracture energy and arrest the

propagation of cracks. Nielsen (1974) had similar observations and stated that the composites with a ductile matrix have a high impact strength due to the crazing mechanism. Such a mechanism might occur in the samples tested here and in order to analyse it the samples were manually opened and the fractured surfaces were photographed (Figure 5.79).

(a)

(b)
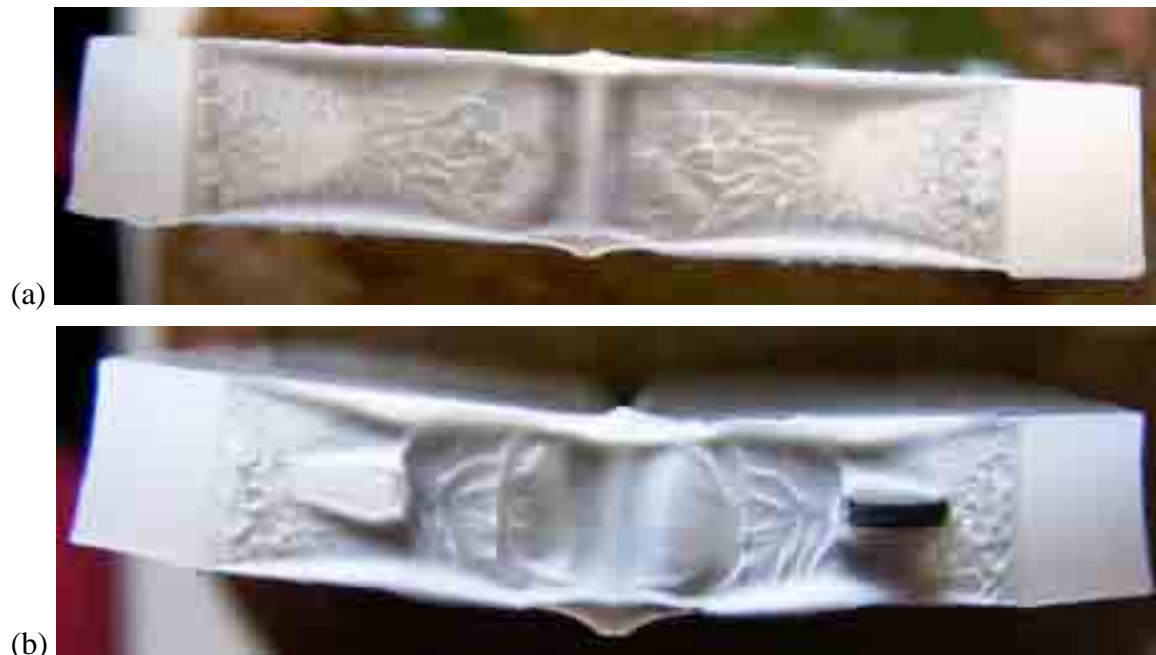
Figure 5.79 Fractured surface of polyethylene samples (a) without and (b) with a silicon chip.

The fractured surface is a mixture of coarse and flatter regions. The coarse fraction is associated with processes such as fibrillation, microvoiding, and matrix yielding contributing to the energy absorption (Suarez & Mano, 2000). The observed white area near the edges (so called sheer lips) and the darker and flatter area in the middle are characteristic for ductile behaviour. The shear lips are a plane stress component associated with ductile drawing in thin sections while the darker area is a plane strain component (see Figure 5.53, page 212). The shear lips are slightly larger in the sample with a chip. The same observed Gedde & Jansson (1985) in the high molecular weight polyethylene and Kratochvilla & Dragun (2008) in the inner and outer polyethylene pipe wall zone (plane strain region).

The surfaces are whitish due to the formation of crazes (Krishnaswamy et al., 2006). The craze initiation zone (white at the beginning) is of a comparable size for both samples. The fracture surface is covered with more or less developed fibrils, which become gradually more developed and form ductile bands with increasing distance from the initiation region. This is more pronounced in the case of the samples with a chip, especially behind the chip. This confirms the observations of Liang & Li (1998) and Tanniru & Misra (2005), who investigated $CaCO_3$ reinforced polyethylene, that the inclusions contribute to the formation of crazes and cavities encouraging plastic deformation increasing the impact strength.

Xanthos (2010) suggests that in the composites based on tough polymers the energy dissipates through mechanical friction when the reinforcement is pulled out of the matrix, which disperses the region of stress concentration through the larger volume stopping crack propagation. It is assumed that similar mechanisms might have been present here. In consequence, the toughness might have increased due to the enhanced crazing mechanism in the sample with a chip. Other researchers had similar observations, e.g. Beaumont & Philips (1972), who stated that debonding of the filler from the matrix due to poor adhesion (which is the case here) improves the toughness of the composite. The details of their discoveries were described in section 2.3.3.6 (page 56).

In contrast, other researchers, e.g. Friedrich & Karsch (1981), claim that stretching of the matrix requires much more energy than the formation of voids and cracking of the matrix-filler interface, thus when there is poor adhesion between the filler and the matrix (which is the case here) the composite has a lower impact toughness than the matrix. Thus, it cannot be excluded that an improved adhesion could further improve the impact strength of the samples.

The orientation of the filler in relation to the load direction is another factor, which influences the impact strength of the composite and the tested orientation (parallel to the direction of the

impact load illustrated in Figure 2.24a, page 42) is considered as the most advantageous after Xanthos (2010). The extra pull-out and debonding work associated with the presence of a chip increases the amount of energy required to break the sample improving the impact resistance (Nielsen, 1974; Piggott, 1980). This extra work can be calculated on the basis of the area of the chip and the shear strength of the polymer; however, the latter value is not known here, thus the calculation is impossible.

From the results and observations of the fractured surfaces it can be concluded that the chip reduces the crack propagation improving the impact fracture resistance of polyethylene.

As it was already mentioned while analysing the results and as the literature indicated (section 2.3.3.6) the character of the inclusion-matrix interface is another important factor influencing the performance of the samples with inclusions. Different researchers had different observations and in some cases the good adhesion improved, while in other cases it reduced the mechanical properties of the samples as summarised in Table 2.4 (page 61). Therefore, it was decided to modify the interface between the silicon chip and the polyethylene matrix using different types of coatings. This is analysed in the next chapter.

Chapter 6 RESULTS & DISCUSSION OF THE ADHESION TESTS

6.1 Introduction

During production and testing of the samples it was apparent that there is no proper adhesion between the chip and the polyethylene matrix, and thus confirms the current knowledge on polyethylene, which is a non-polar polymer, and thus only bonds to very few materials (section 2.3.3.6). The polished side of the silicon chip is very smooth, which is usually not advantageous in terms of adhesion (Packham, 2002).

In this Chapter the experimental analyses of the adhesion aspects associated with chips in polyethylene are presented and discussed. The adhesion was investigated in a direct way using the pull-off test and in an indirect way using the tensile and flexural bending tests. The chips were coated with several materials, especially HMAs (hot melt adhesives) in order to modify their surface and investigate its influence on the adhesion.

The pull-off test was introduced in section 4.4.5 (page 141), while the test procedures in tension and bending were the same as for the samples with non-coated chips analysed in Chapter 5. In the indirect tests only 4.2mm thick samples were tested. The dimensions of the coatings were listed in section 4.3.5.4 (page 116). Table 6.1 summarises number of particular samples tested in each test with regards to chip orientation, adhesive type and thickness.

Table 6.1 Number of samples tested at particular stress levels and environments.

	Test						
	Pull-off		Tensile			Bending	
	Sample						
Adhesive	rectangle	square	plain	SC/surf	SC/0/90	LC/surf	LC/0/90
thin HMA1 layer	6	12[+]	5	7	10	5	5
thick HMA1 layer	-	3	-	7	8	-	-
HMA1 as a matrix	-	6	7	-	5	-	-
thin HMA2 layer	-	5	-	-	9	-	-
thick HMA2 layer	-	-	-	7	-	-	-
HMA2 as a matrix	-	-	8*	-	10*	-	-
Teflon coating	-	-	-	-	7	-	-
photoresist coating	-	-	-	-	6	-	-
Total number of samples	25		106			10	

[+] In the pull-off test the strain rate effect was investigated, thus 7 extra square samples with a thin HMA1 layer were tested at the speed of 1mm/min.

* 5 extra plain and SC/0/90 HMA2 samples produced at the temperature of 210°C were examined in the tensile test.

6.2 Pull-off adhesion test

The pull-off test is a direct method for determining the strength of the bond, which is a modified version of a standard test applied to coatings (ASTM, 2006). The aim was originally to test two types of HMAs, a photoresist, and a Teflon coating; however, after manufacturing and cutting out the samples it appeared there was not enough (or no) adhesion between the chip and polyethylene matrix when using the photoresist or Teflon coatings. Therefore, in this test only the HMAs were analysed.

There are different parameters, which might influence the strength of the bond. After Lakrout et al. (1997) the strain rate of testing is important, thus a few samples with HMA1 coating

259

were tested also at 1mm/min. The thickness of the coating influences both the strength of the bond (Downs, 2010) and the character of the failure (Creton & Fabre, 2002), so additional tests were conducted for a thicker (0.60mm) HMA1 interlayer. As an extreme case the strength of the bond between only the silicon chip and the HMA1 (as a matrix) was measured. Further, the HMA2 coating was also used and two HMAs were compared. The results of these tests are introduced an discussed in the next section.

Initially, the samples with rectangular chips of dimensions $8mm \times 4mm$ (cross-section) and a thin (0.26mm) HMA1 layer between the chip and the polyethylene matrix were produced and tested and the shape of the samples for further tests was chosen. The samples were pulled at the speed of 0.1mm/min.

6.2.1　Test of rectangular samples with a thin HMA1 layer

Initially, six rectangular samples were tested in order to prove the effectiveness of sample preparation and repeatability of the results. In the adhesion test sometimes only the maximum (peak) force of the debonding curve (which is the case here), sometimes the whole process is recorded (Creton & Fabre, 2002). Figure 6.1 and Table 6.2 show the results.
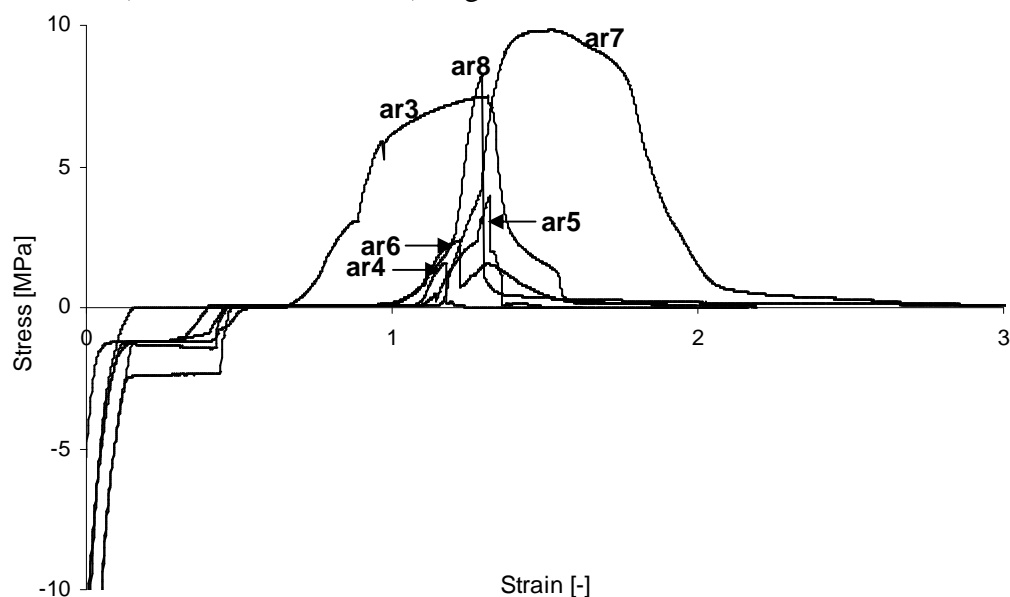
Figure 6.1 Stress-strain curves for the rectangular samples with a thin HMA1 layer obtained in the pull-off test.

Table 6.2 The peak stress values for the rectangular samples with a thin HMA1 layer tested in the pull-off test.

Sample	Peak stress MPa
ar3	7.5
ar4	1.6
ar5	4.0
ar6	2.4
ar7	9.8
ar8	8.3
Average	5.6
SD	3.4

Before analyzing the results it is important to justify the accuracy of the measurement. The error related to the dimensions was negligible as the contact area between the chip and coatings was equal to the area of the chip, which was very accurate due to the sophisticated chip cutting method used (section 4.3.6.1). The strain measurement was very inaccurate and the error was difficult to estimate. The value of depth/length of the sample was very small (4.2mm). There was no narrow section in the sample so the exact length of the stretched region was unknown. The polyethylene might have also extended and thus the sample extension could not only be assigned to the coating. The peak stress value was more reliable. The error for the load was equal to 0.5% of the measured value.

Additionally, the sample was fixed within the grips manually with limited accuracy as they were visually positioned. This might also have had an influence on the results as the samples were very small and thus such errors could be important. If the sample was installed unevenly, the load was not applied perpendicular to the cross-section causing uncontrolled twisting of the sample, which could have had an influence on the sample performance and the results.

All these factors and, in addition, the differences among the samples due to their preparation process, which was difficult to control, contributed to the large variation in the results, thus the theoretical errors, which consider only the load, dimension and strain measurement errors, were not calculated.

From Figure 6.1, the section of the curves under the strain axes (negative stress) is associated with the repositioning of the sample after it was installed in the instrument clamps. As already explained, due to the small dimensions of the samples it is difficult to place them accurately and repeatably in the instrument, thus, some energy (load) is used for this adjustment at the beginning of the test.

The next part of the curves (positive stress region) is associated with the deformation and debonding of the sample. The curves have very diverse shapes and peak stress values with an average of 5.6MPa, and a high SD of 3.4MPa. The variations in the results can be more easily understood by analysing the debonded samples shown in Figure 6.2.

The residual stresses due to shrinkage of the coating and matrix have an effect on adhesion (Adams & Davies, 2002). In addition, part of the energy (impossible to justify) is possibly used for the stretching/plastic deformation of the viscoelastic coating and the matrix.

ar3   ar4   ar5

ar6   ar7
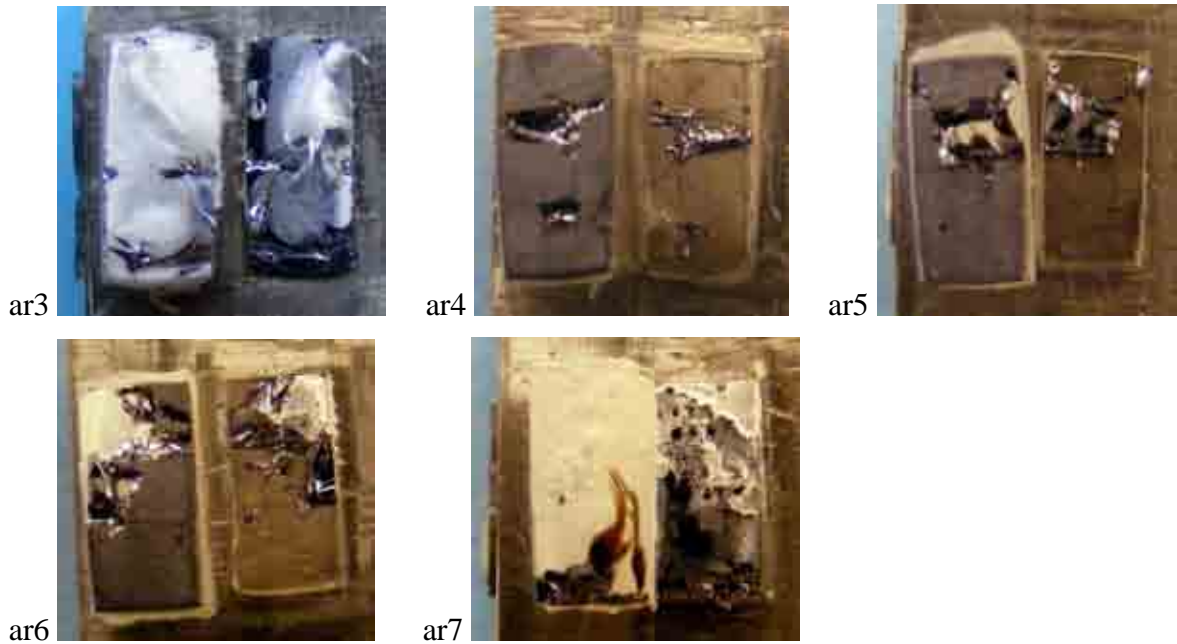
Figure 6.2 The cross-section of the debonded rectangular samples after the pull-off test.

From Figures 6.1 and 6.2 it can be seen that the differences in the results are associated with the differences in the failure patterns of the samples. Due to high brittleness of the silicon and internal defects formed during the preparation of the samples (as explained in section 4.3.6.5) the chip broke and crumbled in most cases and therefore absorbed some energy (Figure 6.2, ar3-ar7).

In addition, in some samples the debonding occurred between the metal block and the chip due to a break in the superglue bond (ar4-ar6). This might mean that the superglue bond was weaker than the HMA bond between the polyethylene and the silicon chip and/or it might be associated with a discontinuity/break of the chip acting as a stress concentration and causing the discontinuity/break in the superglue layer. The potentially weaker superglue bond might be a result of a poor glue curing process and/or poor preparation of the samples due to the varied environmental conditions in the room (humidity and temperature), or possibly even human error. For these samples lower peak stress values were obtained with the minimum reached by the ar4 sample where only a small part of the silicon delaminated (crushed). When

the fracture and delamination of the silicon was more extensive, the sample sustained a higher load (peak stress) before it debonded (samples ar5 and ar6).

In the case of samples ar3, ar7 and ar8, where the superglue sustained the load and the debonding occurred mostly due to the failure of the HMA, the shapes of the curves differ. For the ar3 and ar7 samples with partly broken chips the peak stress is not so clear and the areas under the curves (separation energy) are relatively large (see Figure 6.1). However, it is difficult to justify how much energy was consumed respectively for the final breaking of the bond, stretching of the matrix and HMA, and breaking of the chip. When comparing this with the ar8 sample, in which the chip did not break at all and so most of the energy was consumed for breaking the chip-matrix bond formed by the HMA, the stress-strain curve has a noticeable peak and the failure is close to being brittle (steep drop in the stress-strain curve after the peak stress). This indicates that no extensive stretching/plastic deformation of the sample occurred. It is assumed that in this sample, the result is closest to the real strength of the HMA.

The observations can be compared to the research of Swaminathan et al. (2003) who developed a non-destructive method for determining delamination in chip-to-chip bonded MEMS where the silicon chips had an area of $13mm \times 16mm$ and a thickness of $525\mu m$. The thermoplastic film was used as an adhesive. They verified the reliability of the delamination measurement method through destructive die-shear testing, where a pure shear force was applied to a thermoplastic or epoxy film adhesive interlayers (between 178 and $5\mu m$ thick) until it yielded.

Even though many parameters in this test differed as it was carried out in the shear instead of tensile mode, the adhesion between two chips instead of chip and polyethylene was investigated and different materials were used, the plot obtained by Swaminathan et al. (2003)

(see Figure 6.3) has a comparable shape to the curve obtained for the sample ar8, where the whole chip debonded from the polyethylene matrix.
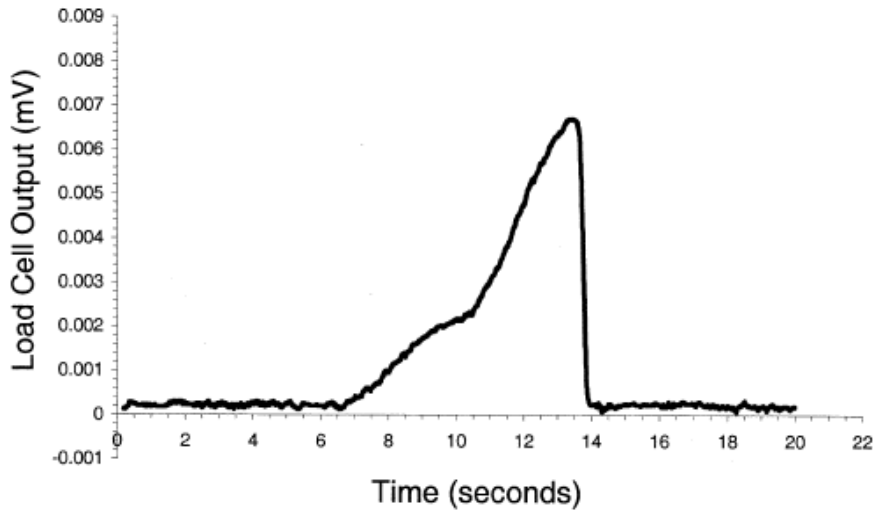
Figure 6.3 Sample die-shear testing data for thermoplastic film (Swaminathan et al., 2003).

Swaminathan et al. (2003) observed that most of the packages did not completely fall apart at failure, which was also the case here. They obtained the ultimate shear stress values by reducing the as-designed bond area by the delamination percentage at the failure interface (see Figure 6.6), while in the current project the original as-designed bond area was used in the calculation. Therefore, for the samples ar4 and ar6 in which the superglue debonded and the chip broke, very small stresses were obtained.

Swaminathan et al. (2003) also observed silicon breakage in some packages and assigned it to uneven distribution of the adhesive (no adhesive in the centre of the package), which could cause the chips to bow in the centre during force application and eventually break. In the current project the adhesive might have also been unevenly spread (as this could not have been controlled during sample production) causing non-uniform stress distribution. Another source of chip failure might be due to the already mentioned chip defects generated during sample production.

265

In the current research only the samples where the whole chip debonds from the polyethylene matrix are valuable for quantitative analyses of the results as only in these samples the strength of the chip-polyethylene bond formed by the HMA can be relatively accurately estimated.

As only one rectangular sample gave the required result (i.e. an indication of the strength of the HMA) from six samples tested, it was therefore decided to test square samples as it was thought these might be easier to prepare due to their smaller surface and circumference and thus smaller possibility of formation of defects during the samples preparation and installation.

6.2.2   Test of square samples with a thin HMA1

In the case of square samples, 12 were tested in order to have a wider range of possible results and failure patterns. Figure 6.4 presents the complete data and Table 6.3 lists the peak stress values.
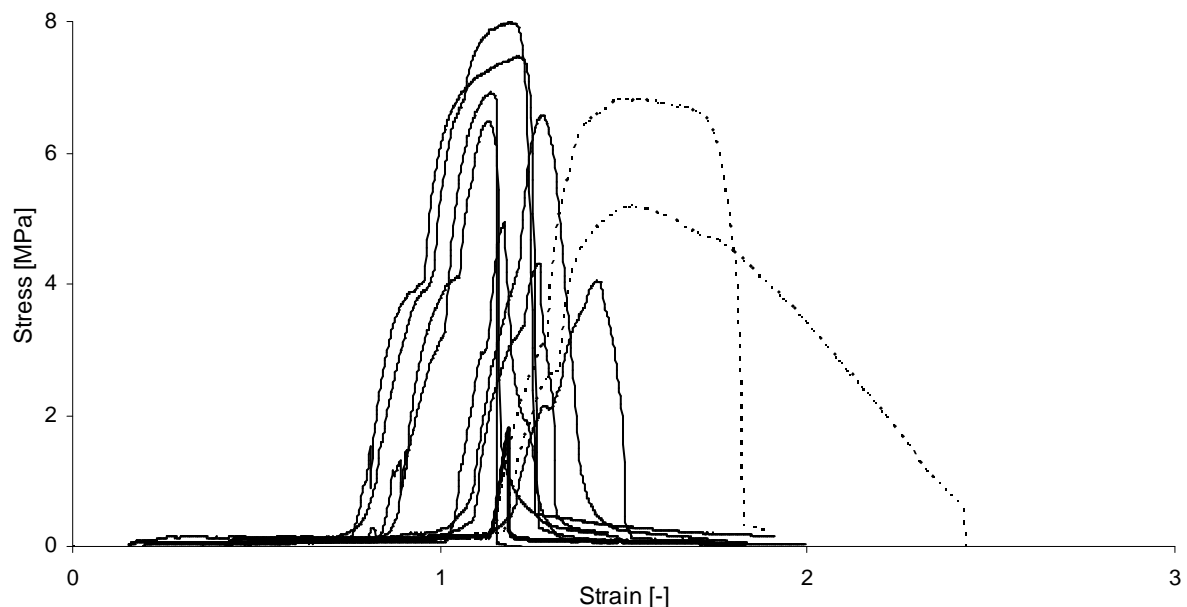
Figure 6.4 Stress-strain curves for the square samples with a thin HMA1 layer obtained in the pull-off test, where: (——) typical sample, (- - -) slipped samples (a14 and a15), and (—) superglue debonded sample (a44).

266

Table 6.3 The peak stress values for square samples with a thin HMA1 layer tested in the pull-off test.

Sample	Peak stress MPa	Sample	Peak stress MPa
a1	5.1	a13	4.1
a2	6.9	a14	6.8
a3	8.0	a15	5.2
a4	6.5	a16	4.3
a5	7.5	a36	4.9
a6	6.6	a44	1.8
		Average	5.6
		SD	1.7

From Figure 6.4 it can be seen that the shapes of the stress-strain curves for the square samples are also very variable, although, similar to the one obtained for the rectangular ar8 sample in which the chip totally debonded from the matrix and also to the one obtained by Swaminathan et al. (2003) in the shear test (Figure 6.3). The peak stress values are less variable (SD of 1.7MPa) in comparison with the rectangular samples (SD of 3.4MPa) while the average peak stress is equal for both samples (5.6MPa).

For a14 and a15 samples different shapes of the plots were obtained (Figure 6.4), which is associated with the samples slipping out of the grips during the test. This is probably due to the small size of the samples, thus small contact surface between the sample and the grips making it difficult to hold the sample stable. Even though the samples after the test looked like a typical sample with a chip debonded from the polyethylene matrix, some energy was consumed to overcome the friction between the sample and the grips as at the end of the test the sample was almost totally removed from the grips.

Sample a44 (Figure 6.5d) totally debonded from the metal block as it was already observed for the rectangular samples. The potential reasons for this have been explained in the previous section.

When the three samples, a14, a15 and a44, are excluded from the calculation for the average peak stress and SD, values of 6.0 and 1.4MPa, respectively, are obtained. This is 2.3MPa smaller than the value obtained for the rectangular sample ar8 in which the chip also fully debonded from the polyethylene matrix. The higher value in the case of the rectangular sample might be due to a smaller proportion of the sample circumference to its surface area. Around the sample circumference the boundary conditions are present and the bond might not be as strong as in the centre. In addition, the edges of the chip are slightly abraded in the sample preparation process associated with the removal of the superglue from the sample sides. In consequence the cross-section of the sample is slightly reduced, the effect of which is smaller in the case of the rectangular samples. This reduction is not considered in the calculation as the differences are very small and the results very variable. However it might at least partly contribute to the variation in the results for the rectangular and square samples.

As the preparation of the square samples is more effective resulting in a higher percentage of correct tests in which the strength of HMA was measured (75% as compared with 16.7% effectiveness obtained for rectangular samples), for all the further tests only square samples are used.

The typical debonded surfaces between the polyethylene matrix and the chip are illustrated in Figure 6.5a-c. They are either relatively smooth as in Figure 6.5a, or plastically deformed with visible fibrils on the matrix and on the chip (Figure 6.5, b and c).
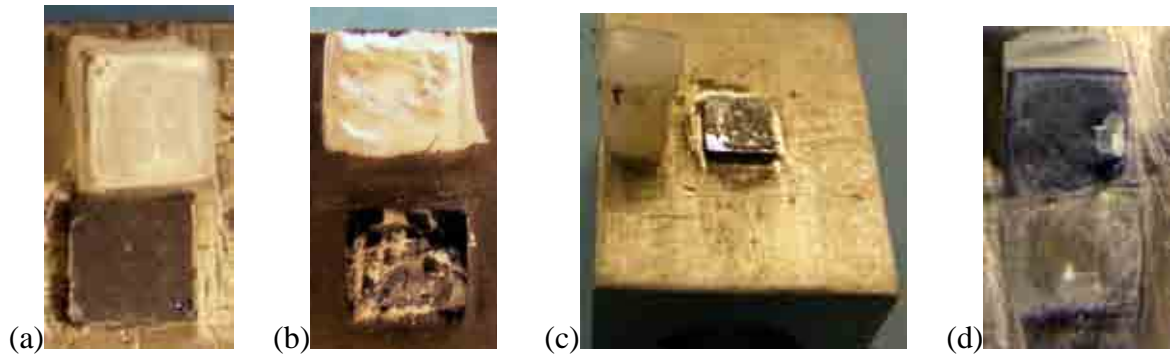
Figure 6.5 The cross-section of the debonded square samples after the pull-off test: (a) smooth even surface, (b) deformed surface with fibrils, (c) deformed surface from the side, (d) debonded superglue.

The debonded surface in the case of the first sample (Figure 6.5a) is similar to the one obtained for the silicon chips with a thermoplastic film tested by Swaminathan et al. (2003) and illustrated in Figure 6.6.
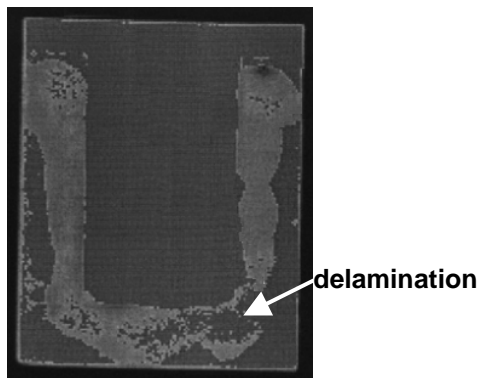
Figure 6.6 The chip with a U-shaped area of thermoplastic film partly delaminated in the debonding process (Swaminathan et al., 2003).

In the cases shown in Figure 6.5b and c, the residue of the adhesive also did not remain on the whole chip surface, however in these samples it had a fibrillar structure. After Zosel (1989) good polymer adhesives can form bridging fibrils between two bonded materials, thus HMA formed a good bond in these samples. In accordance with Andreas & Brian (1991) such cohesive failure, which produces high energy dissipation and thus a high debonding force, and leaves a residue on the substrate surface after peeling, is due to low modulus and strength of adhesive typical for adhesive polyolefin grades (Godfrey, 1998).

The HMA can be to some extent compared with pressure sensitive adhesives (PSA), which have lower Young's modulus and thus are even more ductile as they are based on a modified rubbery material. PSAs differ from HMAs as they adhere without the need of more than a hand pressure and require no activation by water, solvent, or heat (Devries & Adams, 2002).

Figure 6.7 illustrates the tensile pull-off test procedure for PSA.
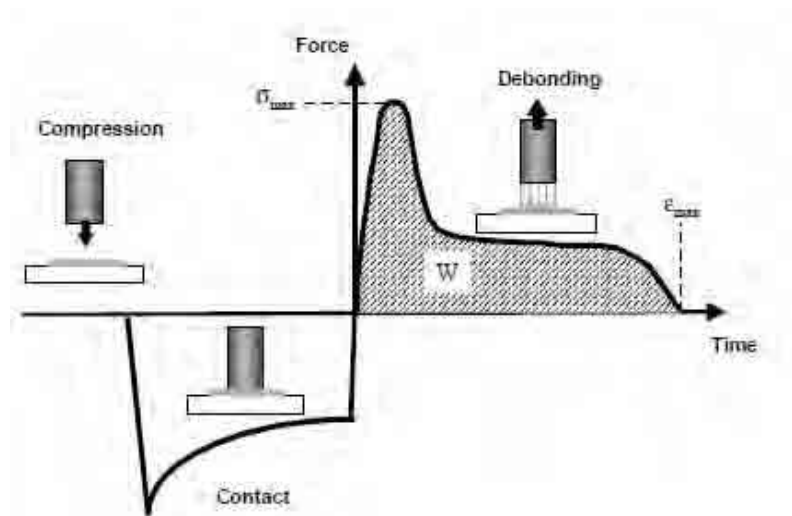
Figure 6.7 Schematic of an adhesion test; W is the work of separation defined as the integral under stress-strain curve, ε_{max} and ε_{max} are the maximum stress and extension, respectively (Creton & Fabre, 2002).

In the case of the procedure used in this project pressure was also applied to the sample during manufacturing process and during bonding of the chip to the metal block with superglue. As illustrated in Figure 6.7 the stress due to compression is relaxed during the initial stage of the test. However, in the current project this could not be quantified but probably contributes to the stress in the initial part of the curve (Figure 6.4).

PSAa have sufficient cohesiveness and elasticity so that they can be removed from smooth surfaces without leaving a residue (Everaerts & Clemens, 2002). Their final rupture often occurs through the formation of fibrillar structure and separation of the two surfaces by failure of the fibrils (cohesive failure when some adhesive remains on both surfaces) or by detachment of the fibrils from the surface (no adhesive left on the probe surface) (Creton &

270

Fabre, 2002; Lakrout et al., 1997). In the case of the HMA test, the residua of the adhesive usually remained on both surfaces and the extension of the adhesive film was much smaller.

Further, the strain rate effect was analysed for a few samples with a thin HMA1 coating pulled at 1mm/min.

6.2.3   Strain rate effect for the HMA

Due to the small gauge length of the samples (approximately 1mm) most tests are carried out at low speed of 0.1mm/min (strain rate $0.1min^{-1}$). In order to analyse the effect of increased speed on the results six samples are tested at 1mm/min, which is a standard speed for Young's modulus measurement in the tensile test recommended in the British Standard (BSI, 1996c). Figure 6.8 presents the data while Table 6.4 lists the numerical values.
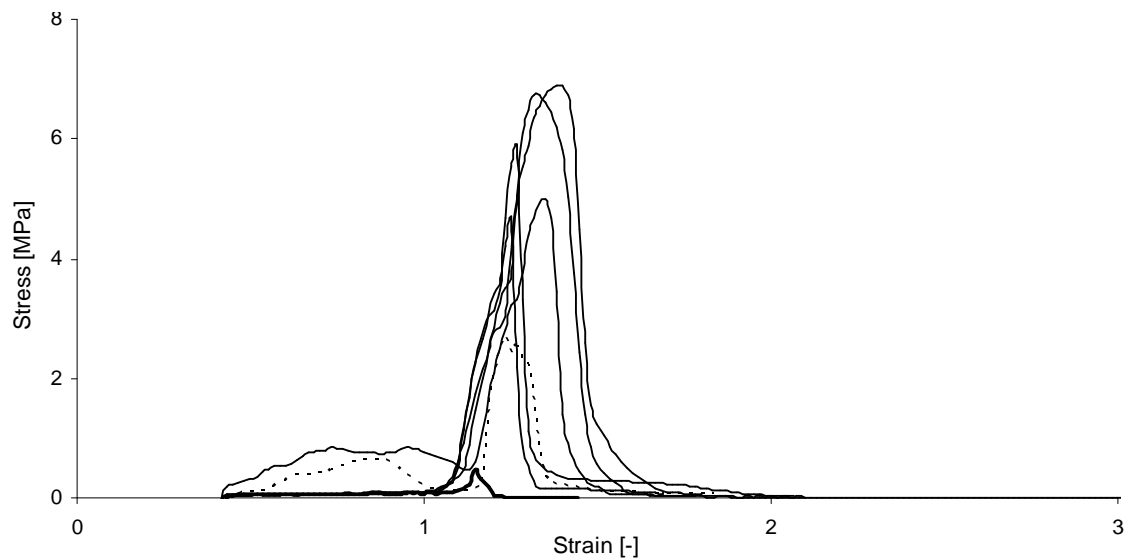
Figure 6.8 Stress-strain curves for the samples with a thin HMA1 layer obtained in a pull-off test carried out at 1mm/min, where: (——) typical sample, (- - -) broken chip (a40), (━) superglue debonded (a38).

Table 6.4 The peak stress values for samples with a thin HMA1 layer tested in a pull-off test carried out at 1mm/min.

Sample	Peak stress MPa
a37	5.1
a38	0.5
a39	6.6
a40	2.7
a41	5.0
a42	5.9
a43	4.6
Average	4.3
SD	2.1

It can be seen that for two samples, a38 and a40, significantly lower peak stress values were obtained, 0.5 and 2.7MPa, respectively. In the case of sample a38 the superglue did not sustain the load and the whole sample debonded from the metal block, while in the case of sample a40 the chip broke and approximately 2/3 of the chip debonded from the metal block as illustrated in Figure 6.9. Therefore, the energy was consumed for debonding only 1/3 of the chip area/sample cross-section and for the chip breakage.

Figure 6.9 The cross-section of the debonded sample with a thin HMA1 layer with the broken chip after the pull-off test carried out at 1mm/min.

The average peak stress, without considering samples a38 and a40 for which something else than the HMA bond strength was measured is 5.4MPa with an SD of 0.8MPa. This gives a value 0.6MPa smaller than that obtained for the nine successful samples tested at 0.1mm/min

(6.0MPa) and a higher repeatability of the results (SD equal to 1.4MPa for the lower speed). However, due to the SD values this difference is insignificant.

Lakrout et al. (1997) who investigated the effect of debonding speed on the peak stress debonding energy of PSA observed other trends as shown in Figure 6.10.
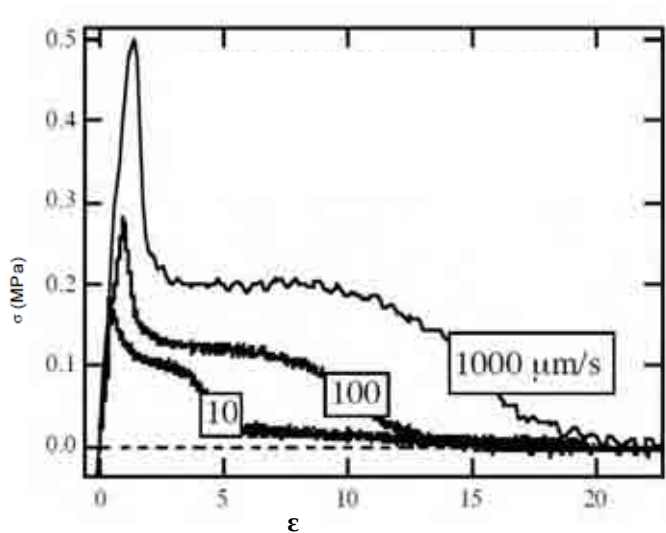
Figure 6.10 Influence of the debonding velocity for PSA (Lakrout et al., 1997).

For higher speeds, higher peak stress, strain at break and separation energy were obtained (Lakrout et al., 1997), which is in accordance with the observations of other researchers (e.g. Zosel, 1985). However, even though in each case the test was carried out in the tensile mode, the materials tested and the test conditions differed.

In the next section the effect of HMA layer thickness is analysed in detail.

6.2.4 Effect of the HMA layer thickness

The effect of HMA thickness is studied for two layer thicknesses and for an extreme case when the HMA serves as a matrix. Among the samples tested only three out of six samples with thick HMA1 layer failed due to a break in the HMA bond, while when the HMA1 served as a matrix each sample failed at the HMA-silicon chip interface. The data are presented in Figures 6.11 and 6.12 while the peak stresses are listed in Tables 6.5 and 6.6.
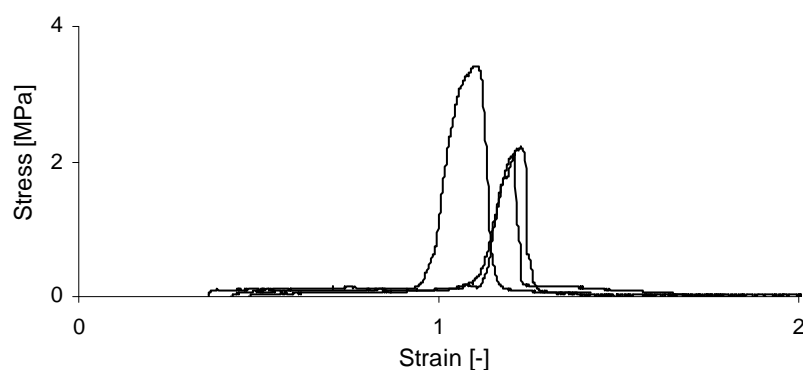
Figure 6.11 Stress-strain curves for the samples with a thick HMA1 layer obtained in a pull-off test.
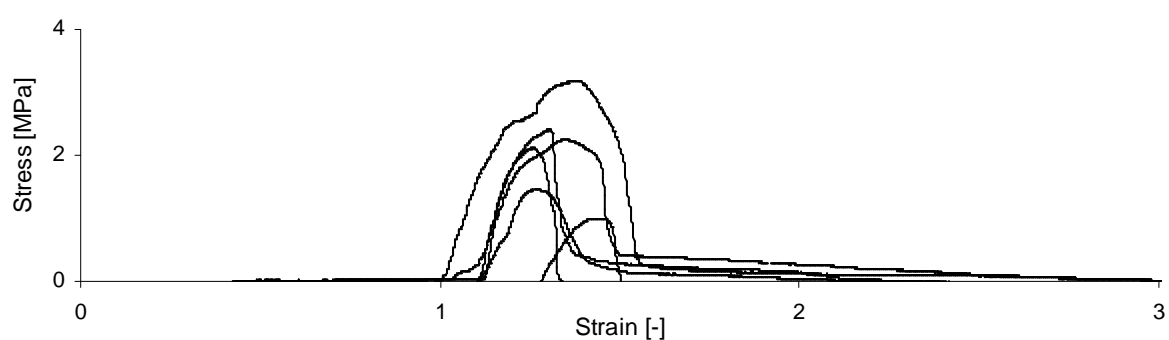
Figure 6.12 Stress-strain curves for the HMA1-silicon chip samples obtained in a pull-off test.

Table 6.5 The peak stress values for samples with a thick HMA1 layer tested in a pull-off test.

Table 6.6 The peak stress values for the HMA1-silicon chip samples tested in a pull-off test.

Sample	Peak stress MPa
a23	3.4
a24	2.2
a26	2.1
Average	2.6
SD	0.7

Sample	Peak stress MPa
a7	1.0
a8	1.5
a9	2.1
a10	2.3
a11	3.2
a12	2.4
Average	2.1
SD	0.8

274

The peak stress was significantly lower for the thick HMA1 layer (2.6MPa in comparison with 6.0MPa obtained for the thin layer), while the lowest value was obtained when the HMA1 served as a matrix (2.1MPa). The reasons for this are better understood by analyzing the broken sample cross-section (Figure 6.13).

Figure 6.13 The cross-section of the debonded sample showing the broken chip after the pull-off test on a HMA1-silicon chip sample.

When comparing Figure 6.5a-c (page 269) and Figure 6.13 it can be seen that in the case of a thin HMA layer between the polyethylene and the silicon chip the debonded surface is rougher with visible fibrils. The extensive plastic deformation contributed to a peak stress (associated with the bond strength) almost three times larger than for the samples where HMA was used as the matrix. In these samples no visible deformation occurred as the matrix and chip surfaces are smooth (no visible fibrils) after failure (Figure 6.13) thus the peak stress was very low.

Until now only the HMA1 was investigated. In the next section two HMAs are compared.

6.2.5   Comparison between two HMAs

In this test series six samples were also tested, however in one case the chip broke and thus this result is not included. Figure 6.14 presents the data for five samples and Table 6.7 lists the peak stress values.
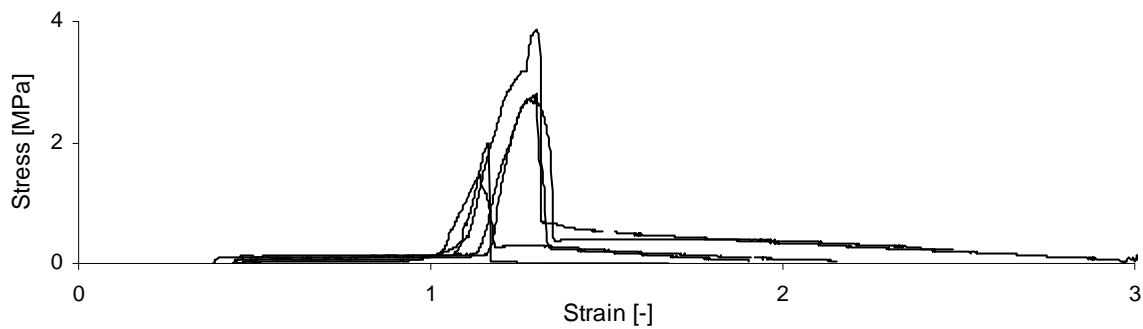
Figure 6.14 Stress-strain curves for the samples with a thin HMA2 layer obtained in a pull-off test.

Table 6.7 The peak stress values for samples with a thin HMA2 layer tested in a pull-off test.

Sample	Peak stress MPa
a7	1.0
a8	1.5
a10	2.3
a11	3.2
a12	2.4
Average	2.1
SD	0.8

From the results (Tables 6.3 and 6.7) it can be seen that the bond formed by the HMA2 is almost three times weaker than the one formed by the HMA1 layer, with the peak stress values being 2.1 and 6.0MPa, respectively. This confirms the statement of the manufacturer of HMAs that the HMA1 contains additives, which lead to its better adherence to polar materials (like silicon) even though the character of the bond is similar for both adhesives as they are based on the same chemistry (LLDPE with maleic anhydride) (Chiche, 2010).

The low peak stress value for the HMA2 might also be partly a result of different dispersions of both HMAs, which might remain more concentrated in the case of the HMA2. As noticed

during production of the tensile samples the HMA2 does not remelt easily and thus might disperse less extensively within the HDPE matrix.

Table 6.8 summarises the results of the pull-off test on the square samples.

Table 6.8 Key results of the direct pull-off adhesion test on the basis of the successful samples tested.

Sample	Number of successful samples tested	Peak stress MPa	
		Average	SD
HMA1 thin	9	6.0	1.4
HMA1 thin (1mm/min*)	5	5.4	0.8
HMA1 thick	3	2.6	0.7
HMA1 as a matrix	6	2.1	0.8
HMA2 thin	5	2.1	0.8

*Note: the speed of testing for other samples was 0.1mm/min.

The data show that the thin HMA1 layer is the most effective adhesive, three times stronger than thicker layer of this adhesive or HMA2.

Further, the indirect adhesion tests (tensile and bending) were carried out and their results are analysed in the next sections.

6.3 Indirect adhesion test – tension

In this section the effect of different coatings on the tensile behaviour of pipe-grade HDPE with SC chips at the orientation 0/90 is investigated. In the tests two types of HMAs, the photoresist and the Teflon coatings were used.

First, the tensile properties of HMAs were determined for the plain and SC/0/90 samples where the HMA was the matrix.

6.3.1 Properties of different polyethylene grades with and without a chip

The properties of the plastics samples with and without a chip were compared for two HMAs and pipe-grade HDPE. Figures 6.15 and 6.16 present the stress-strain curves and Table 6.17 lists the key numerical data for the samples with and without a chip based on different matrix materials, while Tables 6.9-6.14 list the data for both HMAs and HDPE samples with and without chips. In the case of HMA2 the delamination of some samples occurred and these are marked as HMA2-delam in graphs and underlined in the tables. The '+' next to the strain at break value means that some samples (on which the average value is based) did not break within the instrument range and the last recorded values were considered in the calculation. An example of delamination was illustrated in Figure 4.10 (page 104).
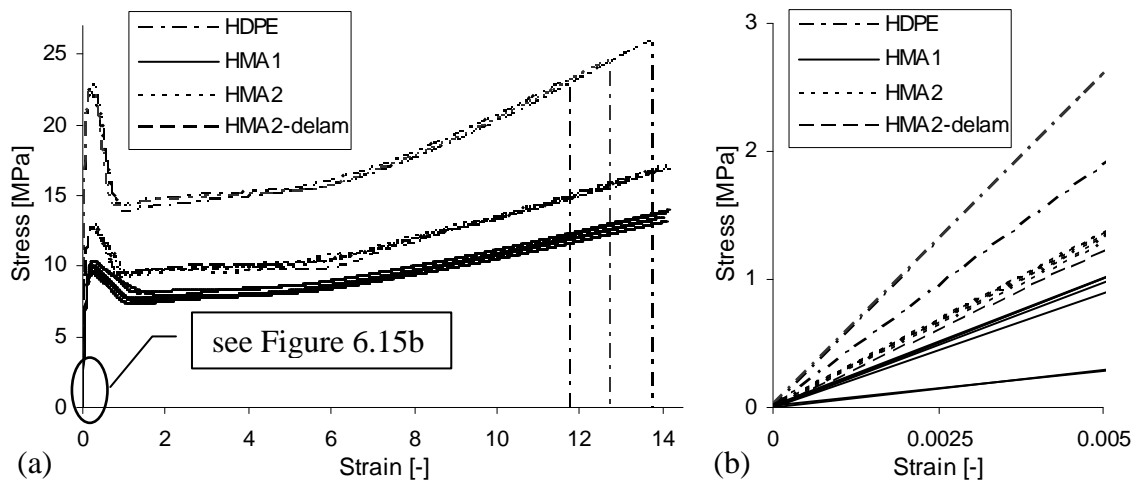
Figure 6.15 (a) Stress-strain curves for plain HMA1 and HMA2 samples and selected HDPE samples, (b) enlarged elastic region of (a).

278
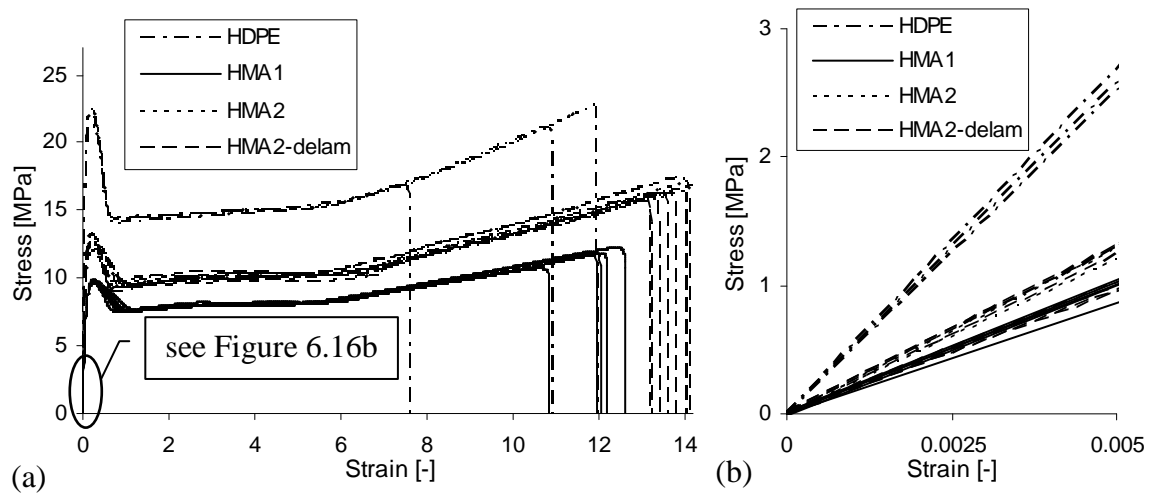
Figure 6.16 (a) Stress-strain curves for the HMA1 and HMA2 samples and selected HDPE samples with chip (SC/0/90), (b) enlarged elastic region.

Table 6.9 Tensile values for the plain HMA1 samples.

Sample	Young's modulus MPa	Yield stress MPa	Strain at break
t191	117	10.4	14.1+
t192	126	10.4	14.1+
t193	175	9.4	14.1+
t194	174	9.6	14.1+
t195	177	9.9	13.8+
t224	172	9.9	14.0+
t225	173	10.1	14.1+
Average	159	10.0	14.0+
SD	26	0.4	0.1

Table 6.10 Tensile values for the SC/0/90 HMA1 samples.

Sample	Young's modulus MPa	Yield stress MPa	Strain at break
t196	202	9.7	12.6
t197	205	9.6	12.0
t198	198	9.7	10.8
t199	205	9.7	12.2
t200	173	9.9	12.0
Average	197	9.7	11.9
SD	14	0.1	0.7

Table 6.11 Tensile values for the plain HMA2 samples.

Sample	Young's modulus MPa	Yield stress MPa	Strain at break
t201	272	12.7	14.2+
t202	265	12.9	14.1+
t203	273	12.7	14.1+
t204	257	13.1	14.0+
t205	248	13.4	14.0+
t226	264	12.5	14.3+
t227	245	12.7	14.0+
t228	255	12.7	14.1+
Average	258	12.8	14.1+
SD	10	0.3	0.1

Table 6.12 Tensile values for the SC/0/90 HMA2 samples.

Sample	Young's modulus MPa	Yield stress MPa	Strain at break
t206	259	13.3	13.2
t207	202	12.7	14.2+
t208	196	12.6	13.4
t209	190	13.1	14.1
t211	257	12.6	14.1
t212	256	12.7	13.9+
t213	241	12.7	13.9+
t214	196	12.0	14.0
t229	247	12.5	13.8
t231	260	12.6	13.2
Average	231	12.7	13.8+
SD	30	0.4	0.4

Table 6.13 The average tensile values with SDs obtained for the plain HDPE samples.

Sample	Young's modulus MPa	Yield stress MPa	Strain at break
Average	476	22.5	12.8
SD	50	0.2	0.7

Table 6.14 The average tensile values with SDs obtained for the SC/0/90 HDPE samples.

	Young's modulus MPa	Yield stress MPa	Strain at break
Average	523	22.2	10.7
SD	9	0.3	1.2

It can be concluded that both the HMAs are much more ductile than the HDPE, which is associated with their molecular structures resulting in lower crystallinities and densities (given and discussed in section 3.3.5). Many plain HMA samples reach strain at break values that are larger than are measurable by the instrument. Similar behaviour is observed in the HMA2 samples with a chip and is assigned to the potential delamination of the samples caused by the method of production (remelting of two sheets with chips in between), as explained in 4.3.3.2. In order to possibly eliminate the delamination effect the temperature to which the polymer is

heated during sample manufacture was increased from 190 to 210ºC. The plots are shown in Figures 6.17 and 6.18. Tables 6.11 and 6.12 listed the tensile values for 190°C and Tables 6.15 and 6.16 list the tensile values for 210°C.
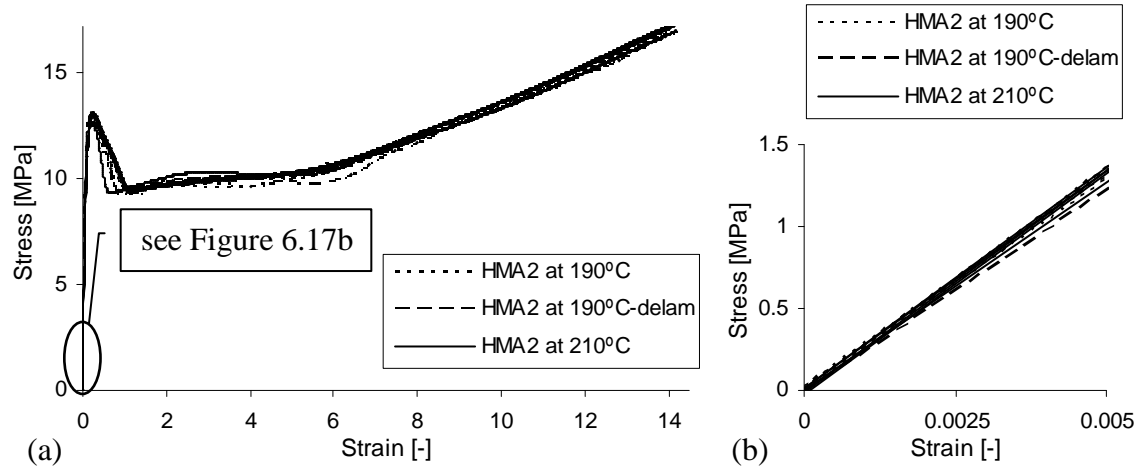
Figure 6.17 (a) Stress-strain curves for the plain HMA2 samples heated up to 190 and 210ºC during compression moulding, (b) enlarged elastic region.
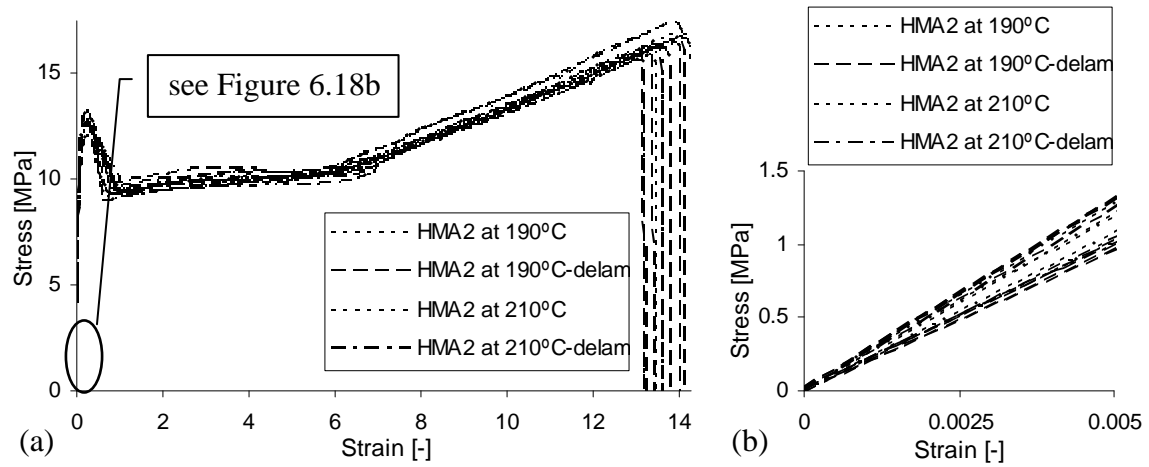
Figure 6.18 (a) Stress-strain curves for the SC/0/90 HMA2 samples heated up to 190 and 210ºC during compression moulding, (b) enlarged elastic region.

281

Table 6.15 Tensile values for the plain HMA2 samples heated up to 210ºC during compression moulding.

Sample	Young's modulus MPa	Yield stress MPa	Strain at break
t339	267	13.1	14.0+
t340	269	13.0	14.0+
t341	268	13.0	14.3+
t342	255	12.7	14.1+
t343	269	13.6	14.1+
Average	266	13.1	14.1+
SD	6	0.3	0.1

Table 6.16 Tensile values for the SC/0/90 HMA2 samples heated up to 210ºC during compression moulding.

Sample	Young's modulus MPa	Yield stress MPa	Strain at break
t322	238	12.8	13.5
t323	216	12.7	13.6
t324	209	12.5	14.0+
t325	197	12.0	14.3+
t326	203	12.7	13.2
Average	213	12.6	13.7+
SD	16	0.3	0.4

The delamination did not occur in the plain samples produced at higher temperature (Figure 6.17), but was still observed in the SC/0/90 samples (Figure 6.18). Further increases in temperature and pressure might improve it this situation, however if the temperature is too high, this accelerates the polymer degradation (Peacock, 2000).

Table 6.17 lists the key numerical values for the HDPE and HMA samples.

Table 6.17 Key tensile values for the plain and SC/0/90 polyethylene samples made of different grades.

Sample	Young's modulus MPa		Yield stress MPa		Strain at break	
	Average	SD	Average	SD	Average	SD
plain						
HDPE	476	50	22.5	0.2	12.8	0.7
HMA1	159	26	10.0	0.4	14.0+	0.1
HMA2	258	10	12.8	0.3	14.1+	0.1
HMA2 (210°C)	266	6	13.1	0.3	14.1+	0.1
SC/0/90						
HDPE	523	9	22.2	0.3	10.7	1.2
HMA1	197	14	9.7	0.1	11.9	0.7
HMA2	231	30	12.7	0.4	13.8+	0.4
HMA2 (210°C)	213	16	12.6	0.3	13.7+	0.4

The densities of the HMA2 samples produced under different temperature did not differ (section 4.3.2.5, page 99) and so do the tensile properties. The reason for it might also be poor adhesion between the chip and the matrix compared to the HMA1 as indicated in section 6.2.5 (page 275).

The HMA1 and HDPE with a chip reach significantly smaller strains at break than the plain samples. The Young's modulus and yield stress of the HDPE are the highest. The next much lower values are obtained for the HMA2 even though it seems to be more ductile (higher strain at break) than the HMA1, which reaches the smallest tensile values.

The chip causes a reduction in strain at break and yield stress of all samples, while in the HDPE and HMA1 it improves the Young's modulus, thus has a reinforcing effect. However, in the HDPE samples the difference between the samples with and without a chip is within the SD, thus insignificant. The other research on this topic has already been discussed in section 5.2.3, where the chip effect for the HDPE was analysed.

As for the HMA2, higher Young's modulus and peak stress values were observed while the peak stress in the pull-off test was significantly lower for this coating (2.1MPa) as compared with HMA1 (6.0MPa), this suggests that the peak stress value is only partly related to the modulus of the matrix and the coating and reflects mostly the strength of the bond.

The profiles of the samples during the tensile test differed thus are illustrated in Figure 6.20 and characteristic stages marked in Figure 6.19.
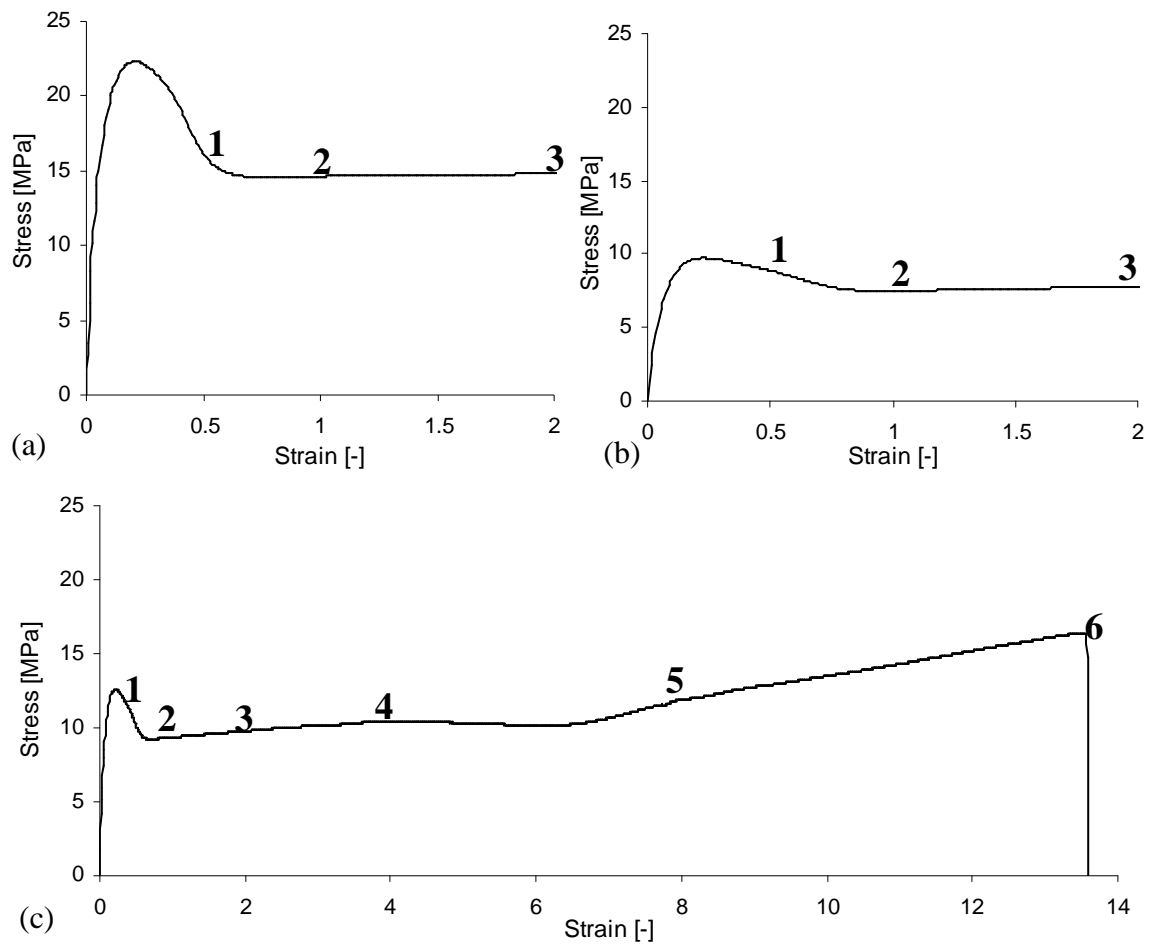
Figure 6.19 Stress-strain curves for the SC/0/90 (a) HMA1, (b) HDPE and (c) HMA2 samples with initial stages marked and shown in the photographs in Figure 6.20.
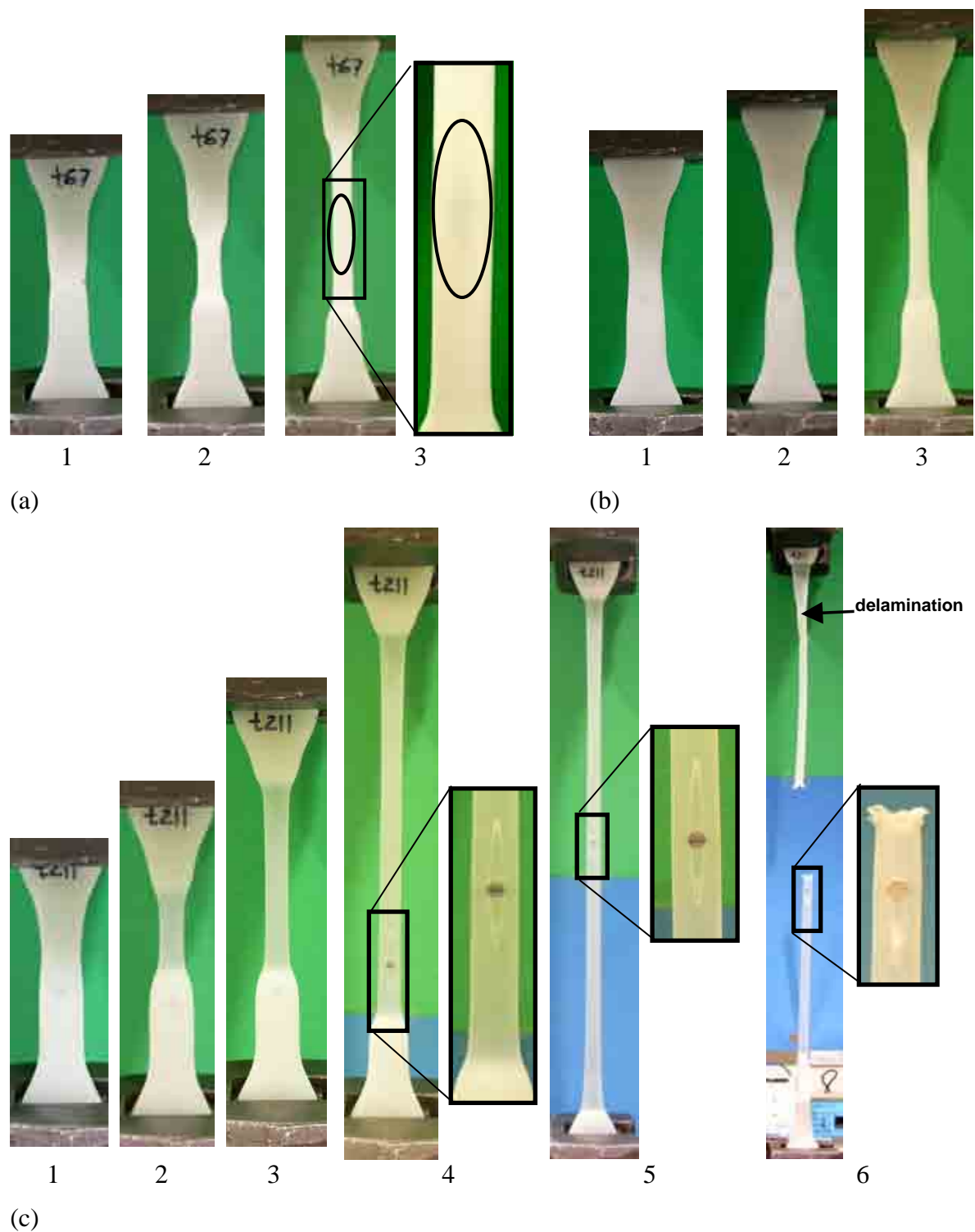
Figure 6.20 Profiles of the SC/0/90 (a) HDPE, (b) HMA1 and (c) HMA2 samples during characteristic stages (see Figure 6.19) of the tensile test. Note: the crack around the chip in (b) marked by the ellipse.

Due to the transparency of the stretched HMA2 sample, the shape of the crack can be seen

and it is similar to the crack observed for the SC/surf HDPE sample (Figure 5.21, page 178).

The performance of both HMA samples with a chip is similar. The neck forms initially above the chip location, but as the neck extends it eventually encompasses the chip. Ultimately, both samples break at the crack tip which develops around the chip as can be clearly seen in Figure 6.20c for HMA2. In the case of HMA2 the neck is slightly sharper, which is reflected in the slightly steeper curve after the yield stress (see Figure 6.16). In the HDPE sample the neck develops in the vicinity of the chip (Figure 6.20b), which causes a stress concentration, and the neck is sharpest and the slope is steepest in comparison with other samples (Figure 6.16).

The fact that the neck does not start in the vicinity of the chip in HMA samples suggests good adhesion between the chip and the matrix. In addition the HMAs are more ductile than HDPE. In consequence, the stress concentration around the chip is smaller than in the HDPE sample. Debonding can contribute to the formation of voids and stress concentrations especially in brittle polymers. Bramuzzo et al. (1985) observed that in the case of mica in PP composite, debonding usually leads to microductility ahead of the crack tip. The matrix stretches and work hardens as it separates from the filler (Friedrich & Karsch, 1981). The adhesion between the filler and matrix can affect the micro mechanism of plastic deformation (drawing) of the matrix (Vu-Khanh & Fisa, 1986). When comparing the HMA1 and HDPE samples it can be seen that in both cases (adhesion and lack of adhesion between the filler and the matrix, respectively) the chip reduced the ductility of the samples.

Once the bonding and tensile properties of both HMAs are known, the HMAs as well as other materials such as Teflon and photoresist as the coatings of silicon chips embedded within polyethylene matrix are analysed.

6.3.2 Effect of different coatings on the polyethylene samples with a chip

First, it is important to determine how the coatings affect the HDPE matrix, thus the plain HDPE samples are compared with the samples with HMA coating (without a chip) on the surface. Then the samples with a coated chip on the surface are analysed for both HMAs and two coating thicknesses. Further, the same is investigated for the samples with a chip inside (SC/0/90) where in addition, the Teflon and photoresist as a coating were studied.

6.3.2.1 Effect of the coating on the surface

Figure 6.21 presents the results for selected plain HDPE samples and the samples with a HMA1 on the surface in the form of small a circle and Table 6.18 lists the numerical values. The thickness and diameter of the coating are comparable with the dimensions of the coating surrounding the chip in further tests (see section 4.3.6.2, page 120).
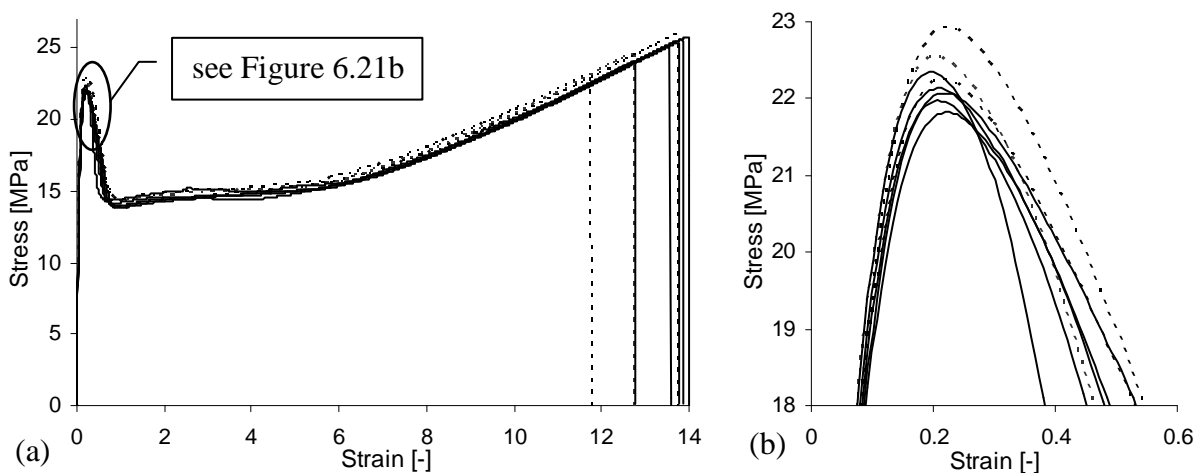
Figure 6.21 (a) Stress-strain curves for (- - -) the selected plain HDPE samples and (——) the samples with HMA1 coating (in the form of a small circle) on the surface, (b) enlarged peak stress region.

Table 6.18 Tensile values for the HDPE samples with a HMA1 coating (in the form of a small circle) on the surface.

Sample	Young's modulus MPa	Yield stress MPa	Strain at break
t161	461	22.2	13.6
t162	487	21.8	13.6
t163	521	22.1	13.8
t164	495	22.1	13.8
t365	530	22.3	12.8
Average	499	22.1	13.5
SD	27	0.2	0.4

Table 6.19 The average tensile values with SDs for the plain HDPE samples.

	Young's modulus, MPa	Yield stress, MPa	Strain at break
Average	476	22.5	12.8
SD	50	0.2	0.7

The Young's moduli for both types of samples are similar and the difference between them is insignificant. The yield stress is slightly lower for all but one sample with a HMA1 coating on the surface and the strain at break is in a higher range for these samples, which suggests their higher ductility. This is probably due to higher ductility (associated with lower crystallinity) of HMA1 than HDPE (section 3.3.5, page 82).

6.3.2.2 Effect of the coating on the SC/surf samples

Further, the samples with a coated chip placed on the surface are investigated for two thicknesses of the HMA1 coating (thin: 0.26mm, and thick: 0.60mm) and a thin HMA2 coating (0.23mm). The plots are presented in Figures 6.22 and 6.23 and compared with the samples with non-coated chips. Tables 6.20-6.22 list the tensile data for the SC/surf samples with different coatings, which are summarised in Table 6.23 including non-coated samples.
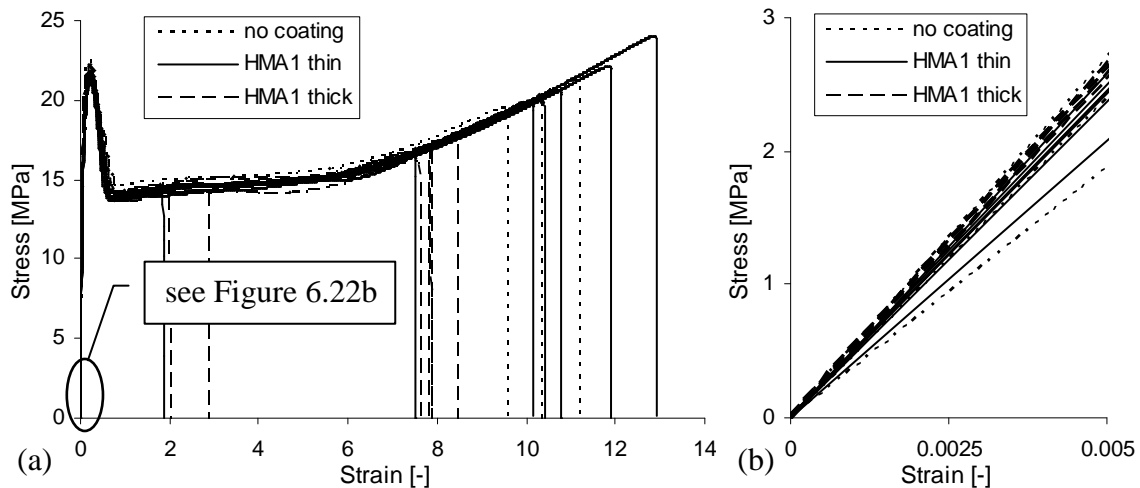
Figure 6.22 (a) Stress-strain curves for the SC/surf samples with the chip coated with thin and thick HMA1 layers and selected samples without coating, (b) enlarged elastic region.
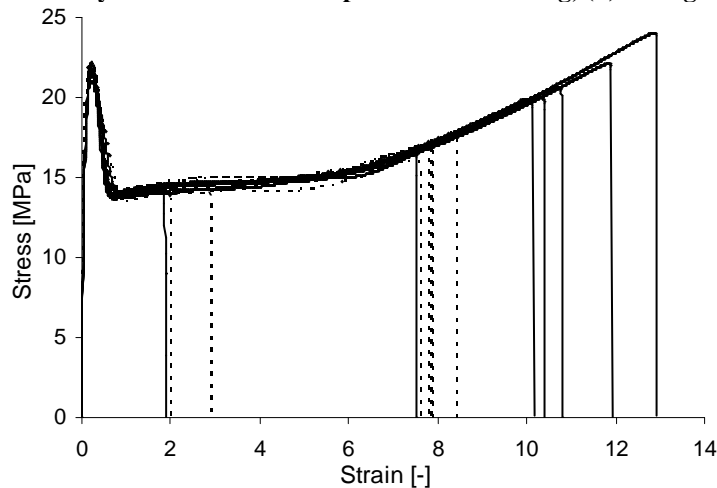
Figure 6.23 Stress-strain curves for the samples with an SC chip on the surface coated with thin (——) HMA1 and (- - -) HMA2 layers.

Table 6.20 Tensile values for the SC/surf samples with a thin HMA1 coating.

Sample	Young's modulus MPa	Yield stress MPa	Strain at break
t174	414	22.2	11.9
t175	487	21.4	10.4
t176	520	22.2	10.8
t177	474	21.2	10.2
t178	485	21.0	12.9
t232	490	21.8	1.9
t233	498	21.8	7.5
Average	481	21.7	9.4
SD	33	0.5	3.7

Table 6.21 Tensile values for SC/surf samples with a thick HMA1 coating.

Sample	Young's modulus MPa	Yield stress MPa	Strain at break
t280	521	21.8	7.9
t281	507	21.3	7.6
t282	527	22.2	8.4
t283	526	21.9	7.8
t284	515	21.8	2.0
t317	519	21.8	2.9
t318	527	22.1	7.9
Average	520	21.8	6.4
SD	7	0.3	2.7

289

Table 6.22 Tensile values for the SC/surf samples with a thin HMA2 coating.

Sample	Young's modulus MPa	Yield stress MPa	Strain at break
t183	524	22.1	6.8
t184	390	21.9	6.9
t185	352	22.5	2.0
t186	486	21.3	8.8
t234	497	22.1	6.7
t235	499	21.7	8.1
t236	493	21.9	9.4
Average	463	21.9	7.0
SD	65	0.4	2.4

Table 6.23 Key tensile values for the SC/surf samples with a coated and non-coated chip.

Coating	Young's modulus MPa		Yield stress MPa		Strain at break	
	Average	SD	Average	SD	Average	SD
non-coated	449	70	21.6	0.5	10.5	0.6
HMA1 thin	481	33	21.7	0.5	9.4	3.7
HMA1 thick	520	7	21.8	0.3	6.4	2.7
HMA2 thin	463	65	21.9	0.4	7.0	2.4

The shapes of all curves are very similar as they are based on the same matrix. In general, it can be concluded that for the SC chip orientation on the surface, the HMA coating only marginally improves the tensile strength (Young's modulus and yield stress) of the samples and this effect is most significant for a thick HMA1 layer. The improvement in the reinforcing effect by the coatings might be reduced due to the fact that the coating itself has lower Young's modulus (Table 6.17). However, the strain at break, and thus ductility of the samples are significantly reduced due to the coating even though the coating itself is more ductile. This effect is greatest in the case of a thick HMA1 and thin HMA2 coatings. However, it has

to be noted that the differences are within maximum SDs being 65MPa for Young's modulus, 0.5 MPa for yield stress and 3.7 for strain at break, thus might be due to variations of the matrix. Non-uniform spreading of the coating around the chip might also have an influence on large spread in the results in some cases, however this could be not verified here. Therefore no certain conclusions can be drawn on the basis of available data.

Other researchers also observed that improved interfacial adhesion increases the reinforcing effect of the composite increasing the tensile modulus (Marshal et al., 1985, Shucai et al., 1996 and Majeed, 2001). Regarding the impact of the adhesion on the ductility Beaumont & Philips (1972) stated that debonding reduces the strain at break while here the highest value was recorded for non-coated chips – no adhesion between the chip and the matrix, which is in contrast to current observations. However, the test conditions and materials tested differed, thus cannot be directly compared. In this project the coating made relatively large volume of the sample and thus might have influenced the integrity of the material. In addition, all researchers considered the chip inside the matrix, while here it was located on the sample surface.

The profiles of the samples with coated chip on the surface were very similar to the samples with non-coated chip (Figure 5.21, page 178). However, in the case of a thick HMA1 layer the crack propagation mechanism slightly differed.
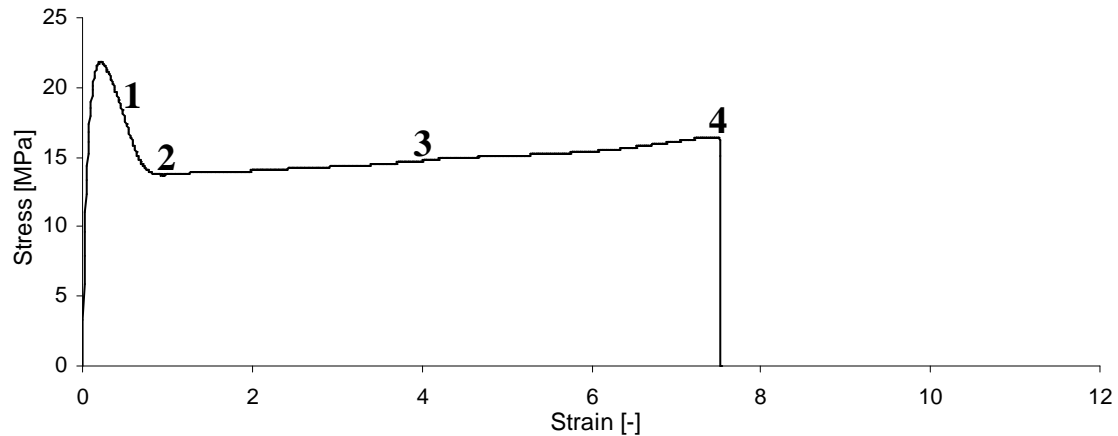
Figure 6.24 Stress-strain curve for the SC/surf sample with a chip coated with a thick HMA1 layer with characteristic stages marked and shown in the photographs in Figure 6.25.

| 3 | 5 | 8 | 10 |
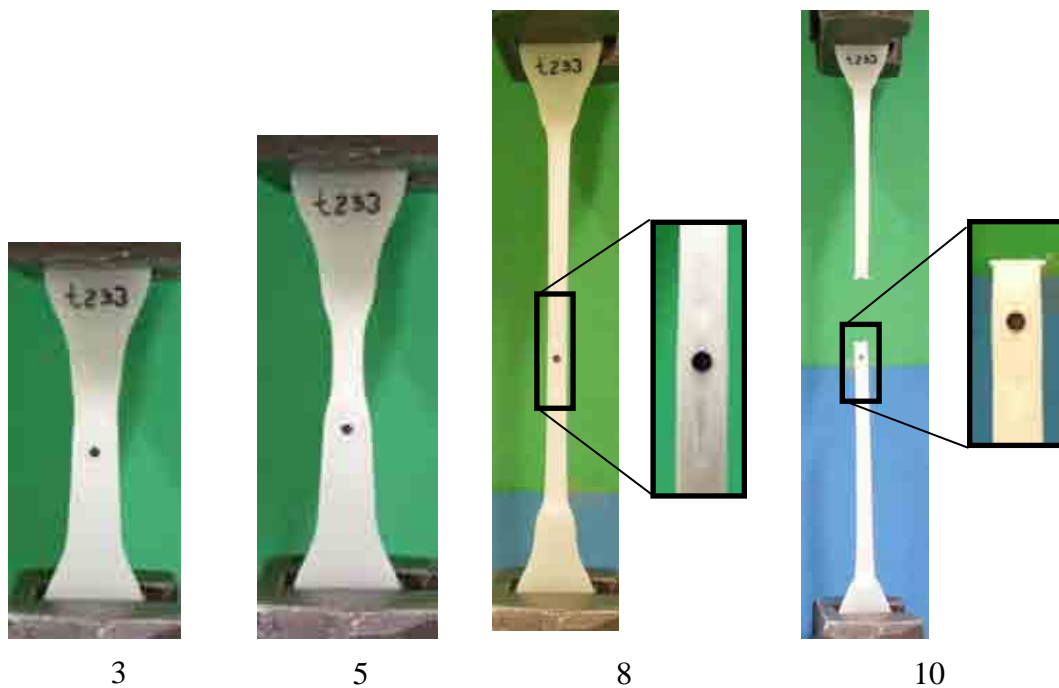
Figure 6.25 Profiles of the SC/surf sample with a thick HMA1 chip coating during characteristic stages (see Figure 6.24) of the tensile test.

The neck started above the chip location, which means that the adhesion between the chip and the matrix contributed to the reduction in the stress concentration around the chip. The HMA increases the discontinuity of the matrix favouring formation of larger cracks. The crack tip expands quicker leading to sample failure at a low strain of approximately 7.5.

As the improved in the reinforcing effect of a chip by the coating is very small while the reduction in ductility is very significant especially in the case of thick layer of the coating,

thus overall mechanical performance is best for the samples with non-coated chip on the surface. Further, the effect of the coatings on the chip embedded within HDPE is investigated.

6.3.2.3 Effect of the coating on the SC/0/90 samples

The samples with a coated chip placed on the surface are investigated for two thicknesses of the HMA1 coating (thin: 0.27mm, and thick: 0.42mm), a thin HMA2 coating (0.27mm), Teflon (0.03mm) and photoresist (0.018mm). The plots are presented in Figures 6.26-6.28 and compared with the samples with non-coated chips. Tables 6.24-6.28 list the tensile data for the SC/0/90 samples with different coatings, which are summarised in Table 6.29 including non-coated samples.
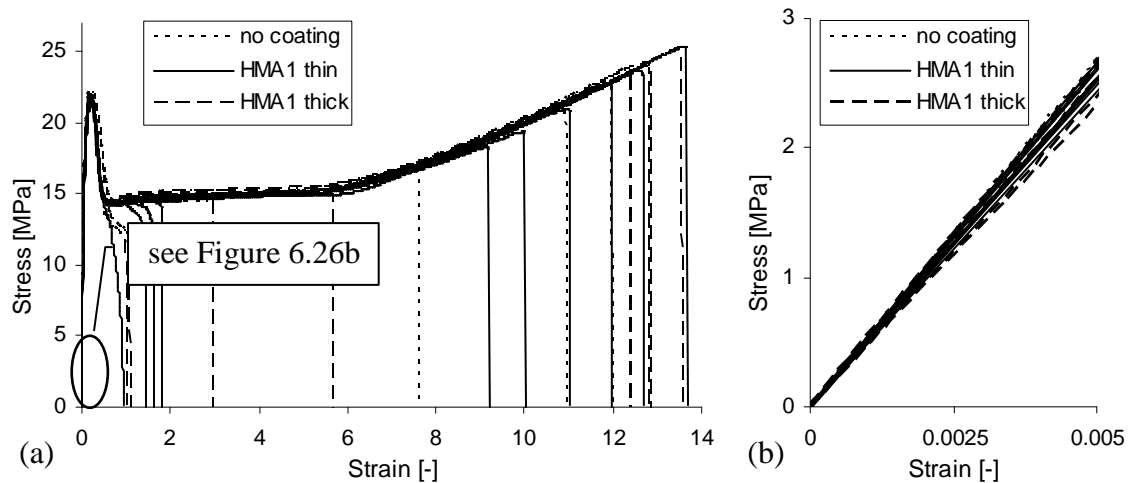
Figure 6.26 (a) Stress-strain curves for the samples with a chip inside (SC/0/90) coated with thin and thick HMA1 layers and selected SC/0/90 samples without coating, (b) enlarged elastic region.
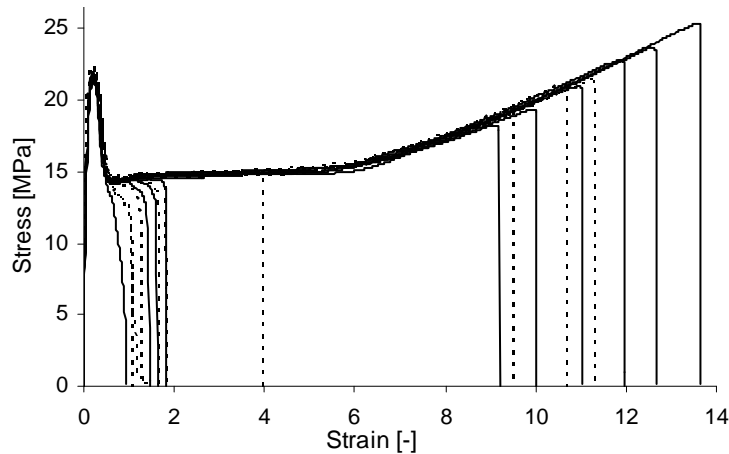
Figure 6.27 Stress-strain curves for the samples with a chip inside (SC/0/90) coated with thin (——) HMA1 and (- - -) HMA2 layers.
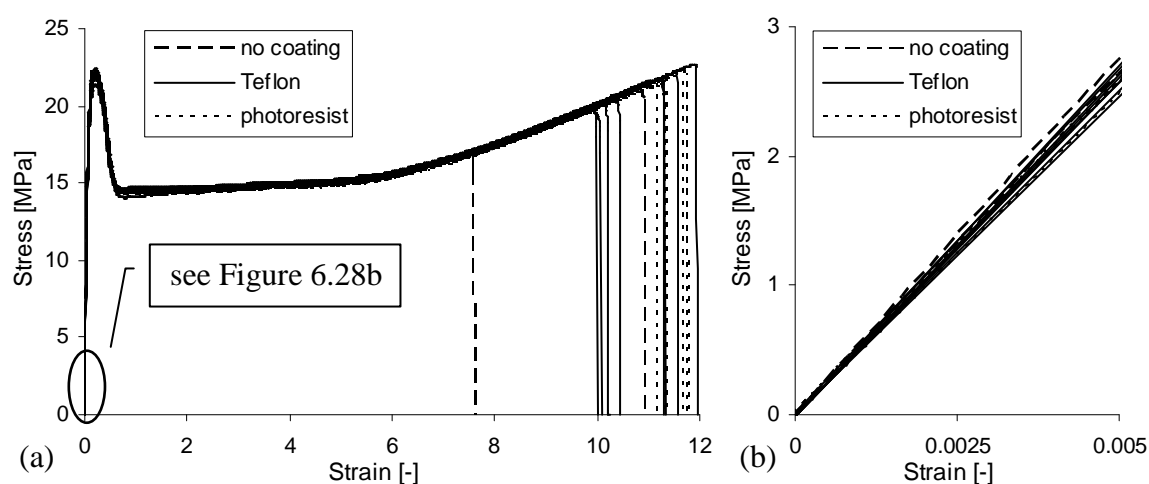
Figure 6.28 (a) Stress-strain curves for the samples with a chip inside (SC/0/90) coated with Teflon and photoresist and selected SC/0/90 samples without coating, (b) enlarged elastic region.

Table 6.24 Tensile values for the samples with a chip inside (SC/0/90) coated with a thin HMA1 layer.

Sample	Young's modulus MPa	Yield stress MPa	Strain at break
t156	533	21.8	0.9
t157	519	21.7	10.0
t158	509	21.8	1.8
t159	506	21.7	1.5
t179	494	21.4	12.7
t180	507	21.9	13.7
t182	506	21.7	1.6
t240	529	22.0	11.0
t241	522	21.8	9.2
t344	486	21.3	12.0
Average	511	21.7	7.4
SD	15	0.2	5.3

Table 6.25 Tensile values for the samples with a chip inside (SC/0/90) coated with a thick HMA1 layer.

Sample	Young's modulus MPa	Yield stress MPa	Strain at break
t259	521	21.7	12.4
t260	527	21.9	12.8
t261	528	21.9	12.8
t315	528	21.7	2.9
t316	521	21.8	5.6
t319	506	21.5	1.0
t320	482	21.6	1.1
t321	464	21.6	13.5
Average	510	21.7	7.8
SD	24	0.2	5.7

Table 6.26 Tensile values for the samples with a chip inside (SC/0/90) coated with a thin HMA2 layer.

Sample	Young's modulus MPa	Yield stress MPa	Strain at break
t275	538	22.2	9.5
t276	534	22.4	1.8
t277	526	22.3	1.1
t278	518	21.9	1.6
t279	508	21.8	11.3
t301	509	21.4	10.7
t302	538	22.2	1.3
t303	502	21.7	1.4
t304	507	21.5	4.0
Average	520	21.9	4.7
SD	14	0.4	4.4

Table 6.27 Tensile values for the samples with a chip inside (SC/0/90) coated with Teflon.

Sample	Young's modulus MPa	Yield stress MPa	Strain at break
t290	528	22.0	10.0
t291	531	22.1	10.4
t292	524	22.3	10.2
t293	542	22.4	11.3
t294	518	21.9	10.1
t346	501	21.8	11.3
t348	491	22.0	11.6
Average	519	22.1	10.7
SD	18	0.2	0.7

Table 6.28 Tensile values for the samples with a chip inside (SC/0/90) coated with photoresist.

Sample	Young's modulus MPa	Yield stress MPa	Strain at break
t270	518	21.9	11.1
t271	514	21.5	11.3
t272	519	21.4	11.3
t273	510	21.7	11.6
t300	514	22.1	11.8
t347	499	21.9	11.7
Average	512	21.8	11.5
SD	7	0.3	0.3

Table 6.29 Key tensile values for the polyethylene samples with and without a coated and non-coated chip.

Coating	Young's modulus MPa		Yield stress MPa		Strain at break	
	Average	SD	Average	SD	Average	SD
non-coated	523	9	22.2	0.3	10.7	1.2
HMA1 thin	511	15	21.7	0.2	7.4	5.3
HMA1 thick	510	24	21.7	0.2	7.8	5.7
HMA2 thin	520	14	21.9	0.4	4.7	4.4
Teflon	519	18	22.1	0.2	10.7	0.7
photoresist	512	7	21.8	0.3	11.5	0.3

The thickness of the HMA1 layer does not have any significant influence on the performance of the samples. When comparing different coatings the Young's modulus values are very close for all the samples while the yield stress is slightly reduced especially when the HMA1 coating is used. The reduction in yield stress in the case of HMAs could be due to lower stiffness of these coating materials (see Table 6.17, page 282), while in the case of the photoresist the lower value is associated with a higher strain at break, thus might be due lower crystallinity of the matrix. Even though the photoresist slightly sticks to the silicon chip it should not bind to non-polar HDPE matrix and its layer is very thin (0.018mm), thus its influence should be insignificant. For the Teflon coating the values are very close to the values obtained for non-coated samples. This result is as expected as the Teflon does not stick to silicon or HDPE matrix and its layer is also very thin (0.03mm) thus it has no influence on the adhesion.

The HMAs caused a significant reduction in the ductility. This suggests that the HMA causes a discontinuity in the HDPE matrix and this weakens its strength and reduces ductility. This effect was most significant for the HMA2 coating, which forms three times weaker bonding

between the chip and the HDPE matrix as indicated in section 6.2.5, page 275. The HMA coating caused also embrittlement when the chip was located on the sample surface, however, then it simultaneously improved the Young's modulus and yield, whereas in the case of chip inside the sample it seems to slightly reduce these parameters. The HMA2 had less detrimental effect on the SC/surf samples as the strain at break reduced to 7.0 (9.4 and 6.4 for thin and thick HMA1 layers). It can be concluded that the chip coating for the positions investigated inside the sample and for particular coating thicknesses is not beneficial in terms of improving the tensile properties of the composite.

The profiles of the samples with a HMA coated chip during a tensile test were very similar to the sample with a non-coated chip illustrated in Figure 5.11 (page 164), thus the pictures are not included here. The only difference was that the final failure did not occur at the crack tip when the HMA1 coating was used even though it occurred when the HMA2 was used or when the HMA1 served as a matrix. Thus, it is assigned to the bond between the chip and HMA, which is better when the HMA1 is used and when the adhesive serves only as an interlayer between the chip and HDPE instead of being the matrix itself as indicated in the pull-off test (section 6.2.4, page 273).

The specimen profiles during the tensile of the samples with Teflon and photoresist coating were also similar to the non-coated SC/0/90 sample, however the failure pattern of some samples with Teflon coating differed and is illustrated in Figure 6.29.

The sample with a Teflon coating breaks also at the crack tip, however in a different manner. Initially the top layer of the HDPE matrix debonds from the bottom layer at the upper crack tip, then it delaminates from above the crack area and the final break of the sample occurs at the bottom crack tip. This might be explained by the fact that the Teflon coating does not adhere to anything (section 3.1.5, page 67) and it might spread around the chip during sample production, and cause poor adhesion between the two remelted sheets in the vicinity of the chip. However, as the neck originates at the chip it suggests that the chip is clamped tight enough within the HDPE matrix to cause stress concentration leading to the neck formation.
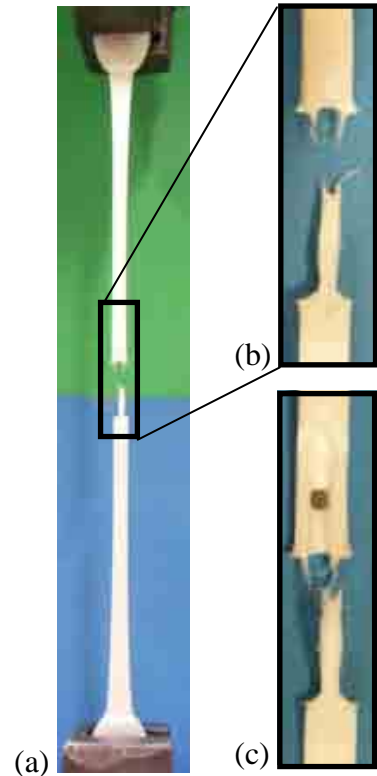
Figure 6.29 (a) Specimen profile at failure in the tensile test of the sample with a chip inside (SC/0/90) coated with Teflon, (b) enlarger broken section, (c) enlarger broken section from the other side.

In the next section, the adhesion between the polyethylene matrix and the silicon chip is investigated in bending.

6.4 Indirect adhesion test – bending

In this section the effect of a coating on the flexural behaviour of pipe-grade HDPE with a chip is studied. As the results of the bending tests on the samples with and without a chip indicated, there are no significant detectable differences between flexural moduli and peak

stresses of different types of samples (section 5.3.9, page 248). Therefore, no significant differences in flexural properties are expected either and the influence of the HMA coating on the material and its performance in bending was only studied for one adhesive (HMA1), one chip (LC), and two orientations (surf and 0/90). All the samples presented in this section were intentionally made from the same polyethylene sheet in order to eliminate the differences associated with potential variations in matrix properties due to variable manufacturing conditions.

Figure 6.30 shows the average plots for the samples with and without a chip at the orientation on the surface and 0/90 with a thin HMA layer between the chip and the matrix. Tables 6.30-6.32 list the flexural values.
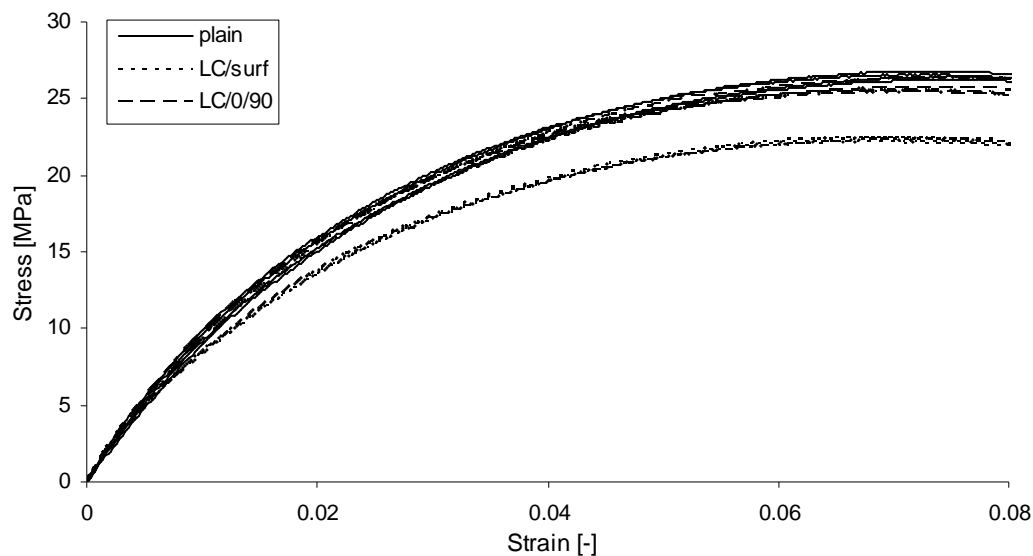
Figure 6.30 Stress-strain curves for the plain polyethylene samples and the LC/surf and LC/0/90 samples with a thin HMA1 coating between the chip and the matrix, all produced from the same sheet.

Table 6.30 Flexural values for the plain polyethylene samples.

Sample	Flexural modulus MPa	Peak stress MPa
226	1134	26.4
227	1090	26.8
228	1008	26.2
229	1146	26.6
230	977	26.8
Average	1071	26.6
SD	75	0.2

Table 6.31 Flexural values for the LC/surf samples with a chip on the outside fibres (bottom of the sample) coated with a thin HMA1 layer.

Sample	Flexural modulus MPa	Peak stress MPa
220	1041	22.3
221	997	22.4
222	1108	22.5
223	1026	22.3
224	1072	22.2
Average	1049	22.3
SD	43	0.1

Table 6.32 Flexural values for the LC/0/90 samples with a chip coated with a thin HMA1 layer.

Sample	Flexural modulus MPa	Peak stress MPa
231	1100	26.4
232	1085	25.7
233	1158	25.4
234	1182	25.5
235	1195	25.6
Average	1144	25.7
SD	49	0.4

From the plots and data it can be seen that there are some slight differences in the flexural moduli of the samples, however they are within the maximum SD obtained for the plain samples (75MPa), thus insignificant. It can only be suspected that the coating in the LC/0/90 sample slightly improves the reinforcing effect of a chip, which was not observed for the non-coated LC/0/90 sample (section 5.3.5, page 235) where the values for the samples with and without a chip were equal.

In contrast, the peak stresses differ significantly and the spread of the values for the same type of sample is relatively small (maximum SD of 0.4MPa). The coated chip on the sample surface causes a significant reduction in the peak stress (22.3MPa in comparison with 26.6 and 25.7MPa for the plain and LC/0/90 samples), which is associated with the reduction in sample stiffness (less energy required to deform the sample to the same strain).

When the samples with a non-coated LC chip were analysed in section 5.3.5 (page 235) no significant difference in the flexural values between the samples with and without a chip was noticed for the location on the surface. Thus this change in the peak stress seems to be due to

the HMA, which is less stiff (lower Young's and flexural modulus) and spreads within the matrix reducing the overall stiffness of the sample.

The coated chip inside also causes a reduction in the flexural peak stress, however the difference between the LC/0/90 and plain samples is only 0.9MPa. When the LC/0/90 samples with a non-coated chip were compared with the plain samples from the same sheet (section 5.3.5) a similar effect was observed, i.e. the chip reduced the peak stress by 1.0MPa. This was explained by the fact that the brittle chip breaks during the test and after that does not resist the bending force any more. The coating inside causes a smaller reduction in sample stiffness than observed for the samples with a coated chip on the surface. This might mean that when there is adhesion between the chip and the matrix at the orientation 0/90, the chip has some reinforcing effect, which partly balances the reduction in sample stiffness cause by the HMA.

The tests indicated that the HMAs significantly improve the adhesion between the silicon chip and the matrix. The improved adhesion between the chip and the matrix reduces the ductility of the samples tested in tension, while in the bending mode its effect is rather insignificant.

The tests up to now have concentrated on the short term mechanical properties of the polyethylene samples with and without silicon chips. Due to the viscoelastic character of polyethylene (see section 2.2.4.4, page 27) it is crucial to also investigate the effect of a chip on the long term properties of the samples, which is very important once the silicon chips (in the future microsensors) are used in the polyethylene structures designed to be in service for a long time, e.g. dozens of years like water pipes. In order to analyze the long term strength the pipes are subject to the pressure regression test where the water pressure is applied for a long time and the reduction in the hoop stress is recorded and often the crack propagation (staring from the artificial notch) is monitored as explained in section 2.2.4.6 (page 32). In this project

the small compression moulded samples with chips were produced and analysed and the flexural creep was carried out at Exova. The results are introduced and analysed in the next chapter.

Chapter 7   FLEXURAL CREEP

7.1 Introduction

As polyethylene is a viscoelastic material and thus its properties change over time when subject to constant stress or strain, a few samples were investigated in a flexural creep test which is a cheap and practical method of creep testing (Sancaktar et al., 1987). As the creep test is time consuming and was carried out using the equipment at Exova the number and type of samples had to be limited. The plain and SC/0/90 samples were subject to stresses of 3.25, 6.5 and 13MPa. According to ASTM (2009a) when creep testing at a single temperature, the minimum number of test specimens at each stress shall be three if fewer than four stress levels are used. In the current research, two samples with and without a chip were tested in a water and air environment at stress levels of 6.5 and 13MPa, i.e. eight samples in total at each stress level. For the lower stress level (3.25MPa) special equipment adjustments had to be made and thus only six samples in total were tested (two in air and four in water). Some samples were tested in water as this is a typical operating environment for water pipes. However, this should theoretically not have any influence on polyethylene when tested at room temperature as the permeability reduces with increasing density (Plastics Pipe Institute, 2007) and the samples tested here had a relatively high density of 0.956g/cm³. All tests were carried out in a temperature controlled room at 23±2ºC. Table 7.1 summarises the numbers of samples tested at particular stress levels and environments.

Table 7.1 Number of samples tested at particular stress levels and environments.

Sample	Stress, MPa					
	3.25		6.5		13	
	Environment					
	Air	Water	Air	Water	Air	Water
plain	1	2	2	2	2	2
SC/0/90	1	2	2	2	2	2
Total number of samples	22					

First the results of the flexural creep test are analysed. Further, the deflection which should not be exceeded during the test is determined on the basis of Sancaktar et al. (1987) theory. In the last section the creep modulus at 50 years is determined as a function of stress level.

7.2 Results and discussion of the flexural creep test

Figures 7.1-7.3 and Tables 7.2-7.4 present the data for all stress levels and types of samples. The samples marked in bold were tested in the air. Note that both time and modulus are plotted on a logarithmic scale. For each sample a power law curve fit and the associated coefficient of determination (R^2) (goodness of fit) were obtained. The 50 years flexural creep modulus was extrapolated for each sample as this is a required minimum service lifetime for water pipes for which this polyethylene grade is used (Hoàng & Lowe, 2008). The 50 years are marked in Figures 7.1-7.3 on the time scale. The accuracy of extrapolation of the 50 years value was justified by the coefficient of determination (R^2) expressing the accuracy of linear correlation (how well a regression line approximates real data points), which was generated automatically by Excel.

First, the 3.25MPa stress is analysed.
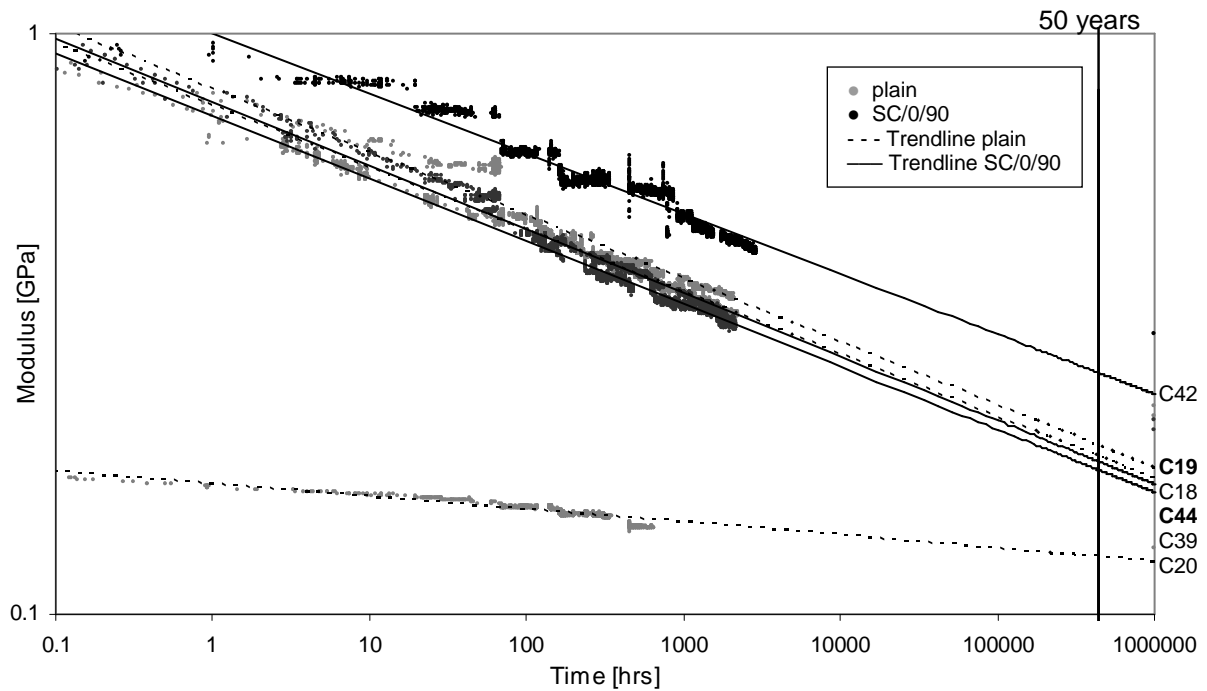
Figure 7.1 Flexural creep modulus for a stress level of 3.25MPa as a function of time.

Table 7.2 The trendline equations with R² and projected creep modulus at 50 years for the stress 3.25MPa (bold – samples tested in air).

Sample	Trendline equation	R²	Modulus at 50 years, GPa
plain			
C19	$E_{fc} = 0.80 \cdot t^{-0.11}$	0.93	**0.19**
C18	$E_{fc} = 0.75 \cdot t^{-0.11}$	0.98	0.18
C20	$E_{fc} = 0.17 \cdot t^{-0.02}$	0.86	0.13
SC/0/90			
C44	$E_{fc} = 0.76 \cdot t^{-0.11}$	0.97	**0.18**
C39	$E_{fc} = 0.72 \cdot t^{-0.11}$	0.97	0.17
C42	$E_{fc} = 1.00 \cdot t^{-0.10}$	0.92	0.26

In order to estimate the reliability of the results, the error in the data collected needs to be calculated. It is related to the accuracy of the deflection measurement, the dimensions of the samples and the actual support span value. Due to the long duration of these tests, which were

carried out at Exova, only a limited number of samples were tested. SDs cannot therefore be obtained. However, the flexural creep modulus error (ΔE_{fc}) can be estimated by applying Equation 7.1.

$$\left(\frac{\Delta E_{fc}}{E_{fc}}\right)^2 = \left(\frac{\Delta F}{F}\right)^2 + 3\cdot\left(\frac{\Delta L}{L}\right)^2 + \left(\frac{\Delta b}{b}\right)^2 + 3\cdot\left(\frac{\Delta h}{h}\right)^2 + \left(\frac{\Delta s}{s}\right)^2 \qquad \textbf{7.1}$$

The Δb, Δh, and ΔL values were already determined as 0.04, 0.05, and 0.05mm, respectively, in section 5.3.1 (page 222), where the flexural bending test error was analyzed. The load measurement error was 0.001kg, giving a force error (ΔF) of 0.01N. The deflection was measured to an accuracy of 0.01mm (Δs).

As an example ΔE_{fc} is calculated for a plain polyethylene sample, where at 1000hrs E_{fc} was 362MPa. The deflection, s, at this moment was 1.70mm. The width and thickness of the sample were 12.65 and 4.33mm, respectively. The load applied was 0.75kg, giving a force of 7.37N. Thus the ΔE_{fc} can be obtained on the basis of Equations 4.17 (page 138) and 5.2 (page 150) as:

$$\left(\frac{\Delta E_{fc}}{362}\right)^2 = \left(\frac{0.01}{7.37}\right)^2 + 3\cdot\left(\frac{0.05}{70}\right)^2 + \left(\frac{0.04}{12.65}\right)^2 + 3\cdot\left(\frac{0.05}{4.33}\right)^2 + \left(\frac{0.01}{1.70}\right)^2 \rightarrow \Delta E_{fc} = 8\text{MPa}$$

The flexural stress is calculated in the same way as the short term flexural stress (Equation 4.12), thus, the error ($\Delta\sigma_{fc}$) is calculated in a similar way (section 5.3.1):

$$\left(\frac{\Delta_{fc}}{3.26}\right)^2 = \left(\frac{0.01}{7.37}\right)^2 + \left(\frac{0.05}{70}\right)^2 + \left(\frac{0.04}{12.65}\right)^2 + 2\cdot\left(\frac{0.05}{4.33}\right)^2 \rightarrow \Delta_{fc} = 0.05\text{MPa}$$

From Figure 7.1 it can be seen that for two samples the results deviate significantly from the average. The lowest curve for sample C20 might be a result of an accidental application of a higher stress to the specimen or a defective specimen (air voids or some degradation).

However, the latter reason is unlikely as multiple samples tested in the tensile and flexural tests did not show such significant variations in the properties. Similarly, in the case of the highest curve for sample C42 a lower stress (load) than to the remaining samples was probably applied.

When excluding the two extremes (C20 and C42) and comparing the samples tested in air (C19 and C44) and water (C18 and C39) slightly larger moduli are obtained for the air environment (0.19 and 0.18GPa) compared with the samples tested in water (0.18 and 0.17GPa). In both environments slightly larger moduli are obtained for the plain samples in comparison with the SC/0/90 samples. However, it is difficult to draw any certain conclusion on the basis of such limited data.

The data scatter at the initial test stages is relatively broad and the records are not consistent, which is a result of a relatively low load applied to the samples (~0.75kg). The creep test equipment and thus its sensitivity and accuracy are designed for higher loads. Scatter in the data may be simply due to people moving round the room, vibration through the floor or even airflow in the room. Thicker specimens may have helped in this respect as the span and loads etc. would have been higher and smaller movements would have had less of an effect on the data (Hesketh, 2009).

Further, the results of the test for the stress level of 6.5MPa are presented in Figure 7.2 and Table 7.3 and analysed.
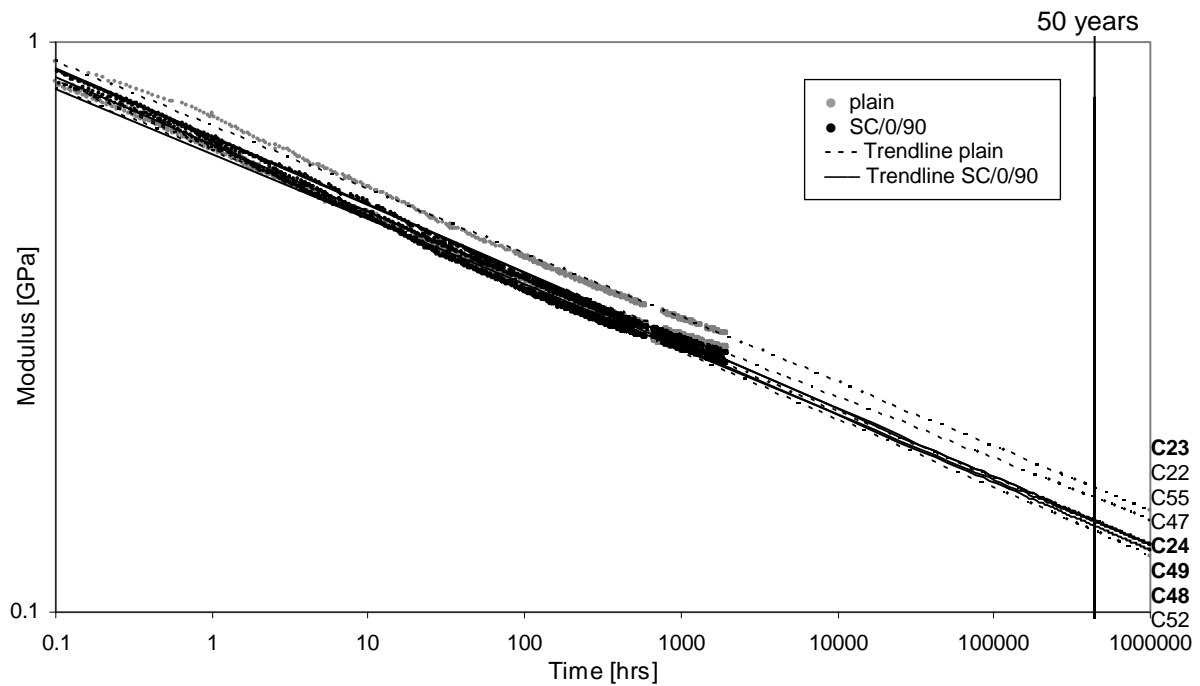
Figure 7.2 Flexural creep modulus for a stress level of 6.5MPa as a function of time.

Table 7.3 The trendline equations with R² and projected creep modulus at 50 years for the stress 6.5MPa (bold – samples tested in air).

Sample	Trendline equation	R²	Modulus at 50 years, GPa
plain			
C23	$E_{fc} = 0.71 \cdot t^{-0.11}$	1.00	**0.17**
C24	$E_{fc} = 0.65 \cdot t^{-0.12}$	0.88	**0.14**
		Average	**0.155**
C22	$E_{fc} = 0.64 \cdot t^{-0.11}$	0.98	0.16
C52	$E_{fc} = 0.65 \cdot t^{-0.12}$	0.99	0.14
		Average	0.15
SC/0/90			
C48	$E_{fc} = 0.64 \cdot t^{-0.12}$	0.99	**0.14**
C49	$E_{fc} = 0.66 \cdot t^{-0.12}$	0.89	**0.14**
		Average	**0.14**
C47	$E_{fc} = 0.68 \cdot t^{-0.12}$	0.93	0.14
C55	$E_{fc} = 0.68 \cdot t^{-0.12}$	1.00	0.14
		Average	0.14

The results for the stress level of 6.5MPa are much more consistent compared with those for the lower stress level. No significant difference between different samples is observed. For all SC/0/90 samples the same modulus at 50 years equal to 0.14GPa was obtained regardless of the test environment, while for the plain samples the value is slightly larger (approximately 0.15GPa), however the difference of 0.01GPa is insignificant (smaller than the maximum difference of 0.03GPa between two samples of the same type , C23 and C24).

Further, the samples tested at the stress level of 13MPa are presented in Figure 7.3 and Table 7.4 and analysed.
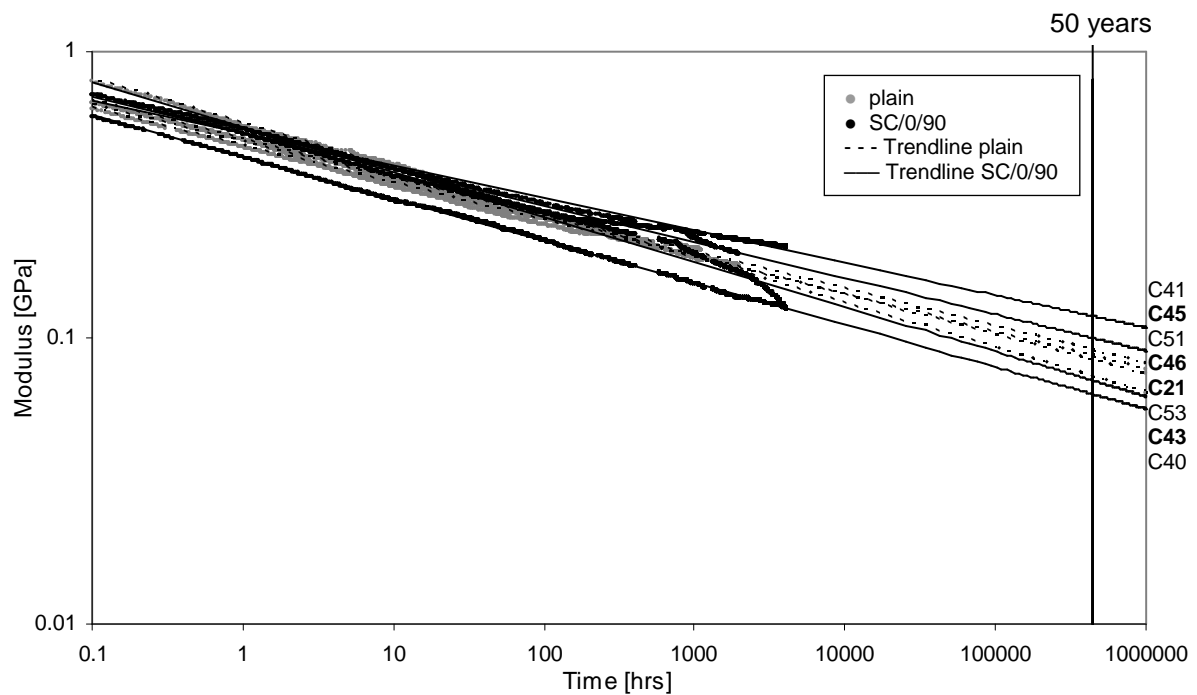
Figure 7.3 Flexural creep modulus for a stress level of 13MPa as a function of time.

Table 7.4 The trendline equations with R² and projected creep modulus at 50 years for the stress 13MPa (bold – samples tested in air).

Sample	Trendline equation	R²	Modulus at 50 years, GPa
plain			
C21	$E_{fc} = 0.50 \cdot t^{-0.14}$	0.97	**0.08**
C46	$E_{fc} = 0.47 \cdot t^{-0.13}$	0.95	**0.09**
		Average	**0.085**
C51	$E_{fc} = 0.48 \cdot t^{-0.13}$	0.99	0.09
C53	$E_{fc} = 0.56 \cdot t^{-0.16}$	0.98	0.07
		Average	0.08
SC/0/90			
C43	$E_{fc} = 0.55 \cdot t^{-0.16}$	0.95	**0.07**
C45	$E_{fc} = 0.52 \cdot t^{-0.13}$	0.99	**0.10**
		Average	**0.085**
C40	$E_{fc} = 0.43 \cdot t^{-0.15}$	1.00	0.06
C41	$E_{fc} = 0.52 \cdot t^{-0.11}$	0.99	0.12
		Average	0.09

The variation in the results for different samples is relatively large. The curve for sample C40 is the lowest and might be due to too high a load being applied. The curve for sample C41 is the highest and may be due to too small a load being applied. The line for sample C43 drops down, which suggests that it fell off the supports as the deflection increases too quickly. Nevertheless, these are also included in the calculation of the averages, because they are not so far from the average as those extreme samples obtained for the stress level of 3.25MPa.

Slipping of the samples is associated with the fact that at higher loads and/or deflection levels the deformed geometry of the specimen causes the vertical support reaction to no longer balance the applied load. In consequence the specimen becomes unstable statistically and slips

through between the supports. Sancaktar et al. (1987) who also tested thermoplastic materials in the bending mode found out that sliding takes place continuously starting from the time of loading. Therefore, BSI (2003c) says that in the creep test the deflection should not exceed 10% of the span during the test, so slipping is insignificant and falling off the supports of the specimen does not happen in this deflection range.

The limitation of the strain to 10% in the test is also assisted with the fact that the equations used for the determination of the stresses and strains (the same as used in the bending test) are designed for small deflections and at larger deflections their use results in large errors. The support span used in the calculations changes with the duration of tests, which is not considered.

Sancaktar et al. (1987) developed a graph on the basis of small and large deflection theories and experiments, which allows the determination of the deflection (strain) values that should not be exceeded during the flexural creep testing procedure in order to obtain accurate results with minimal error. The values are determined with regard to the geometry of the samples and the force (stress) applied.

7.3 Determining the deflection which should not be exceeded during the flexural creep test

In Figure 7.4 the graph showing the stability limit curve after Sancaktar et al. (1987) with marked values obtained for the samples tested in this project is presented.
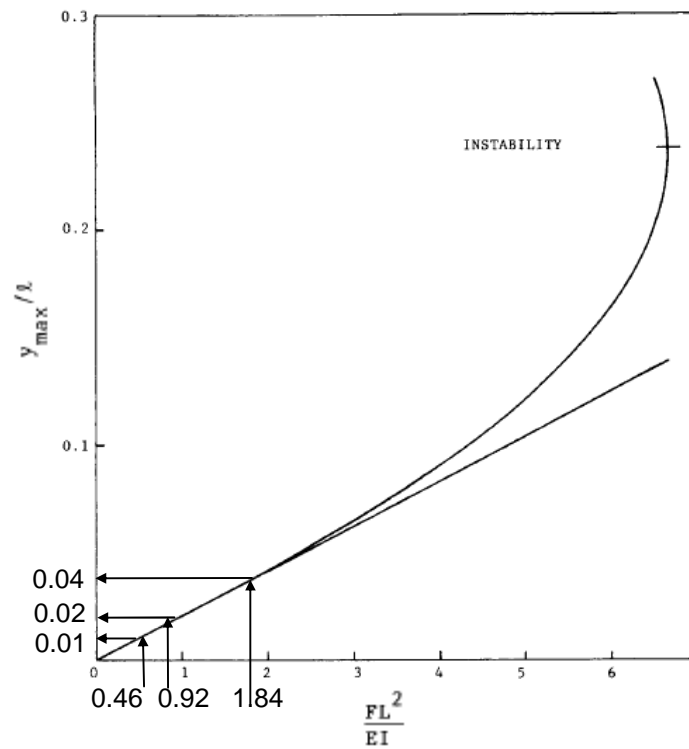
Figure 7.4 Non-dimensional design curve with mid-span deflection versus load parameters for flexural test specimen on cylindrical simple supports (Sancaktar et al., 1987).

The quantities in Figure 7.4 are as follows:

F – force, N

$F_{3.25}$ = 7.35N (on the basis of the load of ~0.75kg for the stress 3.25MPa)

$F_{6.5}$ = 14.7N (on the basis of the load of ~1.5kg for the stress 6.5MPa)

F_{13} = 29.4N (on the basis of the load of ~3kg for the stress 13MPa)

L – support span, L = 0.07m

E – Young's modulus, E = 1000MPa (Borealis, 2008)

I – moment of inertia, m^4 expressed as:

$$I = \frac{bh^3}{12}$$ **7.2**

where: b – specimen width, b = 12.6mm = 0.0126m

h – specimen thickness, h = 4.2mm = 0.0042m

$$I = \frac{12.6 \cdot 4.2^3}{12} = 77.8 \cdot 10^{-12} \, \text{m}^4$$

$l = L/2, l = 0.035 \, \text{m}$

y_{max} − maximum deflection, m

For the stress 3.25MPa:

$$\frac{F_{3.25}L^2}{EI} = \frac{7.35 \cdot 0.07^2}{1000 \cdot 10^6 \cdot 77.8 \cdot 10^{-12}} = 0.46$$

On the basis of obtained value of 0.46 the y_{max}/0.035 is obtained from the graph as 0.01, thus

y_{max} = 0.35mm (8% of the sample thickness).

For the stress 6.5MPa:

$$\frac{F_{3.25}L^2}{EI} = \frac{14.7 \cdot 0.07^2}{1000 \cdot 10^6 \cdot 77.8 \cdot 10^{-12}} = 0.92$$

On the basis of obtained value of 0.92 the y_{max}/0.035 is obtained from the graph as 0.02, thus

y_{max} = 0.7mm (16% of the sample thickness).

For the stress 13MPa:

$$\frac{F_{3.25}L^2}{EI} = \frac{29.4 \cdot 0.07^2}{1000 \cdot 10^6 \cdot 77.8 \cdot 10^{-12}} = 1.84$$

On the basis of obtained value of 1.84 the y_{max}/0.035 is obtained from the graph as 0.04, thus

y_{max} = 1.4mm (32% of the sample thickness).

The limit strain values obtained for the samples tested in this project are 8, 16 and 32% for the stresses 3.25, 6.5, and 13MPa, respectively. Even though the last two values are higher than the 10% recommended in BSI (2003c), they were also exceeded a few times during the tests with the limit strain (10%) achieved within the first few seconds of loading (Hesketh, 2009).

Therefore, the values obtained are only approximations and due to the test conditions (sliding) the error in the data has to be considered.

Further, the flexural modulus at 50 year is determined.

7.4 Flexural creep modulus at 50 years as a function of stress level

The maximum difference between the results for different samples is 0.01GPa, which is much less than the maximum difference between two samples of the same type (0.06GPa), thus insignificant. Therefore, the differences between the results obtained cannot be assigned to different types of samples (with or without a chip) or test environments (air or water) and thus the average modulus at 50 years was calculated for each stress level on the basis of the results obtained for all the types of samples tested.

Table 7.5 lists the average flexural creep moduli at 50 years with SDs for all stress levels tested. For the stress level of 3.25MPa the samples C20 and C42 were not considered in the calculation. The creep modulus is also expressed as a percentage of the short term modulus (1322MPa).

Table 7.5 The averages and SDs of the projected flexural creep modulus at 50 years for the pipe-grade polyethylene at different stress levels.

Stress MPa	Average modulus at 50 years GPa	SD of modulus at 50 years GPa	Modulus at 50 years as % of short term modulus
3.25	0.18	0.01	14
6.5	0.15	0.01	11
13	0.09	0.02	7

On the basis of the stress levels and the projected average moduli at 50 years the linear stress-modulus dependency for the pipe-grade polyethylene is obtained in Figure 7.5.

$$E_{fc50} = -0.009 \cdot \sigma_0 + 0.21$$
$$R^2 = 1$$
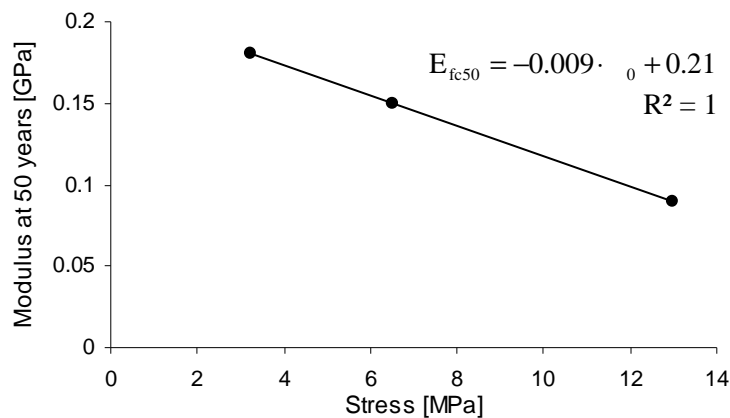
Figure 7.5 Projected modulus at 50 years for polyethylene samples as a function of stress with a trendline equation and R² value.

The creep modulus reduces with stress, which is in accordance with the standards (ASTM, 2001; BSI, 2003c). The modulus at 50 years reduced to between 7 and 14% of the initial value depending on the stress applied, reaching a minimum value of 90MPa, which is very small and unacceptable for the water or sewage pipes. However, it has to be remembered that the stresses applied in the tests are much larger than the stress applied to the pipes during normal operation conditions (BSI, 2003a). In the case of other polyethylene applications relevant operation times, loads and environmental conditions should be considered by evaluating the long term performance of the samples and suitability of the materials tested.

No chip effect was detected on the basis of the limited data obtained. The influence of the fillers on the creep behaviour of polymers based on the literature (e.g. Chevali et al., 2009; Turner, 1965) was introduced in section 2.3.3 (page 37).

In the next chapter the conclusions derived from the research results are presented and the recommendations for further work are given.

Chapter 8   CONCLUSIONS AND RECOMMENDATIONS FOR FURTHER WORK

8.1 Conclusion

The aim of this PhD was to test the impact of introducing silicon chips into polymer samples with the view of using small silicon chips in the order of a few millimetres as the basis of MEMS sensors in order to monitor structures made of polyethylene and in particular plastic pipes. The literature had shown that there was no research conducted in including small rigid inclusions such as the chips into polyethylene although other researchers studied other forms of inclusions such as silica, glass beads and glass flakes. These are significantly different in size and shape as well as volume and hence the research conducted in this PhD can, by its very own nature, be regarded as novel. In order to test a large number of samples, small polyethylene specimens were produced in the laboratory using compression moulding. The main findings can be summarised as follows:

- Polyethylene is a very interesting and complex material. In order to improve the understanding of the polyethylene characteristics, several types of polyethylene were tested. The toughness and ductility of pipe-grade polyethylene was significantly larger than that of off-the-shelf polyethylene. This is likely to be due to a different molecular structure of both materials (different MW and MWD) and the additives used in order to make the pipes more durable in harsh environments.

- Polyethylene behaves very differently to other common civil engineering materials such as steel and concrete. Great care was taken to understand the processes affecting the its quality and associated mechanical properties. Initial tests demonstrated that the temperature of the cooling water and the pressure and temperature applied to the platens

affect the characteristics of the samples. Therefore, whenever possible, samples were produced from the same sheet. However, as the cooling water temperature could not be controlled, some uncertainty remained as samples produced at different times were compared in the analysis. When testing plain polymer samples produced under different conditions significant variations in the test results were observed, which needed to be taken into account when analysing the impacts of inserting chips into the samples.

- The literature review had revealed that there was no standard technique to insert chips into small polymer samples. Thus, new techniques were developed of inserting chips during compression moulding. A number of different techniques were tried and the most effective one involved producing thin sheets of polymer without the chip and then placing the chip between two sheets of polymer, remelting the polymer and thus including the chip. When positioning the chip on the surface, this was much simpler as it could be just placed on the top of a polymer sheet and then remelted. During the remelting process, the chips often moved and hence controlling the orientation and position of the chip was at times difficult. In order to better understand how the chips moved during the remelting process, some samples were scanned using X-rays.

- The orientation perpendicular to the sample surface (orientations 90/0, 90/45 and 90/90) was very challenging to achieve, while inserting the chips at an angle of 45° towards the sample surface (orientation 45/90) was nearly impossible to control. This resulted in a large number of samples being produced and then, after closer inspection by eye of the chip alignment, a significant number of samples were rejected as these did not include chips with the desired alignment.

- In order to obtain information on the impact of inserting chips into polyethylene samples, two different shapes (square and circular), two different sizes (4mm^2 and 16mm^2) at a

number of different positions and orientations were tested in the tensile tests. It turned out that the circular chips have less of an impact on the structural integrity of the samples, which is not surprising, as the square samples provide positions (chip corners) of stress concentrations leading to cracking. Thus, any future sensor design needs to take this into account and from this research the recommendation is to use circular chips whenever possible; although, the square chip had a small reinforcing effect on the samples.

- The tensile tests revealed that the impact of a chip depends also on its orientation. A slight deviation from the alignment parallel to the tension direction caused a significant reduction in the ductility, so the performance of the samples with an SC chip reduced as follows: $0/90 > \text{surf} > 90/0 > 90/0 \text{ slanted} > 90/45 > 45/90 > 90/90,$ where for the first orientation the ductility decreased by 16%, and for the last by 95%. For the LC and SSQ chips this effect was even more significant and even at the most advantageous orientation of 0/90 the ductility reduced by 45% and 88%, respectively. The reduction in ductility (strain at break) and also strength (yield stress) due to the inclusion of a chip was assigned to the reduction in the sample cross-section, thus the volume of polymer, which deforms and sustains the load. Therefore, as small a size of chip as possible is favoured.

- Tensile tests were conducted to determine the influence of the ratio of chip to sample volume by testing samples with different thicknesses and multiple chips. Overall, two thicknesses (thin = 2.2mm, thick = 4.2mm) were tested. The plain thin samples were more ductile due to a larger proportion of the plane stress region, in which more extensive plastic deformation occurs. The tests on thinner samples and samples with multiple chips indicated that a larger volume of small chips in relation to the volume of the matrix gives the best reinforcing effect (higher yield stress), at all orientations except 90/90. Samples with multiple chips are also slightly more ductile.

- Similar findings were obtained for the tests in bending mode. The SSQ chip also acted as reinforcement and the peak stress increased by 5% (at the orientation 90/90). The position of the LC chip (on the outside surface or inside the polymer) was critical as the fibres were either in tension, compression or on the neutral axis. When the chip was placed on the inside fibre, i.e. in compression, the LC chip acted as reinforcement and the peak stress increased by 2%. When it was placed inside the polyethylene, it gave an opposite effect as the chip broke and the peak stress reduced by 4%. For other samples the peak stress reduced with the following: $0/90 > 90/0 > 90/90$. At the last two orientations the peak stresses were lower for the LC chip than for the SC chip, which might be due to a larger void being formed around the debonded LC chip.

- Further, the samples with and without a chip were tested in the impact mode in order to find out if the chip increases or reduces the material resistance to crack propagation, as failure via cracking is a common failure mode of polyethylene structures, e.g. pipes. The chip improved the impact strength of the notched samples by 43% by arresting the crack propagation.

- The preliminary tests and visual investigation of the samples revealed that there is no bond between the silicon chip and the surrounding polymer matrix. This is not surprising as polyethylene is a non-polar material and does not bind to most materials (Huntsman Corporation, 2009). When the samples are subjected to stress, the inclusion behaves like a hole with the chip sitting loosely in this hole, which increases under stress. Therefore, it was regarded as important to investigate the bonding strength between the silicon chip and the polymer. In order to alter the bonding, two HMAs were investigated. The pull-off test indicated that the HMA1 forms a bond three times stronger than the HMA2, and the thin HMA1 layer forms a bond twice as strong compared to the thick layer. However, the

improved adhesion had a rather negative impact on the performance of the samples as it lead to a further reduction in the ductility (for example by 56% in the case of the HMA2 coating). The coatings reduced the stiffness of the whole sample in some cases due to their lower stiffness. From a practical point of view, the findings have shown that, should sensors based on silicon chips be inserted in polymer structures, no adhesion between the chips and the matrix is favoured unless a coating or adhesive is used that does not reduce the polymer integrity.

- It was also important to investigate the impact of the chips on the long term performance of polyethylene. Therefore, a few samples with and without chips were subject to flexural creep test in two environments, water and air. The data did not show any significant differences between the samples.

In addition, to get an appreciation of the scaling effect and the impact of inserting silicon chips into real pipes, a few samples were produced whereby the chips were introduced into pipe joints during the fusion process. The results of the joints tests and the derived conclusions are presented in Appendix A.

Notwithstanding the presented conclusions, there is still a need to gain a deeper understanding of the effect of inclusions of silicon chips on the performance of pipe-grade polyethylene and hence a requirement for additional tests and improvements in the methodology as explained in the next section.

8.2 Recommendations for further work

Having highlighted the main conclusions from this research, there are a number of recommendations for future work. These can be summarised as follows:

- The different manufacturing conditions (especially the cooling water temperature) affected the characteristics of the samples. Better control over the manufacturing conditions would allow any variations in the test results due to the manufacturing processes to be ruled out.

- Improved control over the orientation and alignment of the chips would also allow any variations in the test results due to misalignment of the chips to be ruled out. It would greatly help if this process could be automated.

- More accurate measurement of some parameters, e.g. Young's and flexural moduli, would limit variations in the results due to the measurement error.

- The samples in the bending mode deformed to large strains under low loads due to their small thickness. Testing thicker samples would limit this deformation and improve the accuracy of the flexural and creep moduli measurements.

- The tests revealed that the chip shape and size have an impact on the mechanical performance of the samples. Other chip shapes, sizes and orientations should be also tested to find the optimal one for any particular application.

- As it is envisaged that the chips will be randomly inserted in large numbers into the structure, it is important to test samples containing more than one or two chips. As part of this research, only a small number of samples with two chips were tested. Further tests are required to get a more holistic understanding of large numbers of chips on the structural integrity of the structure. It will be important to vary the ratio of the chip volume to the volume of the sample.

- The effects of different sample thicknesses were investigated, as the thickness of the samples was limited to approximately 4.2mm, and only two thicknesses (4.2 and 2.2mm)

321

were investigated. In order to obtain a better understanding of the effect of the chip relative to the sample thickness, more and greater thicknesses should be tested. This would require different manufacturing equipment (greater press capacity) or process.

- The boundary conditions had a huge impact on the way in which the crack developed in the samples. Testing different sizes of samples would help to better understand this impact, while wider and thicker samples would reduce the effect of boundary conditions.

- More pipe specific tests on the pipe joints and pipes containing chips would allow an improved understanding of the impact of the chips on large structures in the stress modes and test regimes similar to those under which they operate.

- The tests on the coated chips revealed that improved adhesion between the chip and the matrix reduces the ductility of the samples. However, this is thought to be partly due to the uneven spreading of the HMAs within the polyethylene matrix, but could not be verified due to both materials being the same colour. Therefore, it would be recommended to dye the HMAs and monitor how they distribute around the chip and possibly control this process and investigate how this influences the mechanical performance of the samples.

- Even though the surface morphology of a microsensor does not differ significantly from the plain silicon chip as the additional layers are only micrometres thick, once the final microdevice has been manufactured it should be tested directly and the effect of HMAs and the high temperatures likely during the manufacturing process on how it functions should be studied.

List of References

Adams R. D. & Davies R. G. H. (2002) Chapter 4. Strength of lap shear joints. Dillard, D. A. & Pocius, A. V. (Eds.) *Adhesion science and engineering. 1.The mechanics of adhesion.* Amsterdam, Elsevier Science B.V.

Adhikary K. B., Pang S. & Staiger M. P. (2008) Dimensional stability and mechanical behaviour of wood-plastic composites based on recycled and virgin high-density polyethylene (HDPE). *Composites: Part B,* 39 pp. 807-815

Adur A. M. & Flynn S. R. (1987). Proceedings of the: *45th Annual Technical Conference Society of Plastics Engineers.* Los Angeles, CA, May 1987, pp. 508

Air Resources Board (2010) *Heptane.* Available from: http://www.arb.ca.gov/db/solvents/solvent_pages/Hydrocarbon-HTML/heptane.htm, California Environmental Protection Agency, Date accessed: 18 June 2010

American Society of Metals (2003) *Characterization and failure analysis of plastics*, Ohio, USA, ASM International

American Water Works Service Co., Inc. (2002) *Deteriorating Buried Infrastructure Management Challenges and Strategies Characterization and failure analysis of plastics.* Washington, U.S. Environmental Protection Agency

Ames W. A. (1978) *Modified amorphous polyolefin based hot-melt adhesives.* U.S. Patent No. 4159287, U.S. Patent and Trademark Office, USA

Amornsakchai T., Olley R. H., Bassett D. C. et al. (2000) On the influence of initial morphology on the internal structure of highly drawn polyethylene. *Polymer,* 41 pp. 8291–8298

Anderson T. E. (2005) *Fracture mechanics: Fundamentals and applications.* Boca Rato´n, CRC Press

Andres S. & Brian P. (1991) Tailoring HM properties with intra-APAO blending. *Adhesives Age,* 34 (12), pp. 17-20

Argon A. S. & Bailey D. G. (1974) Failure in laminates in tension under increasing stress, constant stress, and cyclic stress. *Journal of Materials Science,* 9, pp. 201-211

323

ASTM (2001) *Standard test methods for tensile, compressive, and flexural creep and creep rupture of plastics*. D2990, ASTM International, USA

ASTM (2005) *Standard specification for polyethylene plastics extrusion materials for wire and cable*. D1248, ASTM International, USA

ASTM (2006) *Pull-off adhesion strength of coatings on concrete using portable pull-off adhesion testers*. D7234, ASTM International, USA

ASTM (2007a) *Standard test method for notch tensile test to measure the resistance to slow crack growth of polyethylene pipes and resins*. F1473, ASTM International, USA

ASTM (2007b) *Standard practice for compression moulding thermoplastic materials into test specimens, plaques, or sheets*. D4703, ASTM International, USA

ASTM (2007c) *Standard test methods for flexural properties of unreinforced and reinforced plastics and electrical insulating materials*. D790, ASTM International, USA

ASTM (2008a) *Flexural properties of unreinforced and reinforced plastics and electrical insulating materials by four-point bending*. D6272, ASTM International, USA

ASTM (2008b) *Standard test method for determining the Charpy impact resistance of notched specimens of plastics*. D6110, ASTM International, USA

ASTM (2008c) *Standard practice for conditioning plastics for testing*. D618, ASTM International, USA

ASTM (2008d) *Standard test method for tensile properties of plastics*. D638, ASTM International, USA

ASTM (2009a) *Standard test methods for tensile, compressive, and flexural creep and creep-rupture of plastics*. D2990, ASTM International, USA

ASTM (2009b) *Standard test method for pull-off strength of coatings using portable adhesion testers*. D4541, ASTM International, USA

Beaumont P. W. R. & Phillips D. C. (1972) Tensile strength of notched composites. *Journal of Composite Matter,* 6 (1), pp. 32-46

Bentley D. J. (2005) Hot melt adhesive use. *Paper, Film & Foil Converter,* March 1

Bigg D. M. (1987) Mechanical properties of particulate filled polymers. *Polymer Composites,* 8 (2), pp. 115-122

Borealis (2008) *Polyethylene BorStar HE3493-LS-H.* Vienna

Borup B. & Weissenbach K. (2010) Chapter 4. Silane coupling agents. Xanthos, M. (Ed.) *Functional fillers for plastics.* Weinheim, Wiley-VCH

Bowman J. (1996) Butt fusion joining polyethylene pipes and assessing the resultant joint strength. *Welding and Metal Fabrication,* 64 (2), pp. 62-65

Bowman J. (2008) Polyethylene pipe: Current & future developments. Proceedings of the: *Polyethylene Pipe Seminar.* Warwick, 10 March 2008

Bowman J., Sandilands G. J. & Barker M. B. (1984) The influence of flaw shape and size on the stress rupture lifetimes of semicrystalline thermoplastics. Proceedings of the: *Creep and Fracture of Engineering Materials and Structures.* Swansea, UK, 25-30 March 1984

Bramuzzo M., Savadori A. & Bacci D. (1985) Fracture behaviour of mica reinforced polypropylene: Mica concentration effect. *Polymer Composites,* 6 (4), pp. 249-260

Brancheriau L., Bailleres H. & Guitard D. (2002) Comparison between modulus of elasticity values calculated using 3 and 4 point bending tests on wooden samples. *Wood Science and Technology,* 36 (5), pp. 367-383

Broutman L. J., Duvall D. E. & So P. K. (1990) Application of crack initiation and growth data to plastic pipe failure analysis. Proceedings of the: *48th Annual Technical Conference.* New York, pp. 1495-1497

Brown N. (2007) Slow crack growth-notches-pressurized polyethylene pipes. *Polymer Engineering and Science,* 47 (11), pp. 1951-1955

Brydson J. (1999) *Plastics materials.* Oxford, Butterworth-Heinemann

BSI (1996a) *Plastics. Determination of tensile properties. General principles.* BS EN ISO 527-1:1996, BSI, UK

BSI (1996b) *Plastics. Determination of tensile properties. Test conditions for films and sheets.* BS EN ISO 527-3:1996, BSI, UK

BSI (1996c) *Plastics. Determination of tensile properties. Test conditions for moulding and extrusion plastics*. BS EN ISO 527-2:1996, BSI, UK. – to references as the standard, which recommends test speed of 1mm/min for modulus measurement

BSI (1998) *Plastics — injection moulding of test specimens of thermoplastic materials — part 1: General principles, and moulding of multipurpose and bar test specimens*. BS EN ISO 294-1:1998, BSI, UK

BSI (2000) *Testing of welded joints of thermoplastics semi-finished products. Part 3: Tensile creep test*. BS EN 12814-3:2000, BSI, UK

BSI (2001a) *Plastics. Determination of Charpy impact properties. Non-instrumented impact test*. BS EN ISO 179-1:2001, BSI, UK

BSI (2001b) *Thermoplastics pipes. Determination of tensile properties. General test method*. BS EN ISO 6259-1:2001, BSI, UK

BSI (2002) *Plastics piping systems for renovation of underground non-pressure drainage and sewerage networks. Lining with cured-in-place pipes*. BS EN 13566-4:2002, BSI, UK

BSI (2003a) *Plastics piping systems for water supply. Polyethylene (PE). Part 1: General*. BS EN 12201-1:2003, BSI, UK

BSI (2003b) *Plastics. Determination of flexural properties*. BS EN ISO 178:2003, BSI, UK

BSI (2003c) *Plastics. Determination of creep behaviour. Flexural creep by three-point loading*. BS EN ISO 899-2:2003, BSI, UK

BSI (2004) *Plastics. Methods for determining the density of non-cellular plastics. Immersion method, liquid pyknometer method and titration method*. BS EN ISO 1183-1:2004, BSI, UK

BSI (2005a) *Plastics - compression moulding of test specimens of thermoplastic materials*. BS EN ISO 293:2005, BSI, UK

BSI (2005b) *Plastics. Determination of the melt mass-flow rate (MFR) and the melt volume-flow rate (MVR) of thermoplastics*. BS EN ISO 1133:2005, BSI, UK

BSI (2007) *Plastics. Polyethylene (PE) moulding and extrusion materials. Preparation of test specimens and determination of properties*. BS EN ISO 1872-2:2007, BSI, UK

BSI (2008) *Plastics. Standard atmospheres for conditioning and testing.* BS EN ISO 291:2008, BSI, UK

BSI (2009) *Plastics. Differential scanning calorimetry (DSC). General principles.* BS EN ISO 11357-1:2009, BSI, UK

Caddell R. M., Bates T. & Yeh G. S. Y. (1972) On the tensile behaviour of high density polyethylene subjected to cold rolling. *Materials Science and Engineering,* 9 pp. 223-229

Callister W. D. (2007) *Materials science and engineering: An introduction.* New Jersey, John Wiley and Sons

Cawood M. J. & Smith G. A. H. (1980) A compression moulding technique for thick sheets of thermoplastics. *Polymer Testing,* 1 (1), pp. 3-7

Chan M. K. & Williams J. G. (1983) Slow stable crack growth in high density polyethylene. *Polymer* 24 (2), pp. 234-244

Channel A. D. & Clutton E. Q. (1992) The effects of short chain branching and molecular weight on the impact fracture toughness of polyethylene. *Polymer,* 33 (19), pp. 4108-4112

Chapman D.N., Cheneler D., Metje, N., et at. (2009) *Smart Sensors for Buried Utility Location and Performance Monitoring*, UKWIR Report Ref. No. 09/WM/12/26

Chen H. C., Chen T. Y. & Hsu C. H. (2006) Effects of wood particle size and mixing ratios of HDPE on the properties of the composites. *Holz als Roh- und Werkstoff,* 64 (3), pp. 172–177

Chen H., Scavuzzo R. J. & Srivatsan T. S. (1998) Influence of joining on the tensile behaviour of high density polyethylene pipe. *Journal of Materials Science Letters,* 16 (11), pp. 897-898

Chevali V. S., Dean D. R. & Janowski G. M. (2009) Flexural creep behaviour of discontinuous thermoplastic composites: Non-linear viscoelastic modelling and time–temperature–stress superposition. *Composites: Part A,* 40 (6-7), pp. 870–877

Chiche A. (2010) *Yparex hot melt adhesives.* Personal email to: Kolonko, A., Sent on: 21 October 2010

Chudnovsky A. & Shulkin Y. (1999) Application of the crack layer theory to modelling of slow crack growth in polyethylene. *International Journal of Fracture,* 97 (1-4), pp. 83-102

Clegg D. W. & Collyer A. A. (Eds.) (1986) *Mechanical properties of thermoplastics.* Essex, Elsevier Applied Science Publishers Ltd.

Cowie J. M. G. (1991) *Polymers: Chemistry & physics of modern materials.* Cheltenham, Nelson Thornes Ltd.

Crawford R. J. & Kearns M. P. (2003) *Practical guide to rotational moulding.* Belfast, Queen's University

Crawford R. J. (1987) *Plastics engineering.* Oxford, Pergamon Press

Creton C. & Fabre P. (2002) Chapter 14. Tack. Pocius, V. (Ed.) *Adhesion science and engineering. 1. The mechanics of adhesion.* Amsterdam, Elsevier Science B.V.

Dastoorian F. & Tajvidi M. (2008) Influence of strain rate on the flexural properties of a wood flour/HDPE composite. *Journal of Reinforced Plastics and Composites,* 27 (16-17), pp. 1701-1708

Devries K. L. & Adams D. O. (2002) Chapter 6. Mechanical testing of adhesive joints. Chaudhury, M. & Pocius, A. V. (Eds.) *Adhesion science and engineering. 2. Surfaces, chemistry & applications.* Amsterdam, Elsevier Science B.V.

Downs S. (2010) *Adhesion measurement of a pressure sensitive adhesive. Development of a nanoindentation-based testing technique for PSA materials.* Available from: http://www.hysitron.com/page_attachments/0000/0431/Adhesion_Measurement_of_a_P ressure_Sensitive_Adhesive.pdf, Hysitron Incorporated, Date accessed: 16/10/2010

DSM Engineering Plastics (2004) *Yparex. Extrudable adhesive resins for multi-layer pipe systems.*

DSM Engineering Plastics (2009a) *Yparex 8702 ES.*

DSM Engineering Plastics (2009b) *Yparex 9403.*

Durelli A. J. & Murray W. M. (1943) Stress distribution around an elliptical discontinuity in any two-dimensional, uniform and axial, system of combined stress. *Experimental Stress Analysis,* 1 (1), pp. 19-31

Durelli A. J., Parks V. J. & Feng H. C. (1966) Stress around an elliptical hole in a finite plate subjected to axial loading. *Journal of Applied Mechanics,* 33 (1), pp. 192-195

Dusunceli N. & Colak O. U. (2008) The effects of manufacturing techniques on viscoelastic and viscoplastic behaviour of high density polyethylene (HDPE). *Materials and Design,* 29 (6), pp. 1117-1124

Everaerts A. I. & Clemens L. M. (2002) Chapter 11. Pressure sensitive adhesives. Chaudhury, M. & Pocius, A. V. (Eds.) *Adhesion science and engineering. 2. Surfaces, chemistry & applications.* Amsterdam, Elsevier Science B.V.

Farshad M. (2006) *Plastic pipe systems: Failure investigation and diagnosis.* Hardbound, Elsevier

Feingold A., Mirza S. & Malhotra R. N. (1972) Photoelastic study of stress concentration in rectangular panels with inserts. Proceedings of the: *International Symposium on Experimental Mechanics.* Waterloo, 12-16 June 1972

Ferry S. (2007) *ASTM D2990 flexural creep testing of CIPP liner materials.* Technical Articles, Microbac Laboratories, Inc.

Friedrich K. J. & Karsch U. A. (1981) Failure processes in particulate filled polypropylene. *Journal of Materials Science,* 16 (8), pp. 2167-2175

FSRM (2003) *World of microsystems.* CD-ROM, VDI/VDE-IT and Yole Development, FSRM Swiss Foundation for Research in Microtechnology

Fu Q., Men Y. & Strobl G. (2003) A molar mass induced transition in the yielding properties of linear polyethylene. *Polymer,* 44 (6), pp. 1941–1947

Gad-el-Hak M. (2002) *The MEMS handbook.* London, Chapman & Hall

Gedde U. W. & Jansson J. F. (1985) Molecular fractionation in melt-crystallized polyethylene: 4. Fracture. *Polymer,* 26 (10), pp. 1469-1476

Godfrey D. A. (1998) *Polyethylene based hot-melt adhesive.* U.S. Patent No. 5763516, U.S. Patent and Trademark Office, USA

Greig J. M., Leevers P. S. & Yayla P. (1992) Rapid crack propagation in pressurised plastic pipe. I. Full-scale and small-scale testing. *Engineering Fracture Mechanics,* 42 (4), pp. 663-673

Griffith A. A. (1920) The phenomenon of rupture and flow in solids. *Philosophical Transactions of the Royal Society of London,* 221 (582-593), pp. 163-198

Halpin J. C. & Kardos J. L. (1976) The Halpin-Tsai equations: A review. *Polymer Engineering and Science,* 16 (5), pp. 344–352

Hartest Precision Instruments Ltd. (2009) *Dimensions of the cutter.* Verbal communication with Hartest Precision Instruments Ltd., August 2009

Hawley G. C. (1987) Flakes. Katz, H. S. & Milewski, J. V. (Eds.) *Handbook of reinforcement for plastics.* New York, Van Nostrand Reinhold

Haynes W. M. (Ed.) (2010) *CRC handbook of chemistry and physics.* Boca Raton, FL, CRC Press/Taylor and Francis

Hearle J. W. S. (1982) Fundamentals of structure and mechanics. *Polymers and their properties.* Chichester, UK, Ellis Horwood, Ltd.

Hesketh (2009) *Creep test of polyethylene.* Verbal communication with D. Hesketh, November 2009

Hoàng E. M. & Lowe D. (2008) Lifetime prediction of a blue PE100 water pipe. *Polymer Degradation and Stability,* 93 (8), pp. 1496-1503

Hoechst Plastics (1982) *Pipes, Brochure No. HKR 111e-8122.* Frankfurt, Hoechst AG

Holding S. (2010) *Characterisation of molecular weight distributions of polyolefin materials using high temperature gel permeation chromatography.* Shrewsbury, Smithers Rapra

Hubert L., David L., Séguéla R. et al. (2001) Physical and mechanical properties of polyethylene for pipes in relation to molecular architecture. I. Microstructure and crystallisation kinetics. *Polymer,* 42 (20), pp. 8425-8434

Huntsman Corporation (2009) *Modification of polyolefins with Elastamine® polyetheramines.* The Woodlands, TX

INEOS Polyolefins (2006) *Eltex TUB 124 Blue.*

Ingham E. J. (2003) *The development of impact toughness and resistance to slow crack growth in modified polyvinyl chloride and polyethylene pipe grade polymers.* PhD, Department of Chemistry and Materials Technology, Metropolitan University, Manchester

Ingham, E. J. (2008) *Plain stress and plain strain regions in pipe walls*. Verbal communication with Ingham, E. J., October 2008

Instron (2005) *5500 Series. Advanced materials testing systems.* User manual

Jaarsma F. (2000) Physical and mechanical properties of plastics. *The Free Library. Health care industry. Medical Equipment Designer,* 1 November, Available from: http://www.thefreelibrary.com/Physical+And+Mechanical+Properties+of+Plastics-a067717233, Date accessed: 7 July 2010

Jilkén L., Mälhammar G. & Seldén R. (1991) The effect of mineral fillers on impact and tensile properties of polypropylene. *Polymer Testing,* 10 (5), pp. 329-344

Jönsson L. (2005) Expandable microspheres as foaming agents in thermoplastics, thermosets and elastomers. Proceedings of the: *Advances in Plastics Technology.* Katowice, Poland, November 2005

Joseph R., McGregor W. J., Martyn M. T. et al. (2002) Effect of hydroxyapatite morphology/surface area on the rheology and processability of hydroxyapatite filled polyethylene composites. *Biomaterials,* 23 (21), pp. 4295-4302

Keller A. (1957) A note on single crystals in polymers: Evidence for a folded chain configuration. *Philosophical Magazine Series,* 8 (2), pp. 1171-1175

Khelif R., Chateauneuf A. & Chaoui K. (2008) Statistical analysis of HDPE fatigue lifetime. *Meccanica,* 43 (6), pp. 567-576

Kobayashi M., Takahashi T., Takimoto J.-I. et al. (1996) Influence of glass beads on the elongational viscosity of polyethylene with anomalous strain rate dependence of the strain-hardening. *Polymer,* 37 (16), pp. 3745-3747

Kousourakis A., Bannister M. K. & Mouritz A. P. (2008) Tensile and compressive properties of polymer laminates containing internal sensor cavities. *Composites: Part A,* 39 (9), pp. 1394-1403

Kratochvilla T. R. & Dragaun H. (2008) Morphological considerations on slow crack growth in polyethylene pipes under different production conditions. Proceedings of the: *Plastics Pipes XIV.* Budapest, Hungary, 22-24 September 2008

Krishnaswamy R. K., Lamborn M. J., Sukhadia A. M. et al. (2006) Rapid crack propagation failures in HDPE pipes: Structure-property investigations. *Polymer Engineering and Science,* 46 (10), pp. 1358 - 1362

Kromminga T. & Van Esche G. (2001) Chapter 7. Zweifel, H. (Ed.) *Plastics additives handbook*. Munich, Hanser Publishers

Kuelpmanna A., Osmana M. A., Kochera L. et al. (2005) Influence of platelet aspect ratio and orientation on the storage and loss moduli of HDPE-mica composites. *Polymer,* 46 (2), pp. 523-530

Kukureka S. N. (1989) *Elasticity and viscoelasticity in polymers.* Birmingham, University of Birmingham, School of Metallurgy and Materials

Kurrer K. E. (2008) *The history of the theory of structures: From arch analysis to computational mechanics*. Berlin, Ernst & Sohn

Lakrout H. (1998) PhD, University of Paris 7, Paris

Lakrout H., Creton C., Ahn D. et al. (1997) Micromechanisms of debonding of pressure sensitive adhesives. Proceedings of the: *European Conference on Macromolecular Physics - Surfaces and Interfaces in Polymers and Composites.* Lausanne, Switzerland, 1-6 June 1997, pp. 253-254

Lang R. W., Stern A. & Doerner G. (1997) Applicability and limitations of current lifetime prediction models for thermoplastics pipes under internal pressure. *Angewandte Makromolekulare Chemie,* 247 (1), pp. 131-145

Lauke B. & Schűller T. (2002) Calculation of stress concentration caused by a coated particle in polymer matrix to determine adhesion strength at the interface. *Composites Science and Technology,* 62 (15), pp. 1965-1978

Liang J. Z. & Li R. K. Y. (1998) Mechanical properties and morphology of glass bead-filled polypropylene composites. *Polymer Composites,* 19 (6), pp. 698-703

Liang J. Z. & Yang Q. Q. (2007) Mechanical, thermal, and flow properties of HDPE–mica composites. *Journal of Thermoplastic Composite Materials,* 20 (2), pp. 225-236

Liang J. Z. (2007) Tensile properties of hollow glass bead-filled polypropylene filled composites. *Journal of Applied Polymer Science,* 104 (3), pp. 1697-1701

Lu S., Yan L., Zhu X. et al. (1992) Microdamage and interfacial adhesion in glass bead filled high density polyethylene. *Journal of Materials Science,* 27 (17), pp. 4633-4638

Lu X., Qian N. & Brown N. (1995) The effect of crystallinity on fracture and yielding of polyethylenes. *Polymer,* 36 (22), pp. 4239-4244

Lu X., Zhou Z. & Brown N. (1994) The anisotropy of slow crack growth in polyethylene pipes. *Polymer Engineering and Science,* 34 (2), pp. 109-115

Lusis J., Woodhams R. T. & Xanthos M. (1973) The effect of flake aspect ratio on the flexural properties of mica reinforced plastics. *Polymer Engineering and Science,* 13 (2), pp. 139-145

MacKellar S. (2007) An auditor's view of PE. Proceedings of the: *Polyethylene Pipe Seminar.* Warwick, 25 January 2007

Madryas C., Kolonko A. & Wysocki L. (2002) *Sewage pipes constructions.* Wrocław, Publishing House of Technical University Wrocław

Maine F. W. & Shepherd P. D. (1974) Mica reinforced plastics: A review. *Composites,* 5 (5), pp. 193-200

Majeed B. (2001) *Investigation of the properties of the polyethylene pipe reinforced with glass flake.* Institute of Science and Technology, University of Manchester, Manchester

Marshall C. J., Rozett R. & Kunkle A. C. (1985) The effects of mica as a filler in polypropylene, HDPE, and PVC. Proceedings of the: *Reinforced Plastics/Composites '85.* Atlanta, Georgia, USA, 28 January -1 February 1985

Marshall J. P. (1991) The influence of welding parameters on the toughness of butt fusion welds in MDPE. Proceedings of the: *Advances in Joining Plastics and Composites.* Bradford, UK, 10-12 June 1991, pp. 202-215

McCrum N. G., Buckley C. P. & Bucknall C. B. (1997) *Principles of polymer engineering.* New York, Oxford University Press

Meinel G. & Peterlin A. (1971) Plastic deformation of polyethylene II. Change of mechanical properties during drawing. *Journal of Polymer Science, Part A-2: Polymer Physics,* 9 (1), pp. 67-83

Metje N., Atkins P. R. & Brennan M. J. et al. (2007) Mapping the Underworld – State-of-the-art review. *Tunnelling and Underground Space Technology,* 22 (5-6), pp. 568–586

Mills N. (2005) *Plastics: Microstructure and engineering applications*. Oxford, Elsevier

Mirza S. & Ansari K. (1974) On stress concentration in rectangular plates having rectangular inserts. *Experimental Mechanics*, 14 (10), pp. 412-416

Mitchell B. S. (2004) *An introduction to materials engineering and science*. New Jersey, John Wiley & Sons, Inc.

Mujika F. (2006) On the difference between flexural moduli obtained by three-point and four-point bending tests. *Polymer Testing,* 25 (2), pp. 214-220

Nicolais L. & Narkis M. (1971) Stress-strain behaviour of styrene-acrylonitrile/glass bead composites in the glassy region. *Polymer Engineering and Science,* 11 (1), pp. 194-201

Nielsen L. E. (1974) *Mechanical properties of polymers and composites*. New York, Mercel Dekker, Inc.

Okoli O. I. & Smith G. F. (2000) High strain rate characterization of a glass/epoxy composite. *Journal of Composites Technology & Research,* JCTRER, 22 (1), pp. 3-11

Özbek P. (2008) *Rapid Fracture resistance of polyethylene: Dependence on polymer structure.* PhD, Department of Mechanical Engineering, Imperial College, London

Packham D. E. (2002) Chapter 7. Surface roughness and adhesion. Chaudhury, M. & Pocius, A. V. (Eds.) *Adhesion science and engineering. 2. Surfaces, chemistry & applications*. Amsterdam, Elsevier Science B.V.

Paizis A. (2004) *Orientation and strain cycle effects on the RCP resistance of polyethylene resins.* PhD, Department of Mechanical Engineering, Imperial College, London

Parker J. (2007) *Mains by material in the UK (data from 2006).* Personal email to: Kolonko, Sent on: 30 July 2007

Paul E. L., Antiemo-Obeng V. A. & Kresta S. M. (Eds.) (2004) *Handbook of industrial mixing: Science and practice.* New Jersey, John Wiley & Sons

Peacock A. J. (2000) *Handbook of polyethylene: Structures, properties and applications.* New York, Marcel Dekker Inc.

Peterlin A. (1971) Molecular model of drawing polyethylene and polypropylene. *Journal of Materials Science,* 6 (6), pp. 490-508

Phua S. K., Lawrence C. C. & Potter R. (1998) Fractographic study of high-density polyethylene pipe. *Journal of Materials Science,* 33 (7), pp. 1699-1702

Piggott M. R. (1980) *Load bearing fibre composites*. Oxford, UK, Pergamon Press, Inc.

Plastics Pipe Institute (2007) *Handbook of PE pipe*. Available from: http://plasticpipe.org/publications/pe_handbook.html, The Plastic Pipe Institute Inc., Date accessed: 12 October 2007

Powell P. C. (1983) *Engineering with polymers*. London, Chapman & Hall

Pukánszky B. (1990) Influence of interface interaction on the ultimate tensile properties of polymer composites. *Composites,* 21 (3), pp. 255-262

Raghupathi N. (1990) Long fibre thermoplastic composites. Mallick, P. K. & Newman, S. (Eds.) *Composite materials technology*. Munich, Hanser Publishers

Rane S. S. & Choi P. (2005) Polydispersity index: How accurately does it measure the breadth of the molecular weight distribution? *Chemistry of Materials,* 17 (4), pp. 926

Reedy E. D. & Guess T. R. (2001) Rigid square inclusion embedded within an epoxy disk: Asymptotic stress analysis. *International Journal of Solids and Structures,* 38 (8), pp. 1281-1293

Rheinländer J. (2009) *Back-scatter X-ray technology for detection of sub-surface defects accessible from one side*. Hvalsø, Denmark, InnospeXion ApS

Roberts R.M. (1989) *Serendipity: Accidental Discoveries in Science*. John Wiley and Sons, New York

Rooke D. R. & Cartwright D. J. (1976) *Compendium of stress intensity factors*. London, Her Majesty's Stationary Office

Sancaktar E., Jozavi H., El-Mahallawy A. H. et al. (1987) Application and limitations of the flexural creep test for polymeric materials. *Polymer Testing,* 7 (1), pp. 39-58

Sandilands G. J. & Bowman J. (1986) An examination of the role of flaw size and material toughness in the brittle fracture of polyethylene pipes. *Journal of Materials Science,* 21 (8), pp. 2881-2888

Savin G. N. (1961) Stress concentration around holes. Johnson, W. (Ed.) *Aeronautics and astronautics, Division 1: Solid and structural mechanics.* London, Pergamon Press

Schouwenaars R., Jacobo V. H., Ramos E. et al. (2007) Slow crack growth and failure induced by manufacturing defects in HDPE-tubes. *Engineering Failure Analysis,* 14 (6), pp. 1124-1134

Seguela R. (2005) Critical review of the molecular topology of semicrystalline polymers: The origin and assessment of intercrystalline tie molecules and chain entanglements. *Journal of Polymer Science, Part B: Polymer Physics,* 43 (14), pp. 1729-1748

Sherman E. & Weston G. J. (1966) *Chemistry of the non-metallic elements.* New York, Pergamon Press

Shucai L., Järvelä P. K. & Järvelä P. A. (1996) Properties of polypropylene copolymer-mica composites. *Plastics, Rubber and Composites Processing and Applications,* 25 (9), pp. 441-447

Smith C. G. (1954) Piezoresistance effect in germanium and silicon. *Physical Review,* 94 (1), pp. 42-49

Squires G. L. (1988) *Practical physics.* Cambridge, Cambridge University Press

Stakenborghs B. (2005) Specific application NDE method leads to development of novel microwave NDT technique. *Inspectionengineering Journal,* 11 (1), pp. 11-13

Suarez J. C. M. & Mano E. B. (2000) Brittle-ductile transition of gamma-irradiated recycled polyethylenes blend. *Polymer Testing,* 19 (6), pp. 607-616

Swaminathan R., Bhaskaran H., Sandborn P. A. et al. (2003) Reliability assessment of delamination in chip-to-chip bonded MEMS packaging. *IEEE Transactions on Advanced Packaging,* 26 (2), pp. 141-151

Tanniru M. & Misra R. D. K. (2005) On enhanced impact strength of calcium carbonate-reinforced high-density polyethylene composites. *Materials Science and Engineering,* 405 (1-2), pp. 178-193

Tay C. J., Wang S. H., Quan C. et al. (2004) Surface roughness investigation of semi-conductor wafers. *Optics & Laser Technology,* 36 (7), pp. 535-539

Taylor J. R. (1982) *An introduction to error analysis*. Mill Valley, California, University Science Books

Testometric (2004) *M500-50 at*. Available from: http://www.testometric.co.uk/attester/atm500-50.asp, Date accessed: 6 June 2010

The Welding Institute (2009) *Mechanical testing - notched bar or impact testing*. Available from: http://www.twiprofessional.com/content/jk71.html, Date accessed: 28 May 2009

Thibodeau W. E. & Wood L. A. (1938) Photoelastic determination of stresses around a circular inclusion in rubber. *Journal of Research of the National Bureau of Standards,* 20 (3), pp. 393-409

Timoshenko S. & Goodier J. N. (1951) *Theory of elasticity*. New York, McGraw-Hill

Ting S. K. M., Williams j. G. & Ivankovic A. (2006a) Characterization of the fracture behavior of polyethylene using measured cohesive curves. I: Effects of constraint and rate. *Polymer Engineering and Science,* 46 (6), pp. 763-777

Ting S. K. M., Williams J. G. & Ivankovic A. (2006b) Characterization of the fracture behavior of polyethylene using measured cohesive curves. III: Structure-property relationship. *Polymer Engineering and Science,* 46 (6), pp. 792-798

Todd D. B. (Ed.) (1998) *Plastics compounding: Equipment and processing*. Munich, Hanser Publishers

Troughton M. J. (2001) Welding with integrated non-destructive examination of polyethylene pipes. Proceedings of the: *Plastic Pipes XI.* Munich, Germany, 3-6 September 2001

Turner S. (1965) Creep in thermoplastics, Nylon 66. *British Plastics,* I. January, pp. 44-47

UK Water Industry (2001) *Polyethylene pressure pipes for water supply and sewerage duties*. WIS 4-32-17, UK Water Industry, UK

UK Water Industry (2008) *Fusion jointing of polyethylene pressure pipeline systems using PE80 and PE100 materials*. WIS 4-32-08, UK Water Industry, UK

Vu-Khanh T. & Fisa B. (1986) Fracture behaviour of mica-reinforced polypropylene: Effects of coupling agent, flake orientation, and degradation. *Polymer Composites,* 7 (4), pp. 219-226

Vu-Khanh T., Sanschagrin B. & Fisa B. (1985) Fracture of mica reinforced polypropylene: Mica concentration effect. *Polymer Composites,* 6 (4), pp. 249-260

Wang J., Silva C. A., Viana J. C. et al. (2008) Prediction of fibre orientation in a rotating compressing and expanding mould. *Polymer Engineering and Science,* 48 (7), pp. 1405-1413

Whelton A. J. & Dietrich A. M. (2009) Critical considerations for the accelerated ageing of high-density polyethylene potable water materials. *Polymer Degradation and Stability,* 94 (7), pp. 1163-1175

Williams J. G. (1984) *Fracture mechanics of polymers*. London, Ellis Horwood

Wu S., Sehanobish K. & Jivraj N. (2001) Defect analysis and high density polyethylene pipe durability. Moalli, J. (Ed.) *Plastics failure analysis and prevention*. Exponent, USA, William Andrew Inc.

Wypych G. (2000) *Handbook of fillers*. Toronto, ChemTec Publishing

Xanthos M. (2010) Chapter 20. Compatibilizers - mechanisms and theory. Manas-Zloczower, I. (Ed.) *Mixing and compounding of polymers*. Munich, Germany, Carl Hanser Verlag

Xanthos M. (2010) *Funtional fillers for plastics*. Weinheim, Wiley-VCH

Xiang C., Sue H.-J., Chu J. et al. (2001) Scratch behaviour and material property relationship in polymers. *Journal of Polymer Science: Part B: Polymer Physics,* 39 (1), pp. 47-59

Xiaomeng W. (2009) Detection of weld line defect for oil-gas pipeline based on X-rays image processing. Proceedings of the: *International Symposium on Web Information Systems and Applications*. Nanchang, China, May 22-24, 2009, pp. 273-275

Yang K., Yang Q., Li G. et al. (2008) Mechanical properties and morphologies of polypropylene with different sizes of glass bead particles. *Polymer Composites,* 29 (9), pp. 992-997

Yayla P. & Bilgin Y. (2007) Squeeze-off of polyethylene pressure pipes: Experimental analysis. *Polymer Testing,* 26 (1), pp. 132-141

Yu T. X. & Zhang L. (1996) *Plastic bending: Theory and applications*. Singapore, World Scientific Publishing Company

Zhang Y. & Tanner K. E. (2008) Effect of filler surface morphology on the impact behaviour of hydroxyapatite reinforced high density polyethylene composites. *Journal of Materials Science: Materials in Medicine,* 19 (2), pp. 761-766

Zhao J. Q., Daigle L. & Beaulieu D. (2002) Effect of joint contamination on the quality of buttfused high-density polyethylene (HDPE) pipe joints. *Canadian Journal of Civil Engineering,* 29 (5), pp. 787-798

Zhuk A. V., Knunyants N. N., Oshmyan V. G. et al. (1992) Debonding microprocesses and interfacial strength in particle-filled polymer materials. *Journal of Materials Science,* 28 (17), pp. 4595-4606

Zosel A. (1985) Adhesion and tack of polymers: Influence of mechanical properties and surface tensions. *Colloid Polymer Science,* 263 pp. 541-553

Zosel A. (1989) Adhesive failure and deformation behaviour of polymers. *Journal of Adhesion,* 30 (1), pp. 135-149

Zhuang X. & Yan X. (2006) Investigation of damage mechanisms in self-reinforced polyethylene composites by acoustic emission. *Composites Science and Technology,* 66 pp. 444–449

Appendix A   JOINTS TEST

A.1   Introduction

All the tests up to now were carried out for small-scale compression moulded samples. As the researchers indicated (see section 2.3.3.3, page 43) and as especially the tensile tests have shown (see section 5.2.9, page 210) the boundary conditions influence the effect of the inclusions on the samples or structures. In addition, the microsensors were originally intended for water pipes, which have walls from a few to dozens of centimetres thick. Therefore, tests on larger samples and ideally pipes with chips should be carried out. However, the chips could not be introduced into pipes as the required equipment was not available. An alternative was to introduce them into the pipe joints in the butt fusion process, which was also practiced by Marshall, 1991 and Troughton, 2001 investigating the quality of the pipe joints. In this project, a new method of introducing the chips into the joints was developed and the samples were tested in tension, which is one of the methods for joint quality testing recommended by UK Water Industry (2008). In this Appendix the methodology associated with this experiment is described and the results of the tests analyzed.

A.2   Characterization of materials used for the tensile joints test

In this section the materials (pipes) used to produce the joint samples are introduced and their physical properties are characterized.

A.2.1   Materials used

The HDPE ProFusion pipes DN250 SDR21 and SDR11 (where DN – nominal outside diameter, SDR – pipe diameter to wall thickness ratio) with average theoretical wall thicknesses of 12 and 23mm, respectively, with coloured polypropylene (PP) skin were used for the joint production and tests (Figure A.4). In addition, the DN90 SDR21 ProFusion pipes

with an average theoretical wall thickness of 4.3mm were used in order to compare the physical properties of same thickness samples produced in different processes.

They were made of the same natural colour polymer grade as the compression moulded samples, and were also supplied by Radius Systems. Normal water and gas pipes are coloured completely blue and yellow, respectively.

In the next section the physical properties of the extruded samples are characterized with regards to their thickness and position within the pipe wall.

A.2.2 Effect of the extrusion on the pipe density/crystallinity

For the DN250 SDR21 pipe the densities of the outside and inside wall were obtained, and for the DN250 SDR11 pipe additionally the density in the middle of the pipe wall was determined. The places from which the samples were cut out are shown in Figure A.1. The values were obtained on the basis of three samples in accordance with BSI (2004), similarly like in the case of compression moulded sheets

Figure A.1 Samples for the density test of DN250 pipes, (top) SDR11 and (bottom) SDR21.

(see section 3.2.4, page 73), and the SDs oscillated between 0.0002 and 0.0004g/cm³. Due to the differences between the results of at least 0.001 g/cm³ the values are presented with an accuracy of three decimal places.

In the extrusion process, the pipes were cooled by the water applied to the pipe surface, thus the outside wall was cooled quicker, which should result in a lower crystallinity and thus density of this region in the pipe. The value should gradually increase towards the pipe bore as explained in section 2.2.3.2 (page 16), what confirmed the results of the test for the DN250

SDR21 pipe. The density was 0.956 and 0.959g/cm³ in the outer and inner pipe wall region, respectively.

In the case of the SDR11 pipe the densities in the outside, middle and inside pipe wall regions also increased gradually, being: $0.958 < 0.959 < 0.960$g/cm³, respectively. As the density of the thickest pipe investigated exceeded the value determined for compression moulded samples, it should manifest a more brittle behaviour.

The crystallinity of the pipe samples ranged between 66.7% (DN250 SDR21, outer pipe wall sample) and 69.5% (DN250 SDR11, inner pipe wall sample). A similar dependency was observed in the density test and thinner pipes are expected to be more ductile.

In order to enable possible comparison between both types of samples, the influence of the manufacturing method, i.e. extrusion and compression moulding, was investigated for the pipes cut out from DN90 SDR21 pipe and 4.2mm compression moulded samples of the same geometry as the samples used in the previously discussed tensile test (Figure 4.29c, page 121).

A.2.3 Comparison between the physical properties of compression moulded and extruded samples

The influence of the manufacturing process on the polyethylene performance in tension was compared for compression moulded and extruded samples of similar thickness produced from the same polymer grade.

The density of the extruded DN90 SDR21 pipes of a similar wall thickness (5.8 mm) to the compression moulded sheets (4.3 mm) was 0.955g/cm³, which is lower than the average density of the compression moulded samples, 0.957g/cm³. Thus, the pipe samples should be more ductile, which will be investigated further in the tensile test.

The extruded samples were cut out from DN90 SDR21 pipe in the axial direction (Figure A.2) and compared with 4.2mm samples of the same geometry. The theoretical thickness of the pipe should be 4.3mm, however the actual value was 5.8mm. A smaller pipe diameter associated with a thinner pipe wall could not have been used due to a larger curvature of the samples making them very challenging to cut out and hold by the grips of the tensile machine.
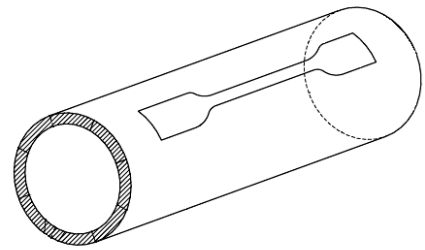
Figure A.2 Schematic of cutting out the dumbbell shape specimen from the pipe (BSI, 2001b).

Figure A.3 shows the data for the extruded samples and some selected compression moulded samples while Table A.1 list the numerical values for the extruded samples, while Tables 5.3 and 5.4 (page 148) listed the values for the compression moulded samples.
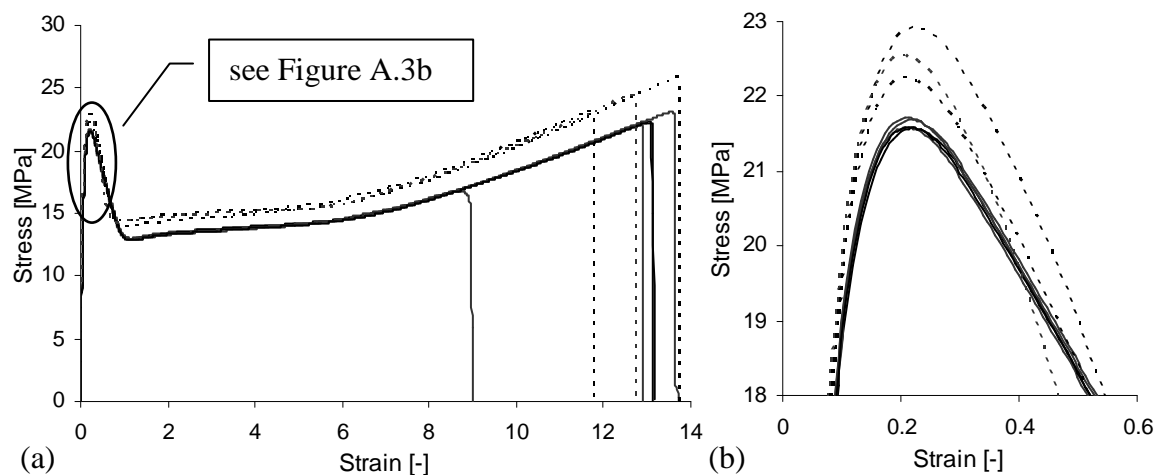
Figure A.3 (a) Stress-strain curves for (——) the extruded samples and (- - -) the selected compression moulded samples; (b) enlarged peak stress region.

Table A.1 Tensile values for the extruded plain polyethylene samples.

Sample	Young's modulus MPa	Yield stress MPa	Strain at break
t96	492	21.6	9.0
t97	467	21.6	13.1
t98	474	21.7	13.7
t99	488	21.7	12.9
t100	475	21.6	13.2
Average	479	21.6	12.4
SD	10	0.1	1.9

In practice, the average Young's moduli for the extruded and compression moulded samples are similar for both samples. The difference is much smaller than SDs, thus the values cannot be relied on. The yield stress and strain at break are lower for the extruded samples (21.6MPa and 12.4, respectively) with a lower density as compared with higher density compression moulded samples (22.5MPa and 12.8, respectively). After Peacock (2000) the yield stress should increase with increasing density, which is the case here, while the strain at break should decrease. The lower strain at break of lower density extruded samples might be associated with their greater thickness as explained in section 5.2.9.1 (page 210), where the thickness effect for the plain compression moulded samples was studied.

Dusunceli & Colak (2008) who tested extruded and compression moulded samples made of the same resin obtained different results than in the current study as both, the Young's modulus and yield stress values, were higher for the extruded samples. However, the degree of crystallinity of extruded and compression moulded samples is not given in Dusunceli & Colak (2008) and hence drawing definite conclusions is difficult.

In summary, the tensile properties of tested compression moulded and extruded samples of similar density and thickness are comparable. Therefore, the results from pipe joints tests can be related to the compression moulded samples. However, it has to be remembered that for thicker pipes lower density and crystallinity values were obtained and thus they are expected to be more ductile. In addition, the larger thickness of the samples and their different geometry might also have an impact on their performance.

Further, the methodology associated with production and testing of the joint samples is introduced.

A.3 Production of the pipe joints with/without chips

Chips were also introduced into the butt-fusion joints and these samples, both with/without chips were tested in tension. In this section the production of the joints with/without chips is described.

A.3.1 Butt-fusion jointing

The butt-fusion joints were made in accordance with UK Water Industry (2008) from DN250 SDR21 and SDR11 ProFuse pipes shown in Figure A.4. The jointing was done at Exova.

The pipe sections were supplied in 1 metre lengths, which were then cut into five portions using a band saw. A line was drawn along each 1 metre pipe in order to align the pieces properly during jointing. The polypropylene (PP) skin was removed using a special pipe peeling tool. The

Figure A.4 DN250 SDR21 and SDR11 pipe sections used to produce butt-fusion joints: (a) side and (b) top view.

pressures and times in the description of the jointing procedure are given for SDR11 pipe and summarized in Table A.2, where the values for SDR21 pipe are additionally listed.

The two pieces of pipe to be jointed were positioned in the clamps ensuring they were properly aligned. The pressure required to push them together (drag pressure) was determined as 7bar. When both pieces were in contact, the position of the clamps and the 12 o'clock position of the pipe were marked, as shown in Figure A.5.

Figure A.5 Marked position of the clamps and the 12 o'clock position of the pipe.

The pipe pieces were moved apart and the trimming tool shown in Figure A.6 was installed between them to level and smooth the edges. The pressure of 10bar was applied to push the pipe pieces towards the trimming tool until the material removed from the edges was in the form of continuous circular scrap.

Figure A.6 Trimming tool.

Then the trimming tool was replaced by a heater plate (Figure A.7) with a surface temperature of 230-240ºC to melt the polymer. The pressure was set at approximately 44bar until an initial 3mm bead (made of displaced polymer) formed around the circumference of the pipe end. It was then reduced to 7bar (heat-soak pressure) and maintained for around 4min 45sec.
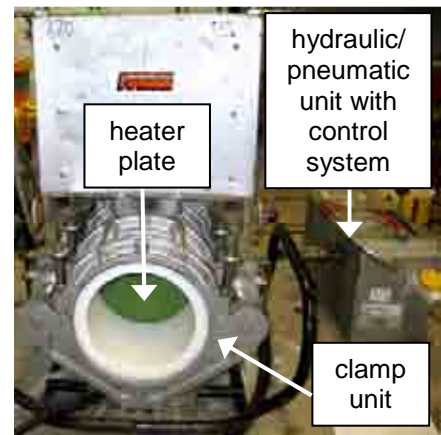

Figure A.7 Butt-fusion equipment (showing heater plate, clamp unit and control unit).

After that, the pressure was released and the heater plate removed. The molten pipe ends were pushed together

immediately at a pressure of 44bar (fusion pressure) for 10sec, which was then reduced to about 13bar and maintained for approximately 15min until the joint cooled down. Finally, the pressure was removed and the clamps opened.

Table A.2 Pressures and times applied during the butt-fusion process of DN250 SDR11 and SDR21 pipes.

	SDR11		SDR21	
	Parameter			
Process	Pressure, bar	Time, sec	Pressure, bar	Time, sec
Drag	7	-	6	-
Bead-up	44	-	26	-
Heat-soak	7	285	6	180
Fusion	44	10	26	600
Cooling	13	900		

The bead generated during the butt-fusion process from the displaced polymer around the joint (Figure A.8) was removed with a debeading tool, which was required for joint scanning and testing. On the basis of the condition of the bead the quality of the joint could be determined. Figure A.9 shows examples of beads in low quality and best practice joints. The bead quality was also examined by twisting it in several places along its length according to the standard (UK Water Industry, 2008). Joints where the bead split during twisting were discarded.

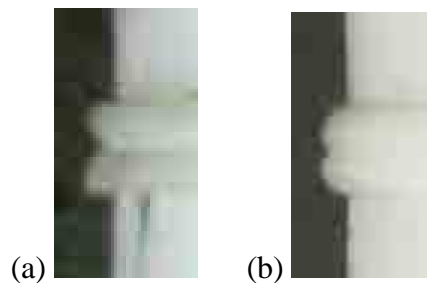**Figure A.8 Butt-fused pipe with a bead.**

(a)   (b)

Figure A.9 (a) A bead in a low quality and (b) best practice joint.

A.3.2 Inserting chips into pipes

Different methods of inserting chips into pipe joints were tested. Initially, the chips embedded within polymer, as shown in Figure A.10, were placed between the molten pipe ends, within 10sec, between heat-soaking and fusion stages. After pushing the molten pipe ends together, the chips moved to the joint bead, which was ultimately removed, thus the method was not effective.

A few chips were inserted into a pipe by drilling a hole of a diameter slightly larger than the diameter of the chip (Figure A.11). However, in this method lots of pipe material was removed and the chip was loose in the hole. In consequence, after the pipe ends were melted and the fusion pressure applied, the chip was washed out by the flowing polymer from its initial position to the joint bead.

surrounding polymer

chip

(a) (b)
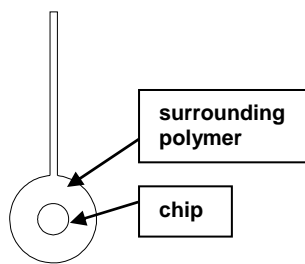
Figure A.10 Chip embedded within polymer. **Figure A.11 Positions of drilled holes in the pipes wall.**
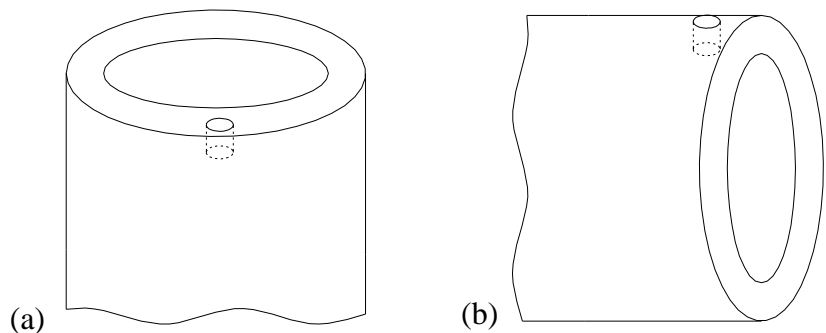
It was eventually decided to insert the chip into the pipe joint by making a hole with a soldering iron at the pipe end in the direction shown in Figure A.11a, and refilling it with molten polymer. In this way the chip being washed out could have been prevented. In order to improve the control of the position/depth of the chip, it was inserted into an already trimmed pipe end as the amount of pipe material removed from the pipe edges during trimming can vary.

The temperature of the soldering iron tip was set at 230-240ºC, which is the approximate temperature of the heater plate. The hole was made in the middle of the wall (Figure A.12a), approximately 5-7mm deep (7-9mm for the LC chip) and enlarged with an screw driver as required. After the chip was inserted (Figure A.12b), the polymer removed to form the hole was melted and used to refill it (Figure A.12c). The edge of the pipe was smoothed with the soldering iron, which was cleaned frequently in order to remove possible polymer residues and prevent their degradation. This process was conducted outside the butt-fusion clamping frame and so the marks made on the pipe (Figure A.5) were useful when repositioning the pipe section back into this frame.

(a)   (b)   (c)
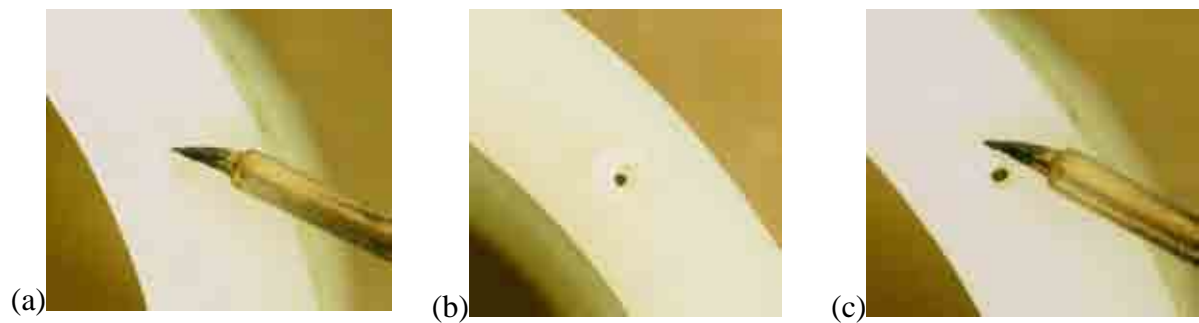
Figure A.12 (a) Making the hole with a soldering iron, (b) chip inserted into the hole, polymer from the hole on the surface, and (c) refilling the hole with molten polymer from the surface.

The position of the chips within the initial joint was verified using microwave non-destructive examination (NDE).

A.3.3 Verification of the position of the chips within a joint by microwave non-destructive examination (NDE)

In order to determine the position of the chips within a pipe joint after processing, NDE was carried out by an experienced person at Exova. Due to the application of pressure during processing the chips should move towards the joint centre from their original positions. However, some chips might move to the joint bead and also some potential air voids might

form during insertion of the chip into polymer due to untight refilling of the hole, which should be detected during NDE.

The technique, developed by Evisive Inc., utilizes microwaves (5-50GHz) and can be applied to dielectric materials. The radiation impinges on the sample and a detectable signal is returned at each interface where the dielectric constant changes, e.g. defects. The signal generated depends on the angle of incidence, the differences in dielectric constant, and the surface geometry. Figure A.12 shows the test arrangement.
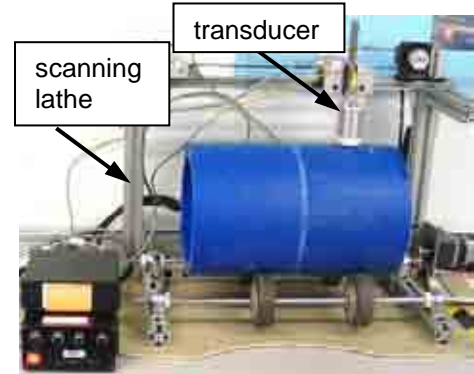

Figure A.13 Pipe joint scanned using the NDE microwave technique.

The transducer from which the waves are radiated can be moved relative to the specimen at any desired speed (Stakenborghs, 2005). The pipe is placed in the scanning lathe, which rotates the sample while scanning the joint along the circumference.

In the trial joint the SCs and SSQs were inserted at a depth of approximately 5-7mm from the edge, and a few LCs were placed at 7-9mm before fusion. The places of chips were marked as shown in Figure A.14. During fusion, once the polymer was melted and thus transparent, it could be seen that the chips from the top and bottom of the joint

Figure A.14 Trial joint with different chips embedded (bead removed).

moved to the bead (internal and external bead, respectively) due to the gravitational force. As the chips are more than two times denser and heavier than the polymer, they drop to the 'bottom' of the molten polymer. Thus, these chips are not expected to be seen within the joint. The joint scan is shown in Figure A.15 with the

chip positions marked. In the image, the X direction is axial (along the pipe length), and the Y direction is radial (along the circumference).

(a)

(b)

(c)

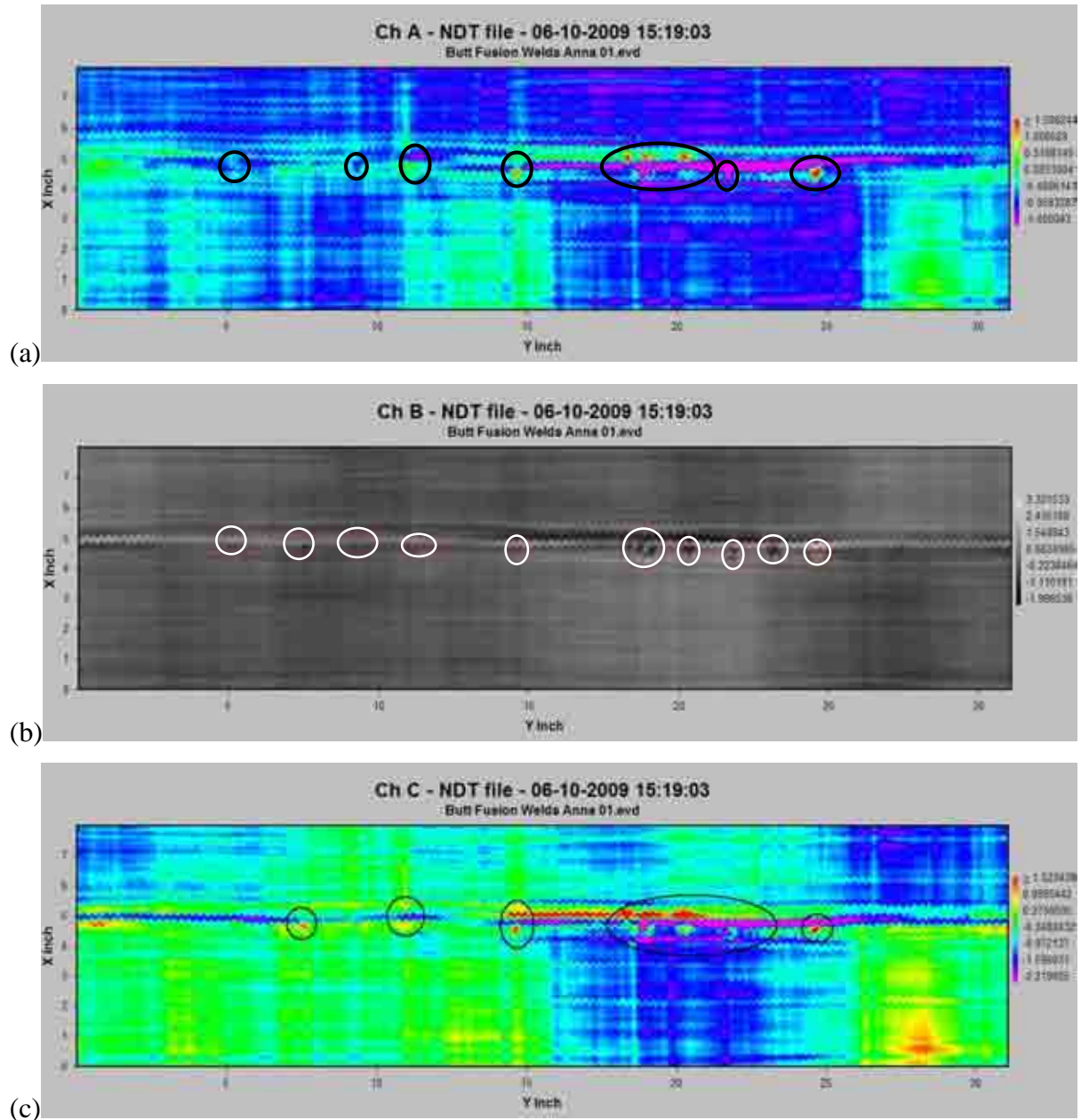**Figure A.15 Results of the microwave scan of the joint at different depths of testing: (a) internal, (b) middle and (c) external pipe wall.**

Some chips were not detected within the joint even though they were not found within the removed joint bead either. The large chips (LC) were easier to localize than the small chips (SC and SSQ) and are more visible in the microwave scans. From Figure A.15 it cannot be

351

identified if there are any air voids around the chips. Most chips detected are positioned very close to the places where they were inserted before fusion of the pipe and they are located within the joint region (characteristic stripe along the pipe circumference in Figure A.15). It means that apart from the areas at the top and bottom of the pipe, chips do not move much around the pipe edge or circumference due to the fusion process. However, they might turn and change their orientation without changing the place, which was verified via the X-ray scanning of the samples. The examples are presented in Figure A.35 (page 371). The X-ray of the whole joint would not give accurate results as the detection capability depends on the interaction volume.

In the next section the choice of sample dimensions is described.

A.3.4 Tensile joint samples

The dimensions of the joint samples were chosen in accordance with UK Water Industry (2008) and are shown in Figure A.16. Samples with a longer gauge section were also considered as this would have meant that the chips were more likely to be positioned within the gauge region. However, it would have been very expensive to cut out such samples due to a lack of appropriate facilities at Exova or at the University.

Figure A.16 Tensile joint sample; dimensions in mm.

The DN250 SDR21 and SDR11 pipes were chosen for jointing as DN250 is the maximum diameter which can be fused using available equipment, and thus the SDR11 has the maximum wall thickness to be fused and SDR21 is approximately twice as thick.
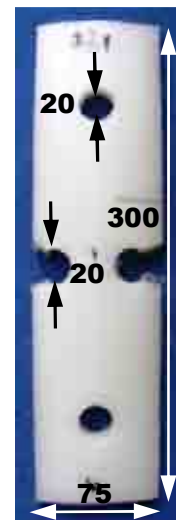
The samples were cut out at Exova by their technicians. The process initially involved cutting out longitudinal rectangular samples across the weld using a band saw. Holes were then drilled on the sides at the weld level to produce the narrowed section and also on both long ends of the sample to enable sample installation in the testing equipment.

A.3.5 Number of samples from one joint

The number of the samples that could be produced from one joint was determined on the basis of pipe circumference (785mm) and sample width (75mm) as: $785/75 \approx 10$. However, as the chips could move during the butt-fusion process, this was reduced to 8. Figure A.17 shows the position of the chips around the pipe circumference.

As explained in previous section, the chips at the 12 and 6 o'clock positions moved into the beads. Therefore, it was decided to not insert the chips at these positions and the samples cut out from these positions were used for testing the joint quality in the tensile test.
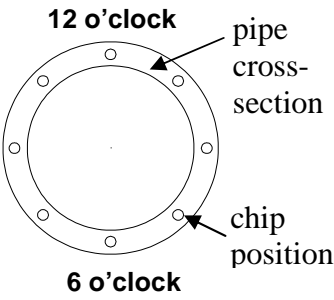

Figure A.17 Chips displaced around the pipe circumference.

A.3.6 Orientation of the chips

Initially, it was planned to produce the samples with different chip orientations, as shown in Figure A.18.
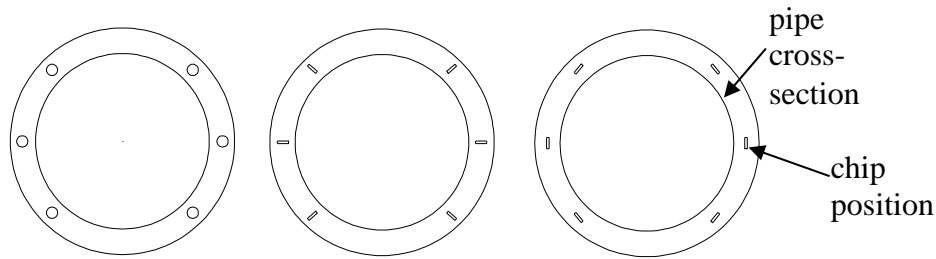

Figure A.18 Pipe joints with chips at different orientations.

Unfortunately, the preliminary experiments, where chips were inserted into joints showed that it was impossible to control the chip position and orientation using the available methods. Therefore, the effect of orientation could not be studied for the joints. Additionally, the joint production and testing was very time consuming and hence only a limited number of tests were conducted.

A.4 Methodology of the tensile joint test

The tensile test is a standard joint quality control test in which the ductility of the joint bond is determined.

A.4.1 Test procedure

The tensile joint test was carried out at Exova on the Testometric M500 machine with a maximum load (force) capacity of 50kN (Figure A.19). Although the speed recommended by UK Water Industry (2008) is 5mm/min, in this case the tests were carried out at 10mm/min, i.e. the same speed as for the compression moulded samples. The load applied was automatically recorded every second. Six samples of each type were tested,
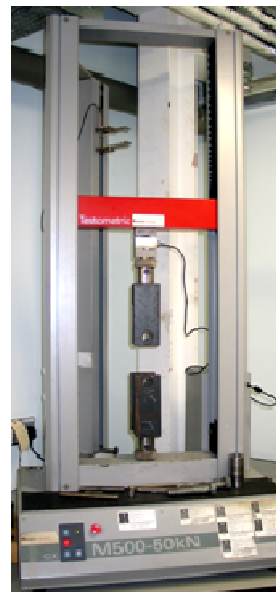

Figure A.19 Testometric M500 testing machine.

Figure A.20 Fixture for the joint sample.

in accordance with UK Water Industry (2008). In addition, two plain samples were tested from each joint to verify the quality of the joint production. Figure A.20 shows the fixture used to hold the sample.

A.4.2 Data analysis

The data were analysed in a similar way as in the case of compression moulded samples (see section 4.4.1.2, page 130). The load was automatically converted into stress as the dimensions of the cross-section of the sample were incorporated into the software. The gauge length was theoretically equal to zero, as it is the narrowest section between the two circular drilled zones (see Figure A.20), thus the strain could not be calculated. The displacement in millimetres was measured instead and the stress-displacement relationship was obtained (Figure A.21). For the same reasons the Young's modulus could not be determined. Therefore, the slope of the stress-displacement curve was calculated as a substitute, for comparison between samples.

It has to be considered that the yield stress and displacement values are also only indicative as the area applied in the calculation is only at a limited range and the sample is stretched at a larger section. Thus, the results cannot be easily compared with samples of other geometries, although, they can be used for comparing samples of the same shape.
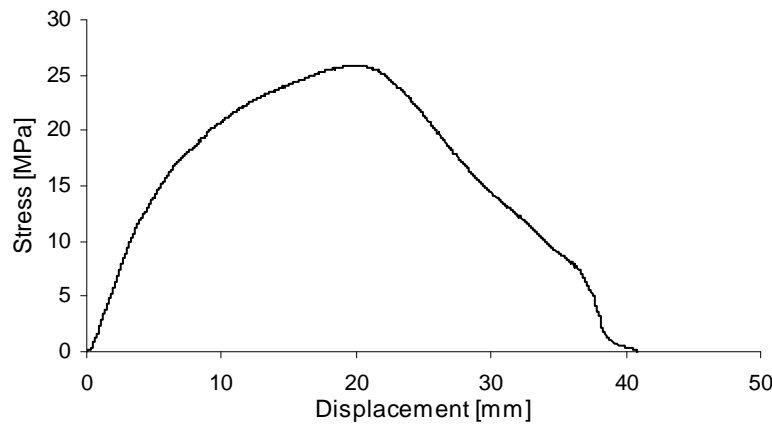

Figure A.21 Example stress-extension relationship for a plain joint sample.

A.5 Results & discussion of the tensile joints test

A.5.1 Introduction

The series of tests on the joints allowed consideration of the effect of including chips within larger structures. The samples cut out from these larger pipes and pipe joints had the geometry specified in Figure A.16 (page 352). Six samples of each type were tested.

Initially, the plain pipe and joint samples of the same dimensions are compared in order to investigate the effect of the jointing process. Further, the influence of the technique used to insert a chip is examined in order to justify the validity of the results for the samples with chips. Finally, the chip size and shape effects as well as the influence of sample thickness are studied.

A.5.2 Joint effect

The joint effect is analysed for the thick samples (cut out from DN 250 SDR11 pipe). The measurements indicated that the actual thickness of the fused pipes/samples is larger than the theoretical (13.5 and 25.0mm for the SDR21 and SDR11 pipes, respectively).

The results for the pipe and joint samples are presented as stress-displacement curves rather than stress-strain curves as due to the shape of the samples the strain cannot be calculated. The Young's modulus values cannot be obtained for the same reason, thus only the slope of the stress-displacement curve is calculated between displacements of 2 and 3mm (for lower displacement values the curves are not uniform due to sample movement at the beginning of the test).

Figure A.22 shows the data obtained for the pipe and joint samples while Tables A.3 and A.4 list the numerical values. The plain joint is called the best practice (BP) joint as it was

prepared under accurately controlled standard conditions according to UK Water Industry (2008).
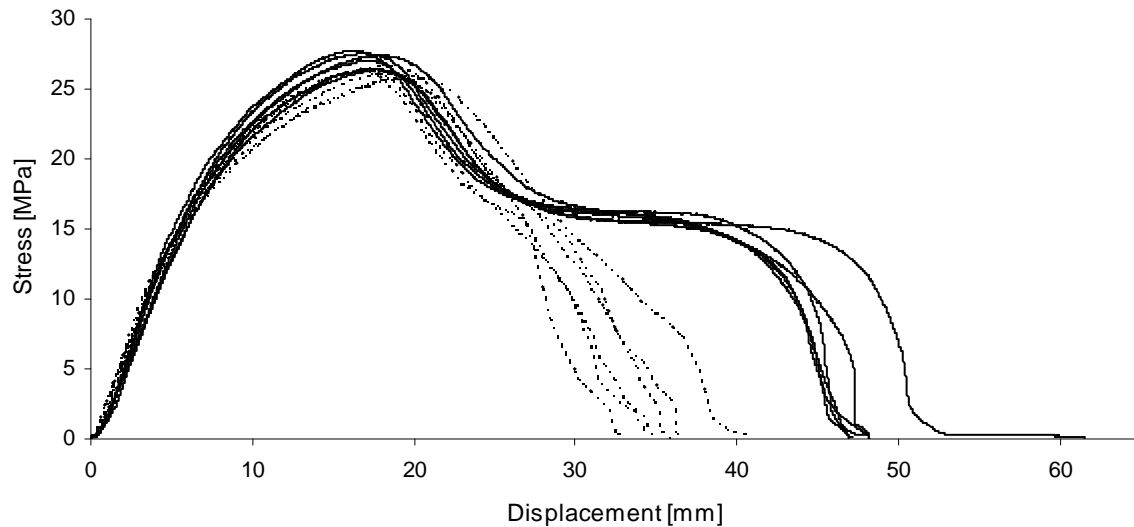

Figure A.22 Stress-displacement curves for DN250 SDR11 (——) pipe and (- - -) BP joint samples.

Table A.3 Tensile values for the DN250 SDR11 pipe samples.

Sample	Slope of the curve MPa/mm	Yield stress MPa	Displacement at break mm
11/1	3.5	27.0	48
11/2	3.3	26.4	62
11/3	3.6	27.8	47
11/4	3.1	27.6	48
11/5	3.0	26.4	47
11/6	2.9	27.4	48
Average	3.2	27.1	50
SD	0.3	0.6	6

Table A.4 Tensile values for the DN250 SDR11 BP joint samples.

Sample	Slope of the curve MPa/mm	Yield stress MPa	Displacement at break mm
6/1	3.5	25.9	41
6/2	3.3	26.2	34
6/3	3.3	26.3	35
6/4	3.1	26.1	36
6/5	2.9	26.6	33
6/6	2.9	25.6	36
Average	3.2	26.1	36
SD	0.2	0.3	3

For comparison with other types of samples the representative curves are chosen similarly as it was done for the compression moulded samples (see section 5.2.1, page 147). Usually, three representative curves are identified and marked in the Tables (e.g. Table A.4): the curve with displacement at break and yield stress closest to the calculated averages (6/4), the curve with

357

the minimum displacement at break, usually associated with the maximum yield stress (6/5) and the curve with the maximum displacement at break, usually associated with the maximum yield stress (6/1). The last two represent the extremes, i.e. the envelopes of all the curves.

Before interpreting the data it is important to justify their reliability by calculating the experimental errors. The accuracy of the tensile data obtained is influenced by measurement of the sample dimensions and instrument precision. The sample thickness and width were measured once at the narrowest place in the sample with vernier callipers with an error of 0.05mm (Squires, 1988). Example values for a sample are 27.92 and 24.94mm, respectively, giving an area of 696.32mm². Thus from Equation 5.2 (page 150), the area error (ΔA) is:

$$\left(\frac{\Delta A}{696.32}\right)^2 = \left(\frac{0.05}{27.92}\right)^2 + \left(\frac{0.05}{24.94}\right)^2 \rightarrow \Delta A = 2\text{mm}^2$$

The errors associated with the instrument accuracy are specified by the manufacturer (Testometric, 2004). The load measurement accuracy is ±0.5% of the reading down to 1/1000 of the load cell capacity (50kN/1000 = 50N). The displacement measurement resolution is 0.01mm.

The error for the yield stress ($\sigma y = 25.87$MPa for the analysed sample) is calculated on the basis of the area and load measurement errors:

$$\left(\frac{\Delta_y}{25.87}\right)^2 = \left(\frac{2}{696}\right)^2 + (0.005)^2 \rightarrow \Delta_y = 0.15\text{MPa}$$

It has to be considered that the data are only approximate as the area applied in the calculation was only at a limited range and the sample was stretched at a larger section. Thus, the results cannot be easily compared with samples of other geometries, although, they can be used for comparing samples of the same shape.

From the plots (Figure A.22) and data (Tables A.3 and A.4) it can be seen that the pipe samples are more ductile than the joints as they reach a significantly higher displacement at break value of 50mm. In contrast to the pipe samples, for the joint samples the proper cold drawing stage cannot be distinguished. The slope of the stress-displacement curve is equal for both samples, 3.2MPa/mm. The yield stress is significantly higher for the pipe samples compared with joints, being 27.1 and 26.1MPa, respectively, with a maximum SD of 0.6MPa. It can be concluded that the pipe samples are both stronger and more ductile than the joints.

The results are mostly in agreement with the observations of Chen et al. (1998) who tested pipes and pipe joint samples in tension and also obtained lower tensile values for joints. Their results are shown in Figure A.23. The difference in yield stress was also 1MPa. The Young's modulus was 26% higher and the strain at break was 9% higher for pipe, while here the moduli are equal and the strain at break is 28% higher for the pipe. From Figure A.23 it can be seen that Chen et al. (1998) recorded a proper cold drawing stage for both, plain and butt-fused pipe samples, which was not observed in the joints tested in this project.

However, it has to be noted that in the test carried out by Chen et al. (1998) the samples were made of different pipe grade and had a different shape, similar to the compression moulded samples analysed in this project and to the sample shown in Figure A.24a. The samples tested here had a shape like the one presented schematically in Figure A.24c.
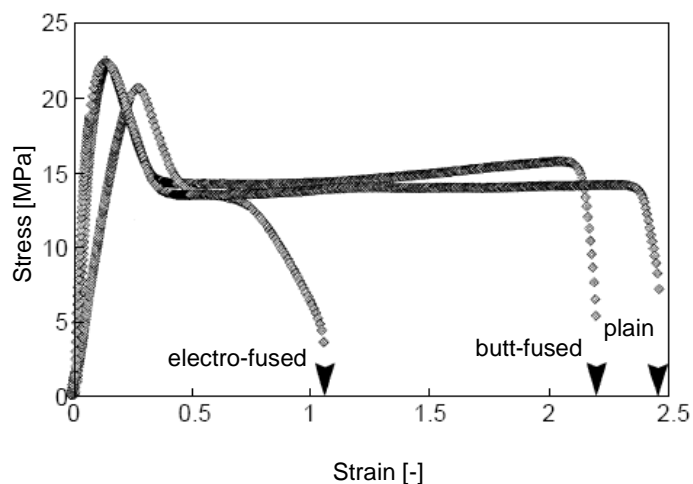
Figure A.23 Comparison of the stress–strain response of the fused samples with the plain pipe samples (Chen et al., 1998).
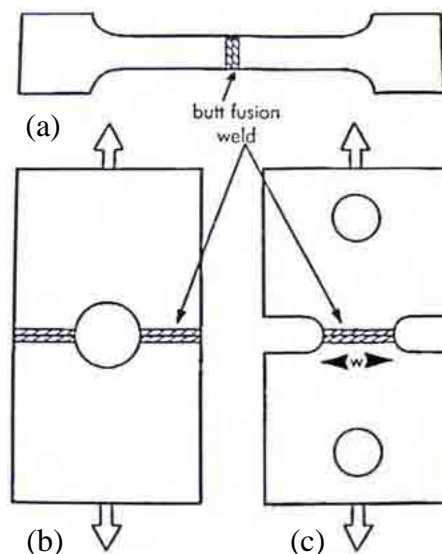

Figure A.24 Examples of shapes of tensile samples used to determine the properties of butt-fusion joints (Bowman, 1996).

Bowman (1996) concluded on the basis of available literature that the shape of the joint samples has an influence on the results of the tensile test and among the shapes in Figure A.24 the lowest strain at break in relation to the plain pipe samples was recorded for shape (c), which is used in this project.

Further, the profiles of the samples tested in tension (Figures A.25 and A.26) and the broken specimens (Figure A.27) are analysed.
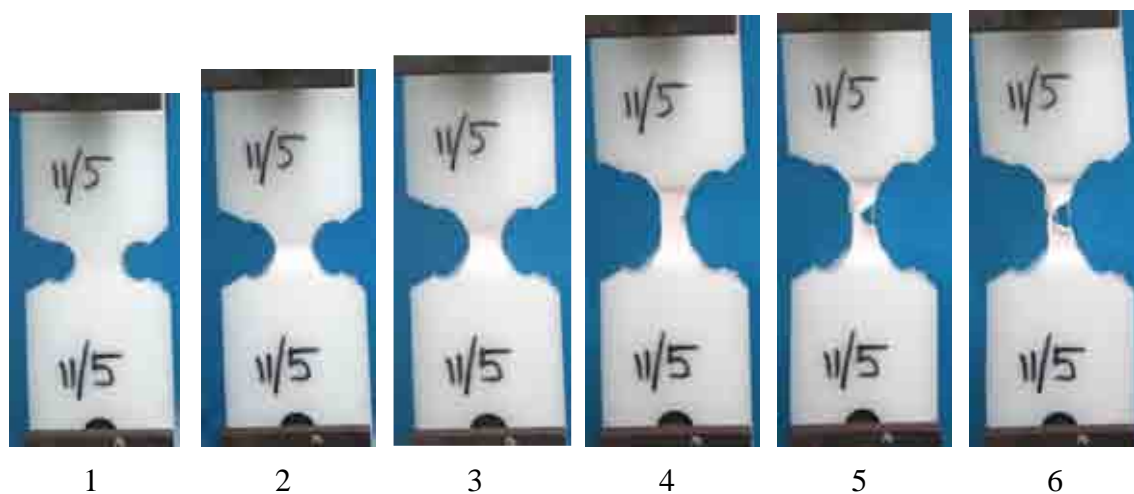

| 1 | 2 | 3 | 4 | 5 | 6 |

Figure A.25 Profiles of the DN250 SDR11 pipe sample during different stages of the tensile test.
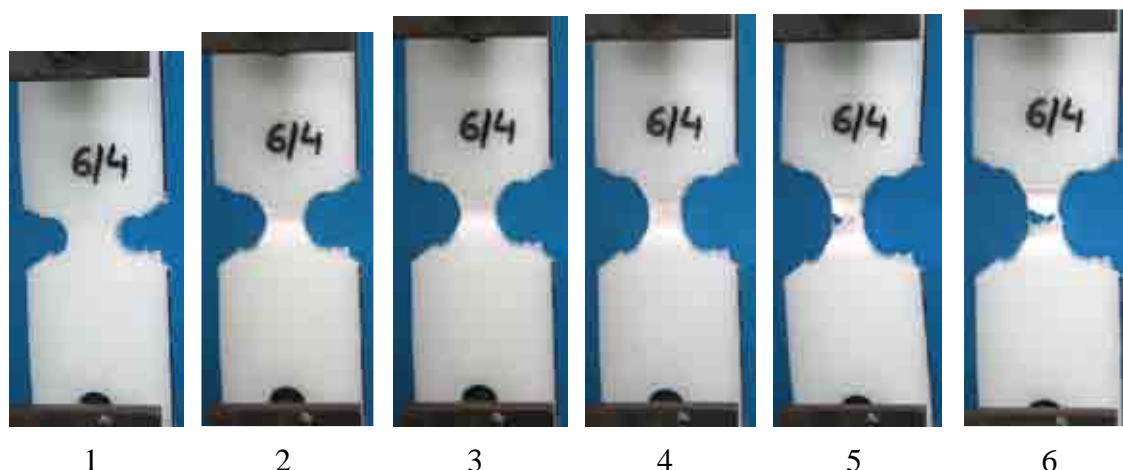
Figure A.26 Profiles of the DN250 SDR11 PB pipe joint sample during different stages of the tensile test.

From Figures A.25 and A.26 it can be seen that the stretching process is comparable for both types of samples. Due to the shape of the sample with a discrete narrowing in the centre the deformation always starts in the same place, which is the joint region in the case of the joint sample. As the sample elongates and the central part narrows down, whitening can be observed associated with the alignment of the polymer forming fibrous structure. For the joint sample the stretched region is more distinguished and limited by the joint/pipe boundary. For the pipe sample the stretched region is slightly larger and this might also be the reason for the larger displacement at break values obtained for these samples. However, it does not change the fact that in service the joint/pipe boundary will have the same effect causing stress concentration in this region limiting the stress transfer to other pipe regions. The failure pattern of the pipe sample is similar to the compression moulded plain polymer sample illustrated in Figure 5.9, page 163.

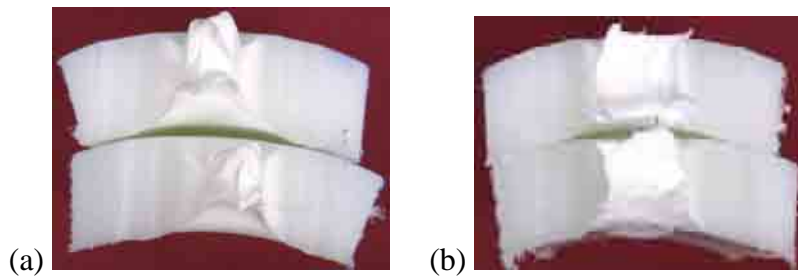Later, the failed samples are investigated.

(a)　　　(b)

Figure A.27 Cross-section of the broken DN250 SDR11 (a) pipe and (b) joint samples.

From Figure A.27 it can be seen that the final cross-section is smaller in the case of the pipe sample due to more extensive stretching. Both samples stretched more at the edges of the cross-sections and for the joint sample a flatter area in the middle can be better distinguished. This might be associated with the plane stress region (at the edges of the sample) being more prone to plastic deformation (absorbing more energy) and the plane strain region in the middle where less deformation occurs as explained in section 5.2.9.1 (page 210). Even though the thickness of both samples is similar and they both fail in a ductile manner, the pipe sample is more plastically deformed (neck developed) thus it is more ductile.

The joint samples can be compared with the results of Marshall (1991) who tested butt-fusion joints made of different polyethylene pipe grades and observed five different failure patterns. Some behaved like the pipe samples while in the samples over 12mm thick the cold drawing was confined to the surface (edge) regions as illustrated in Figure 2.29a (page 47), which is similar to the joint samples tested here and is still considered as a satisfactory mode with respect to the overall failure behaviour. He also observed the flat fracture mode illustrated in Figure 2.29b in some samples, which is unacceptable due to the potential of embrittlement of such a joint. The joint samples over 25mm thick exhibited brittle behaviour leading to slow crack growth in service. The samples tested here are approximately 25mm thick, however they are made of a modern very tough pipe-grade polyethylene, therefore even very thick sections exhibit ductile behaviour.

In summary, the tests have shown that the pipe is stronger and tougher than the joint. Therefore, the joint seems to be the weakest place within the pipe, which was also observed by other researchers (Chen et al., 1998; Marshall, 1991). Introducing the chips into the joints can additionally weaken the structure; however, this effect needs to be analysed further in order to determine the scale of the chip effect.

As the parameters such as time and pressure during the joint production process can differ slightly because they are manually controlled, some variations between samples can occur even though every effort was made to produce the best quality samples in accordance with the standards. Therefore, in the case of joints with chips, the plain joint samples are cut out from the top and the bottom of the pipe circumference and tested in order to verify the joint quality and compare it with the BP joint. These positions were chosen as initial joint production indicated that the chips in the top and bottom of the pipe circumference move to the beads due to gravitational force (see section A.3.3). Therefore, in these regions no samples with chips can be produced.

As the production process of the samples with chips causes slight modifications in the joint and hence the quality of these joints might differ, the effect of the chip inserting technique on the joint performance is studied in the next section.

A.5.3 Effect of the chip inserting technique

The method of inserting chips is verified by testing samples with refilled holes without chips. As the holes for the chips are made and refilled manually, it is difficult to control accurately. In addition, even though a high temperature is used the polymer is not heated up uniformly and some portions might not be melted enough to fill the space accurately. Figure A.28 shows the results for the selected extreme samples with refilled holes, the test samples from the same

joint, and the selected extreme BP joint samples. Table A.5 lists the numerical values for the

samples with refilled holes, while Table A.6 lists the key values for the BP joint.
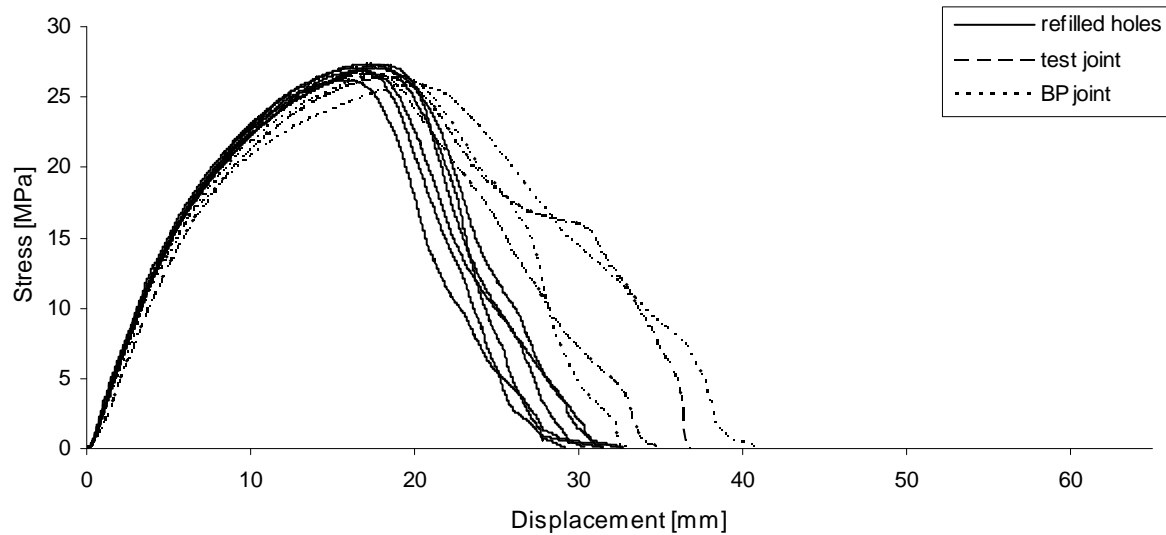

Figure A.28 Stress-displacement curves for the DN250 SDR11 pipe joint samples with refilled holes, test joint samples, and the selected extreme BP pipe joint samples.

Table A.5 Tensile values for the DN250 SDR11 joint samples with refilled holes and the test samples.

Sample	Slope of the curve MPa/mm	Yield stress MPa	Displacement at break mm
9/1	3.2	27.3	31
9/2	3.0	26.2	33
9/3	3.1	27.1	31
9/5	3.1	26.9	33
9/6	3.0	27.1	30
9/7	3.2	27.4	29
Average	3.1	27.0	31
SD	0.1	0.4	2
Test samples			
9/4	3.3	26.7	35
9/8	2.9	26.4	37

Table A.6 Average tensile values with SDs for the BP joint.

Sample	Slope of the curve MPa/mm	Yield stress MPa	Displacement at break mm
Average	3.2	26.1	36
SD	0.2	0.3	3

The data show that the test samples (9/4 and 9/8) are within the same range as the BP joint samples, which suggests that the quality of the joint is right. The samples with refilled holes are less ductile reaching smaller displacement at break of 31mm in comparison with the BP joint and joint tests samples (36mm on average). The difference between the stress-displacement slopes is smaller (0.1MPa/mm) than the maximum SD of 0.2MPa/mm, therefore insignificant. The yield stress is higher for the samples with refilled holes (27.0MPa) and the difference (0.9MPa) is greater than the SD of 0.4MPa. Higher yield stress values were also obtained for the test samples (26.7 and 26.4MPa). This means that this joint is slightly stiffer but still equally ductile, while the refilled holes cause slight embrittlement of the samples.

The effect of the holes is further analysed by studying photographs of sample profiles (Figure A.29) and broken samples (Figure A.30). The samples at the initial stages looked like the BP joint samples, therefore are not shown.
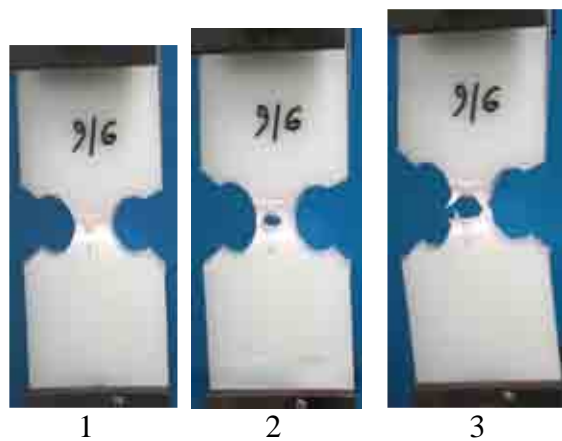

| 1 | 2 | 3 | (a) | (b) |

Figure A.29 Profiles of the DN25 SDR11 pipe joint sample with a refilled hole during different stages of the tensile test.
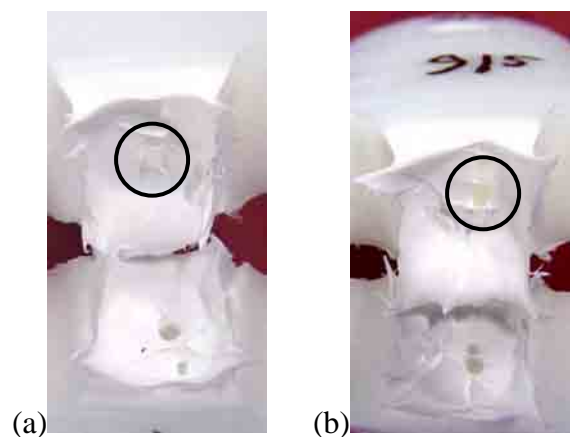
Figure A.30 Cross-sections of the broken DN250 SDR11 pipe joint samples with refilled holes: (a) 9/3, (b) 9/5. Note: the material refilling the hole is marked by the circles.

From Figure A.29 it can be seen that the refilled hole within the joint causes a stress concentration leading to the formation of a crack slightly shifted to the left in relation to the sample centre (stage 1). The enlarged hole splits the neck into four parts and as the hole is

slightly shifted to the left, the left necks narrow quicker and fail first (stage 3) followed immediately by the failure of the necks on the right side.

From Figure A.30a it can be seen that the material refilling the hole indicated by the circle separates from the matrix. It might not totally melt during the butt-fusion process and might not bond properly to the matrix causing a stress concentration on the border between the virgin and remelted regions.

The results indicate that the method of inserting the chip interrupts the structure of the joint and weakens it causing local stress concentration and thus a reduction in ductility. Therefore, it needs to be improved to ensure tight encapsulation of the chip within the matrix.

Further, the impact of the chip included within the joint on its performance is studied for the SC, LC and SSQ chips so the chip shape and size effect is analysed.

A.5.4 Chip shape and size effect

In this section the influence of the chip in general as well as the chip shape and size effect on the joint performance are analysed. Figures A.31-A.33 show the plots for the samples with SC, SSQ and LC chips. In the graphs the test samples from these joints and the extreme samples from the BP joint are also included in order to verify the quality of the joints. Tables A.7-A.9 list the tensile values for the samples with chips. Figure A.34 shows the representative plots (for the samples with the values closest to the calculated averages) while Table A.10 lists the key tensile values.

The joint test samples cut out from each joint (from the bottom and top of the pipe) for verification of its quality were within the range obtained for a BP joint thus their quality was satisfactory. This confirmed the tests of the beads removed from the joints.
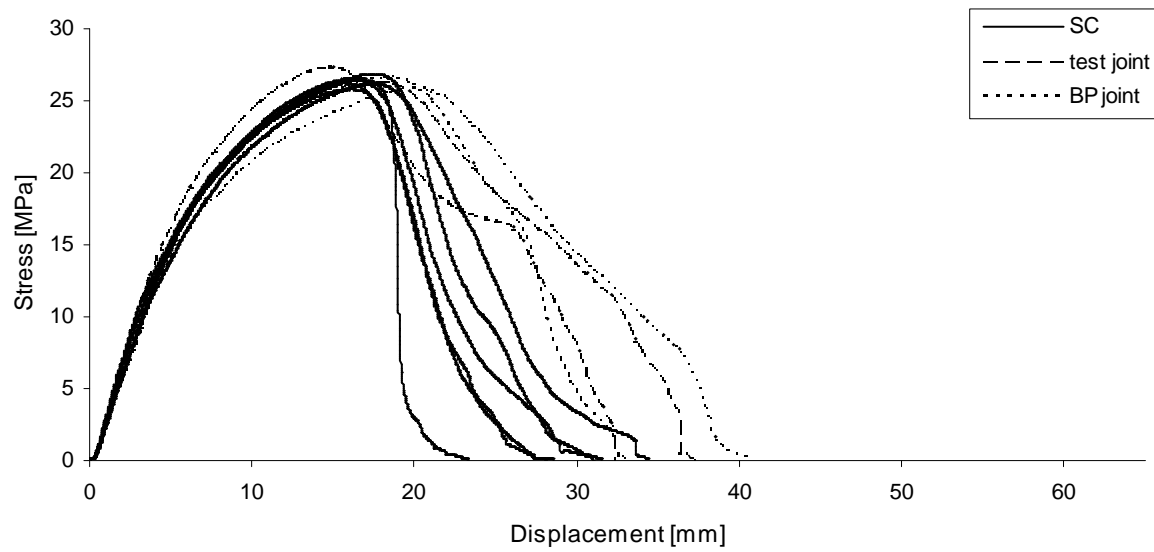
Figure A.31 Stress-displacement curves for the DN250 SDR11 pipe joint samples with SC chips, test joint samples, and the selected BP pipe joint samples.
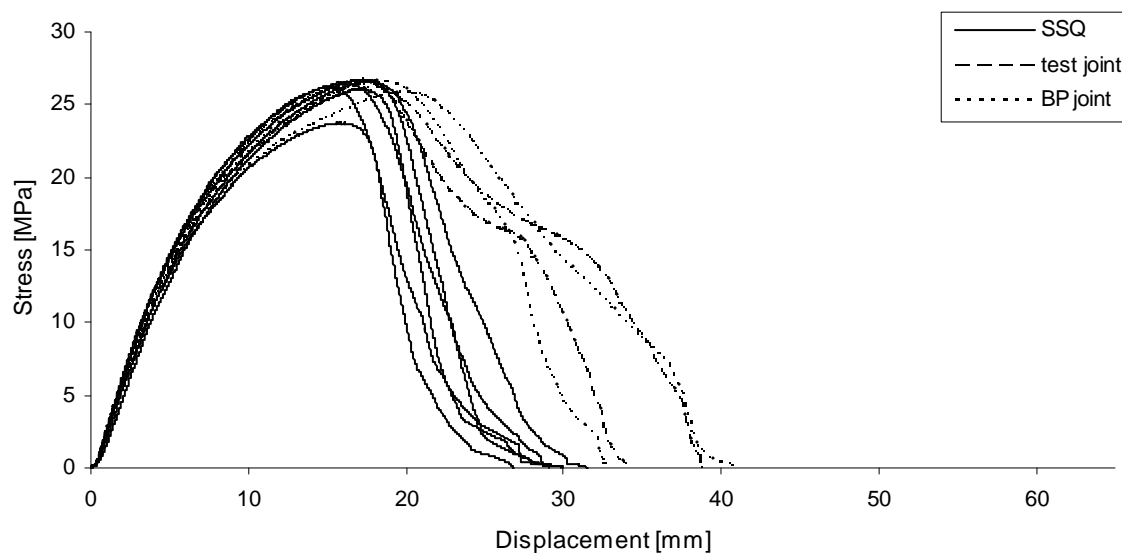

Figure A.32 Stress-displacement curves for the DN250 SDR11 joint samples with SSQ chips, test joint samples, and the selected extreme BP joint samples.
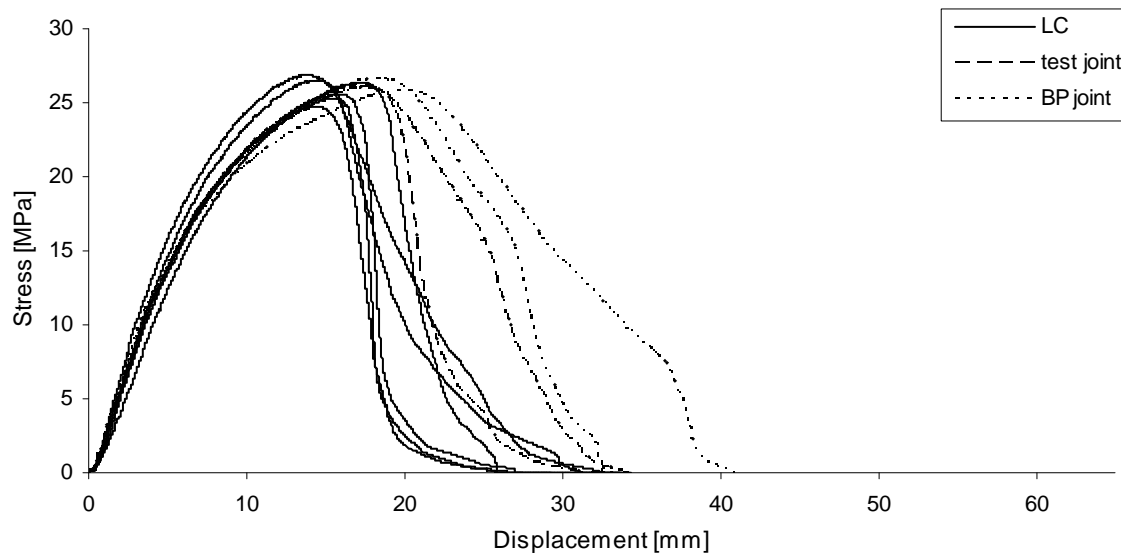
Figure A.33 Stress-displacement curves for the DN250 SDR11 pipe joint samples with LC chips, test joint samples, and the selected extreme BP joint samples.

Table A.7 Tensile values for the DN250 SDR11 samples with SC chips and the test samples.

Sample	Slope of the curve MPa/mm	Yield stress MPa	Displacement at break mm
8/1	3.3	26.2	34
8/2	3.4	26.2	28
8/3	3.5	26.5	31
8/5	3.5	26.5	23
8/6	3.2	26.9	32
8/7	3.4	25.8	29
Average	3.4	26.4	30
SD	0.1	0.4	4
Test samples			
8/4	3.0	26.3	37
8/8	3.8	27.3	32

Table A.8 Tensile values for the DN250 SDR11 joint samples with SSQ chips and the test samples.

Sample	Slope of the curve MPa/mm	Yield stress MPa	Displacement at break mm
10/1	2.8	23.8	27
10/2	3.5	26.8	30
10/3	3.1	26.6	31
10/5	3.2	26.2	29
10/6	3.3	26.5	29
10/7	3.1	26.1	30
Average	3.2	26.0	29
SD	0.2	1.1	1
Test samples			
10/4	3.1	26.6	34
10/8	3.2	26.1	39

Table A.9 Tensile values for the DN250 SDR11 joint samples with LC chips and the test samples.

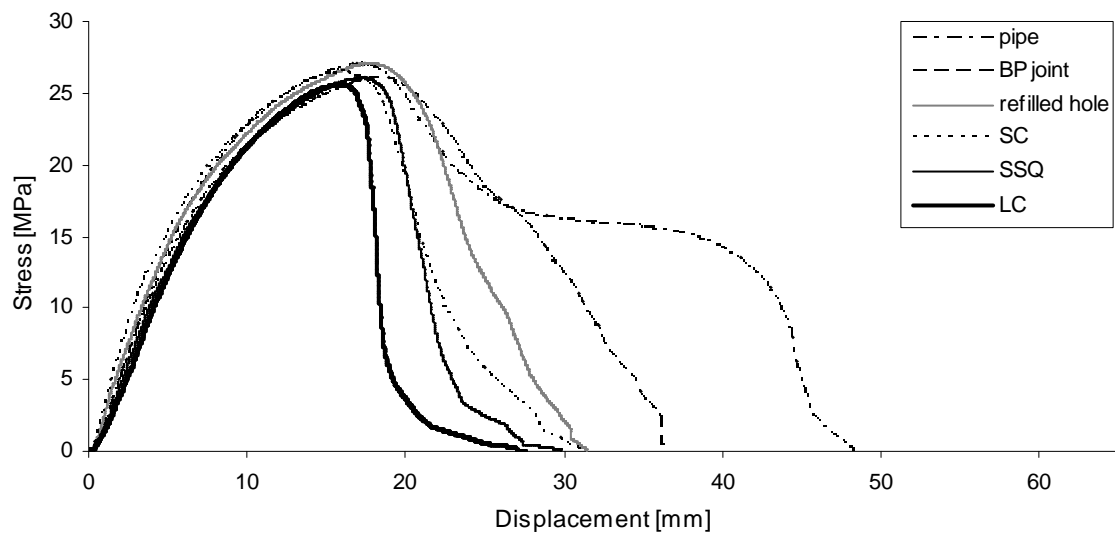| Sample	Slope of the curve MPa/mm	Yield stress MPa	Displacement at break mm
7/1	3.1	25.3	26
7/2	3.9	26.9	32
7/3	3.0	26.4	26
7/5	2.9	25.6	27
7/6	3.3	26.6	31
7/7	3.1	24.8	26
Average	3.2	25.9	28
SD	0.4	0.8	3
Test samples			
7/4	3.4	26.3	34
7/8	3.2	26.1	31

Figure A.34 Representative stress-displacement curves for the pipe and different types of pipe joint samples.

Table A.10 Key tensile values for DN250 SDR11 pipe joints samples.

Sample	Slope of the curve MPa/mm		Yield stress MPa		Displacement at break, mm	
	Average	SD	Average	SD	Average	SD
pipe	3.2	0.3	27.1	0.6	50	6
BP joint	3.2	0.2	26.1	0.3	36	3
refilled hole	3.1	0.1	27.0	0.4	31	2
SC	3.4	0.1	26.4	0.4	30	4
SSQ	3.2	0.2	26.0	1.1	29	1
LLC	3.2	0.4	25.9	0.8	28	3

In the comparison of the samples the slope of the stress-displacement curve (surrogate for the Young's modulus) is not taken into account as the maximum difference between the values is equal to the maximum SD of 0.4MPa/mm, thus insignificant. In addition the measurement of this quantity is very unreliable due to limitations of the instrument and the specific geometry of the sample (theoretically zero gauge length) (see section A.3.4).

As already discussed in section A.5.2 the pipe samples reached the highest yield stress and displacement at break thus are the strongest and toughest. Only for these samples the cold drawing stage (horizontal part of the stress-displacement curve) was recorded, however other samples also exhibited ductility.

As can be seen from Figure A.34 and Table A.10 the joint caused a reduction in the ductility (significantly lower displacement at break of the samples) and energy to break of the joint (smaller area under the curve), which confirms the results of Chen et al. (1998) and was discussed in section A.5.2. The method of introducing a chip caused a further reduction in ductility due to the air void and not complete remelting of the material filling the hole as discussed in detail in section A.5.3.

The chip introduced into the hole caused a further reduction in the ductility and strength. Surprisingly, the yield stress (associated with the strength of the joint) was lower for the joints with SC chips than for the joints with refilled holes. However, the lowest value was obtained for the BP joint, thus it is difficult to justify if the SC chip has any reinforcing effect.

A few samples with an SC chip were X-ray scanned in order to verify the orientation and position of the chip in relation to the sample and the joint region. The examples are shown in Figure A.35.
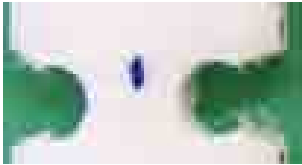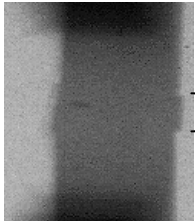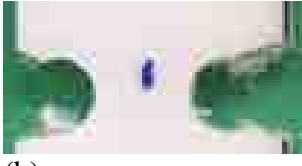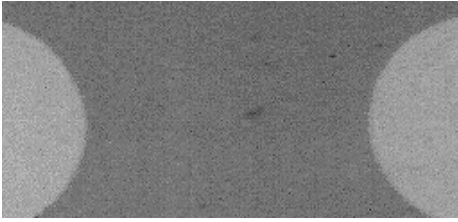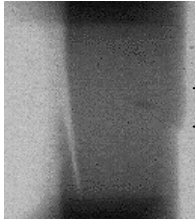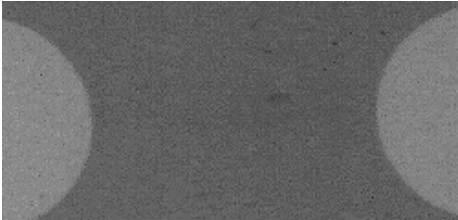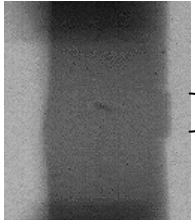

Figure A.35 Pictures of the three example DN250 SDR11 pipe joint samples and their X-ray scans.

From the X-ray scans it can be seen that the chips are located within the joints, close to the centre of the sample (Figure A.35, top views). In some cases they are close to the surface of the sample (Figure A.35a and b, side views). The orientation of all examined chips in the joint

samples is close to SC/90/90. This will also be verified from the broken samples presented in Figure A.37.

The performance of the joint samples in tension was also studied on the basis of sample profiles shown in Figure A.36.

Figure A.36 Profiles of the DN250 SDR11 pipe joint sample with an SC chip during different stages of the tensile test.
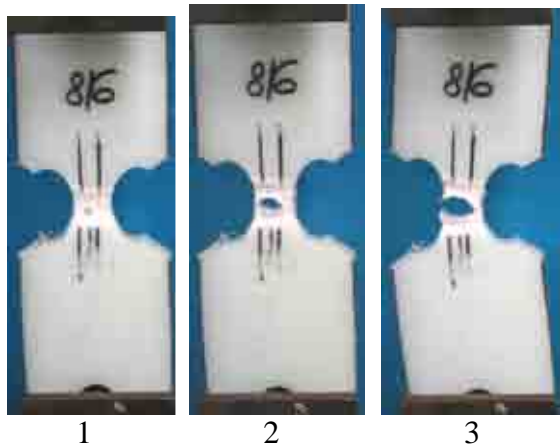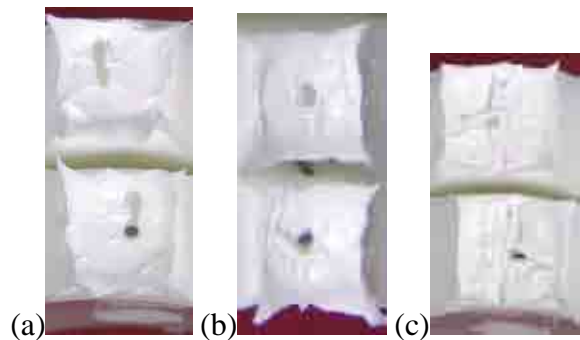
Figure A.37 Cross-sections of broken DN250 SDR11 pipe joint samples with SC chips: (a) 8/2, (b) 8/3, (c) 8/5.

When comparing the profile of the sample with an SC chip at the different tensile test stages with the sample with refilled holes (Figure A.29) lots of similarities can be seen. The chip causes a stress concentration similarly like the refilling polymer and accelerates the sample failure. In Figure A.37a it can be seen that the material in the vicinity of the chip also separates from the matrix. In addition, some space around the chip was probably not totally refilled and the air void within the joint remained.

The pictures of failed samples similar to the X-ray scans indicate that the orientation of the chip is random but close to SC/90/90. Surprisingly, when the chip was more perpendicular to the tension direction (Figure A.37a, sample 8/2) the performance was better than when it was more parallel to the tension direction (Figure A.37c, sample 8/5), which is in contrast to the results obtained for the compression moulded samples (section 5.2.6, page 176). This might

be due to the fact that the space around the chip is not completely refilled and a small air void remains in its vicinity, which dominates the chip orientation effect. In addition, the chip is very small in relation to the sample cross-section in relation to the compression moulded samples, which might also reduce the chip orientation effect. This is further verified by testing other shapes of the chip of the same size in the next section.

The SSQ chip and LC chip caused a further reduction in the ductility, energy at break (area under the curve) and yield stress of the samples. All the values reduce in the order as presented in Figure A.34 and Table A.10, with the highest values obtained for the pipe listed as the first, and with exceptionally high yield stress for the samples with refilled holes, which was already discussed.

The cross-sections of the failed samples with SSQ and LC chips are illustrated in Figures A.38 and A.39, respectively.

The specimen profiles during the tensile test looked similar to the sample with an SC chip, thus are not shown here.

(a)   (b)
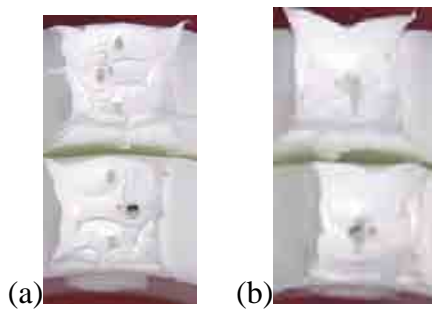
Figure A.38 Cross-sections of broken DN250 SDR11 pipe joint samples with SSQ chips: (a) 10/1, (b) 10/3.

(a)   (b)

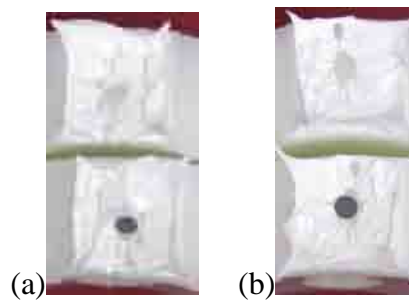**Figure A.39 Cross-sections of broken DN250 SDR11 pipe joint samples with LC chips: (a) 7/1, (b) 7/5.**

From Figures A.38 and A.39 it can be seen that the failure plane of the samples with SSQ chips is similar to the SC samples with visible traces of the air voids of similar size and the polymer around the chip separated from the matrix. As the chip does not stick tightly to the

matrix the sharp corners might not have caused any additional stress concentration as they were probably in the air void and thus had a similar effect to the SC chip and the refilled holes. This effect was different in the compression moulded samples, where the SSQ chip caused significant embrittlement and has a reinforcing effect. However, the pipe joint samples have significantly lager size and different geometry, which might be the reason for these differences. It can be concluded that there is not a significant chip shape effect.

When analysing the chip size effect, from Figure A.34 it can be concluded that the LC chip caused noticeably the highest embrittlement of the joint, because after a steep drop of the curve it continues at a very low stress, which is associated with stretching of the edge region of the sample only. The area under the curve (energy at break) is thus noticeably smaller than for the SC and SSQ chips when comparing the shapes of the curves.

The plots seem to indicate brittle failure; however, the failure plane shows signs of cold drawing in the sample surface regions and microductility in the centre, indicating ductile failure (Figure A.39). Marshall (1991) noticed that the critical defect size ensuring ductile failure depends on the pipe diameter and associated wall thickness. For the same dimensions of a pipe as tested here he determined a critical diameter of 3mm for the orientation of a defect perpendicular to the tension direction. The X-ray scans and pictures of failed samples (Figure A.39) show that the position of the chip was approximately perpendicular to the tension direction; however, even for the LC chip of diameter 4.52mm the failure was ductile. These differences might be due to the fact that Marshall (1991) tested different material (MDPE) while here the modern tough HDPE grade was used, which is probably the reason for these differences.

However, the failure of the samples with an LC chip is slightly less coarse and the fibres group into smaller bands than in other samples, which suggests that less energy was absorbed

by the samples, thus it is less tough (Suarez & Mano, 2000). The largest weakening effect of the LC chip might be associated with the fact that the largest hole is made within the pipe for this chip and the refilling of such a hole is less accurate due to the method applied. Similarly, refilling of the hole around the square chip with sharp corners is also less accurate than in the case of a circular chip of the same size. The LC chip also causes the most significant reduction in the sample cross-section reducing the area of the load bearing polymer matrix by up to 3% (depending on its orientation). This effect was already explained for compression moulded samples (section 5.2.3, page 159).

To sum up the strength and ductility of the samples reduced in the order in which they are presented in Table A.10. All the samples showed signs of microductility and cold drawing was observed in the surface regions, which suggests high toughness of the material and ability to resist crack propagation even when relatively large inclusions are present. However, the chips weaken the joint and in the case of some increased pressure in service, can be the source of a crack.

Further, the thickness effect is studied for BP joint samples and samples with an SC chip made of DN250 SDR21 pipe having a wall thickness of approximately two times smaller than the SDR11 pipe.

A.5.5 Pipe wall/sample thickness effect

The thickness effect is first studied for the joint samples with and without a chip (BP joints) for two thicknesses of the pipe wall, 25mm (DN250 SDR11) called 'thick' and 13.5mm (DN250 SDR21 pipe) called 'thin'. In Figure A.40 the DN250 SDR21 and SDR11 BP joint samples are compared, while in Figure A.41 the plots for the DN250 SDR21 samples with SC chips are shown. Tables A.11 and A.12 list the tensile values for the DN250 SDR21 joint

samples with and without chips. Figure A.42 shows the representative plots (for the samples

with the values closest to the calculated averages) and Table A.13 lists the key tensile values
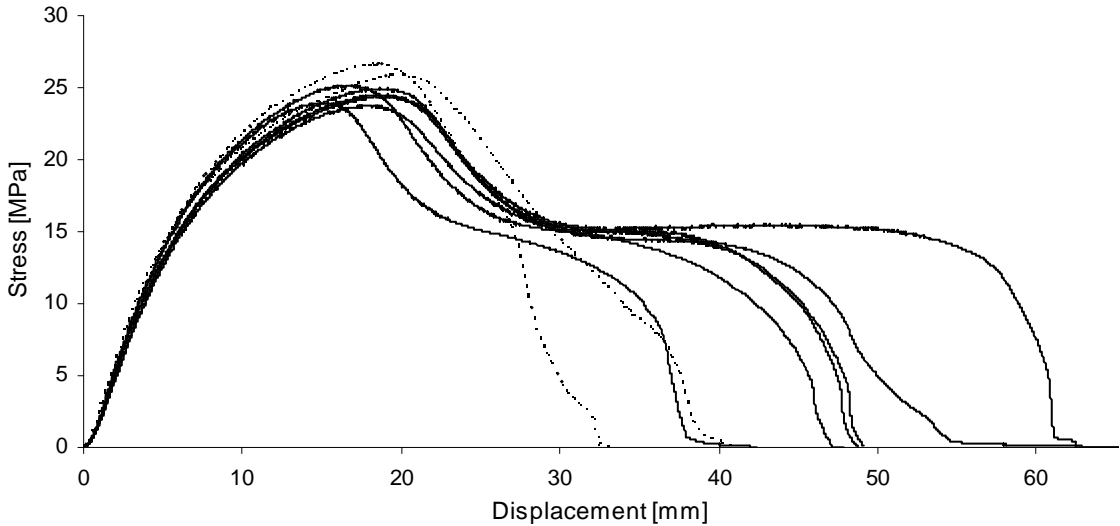
for both pipe joint dimensions.

Figure A.40 Stress-displacement curves for (——) the DN250 SDR21 and (- - -) the selected extreme DN250 SDR11 BP pipe joint samples.
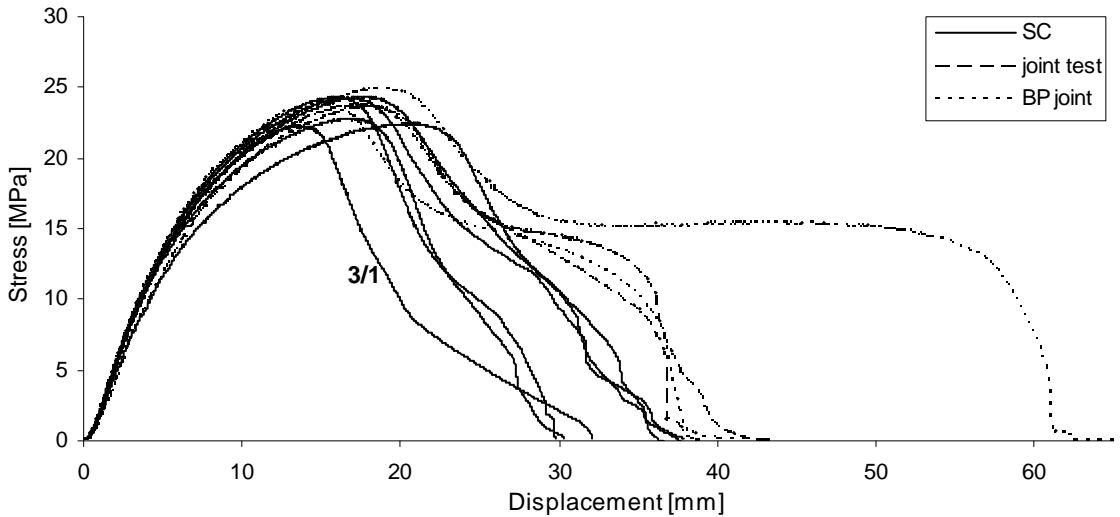

Figure A.41 Stress-displacement curves for the DN250 SDR21 pipe joint samples with SC chips, test joint samples, and the selected BP pipe joint samples.

Table A.11 Tensile values for the DN250 SDR21 BP pipe joint samples.

Sample	Slope of the curve MPa/mm	Yield stress MPa	Displacement at break mm
5/2	3.6	24.0	42
5/3	3.0	23.8	63
5/4	3.0	24.9	62
5/5	3.0	24.5	49
5/6	3.1	24.4	49
5/7	3.3	25.2	47
Average	3.2	24.5	52
SD	0.2	0.5	9

Table A.12 Tensile values for the DN250 SDR21 joint samples with SC chips and the test samples.

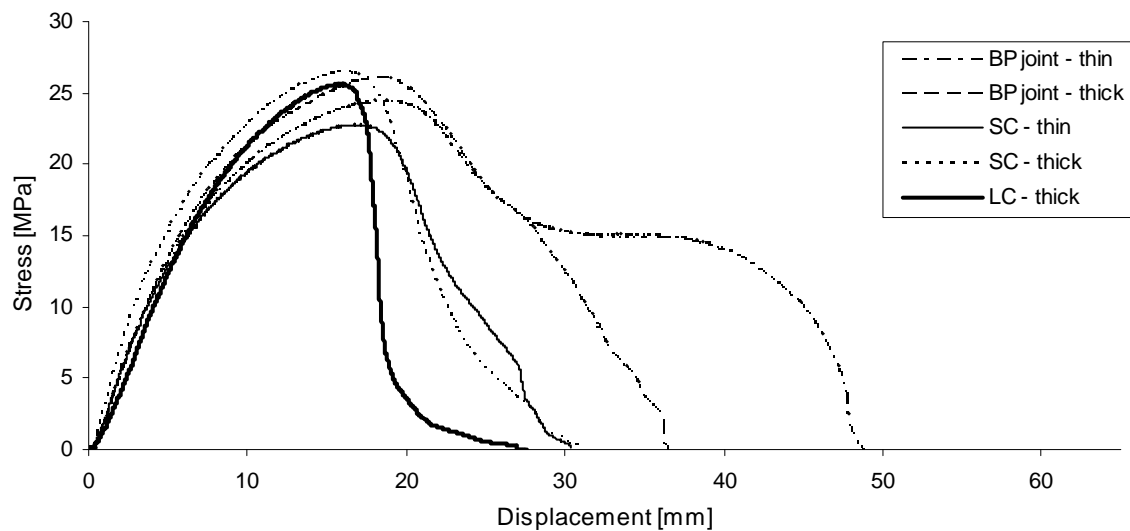| Sample	Slope of the curve MPa/mm	Yield stress MPa	Displacement at break mm
3/1	3.1	22.3	32
3/2	3.0	24.3	38
3/3	3.1	24.4	36
3/5	2.7	22.5	38
3/6	3.2	24.4	30
3/7	2.8	22.8	30
Average	3.0	23.5	34
SD	0.2	1.0	4
Test samples			
3/4	2.9	23.8	42
3/8	3.2	23.7	39

Figure A.42 Representative stress-displacement curves for two thicknesses of pipe joint samples (DN250 SDR11 – thick, and DN250 SDR21 – thin) with and without a chip.

Table A.13 Key tensile values for the DN250 SDR11 pipe joints samples.

Sample	Slope of the curve MPa/mm		Yield stress MPa		Displacement at break, mm	
	Average	SD	Average	SD	Average	SD
DN250 SDR21						
BP joint	3.2	0.2	24.5	0.5	52	9
SC	3.0	0.2	23.5	1.0	34	4
DN250 SDR11						
BP joint	3.2	0.2	26.1	0.3	36	3
SC	3.4	0.1	26.4	0.4	30	4
LLC	3.2	0.4	25.9	0.8	28	3

The density tests indicated that the DN250 SDR21 pipe has a slightly lower average density (0.958g/cm³) than the DN250 SDR11 pipe (0.959g/cm³) having greater wall thickness. This is reflected in the yield stress value being significantly lower (24.5MPa) and the displacement at break value significantly higher (52mm) for thin joint samples in relation to the thick joint samples (26.1MPa and 36mm, respectively).

Another reason for higher toughness of the thin samples is a higher percentage of the plane stress region associated with plastic deformation and energy absorption in these samples, as explained in section 5.2.9 (page 210). The cross-section of the broken sample is totally white (see Figure A.43) due to cold drawing of the whole region, which was observed only in the surface (plane stress) regions in the thick joint samples.

Figure A.43 Cross-section of broken DN250 SDR21 joint sample 5/2.

It is typical that thicker walled sections are less affected by the ductile shear yielding process occurring in the surface regions and are more likely to be under plane strain conditions characteristic for the central regions (Marshall, 1991).

The specimen deformation pattern is between the one for the thick pipe (Figure A.25) and the thick BP pipe joint (Figure A.26), characteristic for a ductile specimen. There can be distinguished a cold drawing stage in the stress-displacement curve as for the thin BP joint samples, which was also recorded only for thick pipe samples (reaching displacement at break of 50mm). Thin pipe samples would have probably reached even higher displacement at break.

In the case of samples with chips the difference between the thin and thick samples was smaller but still a similar pattern was observed. Higher ductility (greater displacement at break) in the case of thin samples is due to the larger percentage of the plane stress region associated with a larger deformation and energy absorption as observed by Broutman et al. (1990) and Marshall (1991). Thus, the thicker pipe joints are more susceptible to embrittlement e.g. due to defects as it was observed here (Bowman, 1996). Another reason for these results might be a slightly lower crystallinity of thin samples.

The reduction in displacement at break and yield stress due to inclusion of a chip (chip effect) in comparison with BP joints of the same thickness was more significant for the thin samples. This effect (difference) was even smaller for the thick samples with an LC chip (when compared with BP joints of the same thickness), which makes a larger percentage of the sample cross-section than an SC chip in a thin sample.

This means that the chip effect is more significant for these samples, which is in contrast to the findings of Bowman (1996) and Marshall (1991) who observed that the thicker sections

are more sensitive to defects leading to embrittlement. However, more tests would be required to confirm this statement as such limited data do not allow drawing of any certain conclusion.

It has to be noted that the measurements were not very accurate. The samples differed due to the method of their preparation where many parameters starting from the pressure during butt-fusion jointing to cutting out of the samples were manually controlled, thus there was a big possibility of human error. Due to the specification of these samples it would be recommended to produce more samples from multiple joints, however this would require a lot of effort and time.

A.6 Conclusions and recommendations for further work associated with the tensile joints test

In order to obtain an information on the impact of inserting chips on large structures, pipe joints with chips were produced and examined. The methods of implementing defects into the joints developed by other researchers did not work for the chips as they moved into the joint bead during the butt fusion process. A new method of inserting chips into joints was developed whereby a hole was made in the pipe end using a soldering iron, the chip was inserted into the hole and it was refilled with the previously removed melted polymer. Although, this method did resolve some of the issues of previous methods it did affect the quality of the joints and did not enable the position nor the orientation of the chips to be controlled. However, the usual chip position was perpendicular to the tension direction. The joint tests revealed that the chip causes a reduction in the joint ductility and strength. However, this effect was similar to the one caused by the method used to insert the chip, i.e. with no chip present, which was tested independently. The LC chip had the largest impact on

the integrity of the joint as the chip and the hole, in which it was placed, caused the largest reduction in the sample cross-section.

The tests on the joints revealed that the effect of, for example, chip shape and size is much smaller in larger samples, however, more tests on higher quality samples are required to confirm the details of these findings.

A more accurate (in terms of position and alignment) method of incorporating chips into pipe joints needs to be developed. In addition, incorporating chips into pipe sections is worthwhile exploring. This might require coatings on the chips to protect them and to protect the pipe manufacturing equipment.